Techniques to Enhance Spectral Efficiency of OFDM Wireless Systems

Das, Suvra S.

Publication date:
2007

Document Version
Publisher's PDF, also known as Version of record

Techniques to Enhance Spectral Efficiency of OFDM Wireless Systems

by

Suvra Sekhar Das, B.Eng.

Dissertation

Presented to the International Doctoral School of Technology and Science

in Partial Fulfillment of the Requirements for the Degree of

Doctor of Philosophy

Aalborg University

$7^{th.}$ September 2007

Supervisors:

Professor Ramjee Prasad
Associate Professor Elisabeth de Carvalho

The Assessment Committee:

Professor Preben Mogensen, Aalborg University, Denmark
Professor Lajos Hanzo, University of Southampton, UK
Professor Shinsuke Hara, Osaka City University Japan

Moderator:

Associate Professor Fleming B. Frederiksen, Aalborg University, Denmark

ISBN: 87-92078-07-9
ISSN: 0908-1224

Suvra Sekhar Das
Center for TeleInFrastruktur (CTiF)
Aalborg University
Niels Jernes Vej 12
9220 Aalborg Ost
Denmark
e-mail: *ssd@es.aau.dk*

Dedicated to my Parents, my Sister and Madhulipa.

Abstract

In recent years Orthogonal Frequency Division Multiplexing (OFDM) based technologies are in wide use for wireless communication systems. This is because OFDM elegantly overcomes the adverse effects of frequency selective fading channels and offers high spectral efficiency. Investigation of techniques to further enhance the spectral efficiency of OFDM based wireless systems is the prime objective of this thesis.

As a first step, a comparison is made between OFDM and Multi Carrier Spread Spectrum (MC-SS) scheme. OFDM is found to offer relatively better performance than MC-SS under channel estimation and synchronization errors. This is the motivation to select OFDM for further investigation and performance enhancement in this thesis.

Though OFDM has many advantages, yet it is severely affected by Inter Carrier Interference (ICI), which is caused by residual phase error, carrier frequency offset and Doppler frequency spread. To track the residual phase error, pilot sub carriers are embedded between the data sub carriers. To reduce the pilot overhead, it is proposed in this thesis to load data bits on pilot sub carriers without degrading system performance. It is found that up to 15% increase in spectral efficiency can be obtained by using this technique.

To mitigate the impact of ICI, due to Doppler frequency spread, a novel technique of using adaptive sub carrier bandwidth is proposed in this work. This technique enhances the spectral efficiency in the range of 10% to 30% over OFDM systems which use fixed sub carrier bandwidth.

OFDM systems need a large Guard Interval (GI) to overcome the effect of Inter

Symbol Interference (ISI). In order to decrease the overhead due to GI, an algorithm to dynamically select the GI duration is derived in this thesis. By adaptively selecting the GI duration, it is found that the spectral efficiency can be increased up to 20%.

The performance of OFDM based wireless systems is also limited by the time variations of the propagation channel. In such situations Link Adaptation (LA) techniques using adaptive bit rate transmission achieves very high spectral efficiency by exploiting the channel variations. OFDM provides a suitable framework for LA. However, the combination of LA and OFDM results in increased implementation complexity. Another aim of this thesis is to provide low complexity techniques to increase spectral efficiency. Hence, low complexity, low overhead LA - OFDM schemes which have near optimal spectral efficiency are proposed in this work. The proposed schemes reduce overhead by 50% as well as significantly bring down the implementation complexity.

The impact of non linear signal distortion caused by the high power amplifier and frequency synchronization errors on the performance of LA-OFDM systems are also analyzed in this work. Methods to overcome the effects of these impairments by suitable adjustments to the LA algorithms are presented in this thesis.

As a result of this work it can be concluded that significant cumulative gain in spectral efficiency can be obtained by using the proposed transmission schemes. The techniques and guidelines for spectral efficiency improvement presented in this thesis are promising enough for future OFDM based wireless systems.

Dansk Resumé

I de seneste år er Orthogonal Frequency Division Multiplexing (OFDM) baserede systemer taget mere og mere i brug i forbindelse med trådløst kommunikationsudstyr. Det skyldes, at OFDM på en effektiv måde kan hindre den ødelæggende virkning af frequency-selective-fading, og at OFDM samtidig kan tilbyde høj spektral effektivitet.

Det primære formål med denne afhandling er undersøgelse af teknikker, som yderligere kan forbedre den spektrale effektivitet af OFDM baserede trådløse systemer. Som det første trin gennemføres en sammenligning mellem OFDM og dets udvidelsessystem MC-SS. OFDM ses her at tilbyde forholdsvis bedre ydeevne end MC-SS m.h.t. modtagereffektivitet og -fejl. Derfor foretrækkes OFDM i denne afhandling og undersøges nøjere med henblik på yderligere forbedring af ydeevnen.

OFDM har mange fordele men er umiddelbart stærkt påvirket af Inter Carrier Interference (ICI). ICI skyldes residuale fasefejl, carrier-frequency-offset og Doppler-frequency-spread. For at spore de risiduale fasefejl er der indført pilot-sub-carriers mellem de enkelte data-sub-carriers. Med sigte på at mindske overheadet i forbindelse med indførelsen af pilot-sub-carriers er det i afhandlingen foreslået at tilføre data bits til de enkelte pilot-sub-carriers for dermed at undgå reduktion af systemydeevnen. Ved undersøgelse findes det, at der med denne teknik kan opnås op til 15% forbedring i spektral effektivitet.

For at mindske den betydelige virkning, som ICI ved Doppler-frequency-spread har på OFDM systemer, foreslås der i nærværende arbejde en ny teknik baseret på adaptiv sub-carrier båndbredde. Der opnås med denne teknik en forbedring på 10% - 30% af den spektrale effektivitet i forhold til OFDM systemer med fast sub-carrier båndbredde.

Der behøves i OFDM systemer et stort Guard Interval (GI) for at overvinde virkningen af Inter Symbol Interference (ISI). Med sigte på at få mindsket overheadet i forbindelse med GI er der i afhandlingen udviklet en algoritme, som dynamisk fastlægger GI-varigheden. Det vises, at hvis GI-varigheden vælges adaptivt v.h.a.

algoritmen, kan den spektrale effektivitet øges op til 15%.

OFDM baserede trådløse systemer er også begrænsede af den tidsvarierende kanal. I sådanne situationer kan man ved hjælp af Link Adaptation (LA) teknik med adaptiv bit-rate-transmission opnå meget høj spektraleffektivitet ved at udnytte variationer i kanalen. OFDM tilvejebringer en passende ramme for LA. Kombinationen af LA og OFDM resulterer dog i forøget implementationskompleksitet. Et andet sigte med denne afhandling er derfor at tilvejebringe en lav-kompleksitets LA-OFDM teknik. I nærværende arbejde foreslås der af den grund lav-kompleksitets, lille-overheads LA-OFDM systemer med næsten optimale spectrale effektiviteter. Det beregnes, at de foreslåede systemer kan reducere overheadet med 50% samtidig med, at kompleksiteten reduceres significant.

Virkningen af en praktisk funktionsbegrænsning - f.eks. i forbindelse med ikke-lineær signalforvrængning forårsaget af effektforstærkere og givet ved resultatet af frekvens-synkroniseringsfejl i forbindelse med driften af LA-OFDM systemer - er også analyseret, og metoder til at få bugt med disse forringelser og fejl ved passende justering af LA algoritmerne er præsenteret i afhandlingen.

Som et resultat af arbejdet kan det konkluderes, at significant kumulativ forbedring af den spektrale effektivitet kan opnås ved brug af de foreslåede adaptive transmissionsteknikker. De adaptive teknikker og retningslinier for forbedring af den spektrale effektivitet, som er præsenteret i afhandlingen, vurderes at være tilstrækkeligt lovende m.h.p. yderligere overvejelser i forbindelse med fremtidige OFDM baserede trådløse systemer.

Acknowledgements

I am deeply indebted to my supervisor Prof. Ramjee Prasad, for giving me the opportunity to work under his supervision and learn from his vast experience which spans beyond technical fields. His continuous motivation helped me sail through this voyage and reach the final destination. I express my gratitude to Elisabeth De Carvalho who has been my co-supervisor for a major duration of my work and has provided important feedback in several aspects of my work. I am also highly obliged to Frank H.P. Fitzek and Ole Olsen who were my supervisors during the early part of my research at Aalborg University without whose support I could not have begun this work.

I am grateful to Dr. Sunil Sherlekar, for taking the initiative for this project and to the management team of Tata Consultancy Services Ltd., India, for funding this work. I specially thank Mr. Debasis Bandopadhay, for providing all support needed to succesfully complete this work without any hindrance. I would like to thank Mr. Arpan Pal, Mr. P. Balamuralidhar and Mr. Prateep Mishra, for giving me the prestigious opportunity to work on this project. I have learnt a lot from my team members of the Embedded Systems group of TCS Kolkata. I would like to thank them all.

I would like to mention my colleague Imadur specially here for he has been a continuous discussion partner throughout the work. I express my sincere thanks to Daniel and Soren who have provided continuous help in understanding technical concepts. I would like to remember Akhilesh, Basuki, Anas , Petar , Huan, Hiro with whom I had the chance of some good technical discussion.

I am thankful to the several MSc. students who have made contributions to this work while working on their graduation projects or on internships. Fuad, Bayu, Carlos, Faisal and Nidcha have been associated with this work is some time or the other. I like to specially cite Yuyuane Wang for his interest in research activities and the contributions he made in many ways to this work.

I thank all my colleagues and secretaries of section of RATE, CTIF, former WING group and former Department of KOM, provided all necessary help needed to do my research smoothly.

Fleming B. Frederiksen was always keen about my progress and supported me in several student projects. I am grateful to him for all his kindness. I would note the help of Sanjay Kumar from BIT Mesra, Ranchi for providing important feedback to make the final version of the thesis. Mrs. Nisha Gupta from BIT Mesra, also helped in making the document complete. I am grateful to her for the help she extended. I also owe a lot my colleague Nicola Marchetti for reading through the thesis and helping to improve it.

It is the sacrifice and blessings of my parents that gave me the strength to reach the completion of this work steadily. My sister kept continuously motivating me to persevere to the end of this long project. It was the tremendous support from my wife, Madhulipa, that helped me put all my effort in this work. She made many sacrifices so that I could devote my time to this thesis. My little daughter Aane, (Debosmita) has been a new inspiration in my life since she was born. Finally it is by God's grace that I could do my research relentlessly to complete the program in time.

Contents

List of Figures

List of Tables

1 Introduction

1.1 Background to OFDM

Orthogonal Frequency Division Multiplexing (OFDM) based access/multiplexing schemes are used in wireless applications such as Wireless Personal Area Network (WPAN), Wireless Local Area Network (WLAN), Wireless Metropolitan Area Network (WMAN), high quality digital radio (Digital Audio Broadcasting (DAB)) and television broadcasting (Digital Video Broadcasting (DVB)) [1]. It is being considered for IEEE 802.20, IEEE 802.16 and 3GPP-LTE [2] systems. OFDM will remain as the key enabling technology for achieving higher data rates in wireless packet based communication systems in the next few years to come [3]. Its extensions with time frequency domain spreading are under investigation for use in future wireless systems [4]. OFDM tackles the frequency selective wireless fading channel effectively by converting a wide band signal into a set of parallel narrow band signals such that each stream of narrow band signal experiences flat fading. With the use of cyclic prefix to eliminate Inter Symbol Interference (ISI), there is need for only a simple one tap equalizer at the OFDM receiver. OFDM brings in unparalleled gains in bandwidth savings, which leads to very high spectral efficiency. These properties make OFDM systems extremely attractive transmission technologies for wireless scenarios.

OFDM was initially used in military systems, such as KINEPLEX in 1958, KATHRYN in 1967, and ANDEFT in 1968 [5]. A bank of conventional transmitters/receivers with overlapping spectra were used in these systems. In 1971, Weinstein and Ebert's proposal to use the Discrete Fourier Transform (DFT) to modulate/demodulate all the sub-carriers, with a single oscillator [6] was a pioneering effort. With its implementation via FFT finally OFDM was realizable in commercial communication system. It started with a number of wire–line standards. High bit-rate Digital Subcarrier Lines (HDSL) [7], Asynchronous Digital Subscriber Line (ADSL)[8], and Very High speed Digital Subscriber Line (VDSL)[8] were a sequence of standards which led to throughput of up to 100Mb/s. Then it was introduced into the wireless arena through DAB[9] and WLAN [10, 11]. Then came DVB[12, 13] around 2004. In the WMAN application, OFDM is considered for the Worldwide Interoperability for Microwave Access (WiMAX) implementation via the IEEE 802.16d,a,e [14, 15] standards. It is also being considered for the 3GPP Long Term Evolution, which in under development.

Table 1.1 summarizes some wireless systems which use OFDM as the transmission technology [1].

Table 1.1: Wireless Systems using OFDM

Application	WMAN	WLAN	WPAN
Cell Radius	1km to 20km	up to 300m	few 10s of meter
Mobility	High and low	Low	very low
Freq Band	2-66Ghz	2-5Ghz	5-10GHz
Data Rate	Few Mbps	upto 100Mbps	upto 10 Mbps
Deployment	IEEE 802.16a, d, e, WiMAX, 3GPP-LTE	IEEE 802.11a, g, HiperLAN2	IEEE 802.15, ZigBee

1.2 Motivation

Now is the juncture where wireless internet access is taking over wire line internet access in several countries. Edinholm, who was the chief technology officer of Nortel Networks, predicted the exponential growth of data rate in wireline and wireless networks [16] and said that wireless data access would eventually catch up with it wireline counterpart but not within 2008. However, the current scenario of Mobile users is tending to shorten the time line.

It is said that currently there are around 2.7 billion mobile phone users. The use of mobile phones is changing the way of life for the next generation, which has already been significantly changed by the Internet.In Japan, South Korea and China, the majority of web access now comes from mobile phones, not Personal Computers (PCs). The need to support higher and higher data rate in wireless systems can be easily understood in this context.

Fig. 1.1 represents a common view of current and future wireless systems. Only two dimensions are present in this picture. Power consumption is also an important dimension along with these metrics. In current systems, there is a tradeoff between mobility, coverage and data rate. The need for next generation systems is to provide higher data rate at high mobility conditions, but at the same time implementation complexity of the devices must be as minimum as possible to reduce power consumption. The systems must also be able to cater to a whole range of mobility conditions, and must consider that devices with different capabilities will coexist in the same network. In other words future generation systems must be able to provide higher data rates at all mobility conditions consuming minimum power and other available resources.

This is supported by the visionary statement "It is dangerous to put limits on wireless data rates, considering economic constraints," by Professor Ramjee Prasad in 1999 [1]. Wireless spectrum available for commercial use is limited and expensive. One of the main ways to support the increasing demand of wireless data services is to push spectral efficiency to its limits.

Increasing the spectral efficiency of wireless communication systems is one of the greatest challenges faced by wireless communication engineers. The available bandwidth is scarce and costly, where as, there is a huge demand for data rate created by increasing number of subscribers and increase in multimedia application which require large bandwidth. Increasing the spectral efficiency is the answer to this growing demand of data rate when the available bandwidth is limited. OFDM already provides very high spectral efficiency but current implementations of OFDM do not fully exploit the capabilities of OFDM. There are still several avenues which can be explored to increase the spectral efficiency of OFDM systems even further. Therefore the necessity to increase the spectral efficiency has been a prime motivating factor for this work.

One of the approaches to increase the spectral efficiency is to design high performance receivers, which leads to increase in signal processing complexity. Increase in receiver complexity contributes to higher power consumption, and costlier compo-

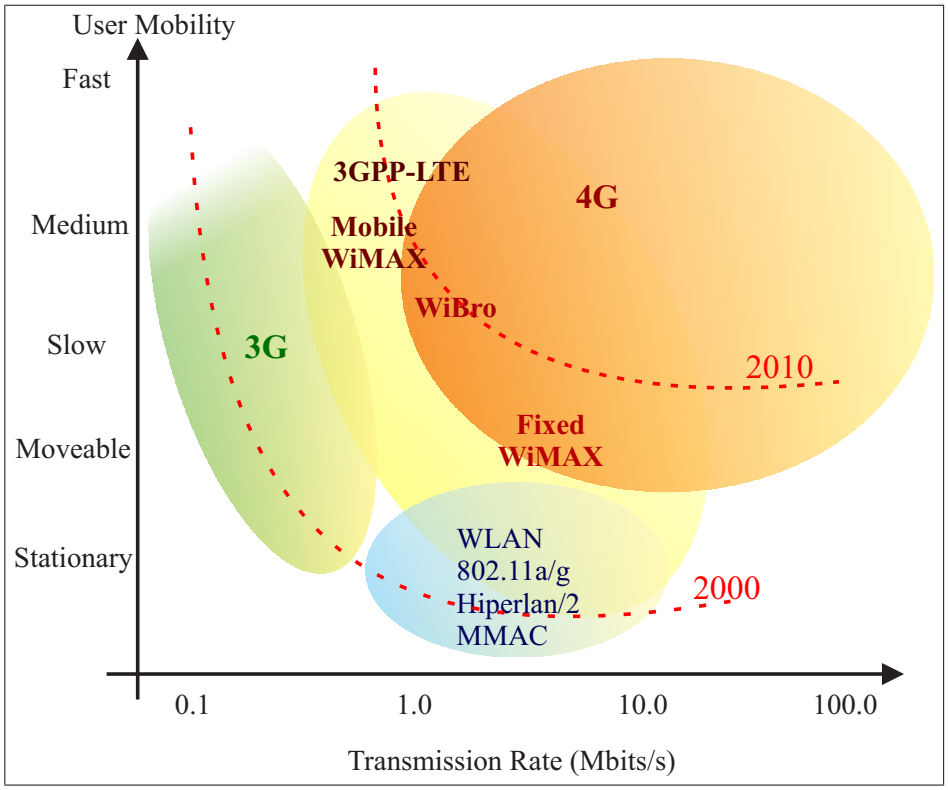

Figure 1.1: Wireless Systems

nents. With increase in multimedia applications, there is a further addition to the processing complexity. With limited battery power available on portable devices to support the full range of operations for long durations the need for low complexity low power consuming algorithms can be easily understood. To target the mass market of wireless modules, low cost solutions have to be found, keeping in mind the tradeoff between efficiency and price. Therefore it is important that the techniques to improve spectral efficiency do not increase the signal processing complexity. Hence one of the motivating factors for this work is the need for low complexity schemes to increase the spectral efficiency of wireless systems.

1.3 Problem Definition

It is known that OFDM is spectrally very efficient and robust in dealing with the frequency selective wireless fading channels, yet some combinations of spread spectrum techniques and OFDM are being considered to develop even better systems [17]. Though some works give details of their performance, it is important to compare them against OFDM in the same test conditions, which include among others non ideal re-

ceiver operations. Thus the first problem addressed is the performance evaluations and enhancements to multi carrier spread spectrum techniques for indoor conditions. This analysis has been extended to the conditions when the receiver cannot obtain perfect frequency synchronization and there exists channel estimation error.

Though OFDM brings several benefits, yet its performance depends on the channel estimation accuracy and residual phase error due to remaining uncorrected carrier frequency offsets [18]. Therefore pilot sub carriers are embedded among data sub carriers [11] so that good estimates of these errors can be obtained. Good estimation of the phase errors helps in better compensation of the errors which leads to improved performance. Since pilot sub carriers do not carry information bits they are overhead and causes loss in bandwidth efficiency. Investigation of methods of reducing this loss in bandwidth efficiency to improve the spectral efficiency of the system is thus considered as a problem area in this thesis.

One of the strengths of OFDM is its closely packed sub carriers. The sub carrier bandwidth is a primary design parameter in OFDM systems. Carrier frequency offset and Doppler frequency spread cause ICI which severely degrade the performance of OFDM based systems. There are several algorithms to estimate and compensate the carrier offset [19]. However, the Doppler frequency spread consists of multiple frequency offsets [20] and cannot be compensated by carrier offset compensation algorithms. Algorithms to address ICI due to Doppler are very complex from implementation point of view [21, 22]. The ratio of the maximum uncorrectable residual carrier offset and the maximum Doppler frequency spread to the sub carrier spacing is an important factor on which the ICI depends. The maximum value of the ratio is usually kept within 2% [23]. Thus once the maximum distortion is known the maximum value of sub carrier bandwidth gets decided. The larger the maximum distortions, the larger is the value of the sub carrier bandwidth needed in order to keep the ratio within the limits mentioned above. The useful signal duration of the symbol is inversely proportional to the sub carrier spacing. Therefore the larger the sub carrier spacing the smaller is the useful signal duration. The OFDM symbol efficiency can be defined as

$$\begin{aligned} \text{OFDM symbol efficiency} &= \frac{\text{useful symbol duration}}{\text{total symbol duration}} \\ &= \frac{\text{useful symbol duration}}{\text{useful symbol duration} + \text{guard interval duration}} \end{aligned} \tag{1.1}$$

The GI duration is dependent on the Root Mean Square (RMS) delay spread of the channel and not on the residual carrier offset or the maximum Doppler frequency spread. Therefore the design of GI length is independent of the sub carrier bandwidth value. Thus the OFDM symbol efficiency decreases as the useful signal duration reduces, due to increasing sub carrier bandwidth, when the GI duration is fixed. This design is based on the worst case scenario which is not always encountered. In other situations there is a large margin in the parameter and there is an unnecessary wastage of resources. Thus one of the problems addressed in this thesis is to investigate adaptive techniques to overcome this situation and improve upon the spectral efficiency without increasing the complexity of the User Equipment (UE).

The GI is an important designed parameter for OFDM systems. Its contribution to the overhead has already been seen in (1.1). A properly chosen length of GI prevents ISI and ICI which enables the use of single tap equalizer per sub carrier. Ideally the length of GI should be larger than the maximum excess delay of the channel. Now similar to the earlier situation, the operating conditions are not that harsh in most occasions. In such scenarios there is wastage of power and bandwidth. If the margins were reduced, then performance would be affected since there would be introduction of irreducible ICI and ISI when worse conditions are encountered. Therefore several attempts to address the situation have been made towards developing high performance receivers, which can reduce the interference but these schemes unfortunately need heavy signal processing [24],[25]. Therefore a technique is proposed in this work, which can reduce the GI overhead, yet does not incur penalty in terms of performance or receiver complexity.

Link Adaptation (LA) through the use of adaptive modulation, coding and power control has been under active investigation to overcome the time frequency selective fading of the wireless channel in an effective manner using feedback of channel state information from the receiver [26]. LA becomes more complex when applied to multi carrier systems because the degrees of freedom available for performance improvement increase. It is vital to investigate schemes with low implementation complexity. It may not be necessary to use all of the degrees of freedom at the same time. Some aspects of reduced LA rate are investigated in [27], however, a much wider scenario and several levels of adaptation are analyzed in this thesis. The tradeoff with performance loss in such mechanisms needs to be identified which is also addressed in this thesis.

Though LA schemes promise significant gains for OFDM based systems, the performance is limited by the handicaps of OFDM. There have been investigations

verifying the performance of LA due to channel feedback delay and channel estimation error [28]. However, their tolerance to synchronization error and non linear operation of the power amplifier, which becomes significant for OFDM with high Peak to Average Power Ratio (PAPR) properties, need a critical study. Hence finding the true performance of OFDM systems using LA under such conditions is a prime area of investigation of this thesis.

1.4 Goal and Scope of the thesis

This project started as a collaboration between Tata Consultancy Services, India and Aalborg University. The objective of this project is to investigate efficient technique for broad band wireless communication system for indoor and outdoor scenarios. The first goal towards the objective is to find a suitable multiplexing scheme among OFDM and MC-SS systems. Therefore in order to make a high efficiency system the second goal is to find transmission mechanisms to overcome the impairments which impede OFDM based schemes. The research focus is in the physical layer.

The environments under consideration are both indoor and outdoor scenarios. Such conditions, would cover WLAN and WMAN applications. Under indoor and low mobility conditions, physical specifications from IEEE 802.11a,g [11] based WLAN standard have been considered for simulations. The parameters for these include a bandwidth of 5 MHz - 20 MHz, with a carrier frequency in the range of 2GHz to 6GHz as per the situation. The channel model used for multi path propagation is from [29]. For outdoor conditions, physical layer system parameters closely adhere to the WIMAX and the developing 3GPP LTE [2] specifications, where bandwidth is 5MHz.

1.5 Research Methodology

The impairments that affect general OFDM systems are first identified. The problems have been evaluated in specific scenarios where they are more prevalent. Each scenario usually maps to either WLAN or WMAN. Accordingly either 802.11a/g parameters or WiMAX/3GPP-LTE parameters have been considered in respective situations.

The analysis presented in this work consists of analytical as well as computer simulation. The system model is usually built on an analytical framework. The appropriate channel conditions are simulated following standard channel models such as [29],[2],[30],[31],[32], etc as applicable. Analysis is made for uncoded systems and

also considering forward error control coding. As found suitable, capacity analysis is also done to find the potential of a scheme. Key performance indicators have been Bit Error Rate (BER), Block Error Rate (BLER), Frame Error Rate (FER), spectral efficiency and outage in different situations.

1.6 Organization of the thesis

Chapter 2: This chapter presents the technical background and introduction to multi carrier techniques needed to explain the work in the following chapters. It details the fundamental description of standard OFDM systems and explains important concepts of multi carrier systems, such as orthogonality of sub carriers and the use of cyclic prefix among others. It also describes the wireless channel model used in the analysis.

Chapter 3: The analysis of MC-SS systems is provided, and the necessity of sub carrier hopping for indoor conditions is evaluated in this chapter. The effect of varying spreading gain, and symbol loading in indoor conditions is evaluated here. The importance of using Successive Interference Cancelation (SIC) receivers under such conditions is also verified. The performance comparison of MC-SS against basic OFDM system under ICI and channel estimation error conditions is also included in the chapter.

Chapter 4 In this chapter, the method of using semi blind pilot sub carriers to enhance spectral efficiency of OFDM systems in WLAN environment is presented. It brings out the possible option of loading the pilot sub carriers with information bits without degrading bit error rate performance of the system. It also discusses a low complexity residual phase tracking algorithm for implementing the scheme.

Chapter 5 This chapter proposes a novel mechanism to deal with inter carrier interference generated due to Doppler effect and carrier frequency offset. Instead of using a compensation mechanism, it proposes adaptive sub carrier bandwidth to dynamically minimize the impact of Doppler. The chapter consists of two parts, where the first part deals with evaluating the system with Orthogonal Frequency Division Multiplexing - Band Division Multiplexing (OFDM-BDM) and Orthogonal Frequency Division Multiplexing - Time Division Multiplexing (OFDM-TDM) systems. The second part of the chapter presents capacity analysis for

a proposed model of Orthogonal Frequency Division Multiple Access - Time Division Multiple Access (OFDMA-TDMA) systems which use ASB.

Chapter 6 This chapter contains the proposal of using adaptive guard interval to reduce the overhead of GI. The algorithm presented here selects the optimal GI length based on the channel condition, residual carrier offset, required SNR margin and received SNR condition. The analysis can be applied to both WLAN and WMAN scenario.

Chapter 7 This chapter presents the proposal of hybrid link adaptation mechanism in OFDM system for spectral efficiency enhancement. Link adaptation discussed in this chapter includes dynamic selection of modulation, coding, and power for the transmitted symbols. The impact of channel condition on the selection of sub band size, modulation and coding rate adaptation interval are investigated. It presents the performance of a proposed low complex system using fast power adaptation along with slow modulation adaptation. Detailed performance analysis is presented which provides guidelines for implementation in a typical outdoor environment.

Chapter 8 Investigation of LA system in presence of non linear distortion due to the HPA and the effect of ICI is made in this chapter. Method to overcome these impairments is also discussed in this chapter.

Chapter 9 This is the concluding chapter of the thesis which summarizes the conclusions of each contributing chapters and lists the possible future works.

1.7 Contributions of this Thesis

1. Multi Carrier Spread Spectrum (MC-SS) techniques enhance the performance of OFDM systems by increasing the frequency diversity gain through spreading over frequency domain. However, for indoor conditions where the coherence bandwidth and coherence time are quite large, then a set of sub carriers will remain in deep fade for a long duration. In such a situation the proposal for Sub-Carrier Hopped Multi Carrier Spread Spectrum (SCH-MC-SS) for indoor systems is made in this work. The proposed SCH-MC-SS can improve the outage performance for indoor scenarios by increasing diversity using fast sub carrier frequency hopping over the entire system bandwidth.

2. Performance evaluation and comparison of OFDM and MC-SS for various practical operating conditions such as channel estimation error and frequency synchronization errors have been made. These analysis bring out the details of performance difference between OFDM and MC-SS. This helps in selecting the best multiplexing scheme in different situations. For this project since increasing the spectral efficiency is a major target, OFDM stands out as the clear winner.

3. Pilot sub carriers used for residual phase tracking in WLAN type systems carry pre-defined symbols and hence are overhead. Semi blind pilots have been proposed which can carry data symbols and can still be used for estimating the phase rotation due to the high SNR content of these sub carriers. This technique of overloading the pilot sub carriers increase the spectral efficiency by 5-15% by reducing the pilot overhead in IEEE 802.11a/g type WLAN environment.

4. A low complexity algorithm for implementing the semi blind pilots is presented in this thesis. The low complexity algorithm does not compute the phase angle using the highly complex inverse tangent function. Instead it uses the complex coefficients directly for estimating the phase coefficients and uses them for compensation.

5. Proposal for Adaptive Sub carrier Bandwidth (ASB) to overcome ICI due to Doppler frequency spread in Orthogonal Frequency Division Multiplexing - Time Division Multiple Access (OFDM-TDMA) systems is made in this work.

6. Proposal for adaptive sub carrier bandwidth to overcome ICI due to Doppler frequency spread in OFDMA systems is made in this thesis. The improvement in spectral efficiency obtained from these schemes is up to 30%.

7. Algorithm for dynamically variable Guard Interval (GI) is developed which reduces the GI overhead up to 60% and contributes towards spectral efficiency enhancement by as much as 15%.

8. Proposal for hybrid link adaptation to suitably use the many degrees of freedom available for link adaptation by combining fast and slow adaptation of the different parameters so as to gain high efficiency while using less complex system is made. The feedback overhead is reduced up to 50% by the proposed techniques. Though primarily parameters from 3GPP LTE have been used, an

investigation of these parameters has been made which provides important insights into possible alternative to the ones selected till now. These results can thus serve as important inputs to future wireless systems.

9. Problem analysis and solution for implementing Link Adaptation (LA)-OFDM under the effect of non linear distortions introduced by High Power Amplifier (HPA) is made in this work.

10. Analysis and solution for implementing LA under practical non ideal conditions of Inter Carrier Interference (ICI) due to Doppler frequency spread is also made.

2

Wireless Channel and Multi Carrier Systems

2.1 Wireless Channel

In 1860s James Clerk Maxwell developed the fundamental laws of electromagnetic theory and Heinrich Hertz proved the existence of electromagnetic waves in 1880s. In the early 1890s Nicola Tesla demonstrated radio telegraphy and Alexander Popov build his first radio receiver in mid 1890s. Then Acharya Jagadish Chandra Bose gave his first public demonstration of electromagnetic waves (at millimeter wavelengths), by using them to ring a bell remotely and to explode some gunpowder. It was reported in The Daily Chronicle of England in 1896: "The inventor (J.C. Bose) has transmitted signals to a distance of nearly a mile and herein lies the first and obvious and exceedingly valuable application of this new theoretical marvel." This was followed by the first successful wireless signalling experiment by Marconi on Salisbury Plain in England in May 1897 [33]. Since then through several developmental stages we have reached an age of near ubiquitous wireless communication network.

To establish any communication system the knowledge of the channel is very important. Its characteristics drive signal design for the system. Professor Ramjee

Prasad's statement is worth mentioning here that understanding of the channel is bread and butter for the communication engineer [1]. A proper understanding of the environment leads to correct parameterizations and optimization of the target solution. Characterization and modeling (for simulation) of the wireless channel is necessary in situation where the error probability computation is too complicated or might not yet have been solved. Through computer simulation we can get an idea about the performance of the system under test in the environment it is supposed to work in. The model to be used for computer simulation must be simple enough for easy and fast implementation. The correctness of the model is also very important. An erroneous characterization and modeling of the channel would lead to improper estimates of the performance of the system. So it is essential that a proper model of the wireless channel is used. In this chapter the wireless channel models commonly used for system evaluation are presented. An introduction on OFDM and LA is also included.

2.1.1 Channel Parametrization

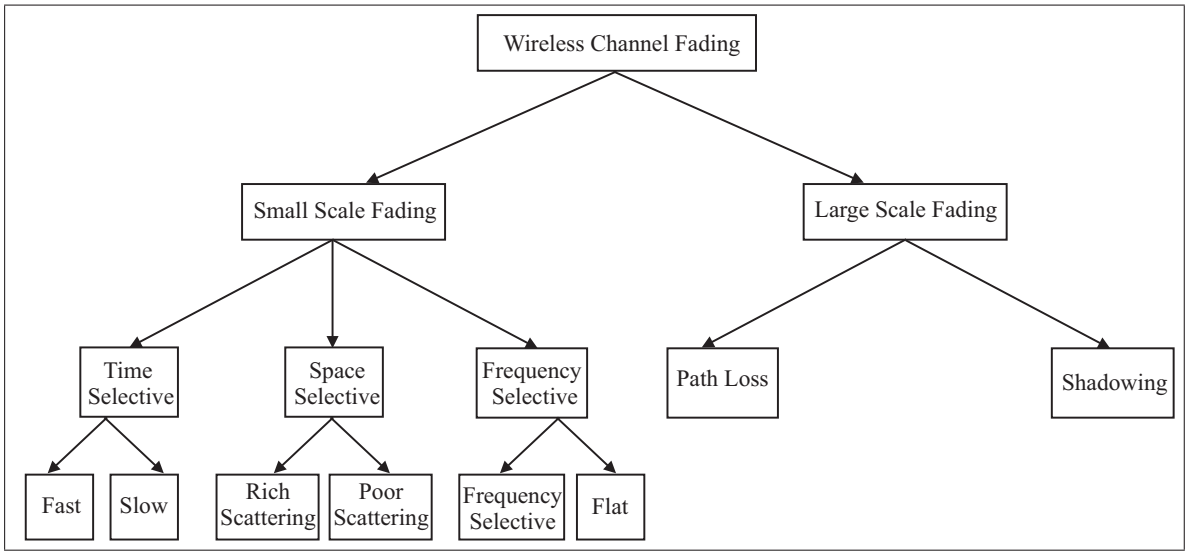

Figure 2.1: Characterization of Fading

The systems analyzed in this thesis are concerned with wide band for both the indoor wireless channel and outdoor channel between 2GHz and 6GHz. The received signal power varies as a function of space, frequency and time in the entire region of described environment. The variation in general is classified as either sarge scale or small scale fading. The different fading conditions can be largely classified as shown in Fig. 2.1.

Large Scale Fading is dealt by propagation model that predicts the mean received signal strength for an arbitrary transmitter receiver separation. The large scale fading model gives such an average with measurements across 4λ to 40λ [34], where λ is the wavelength. This is useful for estimating coverage area. Large Scale fading can be broadly classified as path loss and shadowing. Path loss deals with the propagation loss due to distance between transmitter and receiver while shadowing describes variation in the average signal strength due to varying environmental clutter at different locations.

Small Scale Fading deals with signal strength characteristics within small distance of the receiver location. In such region of space the average signal strength remains constant. Multi path propagation of the electromagnetic waves is the main cause of such effects. It includes the effect of time, space and frequency selective fading characteristics. For each domain, there are broadly two kinds of conditions, one is when the variability is high and the other when the variability is very small over the observation interval.

Thus, the signal strength at a particular location depends on the large scale fading and the small scale fading. As the receiver moves, the instantaneous power of the received signal varies rapidly giving rise to small scale fading. In such a situation the received power may vary by as much as 20-40dB over a range a few order of a fraction of a wavelength depending upon the particular environment. As the distance between the Transmitter and the Receiver increases, the local averaging of the received signal power decreases gradually, this is predicted by the large scale fading statistics. This phenomenon of a combined slow and fast fading is briefly explained in Fig. 2.2.

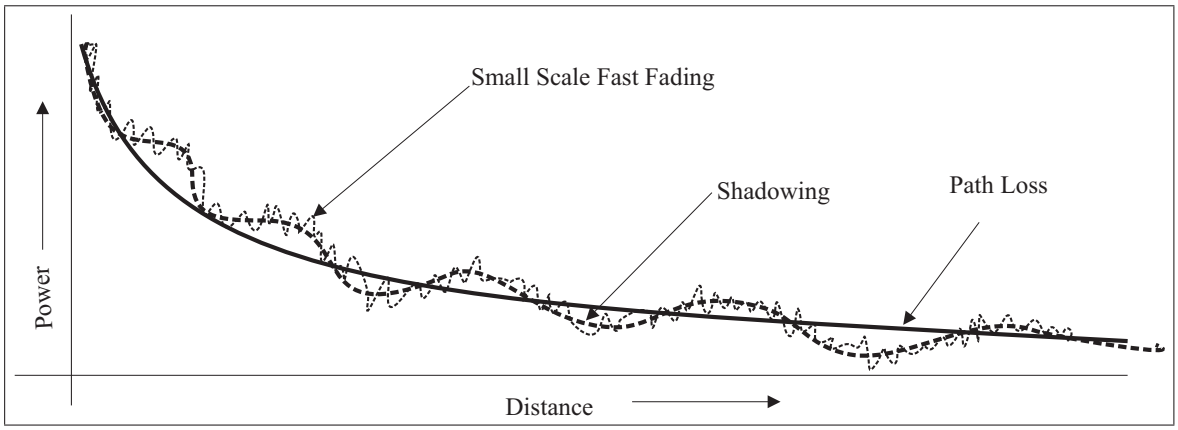

Figure 2.2: Propagation Loss

Three main factors which influence the radio wave propagation are Reflection,

Diffraction and Scattering. **Reflection** is caused when the Electromagnetic Waves (EM) impinge upon surface having dimensions much larger than the wavelength of the impinging wave. **Diffraction** is caused due to effects of sharp edges in the path of the radio waves between the Transmitter and the Receiver. **Scattering** is caused when the EM waves encounter objects of dimension much smaller than the wave in the propagation medium.

Most radio propagation models use a combination of empirical and analytical methods. The empirical approach is based on fitting curves or analytical expressions that recreate a set of measured data. This has the advantage of implicitly taking into account all the propagation factors. However the validity of an empirical model at transmitter frequencies or environments other than those used to derive the model can only be established by additional measured data in the new environment and frequencies. Propagation models and multi path reflection models have emerged over time to enable easy simulation of the wireless channel [34].

2.1.2 Propagation loss

There are many models for predicting the path loss such as Hata-Okumura and COST231-Hata model [34]. However, both these models are for frequency ranges up to 2000 MHz. To modify this a model is proposed in [30]. For a given close in distance[1], d_0 of 100m, the median path loss (P_L), in dB, is given by (2.1) [30].

$$P_L = A + 10n_p \log_{10}\frac{d}{d_o} + s \qquad d > d_o, \tag{2.1}$$

where

$$A = 20\log_{10}(4\pi d_o/\lambda), \tag{2.2}$$

and n_p is the path loss exponent and is given by,

$$n_p = a - bh_b + c/h_b, 10m < h_b < 80m. \tag{2.3}$$

The value of a, b and c are different for different terrain types. Values for urban area are given in Table 2.1 [32]. The shadowing factor is s and follows a log normal

[1]The Friis free space model, which is the basis for large scale propagation models, is valid for values of d which are in the far field of the transmitting antenna, i.e. does not hold for $d = 0$. Therefore, large-scale propagation models [34] use a close-distance, d_0, as known as received power reference point. The received power, $P_r(d)$, at any distance $d \geq d_0$ may be calculated in relation to that received at d_0. The reference distance is chosen so that it lies in the distance used in the mobile communication system.

Table 2.1: Value of parameters for urban terrain.

Parameters	Urban terrain	Unit
a	4.6	
b	0.0075	m^{-1}
c	12.6	m

distribution, with a typical value around 6 dB [30]. This model is proposed for a receiver antenna height of 2 m and operating frequency of 2 GHz, and a correction factor for other frequencies and antenna heights is proposed [32]. The modified path loss in (2.1) is:

$$\mathrm{PL_{mod}} = \mathrm{PL} + \Delta\mathrm{PL_f} + \Delta\mathrm{PL_h}, \tag{2.4}$$

where, PL is path loss given by (2.1), $\Delta\mathrm{PL_f}$ is frequency correction term given by $6\log_{10}(\mathrm{f}/2000)$, f is the frequency in MHz and $\Delta\mathrm{PL_h}$ is receiver antenna height correction term given by $-10.8\log_{10}(\mathrm{h}/2)$, where h is the new receiver antenna height (m) such that $2 < \mathrm{h} < 8$.

The propagation model used for 3GPP-LTE system can be found in [2] where different parameters have been used for different channel condition and cell orientation.

2.1.3 Shadowing

The path loss model does not capture the varying environmental clutter at different locations. However, measurements have shown that at any value d, the path loss PL(d) at a particular location is random and distributed log-normally (normal in dB) about the mean distance dependent values. Since the surrounding environmental clutter may be different at different locations the path loss will be different than the average value predicted by (2.4). This variation is mainly due to refraction and diffraction off Interfering Objects (IO) in the path of the traveling signal, and is an additive term to the path loss, with random values. This phenomenon is called shadowing. It has a log-normal distribution about the mean path loss value [34]. Therefore the modified path loss expression is,

$$\begin{aligned} \mathrm{Pl(d)} &= \overline{\mathrm{PL(d)}} + \mathrm{X}_\sigma & (2.5)\\ &= \overline{\mathrm{PL(d_o)}} + (10\mathrm{n_p})\mathrm{Log_{10}}(\frac{\mathrm{d}}{\mathrm{d_o}}) + \mathrm{X}_\sigma & (2.6)\\ \mathrm{Pr(d)} &= \mathrm{Pt(d)} - \mathrm{Pl(d)};\ \text{antenna gains included in Pl(d)}, & (2.7) \end{aligned}$$

where X_σ is zero mean Gaussian distributed random variable (in dB) with standard deviation σ also in dB.

2.1.4 Small scale Fading

In small scale fading, the signal varies rapidly over a short distance. The variation is caused by the multipath propagation of the received signal and the Doppler frequency shift. The channel impulse response $h(t, \tau)$ is a function of two variables, time t and delay τ [35]. Due to some reflecting objects such as buildings, hills, trees, etc some delayed versions of the transmitted signal, each with different amplitudes (A_{np}), phases (θ_n) arrive at the receiver at different delays (τ_n). The parameters (amplitude, phase, and delay) are random variables, and can be characterized by a channel impulse response. If unit impulse is transmitted and there are N_{SE} scattering elements, then the receiver would receive N_{SE} different signals. Therefore, the channel impulse response would be the sum of these N_{SE} scattered signals as given below [36].

$$h(t, \tau) = \sum_{m=1}^{N_{SE}} A_{np,m} \delta(t - \tau_m) \exp(-j\theta_m). \tag{2.8}$$

The channel impulse response is a function of time frequency and space [37]. A typical channel impulse amplitude response over a region is shown in Fig. 2.3.

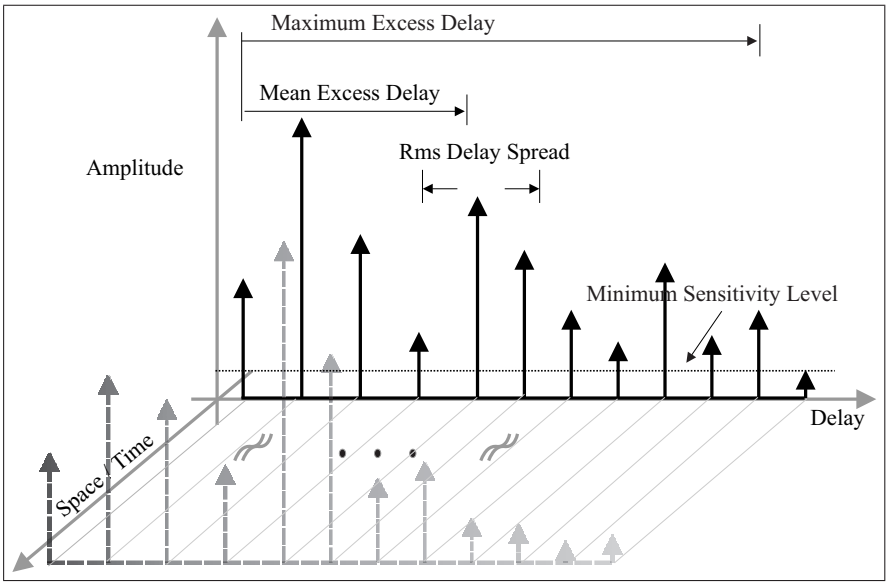

Figure 2.3: Amplitude response

The relationship between the impulse response and the transfer function of the

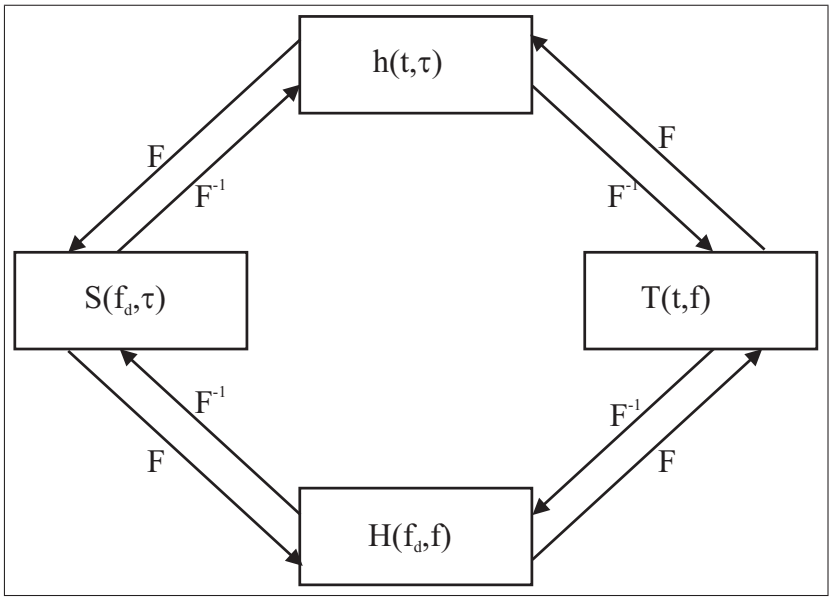

Figure 2.4: channel impulse response and transfer function relationship

channel is shown in Fig. 2.4, where f_d is Doppler frequency, τ is delay, t is time and f is the Fourier domain representation of the delay.

2.1.4.1 Multipath Fading

Multipath propagation as shown in Fig. 2.5 gives rise to small scale fading in time and frequency domain. The multipath properties of a given environment are usually characterized by the power delay profile. Power delay profile denotes the average power of each multipath. Figure 2.6 shows a typical power delay profile. When the first multipath component has the highest power then it is a Ricean channel. Where as when, the first path does not have the highest power which usually happens in non line of sight scenario, then it is usually a Rayleigh channel and this is used in this thesis. The power delay profile of a typical Rayleigh multipath propagation is shown to have a exponential decay profile which is a commonly used model. [31]. There are several other models which consider the cluster effect. i.e. there is a double exponential decay, where each multipath is followed by a sequence of multipath during a very short interval with a steeper decay constant. Another model for the delay profile has the first few taps with same average power followed by exponential decay [38].

The channel impulse response is an instantaneous realization of the power delay profile. A typical method of implementing it is via the Clark's methods as in [34]. Another method is the Rice method [39]. There exists other methods such as ray

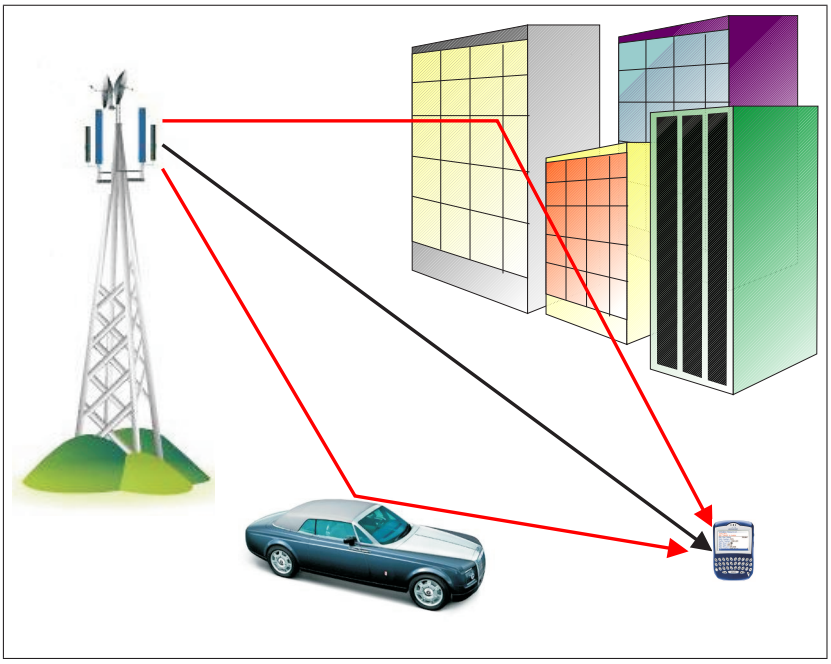

Figure 2.5: Multipath propagation

tracing models. The Clark's method has been mostly followed in this work. In some cases the 'rayleighchan' function of Matlab® has been used. In these models, each multipath component is generated so that they follow a desired Doppler spectrum. The Doppler spectrum can be easily integrated into the system. Though for indoor channels most of the taps in the models are supposed to have Jake's Doppler spectrum, the outdoor multipath channel model taps can have mixed Doppler spectrum, i.e. while some of the taps are advocated to use Jakes's spectrum the one which are towards the tail of the power delay profile may have Gauss' spectrum, details which can be found in [39]. Due to the multipath reflections a transmitted impulse gets time dispersed, i.e. spread in time domain. A measure of this time spread phenomenon is the mean excess delay, which is defined as [34]

$$\tau_{\mathrm{m}} = \frac{\int_0^{\tau_{\max}} \tau \mathrm{E}_{|\mathrm{h}(\tau)|^2}\, \mathrm{d}\tau}{\int_0^{\tau_{\max}} \mathrm{E}_{|\mathrm{h}(\tau)|^2}\, \mathrm{d}\tau} \tag{2.9}$$

where 'E' denotes expectation, $\tau_{\max}$ is the maximum delay of the arriving multi paths, $\mathrm{h}(\tau)$ is the component of the arriving multi path at a delay of τ. The rms delay spread

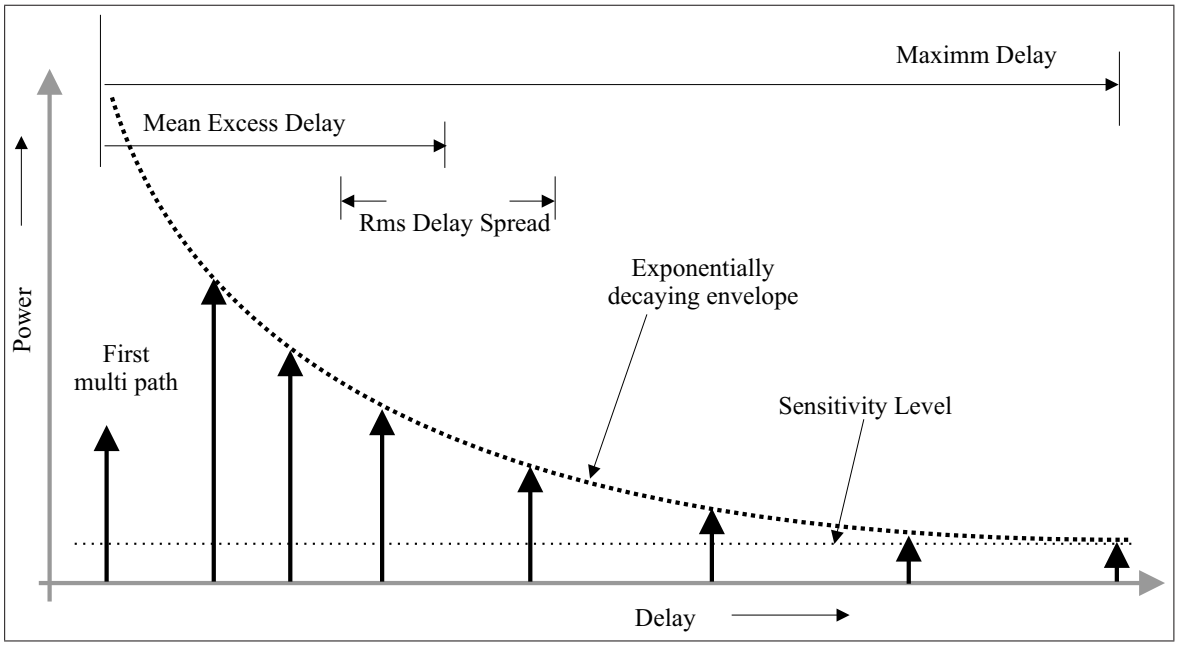

Figure 2.6: A typical power delay profile

of the channel is defined as

$$\tau_{\text{rms}} = \sqrt{\overline{\tau^2} - {\tau_{\text{m}}}^2} \tag{2.10}$$

where

$$\overline{\tau^2} = \frac{\int_0^{\tau_{\max}} \tau^2 \text{E}_{|\text{h}(\tau)|^2}\, \text{d}\tau}{\int_0^{\tau_{\max}} \text{E}_{|\text{h}(\tau)|^2}\, \text{d}\tau}. \tag{2.11}$$

The exponential power delay profile defines,

$$\begin{aligned} \text{E}_{|\text{h}(\tau)|^2} &= \frac{\text{e}^{\frac{-\tau}{\tau_0}}}{\int_0^{\tau_{\max}} \text{e}^{\frac{-\tau}{\tau_0}}}, \qquad \text{for} \qquad 0 < \tau < \tau_{\max} \\ &= 0, \qquad\qquad \text{elsewhere.} \end{aligned} \tag{2.12}$$

In the above τ_0 is the characteristic of the power delay. The rms delay spread is the average information of a certain environment, but it is expected to have a local variation over a few hundred nano seconds [31, 40].

The small scale channel model does not generate or absorb any power. i.e.

$$\int_0^{\tau_{\max}} |\text{h}(\tau)|^2\, d\tau = 1. \tag{2.13}$$

This ensures that we are concerned only with short term multi path fading scenario.

The Fourier transform of the channel impulse response is the channel transfer function, as shown in Fig. 2.7. The signal experiences different levels of fading for dif-

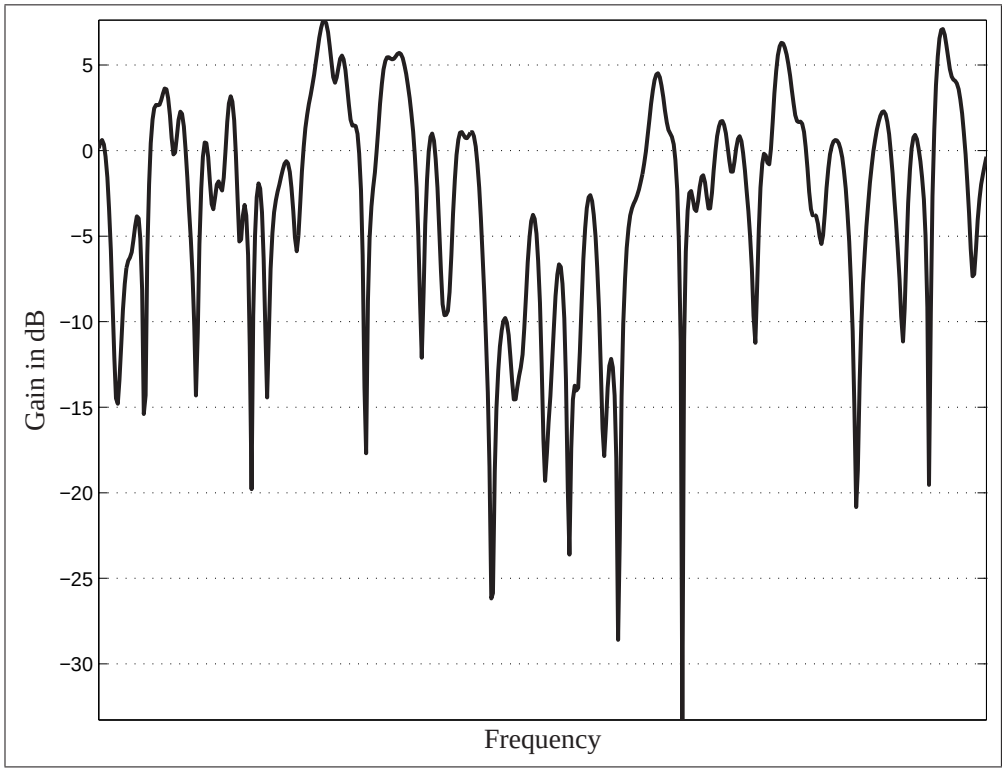

Figure 2.7: Frequency domain channel response

ferent frequencies in the fading channel. With such characteristics, a fading channel could be either frequency or non-frequency selective. This depends on the bandwidth of the system compared with the channel coherence bandwidth, B_c. The coherence bandwidth is defined as the frequency separation Δf such that the correlation coefficient falls below a defined real value between 0 and 1. B_c is inversely proportional to the rms delay spread τ_{RMS} [41, 37].

$$B_c \propto \frac{1}{\tau_{RMS}} \tag{2.14}$$

If the system bandwidth is much smaller compared to the coherence bandwidth, then the channel is said to be frequency non selective. In this case, the correlation coefficient[2] of the sub carrier channel transfer function is almost 1 for the frequencies within the system bandwidth. Physically, the frequency response within the system bandwidth is almost flat, so it is also called flat fading. On the other hand, if the

[2] $E_{H(f),H^*(f+\Delta f)}$, where H is the channel frequency response at frequency 'f'.

system bandwidth is larger than the coherence bandwidth, then the channel is said to be frequency selective. In this case, the frequencies within the channel would experience different level of fading.

2.1.4.2 Time varying channel

Similar to the channel characteristics in frequency domain, there are also signal variations in the time domain due to the time varying nature of the wireless channel. This time varying channel is mainly caused by the movement of either the transmitter, receiver, or the reflectors, which results in the Doppler effect. With a velocity vthe maximum Doppler shift is $\mathrm{f_m} = \frac{\mathrm{v}}{\lambda}$. The coherence time of a time varying channel is inversely proportional to the maximum Doppler frequency. The coherence time is defined as [34]

$$T_c = \frac{9}{16\pi f} \tag{2.15}$$

where f is the maximum Doppler frequency. The above model is true for Jakes' spectrum. The coherence time for Gauss spectrum for the same velocity is much more than in the case of Jake's Spectrum. A Typical Jakes' spectrum is given in Fig. 2.8 and a typical Gauss spectrum is given in Fig. 2.9. Ideally the correlation for a tap of the multipath channel model is given by [42] as,

$$\mathrm{R_{h(\tau,t)h(\tau,t+\Delta t)}} = \mathfrak{F}^{-1}(\tau, \mathrm{S(f)}), \tag{2.16}$$

where $\mathfrak{F}^{-1}$ mean inverse Fourier Transform, $\mathrm{S}(f)$ is the Doppler frequency power spectrum.

2.2 Quadrature Amplitude Modulation

As Quadrature Amplitude Modulation (QAM) is used in this work, the QAM is described in this section. Digital Modulation is a process that maps a digital symbol onto a signal suitable for transmission [43]. This is done in two steps: at first, the k bits of the digital signal are mapped to one symbol of the baseband signal and are represented as complex constellation points. In second step the resultant baseband signal is then up converted to the transmitting frequency via Radio Frequency (RF) modulation. When the amplitude of the modulated signal is varied to carry the source information, the modulation is called Pulse Amplitude Modulation (PAM).

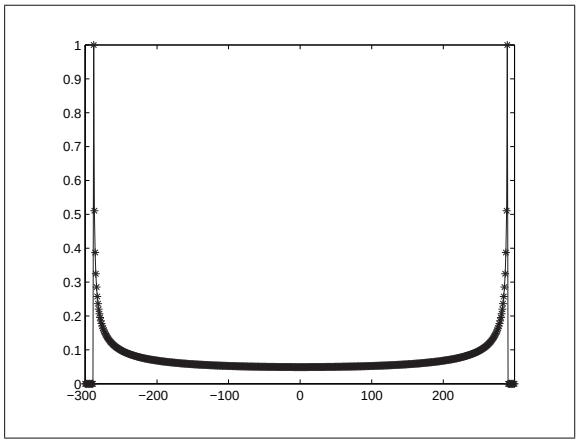

Figure 2.8: Power Spectral Density vs frequency of Jakes' spectrum

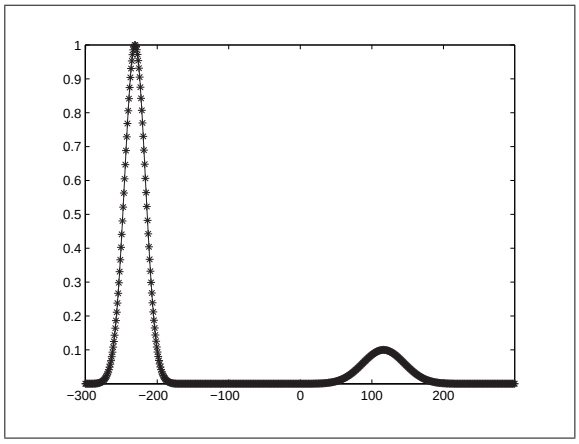

Figure 2.9: Power Spectral Density vs frequency of typical Gauss' spectrum

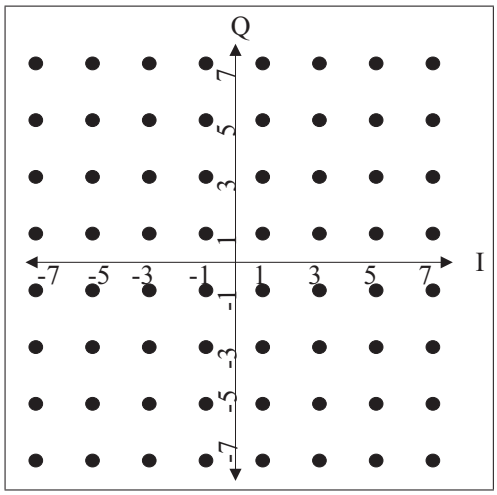

Figure 2.10: Signal space diagram for rectangular 64-QAM

On the other hand, the term Phase Shift Keying (PSK) implies the phase of the modulated waveform has the source information. QAM uses the combination of both these techniques and carries information in the phase as well as the amplitude of the modulated waveform. This can also be seen as embedding two simultaneous sequences of k bits information signal on two quadrature carriers $\cos 2\pi f_c t$ and $\sin 2\pi f_c t$. The corresponding modulated waveform can be written as [35]:

$$s_m(t) = (A_{mc} + jA_{ms})g(t)e^{j2\pi f_c t} \qquad m = 1, 2, ...M \tag{2.17}$$

where A_{mc} and A_{ms} are the information-bearing signal amplitudes of the quadrature carrier and g(t) is the signal pulse.

The signal space diagram of rectangular QAM for different values of M is shown in Figure 2.10 [35], where $M = 2^k$ and k is the number of information bits per modulated symbol. It is common practice to have rectangular QAM where $M = 2^{2j}$, with each symbol representing 2j information bits, because it has the advantage of being generated as superposition of two PAM signal on quadrature carriers.

2.3 OFDM

2.3.1 OFDM Fundamentals

OFDM is an advanced form of Frequency Division Multiplexing (FDM) where the frequencies multiplexed are orthogonal to each other and their spectra overlap with the neighboring carriers. In a standard FDM system the sub carriers do not overlap as shown in Fig. 2.11 which represents the amplitude frequency response of such systems. OFDM is built on the principle of overlapping orthogonal sub carriers. The frequency domain view of the signal is shown in Fig. 2.12. The peak of one sub carrier coincides with the nulls of the other sub carriers due to the orthogonality. Thus there is no interference from other sub carriers at the peak of a desired sub carrier even though the sub carrier spectrums overlap. It can be understood that

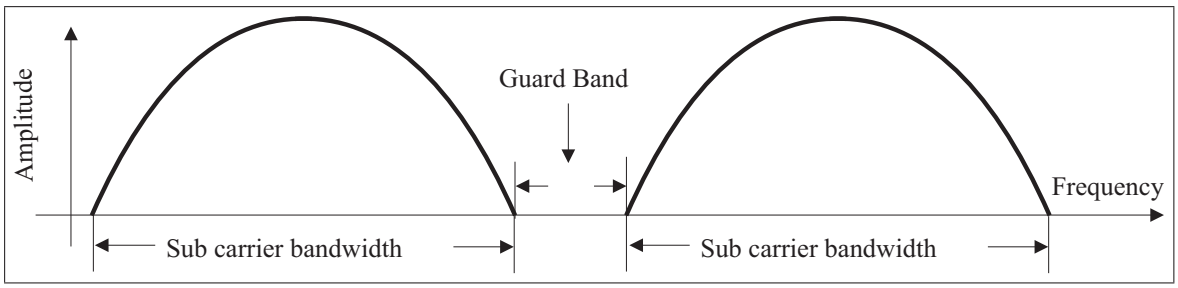

Figure 2.11: Non orthogonal carriers

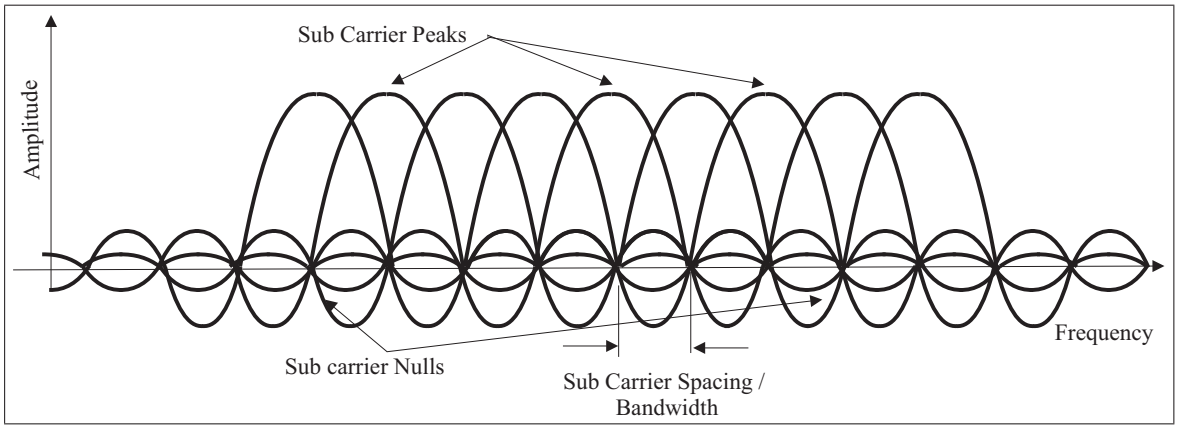

Figure 2.12: Orthogonal Sub carriers in Multi carrier systems (OFDM)

OFDM systems avoid the loss in bandwidth efficiency prevalent in system using non orthogonal carrier set. This brings in huge benefit in spectral efficiency for OFDM systems over earlier systems.

The orthogonality among sub carriers can be viewed in time domain as shown in Fig. 2.13. Each curve represents the time domain view of the wave for a sub carrier. The figure shows that integer number of cycles of each sub carrier is present in the symbol duration. If such is not the case, then orthogonality is not ensured. The mathematical explanation is that two functions f_1 and f_2 are orthogonal in an interval (t1,t2) if the following condition is satisfied.

$$\int_{t=t_1}^{t=t_2} f_1(t) f_2(t)\, dt = 0, \tag{2.18}$$

i.e. the area under the product of the two functions in the region is zero. In case of OFDM, the frequencies are chosen so that all of them form a mutually orthogonal set.

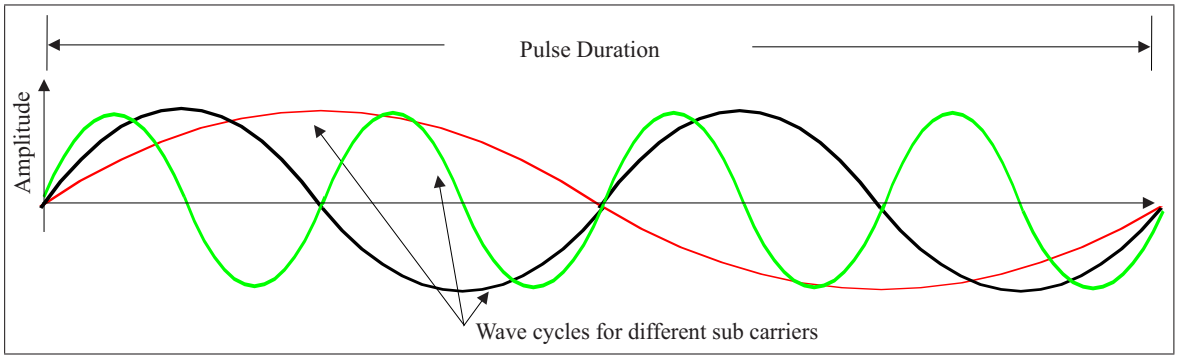

Figure 2.13: Time domain representation of the signal waveforms to show orthogonality among the sub carriers

OFDM is well known for effectively combating the frequency selective fading which arise due to multi path reflections of the wireless channel. To understand this, the OFDM transmitter architecture needs to be studied. Fig. 2.14 shows a typical transmitter structure for the system. The Inverse Fast Fourier Transform (IFFT) replaces the bank of modulators needed in a conventional multi carrier system. It can be considered that the input data symbols to the IFFT modulates the sub carriers, each of which has a pulse period which is the product of the sampling period of the system times the number of sub carriers in the system. In other words, each data symbol modulates one sub carrier.

During the OFDM system design, parameters are chosen in a way such that the sub carrier bandwidth is smaller than the coherence bandwidth of the channel so that each sub carrier experiences flat fading. This together with the use of cyclic prefixed Guard Interval (GI) helps in using a one tap equalizer at the receiver.

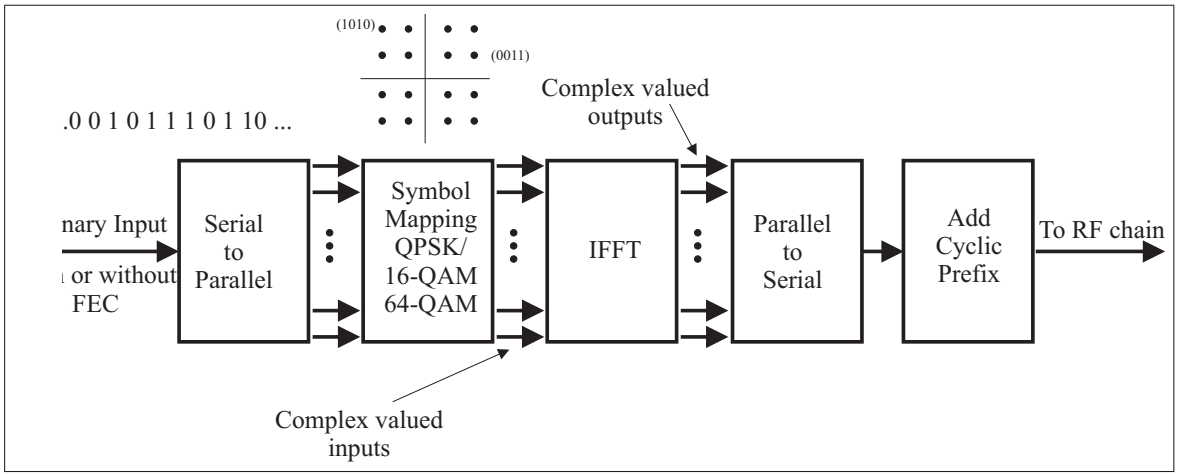

Figure 2.14: Base band modules of the OFDM transmitter

The time frequency diagram of the OFDM signal in Fig. 2.15 shows the difference between single and multi carrier systems with respect to the symbol duration when compared against the channel impulse response. Single carrier system have a symbol duration which is decided by the sampling period of the system. When the channel impulse response is larger than this period, there is ISI. The whole bandwidth is split into a set of parallel orthogonal sub streams each of which has a long symbol duration. The symbol duration becomes significantly greater than the channel impulse response length. This makes each stream, i.e. each sub carrier, experiencing flat fading as is depicted in Fig. 2.16.

The one tap equalizer can be realized if there is no ISI. ISI between consecutive OFDM symbols is avoided by the use of GI, which is discarded at the receiver to reject the ISI. Using Cyclic Prefix (CP) in the GI is a very effective technique to preserve the orthogonality among sub carriers which can be understood from Fig. 2.17. The CP is an extension of the last part of the time domain signal. The length of CP is designed to be larger than the maximum delay of the channel. After the OFDM symbol with the CP passes through a time dispersive channel, the interference from the previous symbol is limited to be within the CP. The contaminated CP is rejected at the receiver. The continuity of the signal waveforms in time domain inside the GI in the form of CP ensures that the remaining portion contains full cycles of the sub carriers as can be seen in the picture. This prevents orthogonality loss among the sub carriers and between consecutive OFDM symbols.

The long symbol duration which brings in several benefits is limited by the Doppler condition of the channel. When the number of sub carriers is made large,

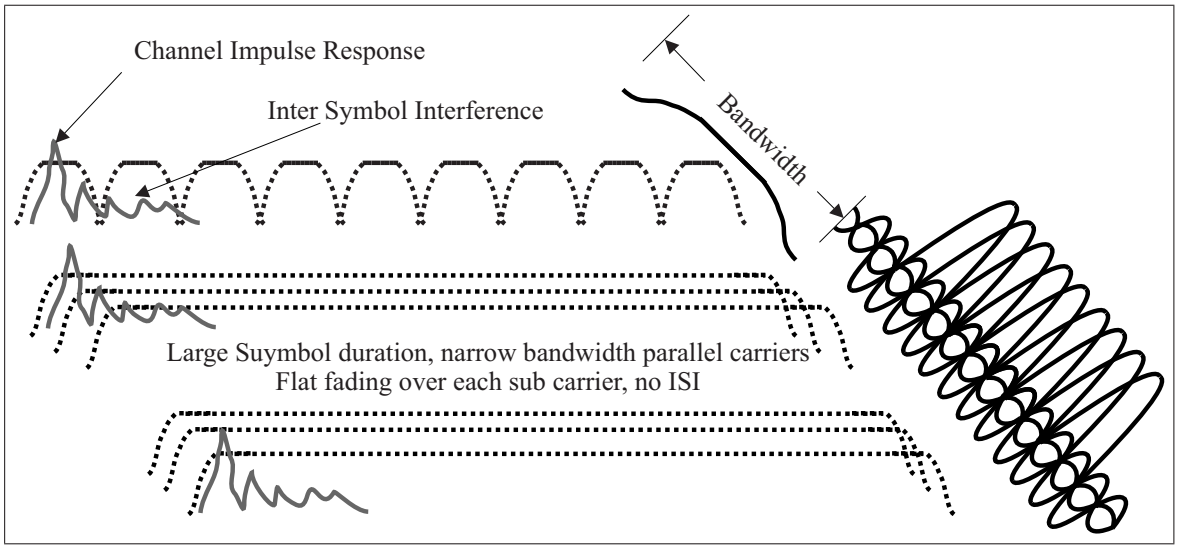

Figure 2.15: Time Frequency representation of OFDM Signal

the system bandwidth is sampled at a higher rate in the frequency domain, which in turn makes the sub carrier bandwidth smaller. This leads to a higher pulse duration. To maintain orthogonality among the sub carriers OFDM systems must have a static channel during the pulse period, i.e. the coherence time of the channel must be much larger than the pulse period of the OFDM symbol.

The sub carrier bandwidth to be selected is also limited by the tolerance of frequency offset due to imperfect carrier synchronization. The ratio of residual carrier offset (due to uncompensated carrier offset because of imperfect carrier synchronization and Doppler frequency spread) to the sub carrier bandwidth must be less than a certain value [23] to get an acceptable BER performance. Usually this value is considered to be around 0.02.

The receiver for OFDM follows similar sequence of operations as in the transmitter but in the reverse direction. There is a front end to this part that is needed usually. This part consists of the synchronization and channel estimation modules. A block diagram of the OFDM receiver is given in Fig. 2.18. The synchronization and channel estimation is usually done with the help of training sequence and embedded pilots. A typical training sequence as used in IEEE 802.11a is given in Fig. 2.19.

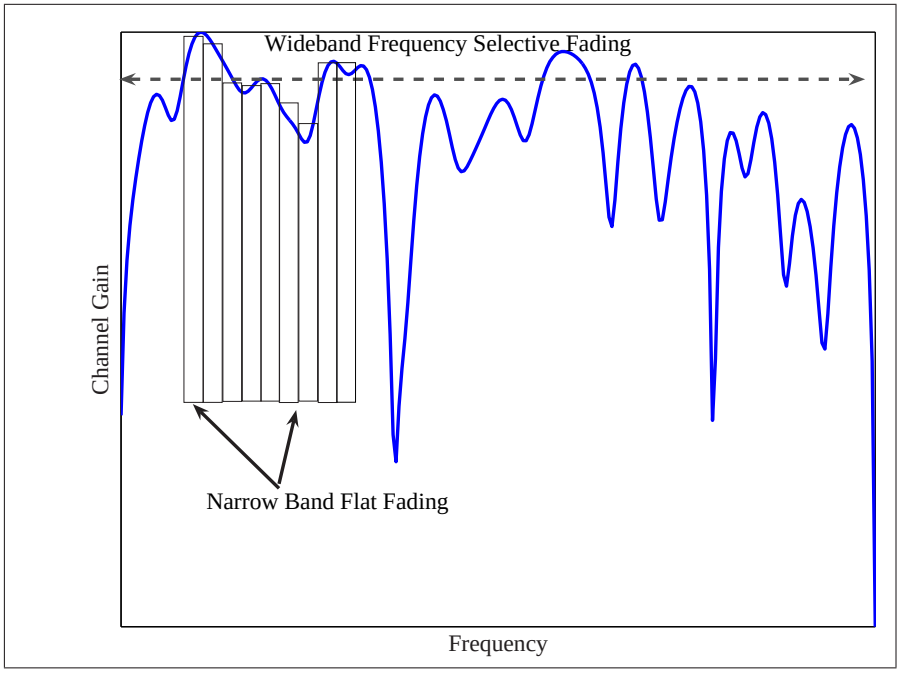

Figure 2.16: Frequency Selective and non Selective Fading

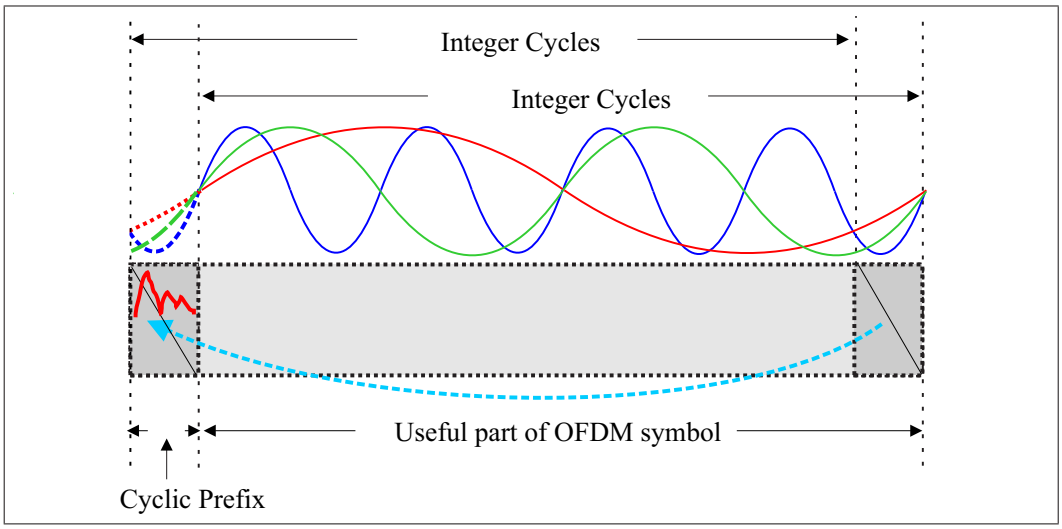

Figure 2.17: The use of Cyclic Prefix

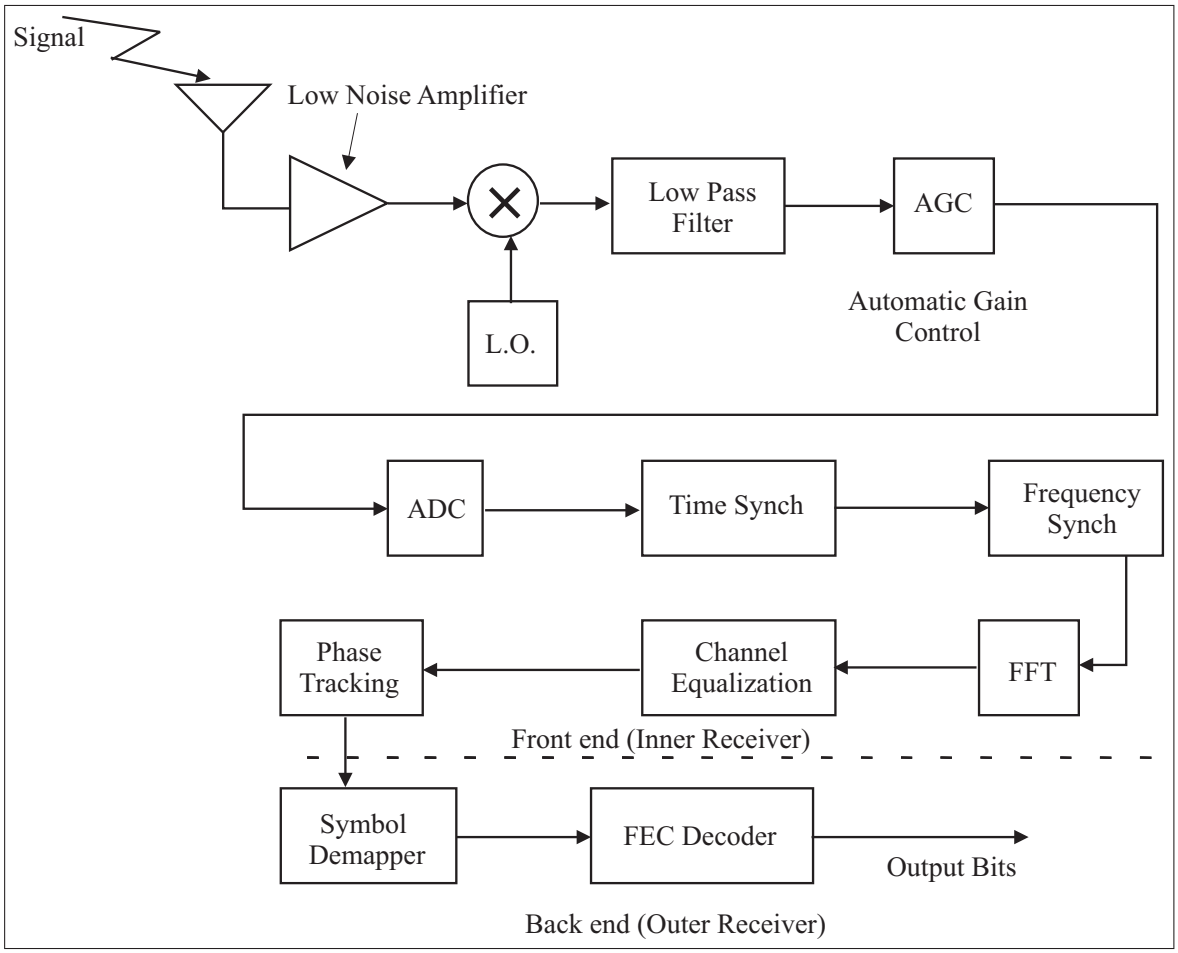

Figure 2.18: Top level architecture of OFDM receiver circuitry showing important signal processing modules in base band part.

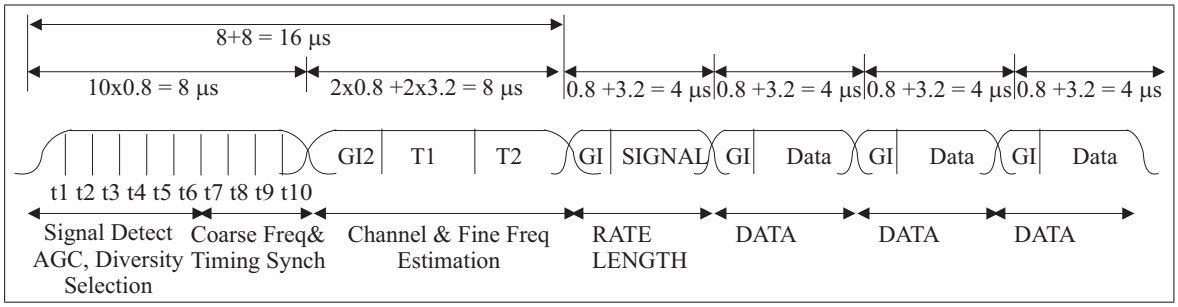

Figure 2.19: Training sequence for WLAN [44]

The analytical model for the OFDM system is presented in this part. The s^{th} baseband transmitted OFDM symbol can be expressed from [45]

$$x_s(t) = \frac{1}{\sqrt{T_f}} \sum_{k=-\frac{N_f}{2}}^{\frac{N_f}{2}-1} X_s[k] e^{j2\pi \frac{k}{T_f}(t-sT_s-T_{gi})} \Xi_{T_s}(t-sT_s), \tag{2.19}$$

with

$$x(t) = \sum_{s=-\infty}^{s=\infty} x_s(t),$$

where T_f is the duration of OFDM symbol except the guard interval, k is the sub carrier index, N_f denotes the number of sub carriers, $X[s,k]$ is the modulated data symbol on the sub carrier, T_s is the symbol duration which is the sum of T_f and the guard interval T_{gi}. $\Xi_{T_s}(t-sT_s)$ is the gate pulse of duration T_s starting from $t = sT_s$, which can be implemented in digital domain [44].

After passing through the channel, the signal can be represented as,

$$r(t) = \int_0^{\tau_{max}} h(\tau) e^{j2\pi f_{d\tau}(t-\tau)} x_s(t-\tau)\, d\tau + \nu(t) \tag{2.20}$$

where τ_{max} is the maximum tail of the channel impulse response $h(\tau)$, $\nu(t)$ is the noise component and $f_{d\tau}$ is the doppler frequency for delay τ. With perfect timing synchronization, but residual carrier frequency offset of 'δf_c' (Hz) , the received OFDM symbol is

$$r_s(t) = r(t) e^{j2\pi\delta f_c t} \Xi_{T_f}(t-sT_s-T_{gi}) \tag{2.21}$$

the signal portion without the noise part is

$$\int_0^{\tau_{max}} h(\tau) x_s(t-\tau) e^{j2\pi f_{d\tau}(t-\tau)} e^{j2\pi\delta f_c t} \Xi_{T_f}(t-sT_s-T_{gi})\, d\tau$$

Since $h(\tau)e^{-j2\pi f_{d\tau}\tau}$ cannot be separated from $h(\tau)$, we re-write the above as

$$r_s(t) = \int_0^{\tau_{max}} h(\tau) x_s(t-\tau) e^{j2\pi(\delta f_c + f_{d\tau})t} \Xi_{T_f}(t-sT_s-T_{gi})\, d\tau. \tag{2.22}$$

Considering ideal conditions of no synchronization error, i.e. $\delta f_c = 0$ and near static

channel , i.e. ($f_{d\tau} \approx 0$), the received sub carrier can be expressed from [45],[46] as,

$$R_{s,k'} = \frac{1}{\sqrt{T_f}} \int_{sT_s+T_{gi}}^{sT_s+T_{gi}+T_f} (r_s(t) + \nu(t))\, e^{-j2\pi \frac{k'}{T_f}(t-sT_s-T_{gi})}\, dt \quad (2.23)$$

which becomes

$$R_{s,k'} = X[s,k']H[s,k'] + \omega[s,k'] \quad (2.24)$$

where $\omega[s,k']$ is the frequency domain noise component and $H[s,k']$ is the channel coefficient for k'^{th} sub carrier of s^{th} OFDM symbol. The above expressions hold when the CP is larger than the maximum tail of the channel impulse response.

Thus the OFDM framework has been developed above, and it is also discussed that OFDM has very high spectral efficiency due to close packing of the sub carriers. It is shown that OFDM elegantly handles multipath fading effect, i.e. the frequency selective fading effect and also needs only one tap equalizer at the receiver due to the long symbol duration and the use of CP.

In spite of these facts OFDM has some weaknesses. The choice of GI duration is very critical. A small value can introduce ISI and ICI thereby destroying the orthogonality and jeopardizing the system performance. Therefore usually a large value is selected which is greater than the largest possible channel impulse response length expected to be encountered in the environment. This adds a high overhead in the system. In one of the chapters of this thesis an algorithm to overcome this problem is addressed. OFDM is also vulnerable to carrier offset errors. The choice of sub carrier bandwidth is very critical in this case. Residual carrier offset and Doppler frequency spread introduces ICI. For large values of the ratio of these offsets to the sub carrier bandwidth, the performance is severely affected. The sub carrier bandwidth is therefore made large enough to sustain a certain amount of such errors. Making the sub carrier bandwidth large in turn implies a smaller useful symbol duration. Now, for a fixed GI duration, the ratio of the useful symbol duration to the total symbol duration (sum of GI period and useful symbol period) becomes smaller thereby affecting the system efficiency. This is also addressed in this thesis and a solution is also proposed. Since an OFDM signal is generated as an addition of several parallel orthogonal carriers, there is high PAPR in the signal. The non linear operation of the power amplifier in the transmitter introduces distortion. Therefore a large back off is usually used and hence a large power inefficiency has to be tolerated in the transmitter. This also has an impact when adaptive modulation and coding are used in OFDM systems. A method to adjust for such distortions in case of adaptive

modulation and coding is also addressed in this thesis.

2.3.2 Parameters values for OFDM based Standards

Some parameters for OFDM system design as used in standards are discussed here. IEEE 802.11a,g [11] is a WLAN standard which is designed for indoor conditions. The path loss is not a very important consideration in this situation since the propagation distance is within 300m. The channel rms delay spread varies between 10ns and 250ns [29]. The user velocity is limited to 5 kmph. The physical layer parameter values related to OFDM used in this standard are in Table 2.2. The sub carrier

Table 2.2: Parameters in WLAN

Parameter	**Values**
System Bandwidth	20MHz
Carrier Frequency	2-5 GHz
Number of points in FFT	64
Sub carrier bandwidth	312.5KHz
Number of useful carriers	52
Number of null carriers	12
Number of pilot sub carriers	4
OFDM symbol duration	4 μs
GI duration	0.8 μs

Table 2.3: WMAN system parameters

Parameter	**WiMAX**	**3GPP–LTE**
Carrier frequency	2-11GHz	2GHz
Bandwidth	1.25MHz,5MHz,10MHz,20MHz	1.25MHz,5MHz,10MHz,20MHz
Number of point in FFT	128,512,1024,2048	128,512,1024,2048
Sub carrier bandwidth	10.94KHz	15KHz
GI ratio	$\frac{1}{4}, \frac{1}{8}, \frac{1}{16}$	$\frac{1}{4}, \frac{1}{8}, \frac{1}{16}$
useful part OFDM symbol duration	91.4μs	66.67μs
Max transmit power	43dBm (10MHz)	38dBm (10MHz)
Minimum Frame size	2ms	0.5ms
Inter site distance in macro cell	2.8Km	1.7Km
Number of sectors	3	3

bandwidth is very wide, and the symbol duration is also very small which allows for

large tolerance of carrier offset and Doppler spread. It can also tolerate the other effect of Doppler i.e. fast fading channel conditions since the symbol duration is very small, though these conditions are not likely to occur in the indoor conditions. The coherence bandwidth can be calculated using the formula $B_c = \frac{1}{5\tau_{rms}}$ as 0.8MHz which is much more than sub carrier bandwidth. Therefore each sub carrier can be expected to experience a flat fading channel.

The values for the standards IEEE 802.16a,e (WiMAX) and the 3GPP-LTE (under development) are in Table 2.3. It can be seen that both systems have very similar parameter values but these are drastically different from the WLAN standard. These standards are more mature than WLAN system and have different channel conditions. The rms delay spread of the channel can be up to 2-3μs. Therefore the GI duration and the OFDM symbol duration is chosen accordingly. The coherence bandwidth is around 66KHz and hence the sub carrier bandwidth is kept smaller than this which is significantly different compared to WLAN systems. The maximum transmit power at the base stations is related to the cell radius, and hence the two systems have different values since the cell radius is different.

2.4 Link Adaptation

The link between the transmitter and receiver is the wireless channel. Taming the wireless channel to gain high spectral efficiency has been one of the greatest challenges of the wireless system design engineer. There has been several ways of approaching the problem. OFDM has been one such proposal. The wireless channel varies in the time and frequency domain. Though OFDM is very effective, yet it is not optimized to handle the dynamically changing conditions. The channel gain of each sub carrier varies in time, and the channel gain varies from one sub carrier to another in one given time as has been seen before. Therefore each sub carrier cannot have the same performance in terms of bit error rate under these circumstances for a certain modulation and coding rate.

The bit error rate performance of different modulation and coding rates are given in Fig. 2.20. The x-axis is the SNR. In a time frequency selective fading channel, if the same modulation and coding rate are used then the BER performance will vary as per the channel gains. In systems using OFDM, the sub carriers experience flat fading. This implies that to each sub carrier the channel appears like Additive White Gaussian Noise (AWGN) but with different Signal to Noise Ratio (SNR) levels.

In practical multi carrier link adapted systems a set of consecutive sub carriers are usually grouped to form a sub-band, and this forms the basic unit of operation. In order to maintain a certain BLER threshold at the receiver, (a value of 10^{-1} has been shown in the figure) the modulation and coding rates need to be dynamically changed as per the measured SNR at each sub band for each OFDM symbol. For example, if the received SNR is below 8 dB, it is better not to transmit any signal since the BLER will be higher than the required level, and when the SNR is between 8 dB and 11 dB, the ideal choice would be 4-QAM, rate 1/2 coding and so on. The objective is to select the bit loading such that the required BLER is satisfied and maximum spectral efficiency is obtained. To realize this, a feedback system is necessary. The system framework is explained in Fig. 2.21.

Usually there are pilot symbols transmitted which are used to estimate the channel coefficients. The channel coefficients are then encoded into a Channel Quality Index (CQI) parameter which is sent back to the transmitter via a feedback channel. The CQI information is then used to adapt the transmit parameters which are used in the next few time slots. The time sequence of these operations is indicated in Fig. 2.22.

The spectral efficiency of each modulation and coding rate reaches a saturation

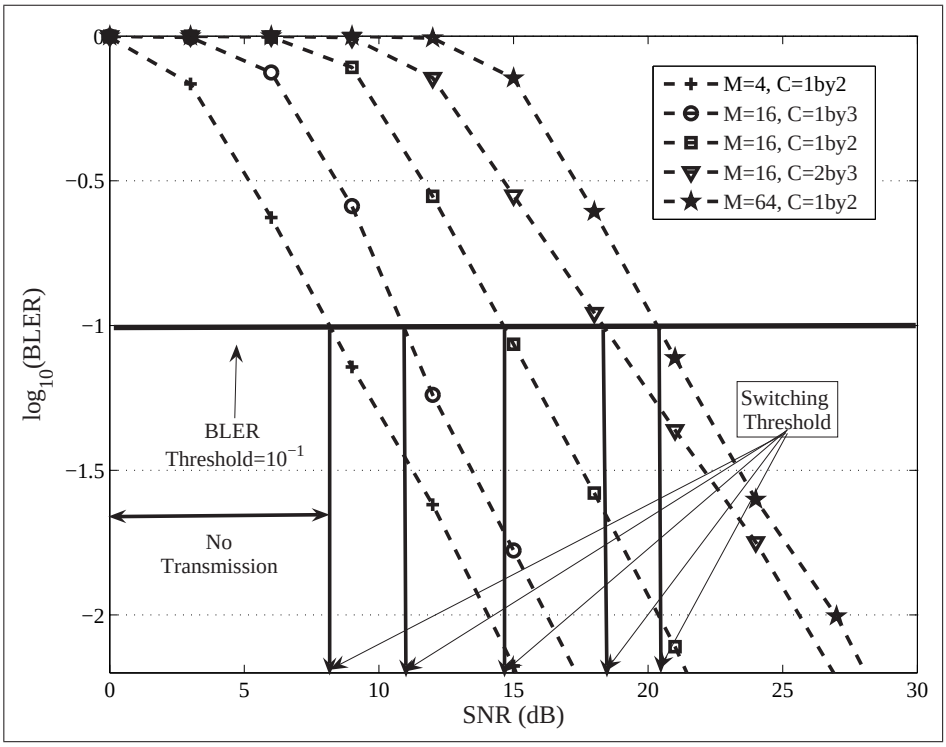

Figure 2.20: SNR switching threshold points for LA System. M=4 indicates QPSK, M=16 is 16-QAM, and M=64 is for 64-QAM, while C represents coding rate

point after a certain SNR. This is because the probability of being in error becomes very small after a certain SNR, and any further decrease in BER/BLER does not improve the spectral efficiency notably. The adaptive bit loading systems select the modulation and coding scheme which has the highest spectral efficiency while satisfying the target BER/BLER. Fig. 2.23 shows the spectral efficiency performance of LA. The curves with different markers represent the SE performance of different modulation and coding. Now, if Link Adaptation (LA) is used then with the increasing SNR the system will choose the modulation and coding rate, which has the best Spectral Efficiency (SE) performance at that SNR. For example, from 0 to 2.5 dB, the only option is 4QAM with $FEC = \frac{1}{2}$ rate and the system will transmit using this scheme. However, after this, and until 5 dB there are two options, one is 4QAM with $FEC = \frac{1}{2}$ and other is 16QAM with $FEC = \frac{1}{3}$. The system will opt for the previous one since it has the better spectral efficiency. At the value close to 8 dB the SE performance of 16QAM with $FEC = \frac{1}{3}$ crosses that of 4QAM with $FEC = \frac{1}{2}$ and immediately the system will switch to 16QAM with $FEC = \frac{1}{3}$. The dashed curve with maroon color represents the SE performance of this system.

However, if some Quality of Service (QoS) constraint is imposed for particular

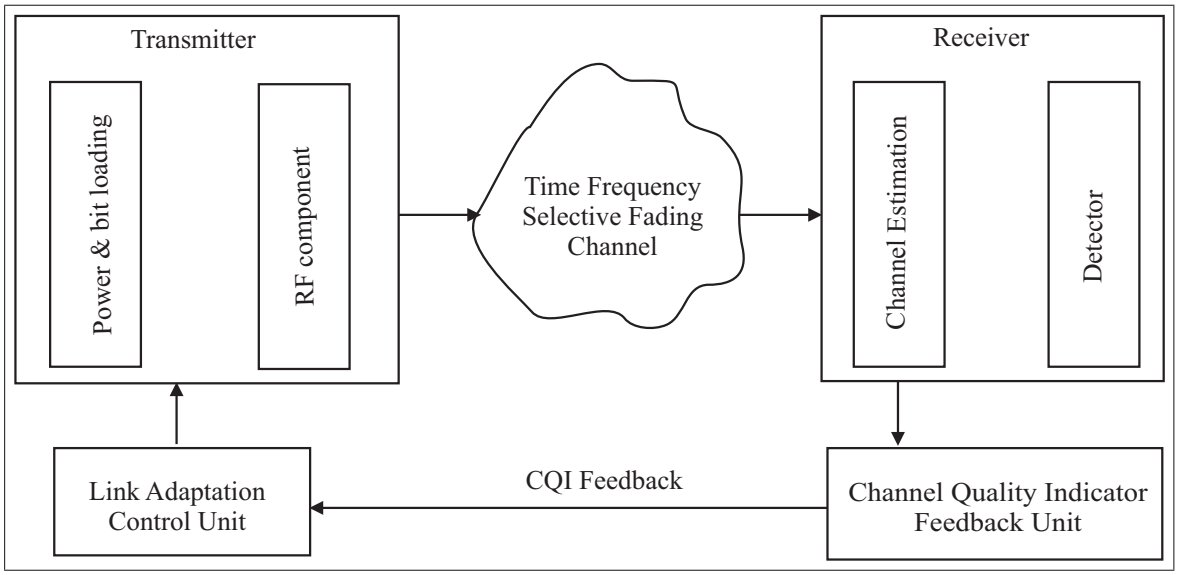

Figure 2.21: Link Adaptation basic framework

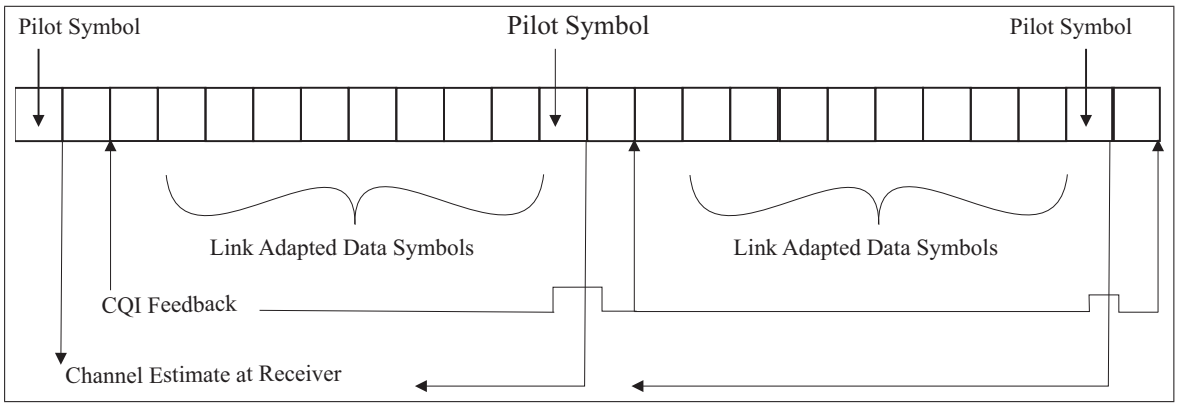

Figure 2.22: Time Sequence of Events in Link Adaptation

application which requires a certain BLER criteria to be met, then the system needs to look at BLER first and if the condition is met, then it will check for the option which will maximize the SE performance. The Fig. 2.20 shows the threshold points when the system can change from one modulation and coding scheme to another while maintaining the BLER constraint of 10^{-1}. To maintain this QoS, the system will not transmit until 8 dB SNR. The spectral efficiency curve for such a case will following the solid blue curve in Fig. 2.23

The analytical framework for adaptive bit loading is given below. The bit load

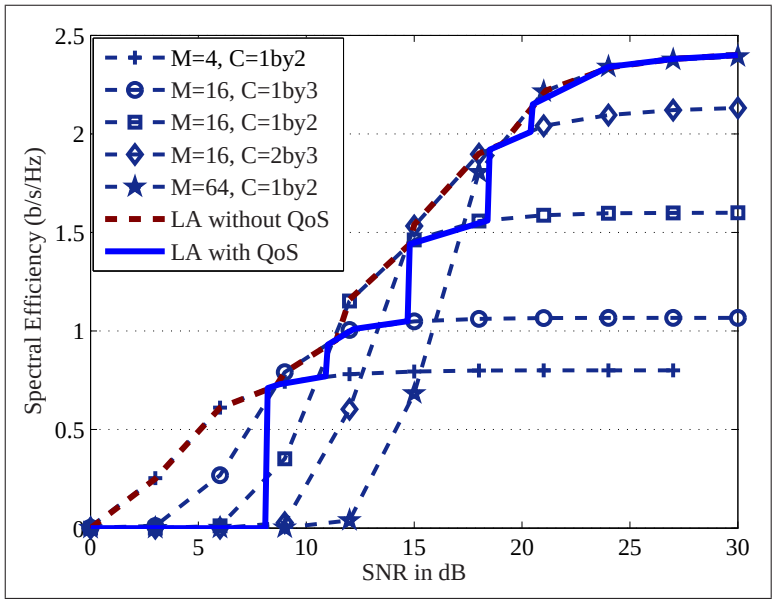

Figure 2.23: Spectral Efficiency Gain for LA System.

Table 2.4: Switching Threshold for Link Adaptation

Modulation & FEC	M=0, C=0	M=4, C= $\frac{1}{2}$	M=16, C= $\frac{1}{3}$	M=16, C= $\frac{1}{2}$	M=16, C= $\frac{2}{3}$	M=64, C= $\frac{1}{2}$
SNR (dB)	0	8.2	10.9	14.7	18.4	20.4

estimate per sub carrier can be expressed as [26]

$$\mathrm{b_L} = 2\lfloor \frac{1}{2}\log_2\left(1 - \frac{1.6}{\ln(\frac{\mathrm{b_{o\ req}}}{0.2})}\Upsilon_{\mathrm{rx}}\right)\rfloor \tag{2.25}$$

The above expression is valid for square constellation, where the operation $\lfloor . \rfloor$ is the floor operation. In the above, $\mathrm{b_{o\ req}}$ is the target BER which is to be satisfied. The BER associated with the chosen bit load is

$$\mathrm{b_o} = 0.2e^{-\frac{1.6\Upsilon_{rx}}{2^{\mathrm{b_L}}-1}} \tag{2.26}$$

which is tight for high SNR and has been claimed to be valid within 1.5dB for 4-QAM to 1024-QAM for bit error rate BER$\leq 10^{-3}$. In the above expression Υ_{rx} is taken as

$$\Upsilon_{\mathrm{rx}} \approx \frac{\mathrm{P_{X[k]}P_{H[k]}}}{\sigma_\omega^2} \tag{2.27}$$

where $P_{\mathrm{X[k]}}$ is the transmitted power per sub carrier, $P_{\mathrm{H[k]}}$ is the channel power per

sub carrier and σ_ω^2 is the noise power. However, for practical purpose forward error control coding is used in systems. Added to this, the fading channels vary over a wide range of conditions. It is very difficult to obtain the closed form expression of the BLER in these conditions and hence extensive simulation based evaluations are done. The details of which are presented in later chapters. The algorithm used for LA is given in Appendix B.

3

Evaluation of Hybrid Multi Carrier Spread Spectrum

The objective of this chapter is to investigate a suitable multiple access/ multiplexing technique for indoor channel conditions. Keeping this in view the performance of a Multi Carrier Spread Spectrum (MC-SS) technique for indoor channel conditions is investigated and it is proposed to use Subcarrier hopping (SCH) along with the MC-SS technique to enhance the outage performance of the system. The MC-SS technique is evaluated for different spreading gains and loading factors. The performance of interleaved and block subcarrier grouping and Successive Interference Cancelation (SIC) receiver is also investigated in this chapter.

Further, the performance of MC-SS technique is compared against OFDM. The comparison is carried out under channel estimation and frequency synchronization errors. The proposed sub subcarrier hopping MC-SS technique improves the outage performance in indoor conditions and OFDM is found to be more robust to receiver impairments when compared against MC-SS under full load conditions.

3.1 Sub Carrier Hopping Multi Carrier Spread Spectrum

3.1.1 Introduction

The search for a suitable access/ multiplexing scheme for next generation wireless networks has produced several combinations of spread spectrum and multi carrier techniques, details of which can be found in [17],[47],[48],[49],[50],[51]. Each of them is specialized to deal with a particular channel condition. The motivation to combine these two is to harness the benefit of two very successful physical layer technologies of the recent years. Both spread spectrum and OFDM techniques are suitable for multi path environment. Spread spectrum techniques such as Code Division Multiple Access (CDMA) combines the frequency selective fading from multi path reflections while OFDM avoids it. Further, CDMA offers the flexibility of fractional loading which is effective in achieving better BER at the cost of throughput, while OFDM provides a very high spectral efficiency. Again, on one hand CDMA has provided very good low data rate connectivity for highly mobile users (voice), on the other hand OFDM has been known to provide very high data rate for low mobility applications such as WLAN systems [11]. This leads to investigation of possible combinations which can be very robust yet have high throughput along with several other flexibility options.

In this section SCH-MC-SS is proposed and described for use in indoor down link environment. It is compared against its parent MC-SS scheme(Orthogonal Frequency Division Multiple Acess with Code Division Multiplexing (OFDMA-CDM) which can also be called Multi Carrier Spread Spectrum Multiple Access (MC-SS-MA) [17]), which is known to be better than other such combinations as it avoids multi user interference [52]. The outage throughput and the mean throughput as experienced by a User Equipment (UE) for both schemes are compared through simulation. Results are presented for different channel conditions following COST259 [29]. Based on the simulation results, guidelines for system implementation are also discussed.

3.1.2 System Description

Primary characteristics of indoor channels are the rich multipath environment and the quasi static nature, i.e. channels remain almost constant over long duration of time. Multi carrier schemes are very effective in such scenarios and have been adopted in wireless local area networks [11] and metropolitan area network [14]. To support mul-

tiple users, either frequency division multiple access or code division multiple access can be used in conjunction with multi carrier systems. Some important contributions are [47]–[51]. OFDMA-CDM [17] which is a special MC-SS scheme, is supposed to be one of the optimal solutions. It avoids multi user interference by using frequency division multiple access while it uses frequency diversity by taking advantage of code division multiplexing by spreading one user's data over the allocated sub carrier set. However, this system will suffer from low outage throughput particularly in quasi static channel conditions. This is because a user is given a set of consecutive sub carriers which span only a part of the entire bandwidth. If the set of sub carriers allocated to a user during one packet (number of consecutive OFDM symbols) are in deep fade, they will remain in deep fade for a long duration. To improve the situation, a highly efficient dynamic channel allocation scheme for multiple users is needed. Such schemes are very complex, require high amount of signalling overhead and still might not be optimal.

As an alternative to overcome the problem of outage, the use sub carrier hopping over a large bandwidth in addition to the MC-SS [17] is proposed in this work. The sub carrier hopping can follow a very elementary cyclic step increment. It will be shown here, that the use of the proposed SCH-MC-SS scheme significantly improves the outage performance over the non hopping system. The transmitter architecture for such a scheme can be represented as in Fig. 3.1. As is shown in the diagram,

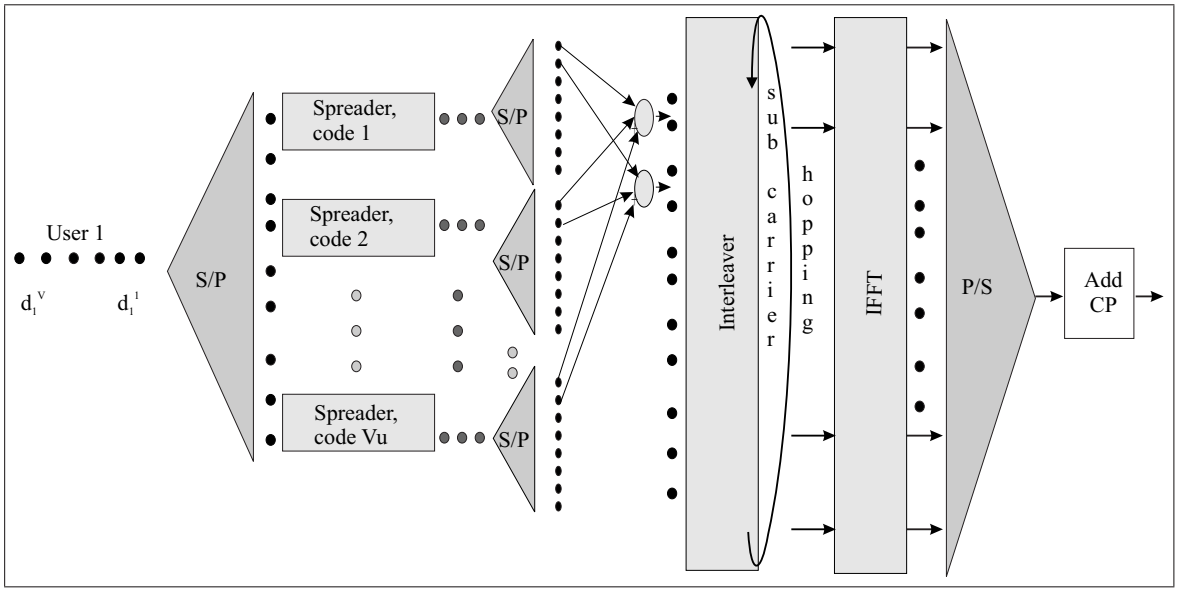

Figure 3.1: Transmitter for SCH-MC-SS

data symbols from a user are first converted from serial to parallel. Then each sym-

bol is spread. Then chips of the spread symbol are added and put on a sub carrier after interleaving. The interleaver is followed by the IFFT, as is used in OFDM systems. The output is converted from parallel to serial. This is followed by the usual addition of guard interval before up conversion. Fig. 3.2 shows the corresponding receiver architecture, where the reverse chronology of events of the transmitter occur. In addition there is a frequency domain channel equalizer [53]. The time frequency

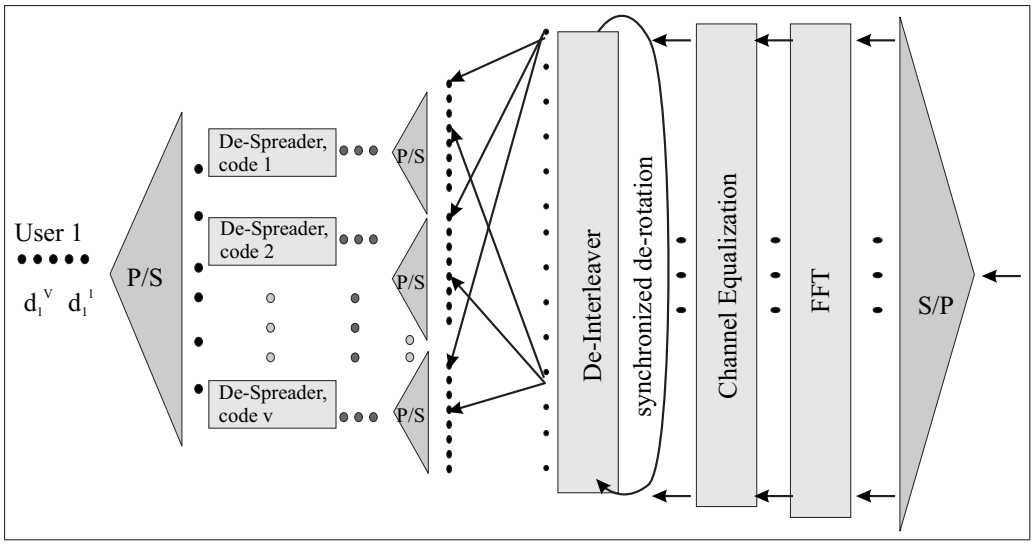

Figure 3.2: Receiver for SCH-MC-SS

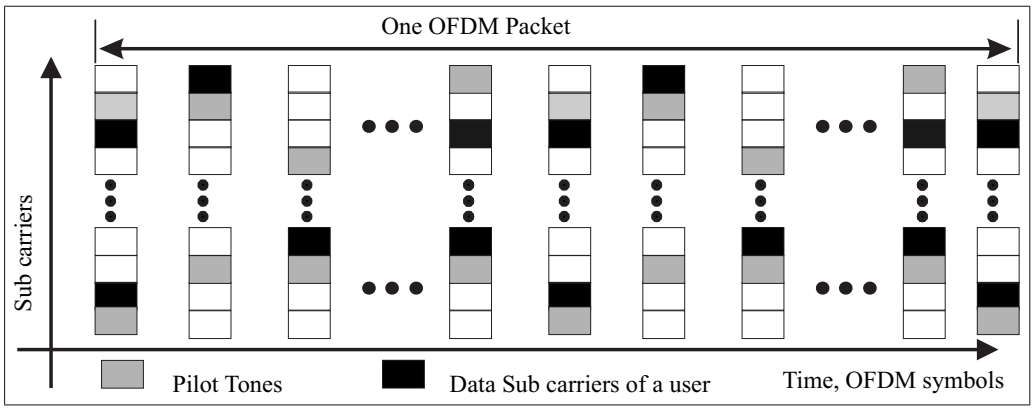

Figure 3.3: Time frequency diagram of the sub carrier hopping scheme. It is shown that a sub carrier allocated, which is represented by a particular colour shade, moves in time and frequency grid in one packet.

diagram for the proposed SCH for a particular user is presented in Fig. 3.3.

3.1.3 Analytical Model

OFDM is the basic system on which the code division multiplexing and sub carrier hopping is used. For the sth OFDM symbol of u^{th} user device a set of sub carriers is allocated, which is indicated by 'Δu_{s}', where '$|\Delta u|$', denotes the number of sub carriers allocated to the user device. $\mathcal{K}_{u,\mathrm{s}}\{n\}$ is a mapping function that maps sequential index from 0 to $|\Delta u| - 1$ onto all sub carrier indices in Δu_{s}. It is defined as,

$$\mathcal{K}_{u,\mathrm{s}}\{n\} \in \Delta u_{\mathrm{s}}; \quad \forall n \in \{0, 1, \ldots, |\Delta u| - 1\} \tag{3.1}$$

$$\mathcal{K}_{u,\mathrm{s}}\{n\} \neq \mathcal{K}_{u,\mathrm{s}}\{n^{'}\}, \text{for} \quad n \neq n^{'}. \tag{3.2}$$

Let v denote the data symbol index in the range 0 to V_u-1 where V_u denote the number of data symbols transmitted by user u in one OFDM symbol, that is kept constant during one transmission burst. Let $\mathrm{c}_{u,v}[n]$ be the n^{th} chip of v^{th} code of u^{th} user. W_u is the code length of user u. The n^{th} chip of u^{th} user, for sth OFDM symbol can be written as

$$\xi_{u,}[n] = \sum_{v=0}^{\mathrm{V}_u - 1} \mathrm{d}_u[\mathrm{sV}_u + v]\mathrm{c}_{u,v}[n]. \tag{3.3}$$

The n^{th} chip of u^{th} user, for sth OFDM symbol $\xi_{u,}[n]$ maps to the sub carrier symbol $\mathrm{X_s[k]}$ and hence $\xi_{u,}[n] = \mathrm{X_s[k]}$. The system needs to be designed such that the guard interval is larger than the delay spread of the channel, this is to avoid inter symbol interference. Another design criteria for OFDM systems is that each sub carrier experiences a flat fading channel. In such situation the expression for a received sub carrier in baseband assuming ideal synchronization can be written as $\mathrm{Y_s[k]} = \mathrm{H_s[k]X_s[k]} + \mathrm{N}$ [38] where N is the noise in one sub carrier bandwidth. With $\mathrm{Z_s[k]}$ as the equalizer coefficient for the kth sub carrier for sth OFDM symbol, the estimated subcarrier is

$$\mathrm{R_s\,[k]} = \mathrm{Z_s[k]H_s[k]} \sum_{v=0}^{\mathrm{V}_u - 1} \mathrm{d}_u[\mathrm{sV}_u + v]\mathrm{c}_{u,v}[(\mathcal{K}_{u,\mathrm{s}}^{-1}\{\mathrm{k}\})] + \mathrm{Z_s[k]N}. \tag{3.4}$$

The recovered $\acute{v}^{th}$ data symbol of sth OFDM symbol of u^{th} user is given as

$$\hat{\mathrm{d}}_{u,\mathrm{s}}[\acute{v}] = \sum_{\mathrm{k:k}\in\Delta u_{\mathrm{s}}} \mathrm{Z_s[k]H_s[k]} \sum_{v=0}^{\mathrm{V}_u - 1} \mathrm{d}_u[\mathrm{sV}_u + v]\mathrm{c}_{u,v}[(\mathcal{K}_{u,\mathrm{s}}^{-1}\{\mathrm{k}\})]\{\mathrm{c}_{u,\acute{v}}[(\mathcal{K}_{u,\mathrm{s}}^{-1}\{\mathrm{k}\})]\}^* + \varpi. \tag{3.5}$$

where ϖ represents the processed noise (due to combining after multiplying with the spreading code). The above expression can be broken into two parts, the useful data symbol part and the inter code interference part. The useful part is,

$$\hat{\mathrm{d}}_{u,\mathrm{s}}[\acute{v}]_I = \mathrm{d}_u[\mathrm{sV}_u + \acute{v}] \sum_{n=0}^{\mathrm{W}_u-1} \mathrm{Z_s}[\mathcal{K}_{u,\mathrm{s}}\{n\}]\mathrm{H_s}[\mathcal{K}_{\mathrm{u,s}}\{\mathrm{n}\}], \tag{3.6}$$

and the total noise term, which includes the processed noise and interference due to orthogonality loss of the codes in the frequency selective fading channel is

$$\chi \triangleq \hat{\mathrm{d}}_{u,\mathrm{s}}[\acute{v}]_{II} = \sum_{\mathrm{k}} \mathrm{Z_s[k]H_s[k]} \sum_{v\neq\acute{v}}^{\mathrm{V}_u-1} \mathrm{d}_u[\mathrm{sV}_u + v] \underbrace{.\mathrm{c}_{u,v}[(\mathcal{K}_{u,\mathrm{s}}^{-1}\{\mathrm{k}\})]\{\mathrm{c}_{u,\acute{v}}[(\mathcal{K}_{u,\mathrm{s}}^{-1}\{\mathrm{k}\})]\}^*}_{\beta=\text{inter code interference}} + \eta, \tag{3.7}$$

where

$$\eta = \sum_{\mathrm{k}\in\Delta u_\mathrm{s}} \mathrm{Z_s[k]N}\{\mathrm{c}_{u,\acute{v}}[(\mathcal{K}_{u,\mathrm{s}}^{-1}\{\mathrm{k}\})]\}^*. \tag{3.8}$$

The proposed sub carrier hopping is involved in the above expressions by the reference to the OFDM symbol index s. By choosing different Δu_s for different OFDM symbols, sub carrier hopping can be ensured.

Assuming BPSK transmit symbol, given that transmitted data symbol is $\mathrm{d}_u[\mathrm{sV}_u + v] = \sqrt{\mathcal{E}_s}$, the probability of error is $\Pr(\text{error}|\{\mathrm{Z_s[k]H_s[k]}\}_{\mathrm{k}\in\Delta\mathrm{u_s}})$

$$= \Pr\left(\hat{\mathrm{d}}_{\mathrm{u,s}}[\acute{\mathrm{v}}]_{\mathrm{I}} < \hat{\mathrm{d}}_{\mathrm{u,s}}[\acute{\mathrm{v}}]_{\mathrm{II}}\right), \tag{3.9}$$

$$= \mathbf{Q}\left(\sqrt{\frac{\mathcal{E}_\mathrm{s}}{\sigma_\chi^2 \mathrm{W_u^2}}} \sum_{\mathrm{k:k}\in\Delta\mathrm{u_s}} \mathrm{Z_s[k]H_s[k]}\right), \tag{3.10}$$

where $\mathbf{Q}(x) = \frac{1}{2}\mathrm{erfc}(\frac{x}{\sqrt{2}})$, where erfc is the complementary error function [35]. It can be easily extended to QPSK and other modulations. The performance of the system depends on the type of equalization–combining. Different options are presented in [54]. The expression for σ_χ^2 (which is the variance of χ in (3.7)) and the term in the summation changes with each type of channel equalization $\mathrm{Z_s[k]}$ and chip combining technique. The performance will also depend on the frequency correlation of the channel. For realistic frequency selective correlated fading channel conditions, it is difficult to assess the performance of the system without using real channel mod-

els. Extensive simulations are done with COST–259 channel parameters to obtain the mean and the 10% outage throughput for each user for the hopping and the non hopping systems. The expression used for computing the normalized throughput is $1 - \text{Ber}$.

3.1.4 Simulation Results and Discussion

Down link indoor COST–259 channel models with rms delay spread of 50 ns (referred as channel 2) and 250 ns (referred as channel 6) are used. The channel is assumed static during one packet. This is a valid assumption knowing that indoor velocities do not exceed 3 kmph and the packet length is limited to 1000 octets. It is considered that each packet experiences independent channel fading.

The total number of sub carriers is set to 64. Walsh–Hadamard orthogonal spreading codes are used. The spreading gain is kept equal to the number of sub carriers in one group. Number of allocated subcarriers per user device tested are 4, 8 and 16.

Successive Interference Cancelation (SIC) receiver is also considered in some cases. For such situations loading is kept as 75%. A loading of 75% means that, when there are 16 sub carriers in a group, i.e. the spreading gain is 16, then only 12 data symbols are loaded, i.e. only 12 spreading codes are used. At the receiver, Minimum Mean Square Error (MMSE)-Equal Gain Combining (EGC) is used for chip combining.

Two kind of sub carrier grouping are considered. One is 'block' which groups a set of consecutive sub carriers together, i.e. the chips of a code are spread over a set of consecutive sub carriers. The other type of sub carrier grouping considered is interleaved. In interleaved sub carrier grouping, the set of sub carriers which form a group are distributed in the entire bandwidth with equal distance between neighboring sub carriers of the same group.

In all cases *un–coded* system is used. Modulation used is QPSK. The following are to be noted for the figures below,

- Sub-Carrier Hopped Orthogonal Frequency Division Multiple Access with Code Division Multiplexing (SCH-OFDMA-CDM) is the proposed sub carrier hopping MC-SS scheme
- OFDMA-CDM is the parent MC-SS scheme
- 'intr' represents interleaved sub carrier arrangement

- 'blk' implies block sub carrier arrangement
- SIC represents successive interference cancelation receiver

3.1.4.1 Channel model 2, rms delay spread 50 ns

In this channel the 50% coherence bandwidth spans on an average up to 13 sub carriers for system using 20 MHz bandwidth.

Figure 3.4 shows the mean throughput of the sub carrier hopped and non hopped system. It can be seen from the figure that the mean throughput is almost

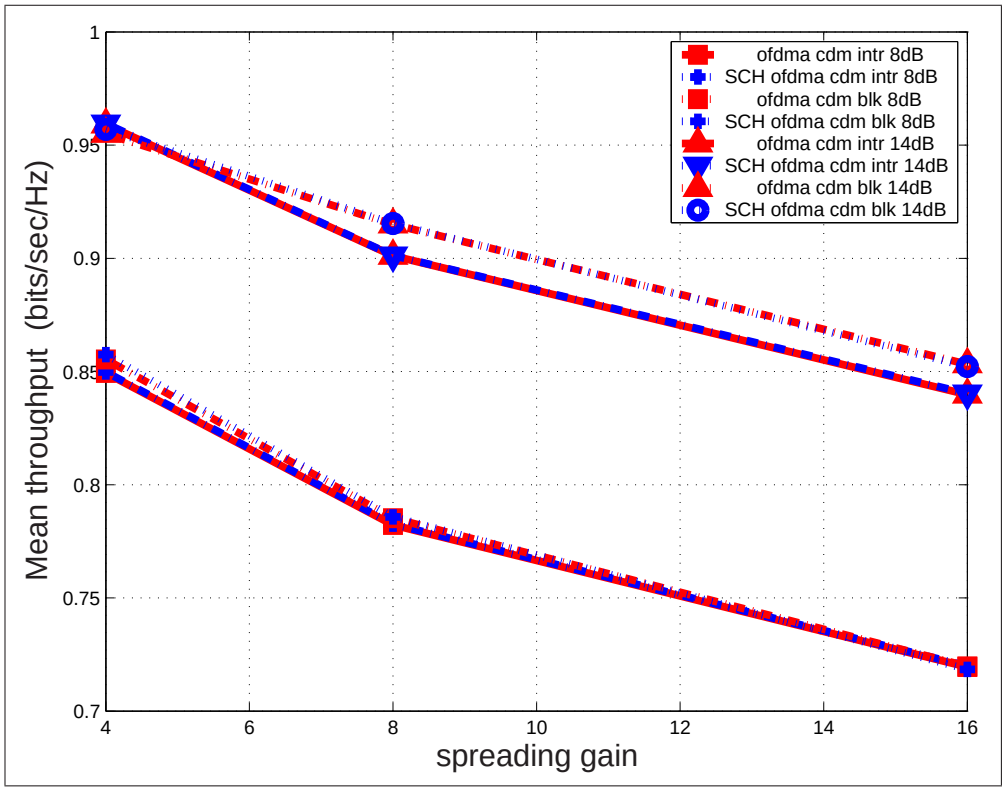

Figure 3.4: Mean throughput Vs spreading gain at different SNRs with single symbol detection, for channel model 2.
'intr' represents interleaved sub carrier arrangement and
'blk' implies block sub carrier arrangement.
OFDMA CDM is the parent MC-SS scheme, while SCH OFDMA CDM is the proposed sub carrier hopping scheme.

same for both the proposed SCH and the parent non hopping schemes. The mean throughput for the block and interleaved sub carrier grouping is also same at a given SNR. This is because the BER shown in the figure is the average over several possible instantaneous channel realizations. It is observed that with increasing spreading

gain the mean throughput is decreasing. It must be remembered that since loading fraction is kept constant (100%), with the increase in spreading gain, the number of data symbols loaded also increases. With increasing spreading gain the number of codes in use is also increasing since full loading (100%) is considered in this case. This performance degradation is because of increasing inter code interference as the the orthogonality of the codes are lost due to the frequency selective fading channel.

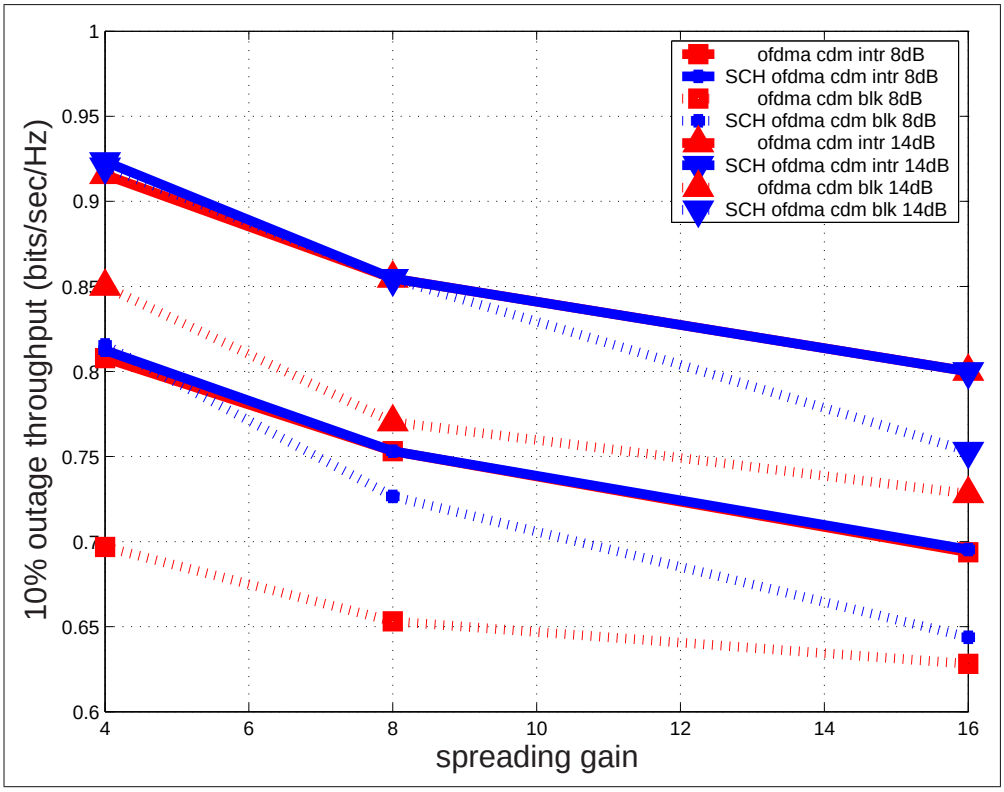

Figure 3.5: 10% outage throughput Vs spreading gain at different SNRs with single symbol detection, for channel 2

Figure 3.5 shows the 10% outage throughput[1] for the proposed SCH scheme and the parent non hopping scheme for both interleaved and block sub carrier arrangement. It can be seen that for block sub carrier assignment at small spreading gain, the improvement with sub carrier hopping is about 15%. Therefore the proposed SCH brings the benefit it has been used for, i.e. to improve the outage. The proposed SCH increases the frequency diversity of the system which provides the benefit of improved outage performance. However it is seen that if interleaved sub carrier grouping is considered the proposed SCH and the non hopped scheme have similar

[1]X% outage throughput is defined as the throughput below which the system is for X% of the time [55].

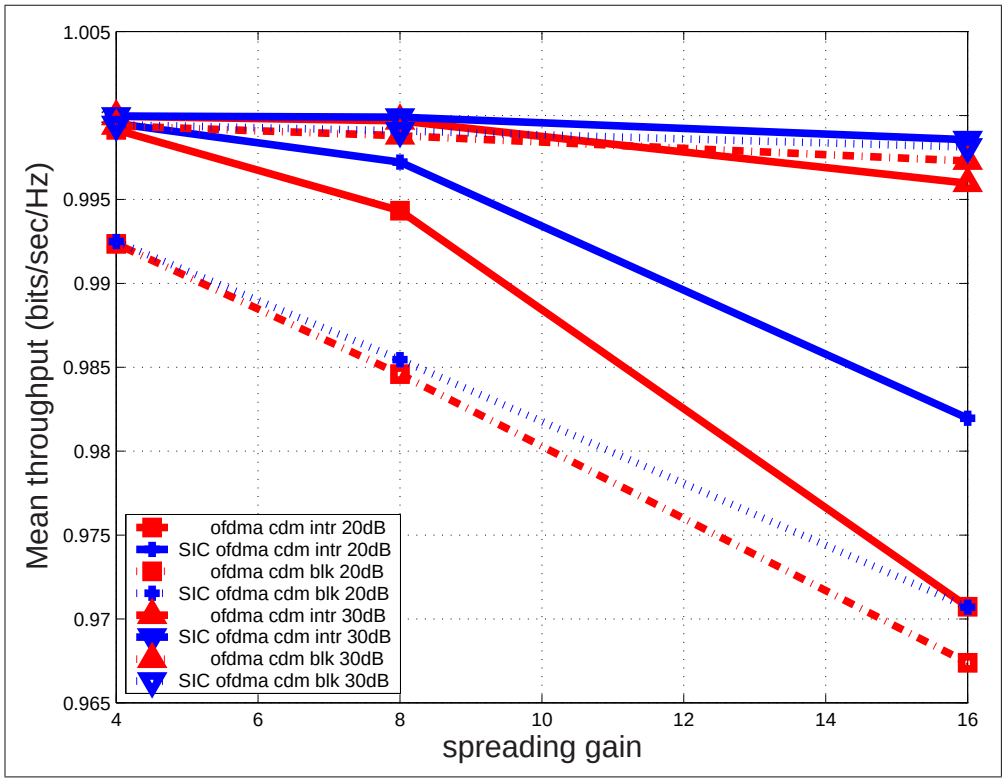

Figure 3.6: Mean throughput Vs spreading gain at different SNRs with successive interference cancelation, for channel 2

performance. The interleaved sub carrier grouping attains the maximum possible frequency diversity and hence SCH does not increase the outage any further.

Figure 3.6 compares the mean throughput of using a SIC and one using a single symbol detector. Both systems were used with sub carrier hopping. The loading considered is 75%. It is seen that SIC is effective for both interleaved and block sub carrier arrangement. It is also seen that SIC is useful for large spreading gains. This is because the diversity order increases with spreading gain.

Figure 3.7 compares the 10% outage performance of using SIC against using a single symbol detector with block and interleaved assignment of sub carriers. The performance is very similar to that of the mean throughput.

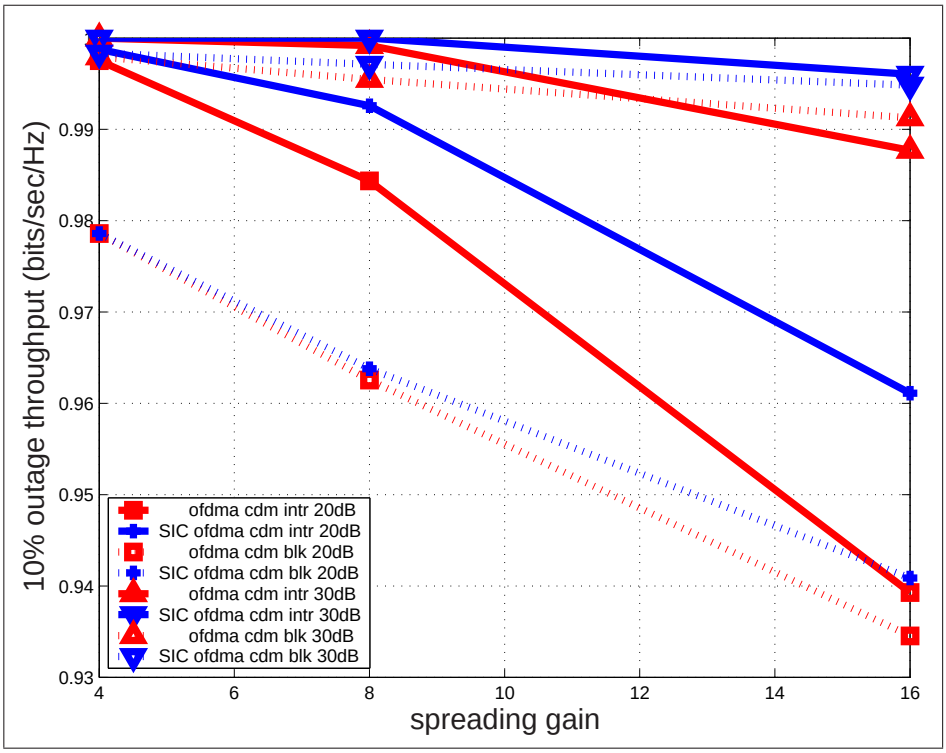

Figure 3.7: 10% outage throughput Vs spreading gain at different SNRs with successive interference cancelation, for channel 2

Recommendations that can be extracted from these results are

- If block assignment is used, at low spreading gain, the proposed sub carrier hopping is necessary to improve performance. Gain of about 15% in outage throughput is achieved in this case.
- If interleaved sub carrier allocation is used, there is no need for the proposed sub carrier hopping as they have same performance.
- At high spreading gains, hopping is not necessary.
- SIC receiver improves performance especially for the high spreading gains, it is a matter of complexity that may decide its use.
- For low spreading gains, SIC does not give much improvement and hence SIC is not recommended. At high spreading gains, if interleaved allocation is used, SIC is suggested for better performance. But, if block assignment is used, SIC has performance only slightly better than single symbol detector and hence may not be used.

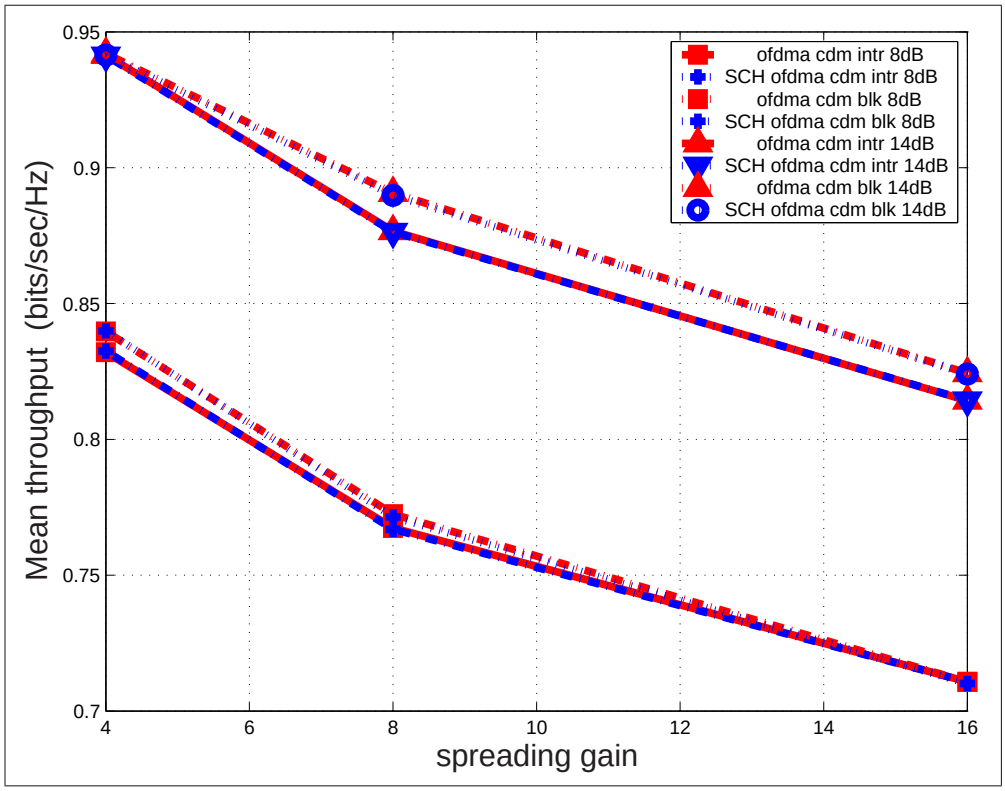

Figure 3.8: Mean throughput Vs spreading gain at different SNRs with single symbol detection, for channel 6

3.1.4.2 Channel model 6, rms delay spread 250 ns

In this channel the 50% coherence bandwidth spans on an average up to 3 sub carriers. Figure 3.8 shows the mean throughput of the proposed sub carrier hopped and non hopped system for interleaved and block sub carrier allocation. It shows that at a given spreading gain, they have almost same performance. This result is almost same as was observed for channel 2.

Figure 3.9 shows the 10% outage throughput for the same conditions as above. It can be seen that that the performance is very similar to that of model 2.

Figure 3.10 compares the performance of a SIC and non–SIC scheme for sub carrier hopping scheme. Once again the earlier conclusions from the previous channel condition hold here.

Figure 3.11 shows outage performance for the same scenario as the previous case. Here again, it is seen that the channel with rms delay spread of 250 ns also have similar effect as does the channel with 50 ns.

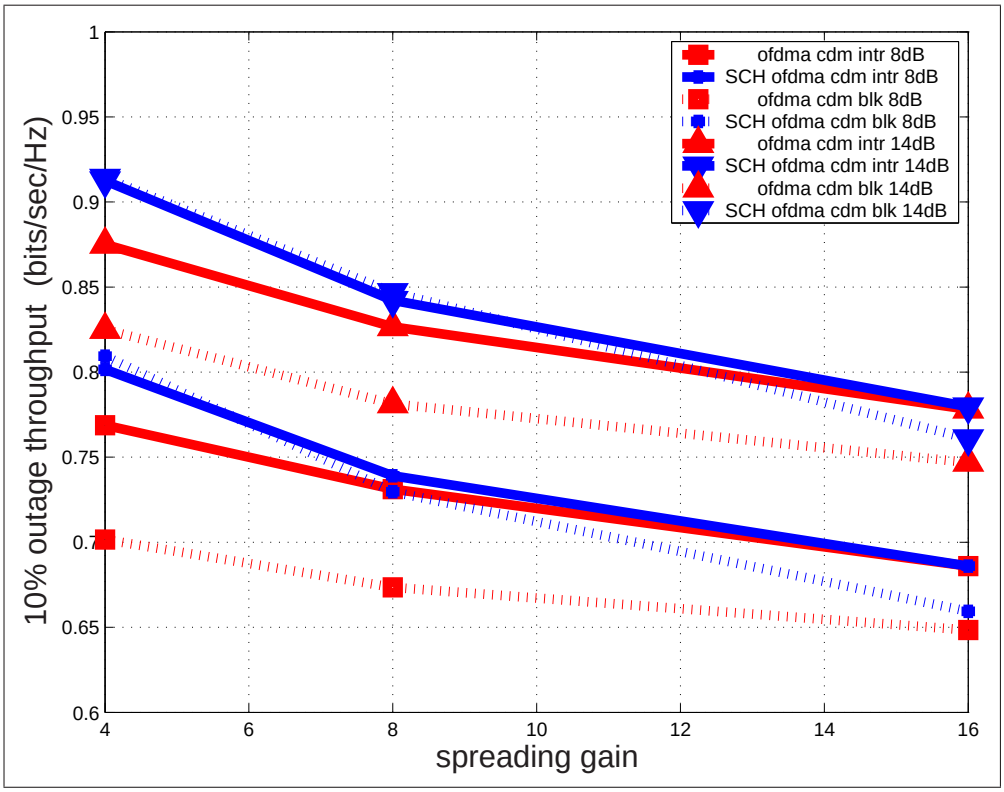

Figure 3.9: 10% outage throughput Vs spreading gain at different SNRs with single symbol detection, for channel 6

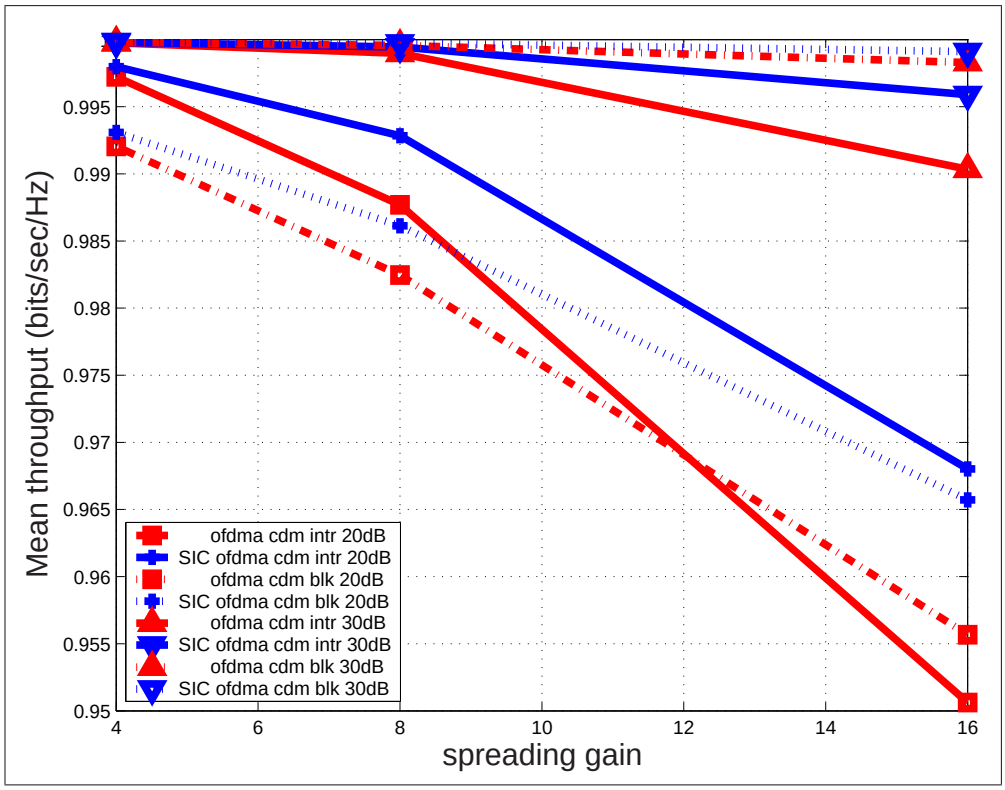

Figure 3.10: Mean throughput Vs spreading gain at different SNRs with successive interference cancelation, for channel 6

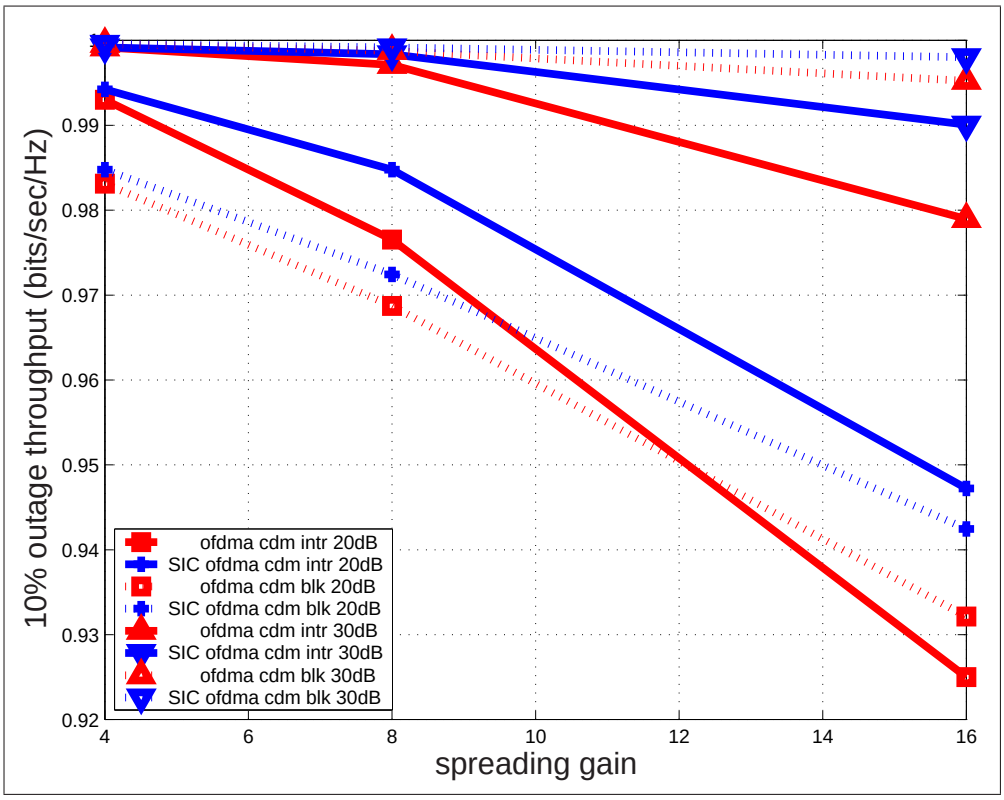

Figure 3.11: 10% outage throughput Vs spreading gain at different SNRs with successive interference cancelation, for channel 6

Recommendations that can be made for these conditions are as follows:

- The gain in outage throughput with hopping in block assignment is about 15%.
- At low spreading gain, block assignment with the proposed hopping has same performance as interleaved assignment.
- With high spreading gain, sub carrier hopping may be avoided, but interleaved sub carrier assignment is suggested.
- For low spreading gain, SIC is not needed for sub carrier hopped systems.
- For higher spreading gains, SIC gives improvement in both mean and outage throughput.

3.1.5 Conclusion

The goal of the study was to analyze the performance of the proposed SCH MC-SS and compare it against its parent non–hopped scheme for indoor conditions. It is found that the proposed hopping scheme improves the outage performance for block sub carrier grouping by about 15%. As part of the analysis the need for SIC receivers was also made. It is seen that SIC improves the performance for higher spreading gain while it is not necessary for small spreading gains. It can also be concluded from the analysis that using interleaved sub carriers rather than block assignment of sub carriers is shown to provide a benefit of about 8% in outage throughput. It is seen that none of the above conclusions are universal. Each situation of spreading gain, sub carrier grouping demands individual attention. Therefore it can be said that the schemes need to be adaptive and choose the best option considering the system parameters and channel condition.

3.2 MC-SS with receiver impairments

3.2.1 Introduction

Factors which influence the performance of the MC-SS schemes, other than the ones considered in the previous section, are the non ideal receiver characteristics. Several works mentioned in the previous section have proposed many new schemes under synchronized environment and with perfect channel estimate at the receiver. Other works analyze the performance of the individual access/ multiplexing schemes with receiver impairments with independent assumptions [56, 45]. Since both channel conditions and receiver impairments influence the performance of the access / multiplexing schemes, it is highly important to evaluate them in a unified framework to decide on the appropriate scheme for the particular situation.

The objective of this section is to analyze the potential multiplexing scheme among OFDM and MC-SS, for different spreading gains and load conditions under carrier frequency offset (due to mismatch in local oscillators) and channel estimation error in the realistic quasi static indoor environment. A comparison of OFDM and MC-SS was made in [57, 58], however it does not delve into the system design analysis of the impact of spreading gain, loading as made in this chapter. Performance comparison of OFDM and MC-SS schemes was made at the same time as this work in this chapter in [59] but the article concentrates on cellular scenario and the focus is not on receiver impairments.

3.2.2 System Description

The MC-SS scheme has been described in the previous section in details. Further important considerations are made here in continuation to the earlier description. Loading is the ratio of the number of codes used in a group of sub carriers, to the length of the spreading gain; i.e. the ratio of the number of modulated symbol in a code group to the spreading gain.

The MC-SS techniques use OFDM as the basic system and apply code division multiplexing on it, as described earlier. The general system model for all the schemes is developed in Section 3.1.1.

The time domain signal of the s^{th} transmitted OFDM symbol is defined in (2.19) through (2.22). Now, considering that channel coefficients remain static over a time period less than the coherence time period of the channel, $\delta f_c + f_{d_\tau}$ can be termed as effective carrier offset and represented as δf. The relative offset, i.e. the ratio of

the effective offset to the sub carrier spacing can be defined as $\epsilon \triangleq \frac{\delta \mathrm{f}}{\Delta \mathrm{f_{sc}}}$, where $\Delta \mathrm{f_{sc}}$ is the sub carrier bandwidth. The change in channel coefficients can be considered over a period greater than the 90% coherence time. The received sub carrier can be computed as [45],[46],

$$\begin{aligned}
\mathrm{R_s}\left[\mathrm{k}^{'}\right] &= \frac{1}{\sqrt{\mathrm{T_f}}} \int_{\mathrm{sT_s+T_{gi}}}^{\mathrm{sT_s+T_{gi}+T_f}} (\mathrm{r(t)}\Xi_{\mathrm{T_f}}(\mathrm{t-sT_s-T_{gi}}) \\
&+ \nu(\mathrm{t}))\, e^{-\mathrm{j}2\pi\frac{\mathrm{k}^{'}}{\mathrm{T_f}}(\mathrm{t-sT_s-T_{gi}})} e^{j2\pi\frac{\mathrm{t}}{\mathrm{T_f}}\epsilon}\, d\mathrm{t} \\
&= \frac{1}{\sqrt{\mathrm{T_f}}} \int_{\Xi_{\mathrm{T_f}}(\ldots)} \left(\int_0^{\tau_{\max}} \mathrm{h}(\tau;\mathrm{t})\mathrm{x}(\mathrm{t}-\tau)\, d\tau \right. \\
&+ \left. \nu(\mathrm{t}))\, e^{-\mathrm{j}2\pi\frac{\mathrm{k}^{'}}{\mathrm{T_f}}(\mathrm{t-sT_s-T_{gi}})} e^{j2\pi\frac{\mathrm{t}}{\mathrm{T_f}}\epsilon}\, d\mathrm{t}\, d\tau. \right. \qquad (3.11)
\end{aligned}$$

With $\mathrm{Z_s[k]}$ as the equalizer coefficient for the k^{th} sub carrier for s^{th} OFDM symbol, the estimated subcarrier is

$$\hat{\mathrm{X}}_{\mathrm{s}}[\mathrm{k}] = \mathrm{Z_s[k]H_s[k]R_s}\left[\mathrm{k}^{'}\right]. \qquad (3.12)$$

The received sub carrier has a useful component and a noise component, which is made of processed additive noise and inter carrier interference (ICI). The useful part of the sub carrier is

$$\mathrm{Z_s[k^{'}]H_s[k^{'}]X_s[k^{'}]e}^{(\frac{\mathrm{j}2\pi}{\mathrm{T_f}}(\mathrm{sT_s+T_{gi}})\phi_{\mathrm{k}^{'},\mathrm{k}^{'},\epsilon})} e^{(\pi\phi_{\mathrm{k}^{'},\mathrm{k}^{'},\epsilon})}\mathrm{sinc}(\pi\phi_{\mathrm{k}^{'},\mathrm{k}^{'},\epsilon}), \qquad (3.13)$$

where $\phi_{\mathrm{k,k}^{'},\epsilon} = \mathrm{k} - \mathrm{k}^{'} + \epsilon$. The inter carrier interference component is

$$\sum_{\mathrm{k,k}\neq\mathrm{k}^{'}} \mathrm{Z_s[k]H_s[k]X_s[k]e}^{(\frac{\mathrm{j}2\pi}{\mathrm{T_f}}(\mathrm{sT_s+T_{gi}})\phi_{\mathrm{k,k}^{'},\epsilon})} e^{(\pi\phi_{\mathrm{k,k}^{'},\epsilon})}\mathrm{sinc}(\pi\phi_{\mathrm{k,k}^{'},\epsilon}). \qquad (3.14)$$

The recovered v^{th} data symbol of s^{th} OFDM symbol of u^{th} user is given in (3.5). The useful data symbol part (decision variable) can be written as

$$\hat{\mathrm{d}}_{u,\mathrm{s}}[\acute{v}]_I = \mathrm{d}_u[\mathrm{s}]\acute{v} \sum_{\mathrm{k}^{'},\mathrm{k}^{'}\in\Delta u_u} \mathrm{Z_s[k^{'}]H_s[k^{'}]e}^{(\frac{\mathrm{j}2\pi}{\mathrm{T_f}}(\mathrm{sT_s+T_{gi}})\phi_{\mathrm{k}^{'},\mathrm{k}^{'},\epsilon})} e^{(\pi\phi_{\mathrm{k}^{'},\mathrm{k}^{'},\epsilon})}\mathrm{sinc}(\pi\phi_{\mathrm{k}^{'},\mathrm{k}^{'},\epsilon}). \qquad (3.15)$$

The combined inter code interference and noise is given in (3.7). Sub carrier hopping can be ensured by appropriately choosing the sub carrier mapping for each OFDM symbol in the above equations. Assuming BPSK transmit symbol, given that transmitted data symbol is $\mathrm{d}_u[\mathrm{s}]v = \sqrt{\mathcal{E}_s}$ the probability of error computation will follow

that as has been mentioned in (3.9) and (3.10). Simulations are done to obtain the mean bit error rate (BER) and the 10% outage throughput for all schemes under different test conditions.

3.2.3 Simulation Environment, Results and Discussion

Simulation results are presents for down link indoor environment. COST–259 channel model with 50 ns of rms delay spread is used. The channel is assumed to be static during one packet. This is a valid assumption knowing that indoor velocities do not exceed 3 kmph and that packet length is limited. The channel impulse response for each burst of packet transmission is considered to be independent.

Total number of sub carriers is set to 256 as per a test parameter set used in the 6^{th} framework EU funded project MAGNET. Walsh–Hadamard orthogonal spreading codes are used for the MC-SS schemes. The spreading gain is varied between 4 and 64. The loading for MC-SS is varied between 50% and 100%. The OFDM system is always considered to be fully loaded, i.e. all sub carriers have data symbols. There is no spreading gain for OFDM. Orthogonality restoration combining is used. Consecutive sub carrier assignment is done. In all cases *un–coded* system, i.e. no error correcting code is considered. The modulation used in QPSK.

Since a relative carrier frequency offset of 0.02 does not introduce significant distortion, therefore to study its impact, the residual carrier frequency offset relative to the sub carrier bandwidth is kept at 0.04. The channel estimation error is modeled as gaussian noise added to the true channel coefficients. The noise added to the channel coefficients to model the channel estimation error is as per the SNR condition.

Ideal Conditions Figure 3.12 presents the performance comparison of OFDM against MC-SS scheme with different spread gains. The loading is taken as 100%, i.e. when the spreading gain is 16, there are 16 sub carriers, and the number of data symbols spread over these 16 sub carriers is 16. It can be seen from the figure that OFDM has the lowest BER performance. The MC-SS scheme with spreading gain of 4, has almost same performance as that of OFDM. When the spreading is 16, the performance degrades but only slightly and when the spreading gain is 64 the performance is the worst. It is mentioned that the coherence bandwidth spans approximately 13 sub carriers for the 50ns rms delay spread channel condition. Therefore as long as the spreading gain is near to this number, the codes do not loose the orthogonality due to the flatness of the channel in the frequency domain over which the chips are spread. At the same time there is not much frequency diversity gain as there is hardly

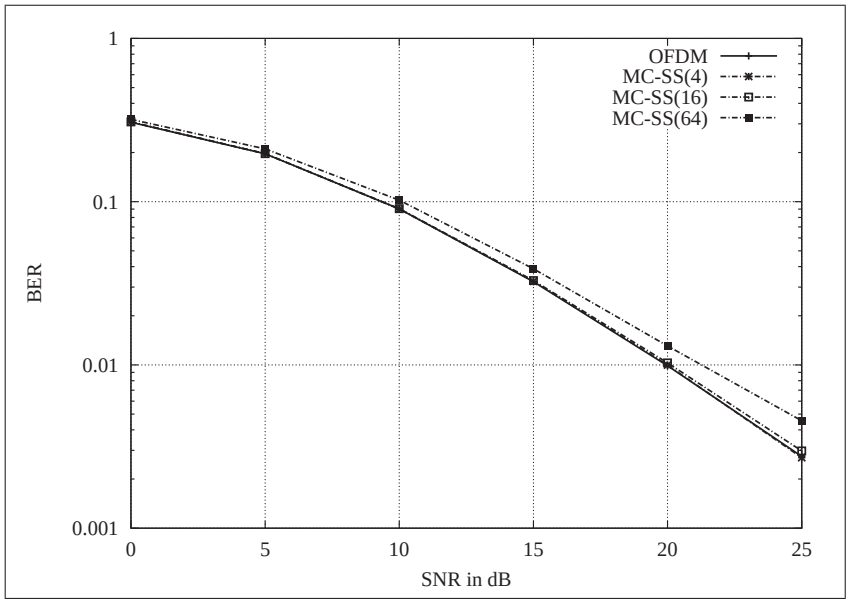

Figure 3.12: Effect of different spreading gain for ideal receiver conditions. The numbers in the bracket, e.g. MC-SS(4) indicates the spreading gain.

any variation in the channel gain over the bandwidth the data symbol is spread. The performance deterioration at high spreading gain is due to the loss in orthogonality of the codes because of frequency selective fading. However up to a spreading gain of 16, i.e. which covers 16 sub carriers, there is not much loss in orthogonality as the coherence bandwidth is very high for the channel under consideration. When the spreading gain is 64, one hand there is diversity gain due to spreading, on the other hand there is orthogonality loss between the codes. When the loss in orthogonality is higher than the diversity gain, there is performance loss.

Figure 3.13 shows the performance comparison of the schemes, under different load conditions for ideal channel estimation and synchronization. OFDM is always considered to be fully loaded, i.e. all its sub carriers carry data symbols. However for the MC-SS when 50% loading is considered, it means that if the spreading gain is 16, then only 8 data symbols are loaded i.e. only 8 code sequences out of 16 are used. It can be seen that MC-SS with 50% loading is the best in terms of BER. The improvement in performance comes from the redundant data transmitted by using spreading with a less than 100% loading. This has some effect similar to the Forward Error Correction (FEC) coding. However , the performance of OFDM is as good as that of MC-SS with 75% loading. Therefore the BER performance of MC-SS schemes are found to improve with decreasing load condition, but only upto a loading of 75%. If the loading is increased, it is expected to perform worse than OFDM. Though the

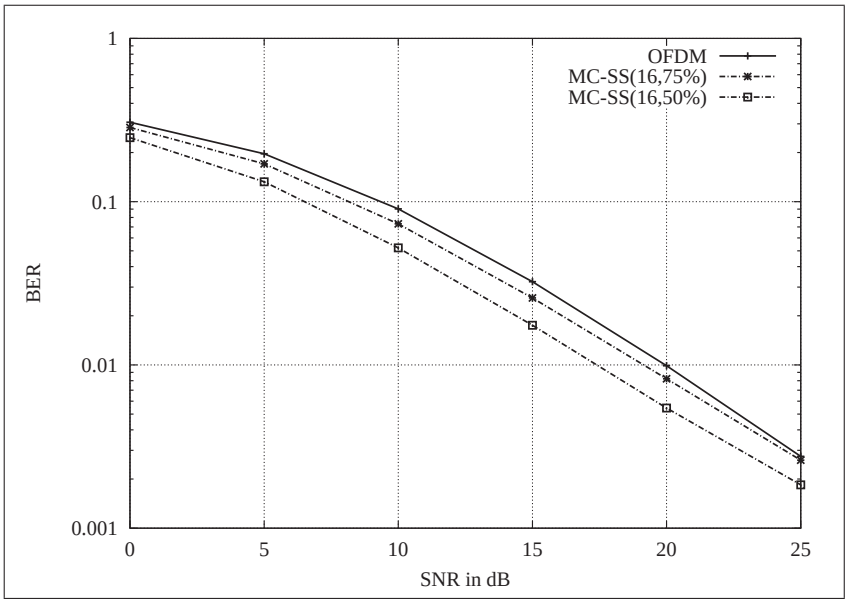

Figure 3.13: Effect of loading for spreading gain of 16 under ideal conditions

BER performance can be improved with low loading, there is a loss in throughput as percentage utilization of the resource is less. Following the previous case, it is to be noted that the BER performance with a certain loading percentage is expected to decrease with increasing spreading gain.

Impact of Carrier Offset: Figure 3.14 shows the performance of the schemes for residual frequency offset of 0.04, under full loading for different spreading gains. The carrier frequency offset introduces ICI as described in (3.13). It can be seen that OFDM has almost identical performance as MC-SS under full loading, with spreading of 4. MC-SS with spreading gain of 16 is only slightly worse compared to the smaller spreading gain while MC-SS with spreading gain of 64 has the worst performance. The performance in this situation is similar to when receiver is assumed to be at condition. Therefore it can be seen that the carrier frequency offset does not influence the relative nature of performance of the schemes under consideration. However, it must be noted that only Quadrature Phase Shift Keying (QPSK) modulation has been used and the residual carrier offset simulated is not very high. The performance could have been different had the residual carrier offset been larger or higher order modulation were used.

Figure 3.15 shows performance of the schemes for residual frequency offset of 0.04, for different amount of loading and for a spreading gain of 16. As observed before, the MC-SS scheme with 50% loading has the best performance, which is

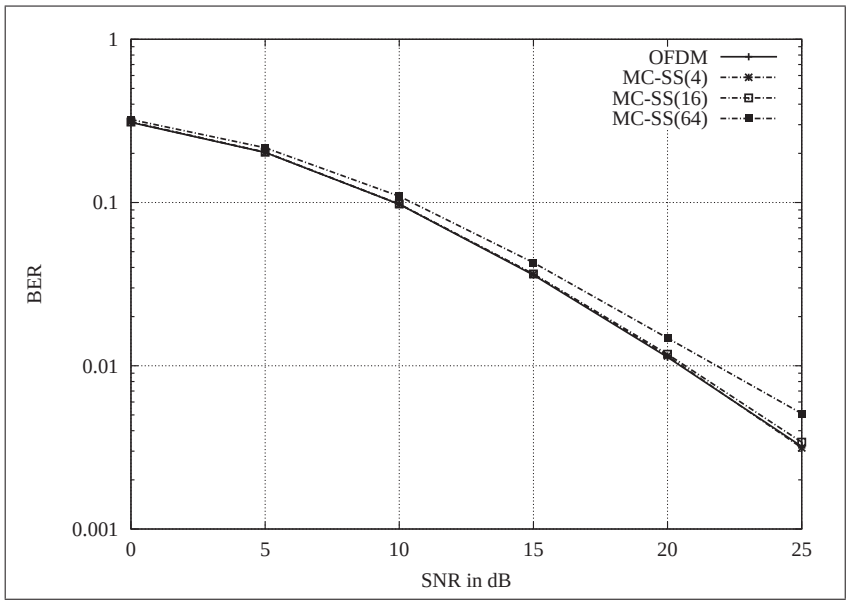

Figure 3.14: Effect of spreading gain in full load under residual carrier frequency offset

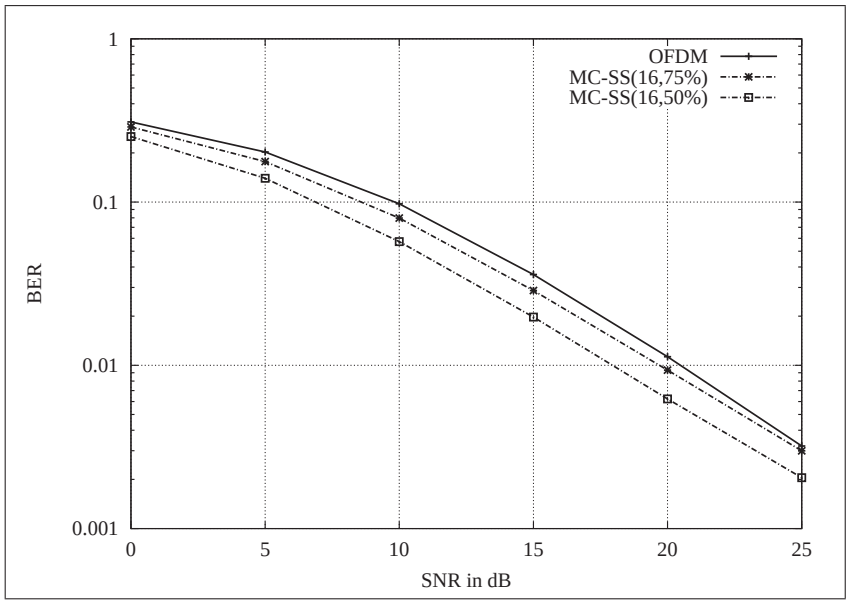

Figure 3.15: Effect of loading for spreading gain of 16 under residual carrier frequency offset

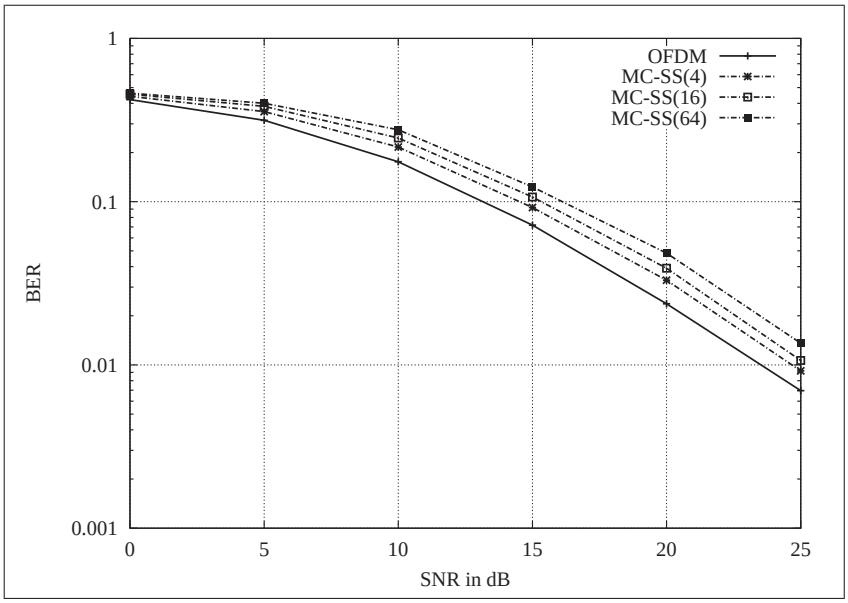

Figure 3.16: Effect of spreading gain in full load under Channel Estimation error

followed by the 75% loading while OFDM has the poorest performance.

Impact of Channel Estimation Error Figures 3.16 and 3.17 shows the performance of the schemes for channel estimation error. The estimated channel coefficients have been assumed to be affected by noise. It can be distinctly observed that channel estimation error affects the performance of the schemes most severely. In Figure 3.16, the observation regarding the relative performance of the different schemes under varying spreading gain, still holds as made for the ideal case earlier in this section. However, it must be noted that MC-SS with spreading gain of 4 now has worse performance than OFDM. In contrast, when ideal channel estimation was assumed, then MC-SS scheme using a spreading gain up to 16 has very close performance to that of OFDM. The channel estimation error degrades the performance of MC-SS scheme more because the noisy channel estimates destroys the orthogonality of the codes and inter code interference becomes higher. A data symbol is recovered by summing the chips which have been spread over the sub carriers. Now, errors due to noisy channel estimates creep into the chips. When these chips are combined then the noise also gets amplified and hence there is no gain from the spreading, rather there is worse performance.

It can be seen from Figure 3.17 that the spreading schemes with 50% load conditions has the best performance but 75% loading has performance which is same as OFDM. Therefore it can be concluded that spreading schemes are severely affected

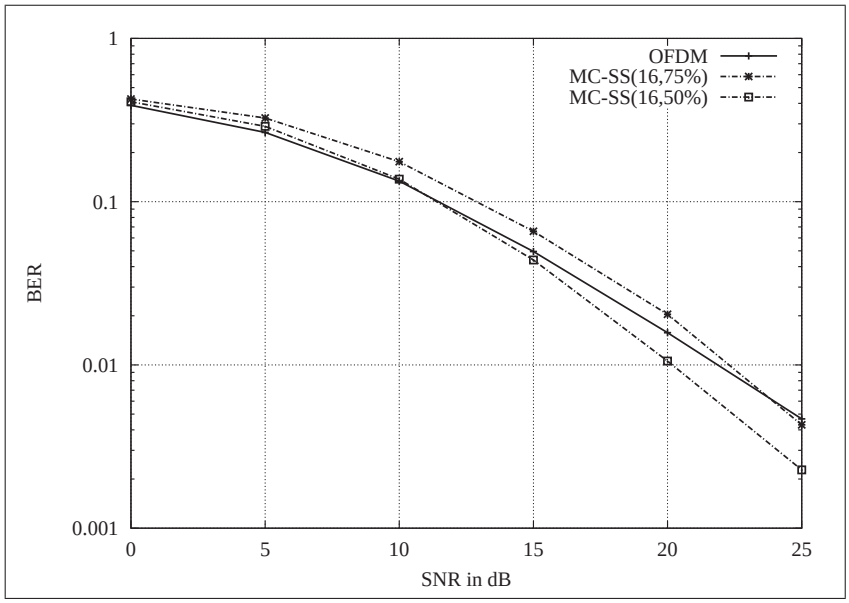

Figure 3.17: Effect of loading for spreading gain of 16 under Channel estimation error

by the channel estimation error.

Outage Performance: Figure 3.18 shows the effect of spreading gain on the 10% outage performance in full load for ideal receiver conditions. It can be observed that the outage throughput of OFDM is best compared to the MC-SS schemes with different spreading gains. The reason is as explained before, i.e. the spread spectrum schemes loose the orthogonality of the codes due to the frequency selective fading channel.

Figure 3.19 shows the effect of loading for spreading gain of 16 on the 10% outage throughput for ideal receiver conditions. It can be seen that MC-SS with 50% loading has the best performance while with 75% loading the performance is similar to that of OFDM, i.e. loading above 75% does not provide any benefit from spreading. The reason for this has been discussed before that there is redundant data information transmitted due to less than 100% loading which provides the extra SNR gain.

Figure 3.20 shows the effect of spreading gain on the 10% outage throughput in full load for channel estimation error and synchronization error. It is seen that OFDM performs better than MC-SS with any spreading gain.

Figure 3.21 shows the effect of loading for spreading gain of 16 on the 10% outage throughput under channel estimation error and synchronization error. The channel estimation error and synchronization error are considered to be in the same

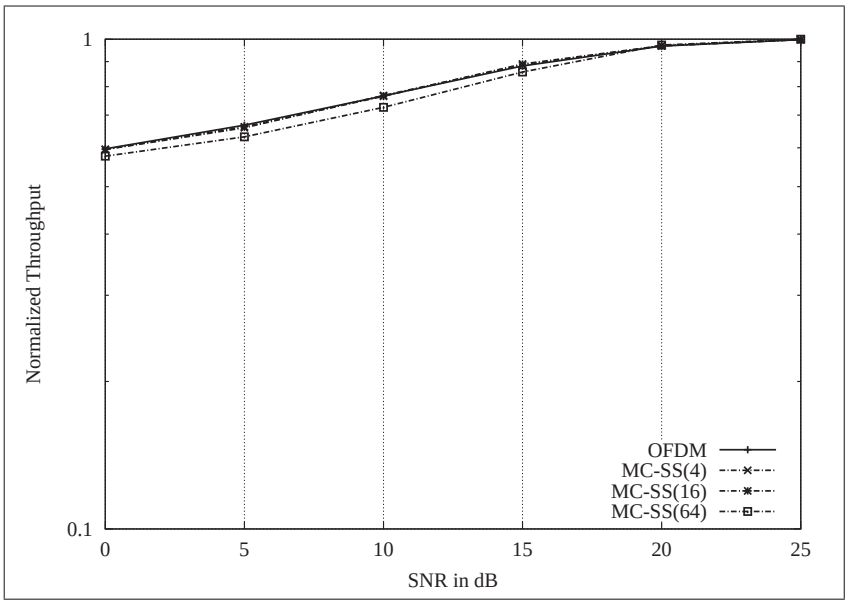

Figure 3.18: Effect of spreading gain on the 10% outage performance in full load for ideal receiver conditions

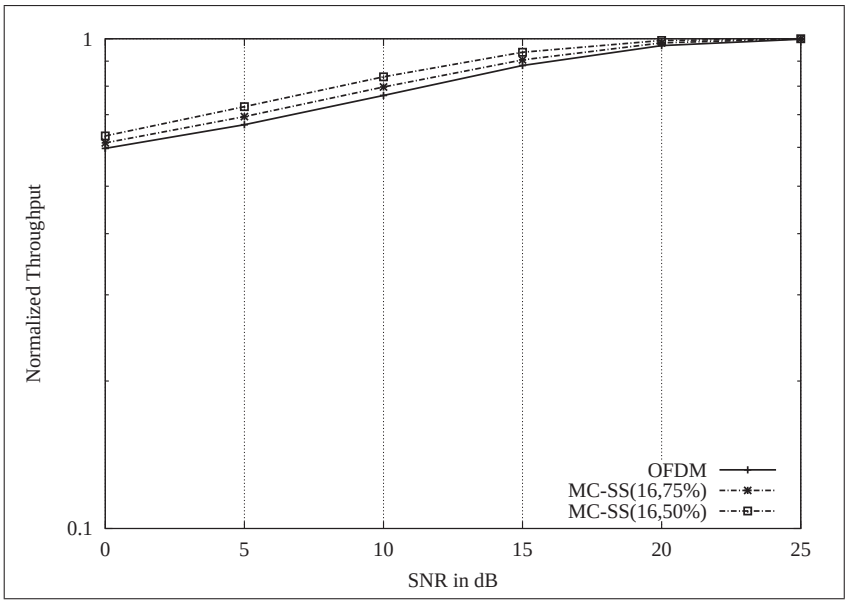

Figure 3.19: Effect of loading for spreading gain of 16 on the 10% outage performance for ideal receiver conditions

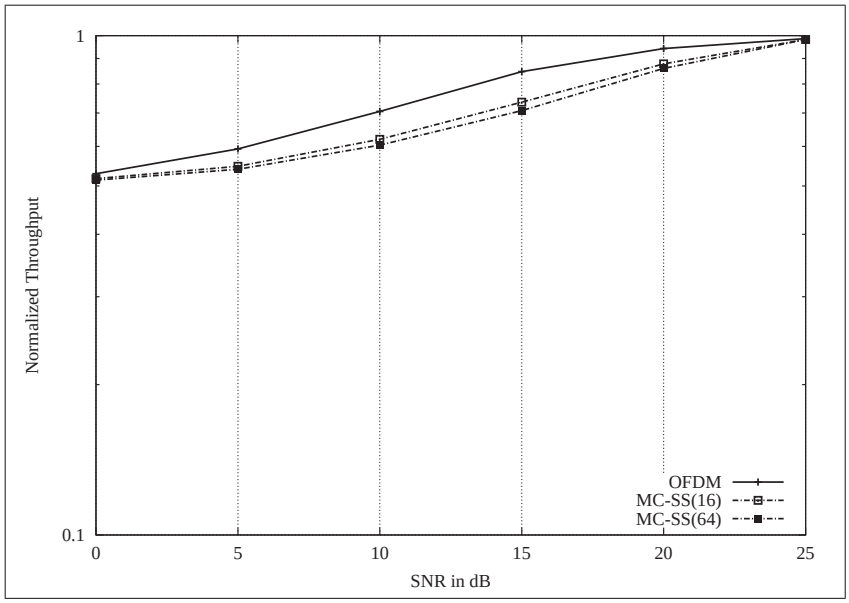

Figure 3.20: Effect of spreading gain on the 10% outage performance in full load for Channel Estimation error and synchronization error

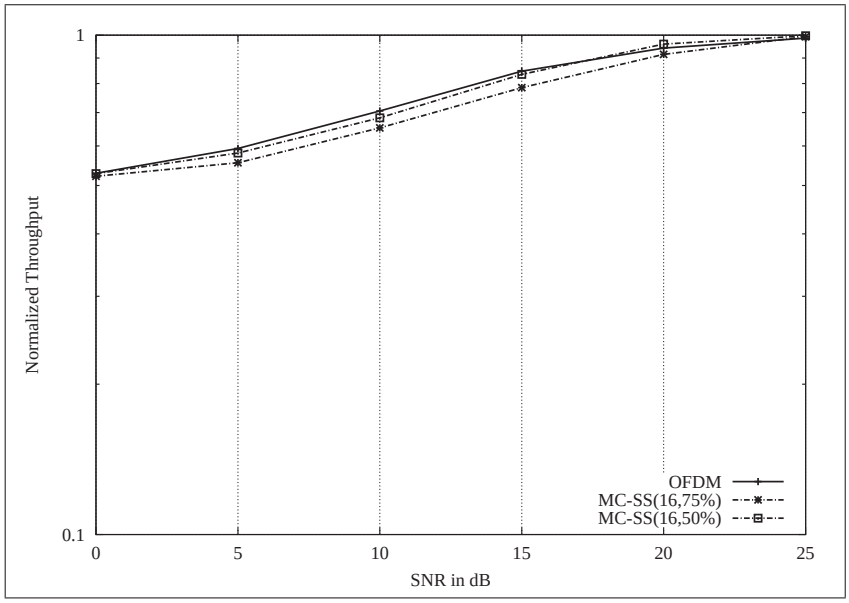

Figure 3.21: Effect of loading for spreading gain of 16 on the 10% outage performance for Channel Estimation error and synchronization error

order as in the earlier cases of non ideal receiver performance. It can be seen that OFDM has better resilience to such errors compared to the MC-SS schemes.

3.2.4 Conclusion

In this study, the performance of OFDM and MC-SS schemes have been evaluated for down link channel in realistic indoor conditions in presence of receiver impairments. For fully loaded conditions it is found that OFDM has the best mean BER performance, while for loading less than 75%, MC-SS outperforms OFDM. It has been distinctly found that increasing spreading gain degrades the performance, but provides the flexibility of changing the loading. Changing the loading can give improved performance as compared to OFDM. Under such conditions the throughput is adversely affected, but BER can be improved. Therefore it can be concluded that, operating the spreading schemes under full load is not desirable, as OFDM outperforms them. Synchronization error has similar effect on the spreading schemes as on the OFDM schemes, for the range of errors considered.

Channel estimation error affects the MC-SS more than OFDM. The flexibility of improving the bit error rate performance of the spreading schemes over OFDM is almost lost for channel estimation error conditions as verified in the work. Similar observations as above has been made for the 10% outage throughput results.

Finally it is important to note that the choice of the scheme depends on the required criteria of performance and hence must be chosen accordingly. It is not possible to claim one scheme to have better performance over other without considering the application it is being considered for. For example, even though it has been seen that OFDM has relatively better performance than MC-SS under full load conditions, yet MC-SS schemes can provide a better BER by simply reducing the loading, which is otherwise not possible in OFDM systems. Thus the results presented in this work can be used to choose the scheme after deciding the performance criteria for particular applications.

3.3 Summary

- A proposal to enhance a MC-SS scheme by introducing SCH has been made.
- The proposed scheme is found to have improved outage performance.
- Detailed guidelines regarding spreading gain, loading, use of SIC are discussed.

- In the second part of the chapter non ideal receiver operation has been considered.
- It is found that channel estimation error severely degrades the performance of MC-SS schemes.
- It is also seen that channel estimation error has a greater influence on the performance of MC-SS schemes than the carrier offset errors.
- Under fully loaded condition, it is found that OFDM has better resilience to receiver impairments over MC-SS schemes.
- If it is considered that full loading will be used for higher spectral efficiency, then it can be concluded that OFDM should be used.
- If full loading is not considered, then MC-SS has better performance.
- The studies made in this chapter did not consider Forward Error Correction (FEC) coding. In OFDM system use of FEC is expected to further enhance the performance by increasing the frequency diversity gain and also time diversity gains if designed carefully. It is already seen that OFDM has better performance in the uncoded set up. Therefore it can be expected with the use of FEC coding the performance of OFDM will be further improved.

4

Bit loading on Pilot Sub Carriers

The aim of this chapter is to increase the spectral efficiency by reducing the pilot overhead. In WLAN type system where a preamble (Training sequence) is used in the front for the packet being transmitted for synchronization and channel estimation, pilots sub carriers are embedded among the data sub carriers to track the residual phase errors [53]. Residual phase errors are the combined effect of residual uncorrected carrier frequency offset error together with the sampling clock offset error. The pilot sub carriers are pre-defined waveforms, does not carry any data information and hence are necessary overhead as they use up some of the sub carriers. In order to reduce the overhead due to these pilot sub carriers a semi blind pilot scheme is proposed in this chapter. Semi blind pilots carry data bits instead of a priori known symbol sequence by exploiting the extra SNR available at the pilots. The term semi blind is used because a preamble is used for initial acquisition of the synchronization and channel estimation while the pilot sub carriers are used for tracking the residual phase errors. Further in the proposed scheme, the pilot sub carriers are loaded with a modulation which is less than that of the data sub carriers, i.e. when the data sub carriers carry 16-QAM and 64-QAM, the pilot sub carriers are made to carry QPSK signal. Since the power of the data and pilot sub carriers are quite similar, (Pilots sometime may have higher power) therefore clearly under the above conditions the data symbols in

the pilots enjoy much more power than required. Thus there is a higher probability of detecting the data on the pilot sub carriers correctly. These correctly decoded data symbols can then be considered as pilots and hence used for estimating the phase errors.

To track the residual phase error a low complexity algorithm is proposed in this chapter. A highly complex computation of the inverse tangent function is needed to estimate the phase errors. The proposed algorithm reduces complexity by avoiding such computation.

The performance of semi blind pilot is investigated with existing and the proposed algorithm. It is observed that the semi blind pilot scheme enhances the spectral efficiency in the range of 5% to 15% without degradation in the BER performance as compared to the data aided pilot based systems. The proposed phase tracking algorithm reduces the implementation complexity significantly at the cost of 1-2 dB loss in BER performance in the semi blind environment, however it is found to be robust against high residual phase errors.

4.1 Introduction

OFDM is spectrally efficient, but high accuracy is needed in synchronization since coherent demodulation of OFDM is extremely sensitive to synchronization errors. In a real environment the synchronization blocks placed at the receiver front end are not able to estimate the exact carrier frequency offset due to thermal noise and fixed word length effects. Moreover due to sampling frequency offset there is a slowly increasing timing offset. The receiver has to continuously track and compensate for these effects in order to keep the BER low. Residual Carrier Frequency Offset (CFO) and Sampling Frequency Offset (SFO) tracking are thus very critical for successful implementation of OFDM systems. Residual CFO and SFO errors are jointly termed as *Residual Phase Errors*.

In WLAN type systems, in order to estimate the channel and get initial acquisition of the frequency offset, a completely data aided Training Sequence (TS) is used as described in Fig. 2.19. Pilot sub carriers, which are a known sequence of waveforms, are embedded in the data part of the packets to enable tracking of residual phase offset. Pilot sub carriers do not carry any information content and thus add significant overhead to the system. To avoid the overhead due to pilot sub carriers blind algorithms [60], [61] can be used but they add very high complexity to the receivers. Therefore a semiblind system is proposed in this chapter.

It is proposed in this work to use the pilot sub carriers embedded in the OFDM symbols to carry data-information, instead of known symbol sequence. This would increase system efficiency by reducing the pilot overhead, while not deteriorating the BER performance, for WLAN systems.

High order modulations such as 16-QAM and 64-QAM are often used for high data rate transmission. Pilot sub carriers used in these systems, which are known a priory at the receiver, are similar to BPSK waveform, i.e sub-carriers have normalized values of ± 1. BPSK modulated signal requires between 12 dB and 16 dB less SNR as compared to 64-QAM, depending on the FEC coding rate to achieve the desired Packet Error Rate (PER) of in a typical WLAN system, which is about 10% for IEEE 802.11a [44]. This additional SNR advantage (Table 4.1) of the pilot may be exploited to transmit additional data bit, thus, increasing the throughput of the system without any increase in bandwidth or SNR requirement or any loss in performance. That is, while transmitting 64-QAM modulated waveform, the pilots can be BPSK or QPSK modulated to carry information bits instead of known a priori symbol sequences.

The increase in efficiency achieved via this scheme though is within modest values yet it has several advantages, such as, utilizing the existing frame format with very little changes. Further the existing demodulation schemes and receiver baseband and front end algorithms can function as usual and do not require any additional hardware extension. Only the phase correction algorithm needs to be changed.

Algorithms used for phase tracking and correction use the search function *argmax* [45, 62, 63, 64] after complex–conjugate–multipy–add operations. They also need to compute the *inverse tangent* [62],[38],[53],[65],[66]. A series implementation of the inverse tangent function, will need up to seven term for appropriate accuracy. This operation needs approximately more than 60 arithmetic operations. In other words the implementation complexity of the phase tracking algorithm is very high. An algorithm for residual phase tracking which does not use complex arithmetic functions is also presented in this chapter. Instead of computing the phase angles using inverse tangent function, the proposed algorithm computes the complex exponential of the phase angle at the pilot-tone locations to minimize the implementation complexity. The design of the algorithm is such that it can be very easily applied to any coherent OFDM based WLAN type of networks.

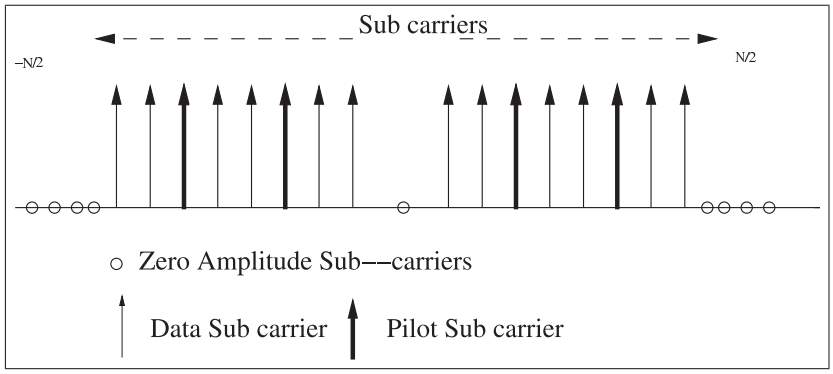

Figure 4.1: OFDM Symbol Format

4.2 System Description

The case for Wireless Local Area Networks (WLAN) systems using a frame format similar to the one used by IEEE 802.11a is considered here. Such systems have a training sequence or preamble (Fig. 2.19) [44]. The initial ten short training sequences are used for packet detection, automatic gain control, Symbol Timing Offset (STO) synchronization and coarse Carrier Frequency Estimation; it is followed by two long training sequences for fine carrier frequency offset (CFO) synchronization and channel estimation [53].

Packet detection and symbol timing synchronization are done by the *Time Synch* block of the receiver. Initial carrier frequency estimation and compensation is done by the *Frequency Synch* block. Channel Estimation and compensation is done by the *Channel Equalization* block (Once per packet). Then follows the residual phase correction done by *Phase Tracking* block. The residual phase occurs because of non–exact carrier frequency compensation and sampling frequency offset (SFO). The residual phase increases with OFDM symbol index [45]. Pilot sub–carriers are embedded in the OFDM symbol among the data sub–carriers to enable the tracking of this residual phase.

Pilot Structure Every OFDM symbol is made of data and pilot sub–carriers as shown in Figure 4.1. Data sub–carriers are modulated using either Binary Phase Shift Keying (BPSK), Quadrature Phase Shift Keying (QPSK) or high order Quadrature Amplitude Modulation (QAM). Pilot sub–carriers are a pseudo random sequence of ± 1 [44], the sequence being known at the receiver. Pilots are the same irrespective of the modulation scheme of the data sub–carriers and are transmitted with the same maximum power as that of data sub–carriers. The minimum SNR required by the

Table 4.1: SNR advantage of pilots in different modulation schemes

Modulation Scheme	Pilots	SNR advantage
64-QAM	BPSK	16dB
64-QAM	QPSK	12dB
16-QAM	BPSK	12dB
16-QAM	QPSK	7dB

highest order QAM (64-QAM) modulation scheme is about 16 dB more than that required by BPSK modulation scheme to achieve a PER of 10% [44],[53],[35]. Hence we know that, the pilots carry more power when a 64-QAM modulated symbol is transmitted than in the case of a BPSK modulated symbol. The additional SNR the pilots enjoy with different modulations is shown in Table 4.1 [44].

Proposed Scheme It is proposed that the pilot sub carriers present in OFDM based WLANs as in IEEE 802.11a can be modulated to transmit data without loss of performance to increase the data rate. The data and pilot sub carrier constellation can be seen in Fig. 4.2 & Fig. 4.3.

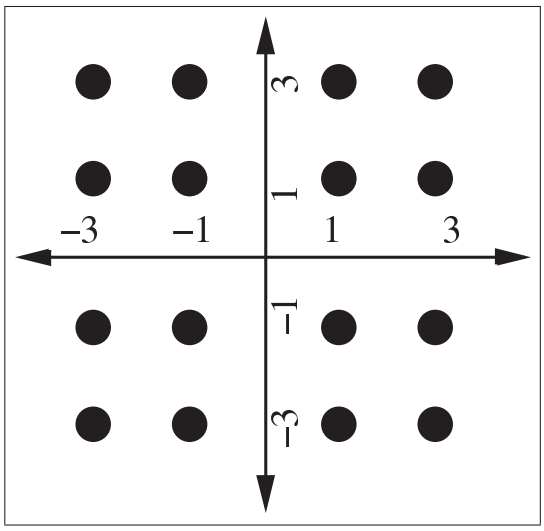

Figure 4.2: 16-QAM Data constellation

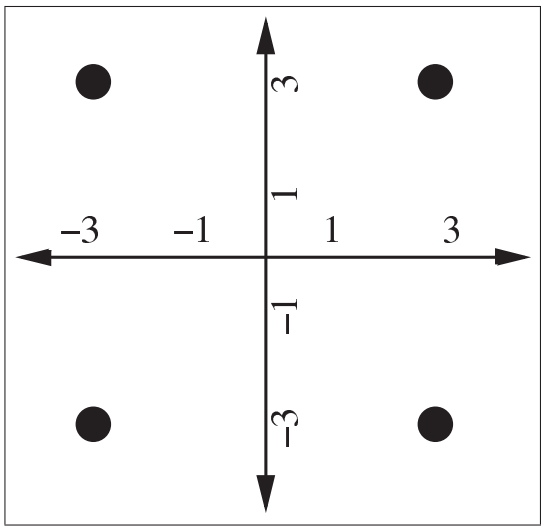

Figure 4.3: QPSK Pilot constellation

Table 4.2: Symbols

Symbol	**Explanation**
$R_{l,k}$	Received OFDM sub–carrier
l	Index of OFDM symbol index
k	Index Sub–carrier symbol index
$H_{l,k}$	Channel coefficient at k^{th} sub–carrier
T	Sampling duration
N	Number of points of DFT
N_g	Number of guard samples
N_s	$=N+N_g$ total number of samples in a transmitted OFDM symbol
T_u	DFT duration = T.N
T_g	Guard Interval = $T.N_g$
T_s	Transmitted OFDM symbol duration = $T.N_s$
$X_{l,k}$	Transmitted symbol
$\phi_{k,i}$	$= (1+\zeta)(\delta f T_u + k) - i$, is the residual phase error
ϕ_k	$= \phi_{k,k} = \delta f T_u + k\zeta$
ζ	Relative Sampling frequency offset between Transmitter and receiver
δf	residual carrier frequency offset
$n_{l,k}$	noise term
ΔF_{sc}	Sub carrier spacing = $\frac{1}{T_u}$
N_o	Thermal noise power density
σ_s^2	Signal power, variance of signal
γ_r	required signal to noise power
γ_s	signal to thermal noise ratio of signal

To prove this statement theoretically, we must consider the reason why pilots are used in OFDM based WLAN systems for indoor communication. Several literatures [38],[53], [67] discuss that pilots are used for residual phase correction. Residual phase effect has been explained briefly before. It happens because of the non–ideal frequency synchronization by the initial carrier frequency offset correction block which uses the training sequence to obtain an initial acquisition. Added to this there is the sampling frequency offset. In some systems the local oscillator and the sampling clock are tied together. This means that they drift between the transmitter and the receiver in the same direction. To correct these effects, the literatures referenced above and several others available treat these two together as residual phase. The algorithms used to track them estimate the progressive phase difference between the sub–carriers of two consecutive OFDM symbols. The effects of the residual phase are many fold as is evident from the equation below. The received sub–carrier after initial carrier frequency offset correction, frame and symbol synchronization and DFT is

$$R_{l,k} = e^{j\pi\phi_k} e^{j2\pi \frac{lN_s+N_g}{N}\phi_k} \frac{\sin(\pi\phi_k)}{\sin(\pi\frac{\phi_k}{N})} X_{l,k} H_{l,k} + \sum_{i=0,i\neq k}^{N-1} e^{j\pi\phi_{k,i}} e^{j2\pi \frac{lN_s+N_g}{N}\phi_i} \frac{\sin(\pi\phi_{k,i})}{\sin(\pi\frac{\phi_{k,i}}{N})} X_{l,i} H_{l,i} + n_{l,k} \tag{4.1}$$

where the symbols are as defined in Table 4.2. The first term is the desired signal component, while the second term is the ICI term [23] due to sub–carrier misalignment, which is caused by the residual carrier frequency error while the third term is the noise term. As can be seen from (4.1) above, the first term has a reduced amplitude and a phase rotation, as well as added to this is the ICI component. Hence the two important effects of the residual phase are rotation of received constellation points and reduction in SNR. Pilots are used to track and compensate for these effects. The principle of operation of these algorithms has been discussed in the above mentioned literature, such that the relative phase rotation between the sub–carriers of consecutive OFDM symbols is computed.

For the proposed semi-blind pilot scheme to work using the above mentioned algorithms for phase compensation, it is desired that the residual phase rotation between two OFDM symbols, satisfy two limiting conditions: i) The angle of rotation of the first component (the desired signal) is less than that required for correct demodulation, ii) The ICI is sufficiently small, so that the BER of the pilot sub–carriers is less than that of the data sub–carriers.

4.3 Analytical Framework and Algorithm

Analysis In this section the two limiting conditions mentioned above for successful deployment of the scheme will be analyzed. First the expression for the maximum residual carrier frequency offset will be given. This will be done assuming initial data aided acquisition using training sequence by commonly used algorithms [38, 62, 53]. Then the expression and limiting allowable phase rotation in the light of constellation rotation of the desired signal will be shown. Next the maximum allowable phase rotation in the light of ICI will be given. The minimum of these two criteria will give the allowable phase rotation for successful demodulation and detection of pilot symbol. This will be equated with the maximum residual carrier frequency offset and the feasibility of the system will be validated.

Residual Carrier Frequency Offset With reference to a generic receiver architecture, there is an initial carrier frequency offset estimation block. This block performs an initial carrier frequency offset acquisition using the training sequence. The estimate is never perfect since the incoming signal is contaminated by noise. The variance of the estimate is dependent on the SNR of the training sequence used to estimate the offset. From [38] it can be written that the variance of the estimate is

$$\sigma_{\delta \mathrm{f}} = \frac{1}{2\pi} \frac{\mathrm{N}}{\mathrm{L}\sqrt{\mathrm{M}\gamma_{\mathrm{s}}}} \tag{4.2}$$

where L is the distance between the corresponding sub–carriers across which phase difference is being measured, M is the number of summations, and γ_{s} is the signal to noise ratio. The residual carrier frequency appears as residual phase error. The maximum carrier frequency offset can be considered as $3\sigma_{\delta\hat{\mathrm{f}}}$. Accordingly the residual phase error at the k^{th} sub–carrier of the l^{th} OFDM symbol can be written as

$$\begin{aligned} \theta_{\mathrm{l,k}} &= \frac{2\pi \mathrm{l} \mathrm{N_s}}{\mathrm{N}} \phi_{\mathrm{k}} \\ &= \frac{2\pi \mathrm{l} \mathrm{N_s}}{\mathrm{N}} (\delta \mathrm{f} \mathrm{T_u} + \mathrm{k}\zeta) \\ &= \frac{2\pi \mathrm{l} \mathrm{N_s}}{\mathrm{N}} (3\sigma_{\delta \mathrm{f}} \mathrm{T_u} + \mathrm{k}\zeta) \end{aligned} \tag{4.3}$$

The algorithms operating on pilots, estimate the residual phase between two consecutive OFDM symbols. Therefore, the residual phase error between the same two

sub–carriers of consecutive OFDM symbol can be written as

$$\begin{aligned}\Delta\theta_{\mathrm{k}} &= \theta_{l,k} - \theta_{l-1,k} \\ &= \frac{2\pi \mathrm{N_s}}{\mathrm{N}}(3\sigma_{\delta \mathrm{f}}\mathrm{T_u} + \mathrm{k}\zeta)\end{aligned} \tag{4.4}$$

Constellation Rotation It has been proposed in this work, to modulate the pilot tones with BPSK or QPSK. Accordingly, the largest constellation rotation allowable is $\pi/2$ and $\pi/4$ for BPSK and QPSK respectively. The residual phase error must be less than this value. i.e. the phase rotation between the same two pilots of consecutive OFDM symbols must be less than these values. Accordingly the equations can be set up as

$$\begin{aligned}\Delta\theta_{\mathrm{k}} &\leqslant \frac{2\pi}{2^{\mathrm{b}+1}} \\ \frac{2\pi \mathrm{N_s}}{\mathrm{N}}\phi_{\mathrm{k}} &\leqslant \frac{2\pi}{2^{\mathrm{b}+1}} \\ \phi_{\mathrm{k}} &\leqslant \frac{\mathrm{N}}{\mathrm{N_s}2^{\mathrm{b}+1}}\end{aligned} \tag{4.5}$$

Where b is the number of bits per symbol used in the modulation scheme. And it can be continued that

$$\phi_{\mathrm{min}_1} = \frac{\mathrm{N}}{\mathrm{N_s}2^{\mathrm{b}+1}} \tag{4.6}$$

Inter Carrier Interference The phenomenon of ICI has been explained previously. Since the symbol in the pilots need to be detected before data in data–sub–carriers, and since the pilots are also needed for correcting the phase of the data–sub–carriers, they are hard decision detected in this work. The pilots must achieve a Bit Error Rate (BER) which is lower than the tolerable limits of the data–sub–carriers. The ICI can be modeled as additive noise [45]. The Signal to Interference plus Noise Ratio (SINR) of the pilots must be such that the BER under ICI conditions must be better than the required BER performance of the data sub–carriers. In IEEE 802.11a type systems with PER of 10% the BER equates to a range between 10^{-4} and 10^{-3}. Hence the BER of pilots can be set to be less than this range. The ICI power which is given by the second term of (4.1) can be approximated [45] to

$$\sigma^2_{\mathrm{ICI,k}} \approx \sigma^2_{\mathrm{s}}\frac{\pi^2}{3}\phi^2_{\mathrm{k}} \tag{4.7}$$

Accordingly the signal to noise ratio can be written

$$\gamma = \frac{\sigma_{\mathrm{s}}^2 \mathrm{sinc}^2(\pi\phi_{\mathrm{k}})}{\sigma_{\mathrm{s}}^2\sigma_{\mathrm{ICI,k}}^2 + \mathrm{N_o}\Delta\mathrm{F_{sc}}} \tag{4.8}$$

This can be reduced with approximations for small angle ϕ_k as

$$\gamma \approx \frac{\sigma_{\mathrm{s}}^2}{\sigma_{\mathrm{s}}^2\sigma_{\mathrm{ICI,k}}^2 + \mathrm{N_o}\Delta\mathrm{F_{sc}}} \tag{4.9}$$

The required PER of 10% for a particular modulation scheme can be mapped to a certain minimum require SNR level. Using γ_r as the minimum required SNR, the second condition is

$$\gamma \geqslant \quad \gamma_{\mathrm{r}} \tag{4.10}$$

Replacing with the expression for γ it can be written as

$$\begin{aligned}
\frac{\sigma_{\mathrm{s}}^2}{\sigma_{\mathrm{s}}^2\sigma_{\mathrm{ICI,k}}^2 + \mathrm{N_o}\Delta\mathrm{F_{sc}}} &\geqslant \quad \gamma_{\mathrm{r}} \\
\frac{\sigma_{\mathrm{s}}^2}{\gamma_{\mathrm{r}}} &\geqslant \quad \sigma_{\mathrm{s}}^2\sigma_{\mathrm{ICI,k}}^2 + \mathrm{N_o}\Delta\mathrm{F_{sc}} \\
\frac{1}{\gamma_{\mathrm{r}}} &\geqslant \quad \sigma_{\mathrm{ICI,k}}^2 + \frac{\mathrm{N_o}\Delta\mathrm{F_{sc}}}{\sigma_{\mathrm{s}}^2} \\
\frac{1}{\gamma_{\mathrm{r}}} &\geqslant \quad \sigma_{\mathrm{ICI,k}}^2 + \frac{1}{\gamma_{\mathrm{s}}} \\
\frac{1}{\gamma_{\mathrm{r}}} - \frac{1}{\gamma_{\mathrm{s}}} &\geqslant \quad \sigma_{\mathrm{ICI,k}}^2
\end{aligned} \tag{4.11}$$

Replacing the value of $\sigma_{\mathrm{ICI,k}}^2$ it can be written as

$$\begin{aligned}
\frac{1}{\gamma_{\mathrm{r}}} - \frac{1}{\gamma_{\mathrm{s}}} &\geqslant \quad \frac{\pi^2}{3}\phi_{\mathrm{k}}^2 \\
\frac{3}{\pi^2}\left(\frac{1}{\gamma_{\mathrm{r}}} - \frac{1}{\gamma_{\mathrm{s}}}\right) &\geqslant \quad \phi_{\mathrm{k}}^2 \\
\sqrt{\frac{3}{\pi^2}\left(\frac{1}{\gamma_{\mathrm{r}}} - \frac{1}{\gamma_{\mathrm{s}}}\right)} &\geqslant \quad \phi_{\mathrm{k}}
\end{aligned} \tag{4.12}$$

In other words it can be written as

$$\phi_{\mathrm{min_2}} = \sqrt{\frac{3}{\pi^2}\left(\frac{1}{\gamma_{\mathrm{r}}} - \frac{1}{\gamma_{\mathrm{s}}}\right)} \tag{4.13}$$

Final Limits on Residual Error Now that the two limits on the residual phase error have been found, the minimum between them needs to be chosen. In other words,

$$\begin{aligned} \phi_{\mathrm{k,max}} &\leq \min\left\{\phi_{\mathrm{min}_1}, \phi_{\mathrm{min}_2}\right\} \\ &= \min\left\{\frac{\mathrm{N}}{\mathrm{N_s}}\frac{1}{2^{\mathrm{b}+1}}, \sqrt{\frac{3}{\pi^2}\left(\frac{1}{\gamma_\mathrm{r}}-\frac{1}{\gamma_\mathrm{s}}\right)}\right\} \end{aligned} \tag{4.14}$$

With parameters from IEEE 802.11a [44], i.e. N = 64, $\mathrm{N}_s = 80$, $\gamma_r = 15$dB, $\gamma_s = 20$ dB, and b=1 and 2 for modulating pilots with BPSK and QPSK respectively, it can be found that, for this particular situation

$$\phi_{\mathrm{k,max}} \leq \phi_{\mathrm{min}_2} \tag{4.15}$$

Therefore it can be written that

$$\begin{aligned} \phi_{\mathrm{k,max}} \leq & \sqrt{\frac{3}{\pi^2}\left(\frac{1}{\gamma_\mathrm{r}}-\frac{1}{\gamma_\mathrm{s}}\right)} \\ 3\frac{1}{2\pi}\frac{\mathrm{N}}{\mathrm{L}\sqrt{\mathrm{M}\gamma}} + \mathrm{k}\zeta \leq & \sqrt{\frac{3}{\pi^2}\left(\frac{1}{\gamma_\mathrm{r}}-\frac{1}{\gamma_\mathrm{s}}\right)} \end{aligned} \tag{4.16}$$

The factor $k\zeta$ is very small and can be neglected from the calculations, thus it can be continued that, for

$$\gamma_\mathrm{s}\frac{1}{1+\frac{3}{4}\frac{1}{\mathrm{M}}\left(\frac{\mathrm{N}}{\mathrm{L}}\right)^2} > \gamma_\mathrm{r} \tag{4.17}$$

the system must be feasible to implement. For large values of M, this leads to

$$\gamma_s > \gamma_r \tag{4.18}$$

To state in words, as long as the required SNR of the pilot modulation is less than that of the data–sub–carriers, the scheme is feasible theoretically. An algorithm for implementing the above scheme will be presented in the next section. Its performance is also analyzed via simulation.

Algorithms for the proposed scheme Channel estimation and equalization can be assumed ideal for now, though imperfections can be modeled with equivalent SNR loss [45], [62]. Some SNR loss can be used in the model to account for channel estimation inaccuracies. Further, the constant carrier phase offset can be included

into the channel effect and thus after channel equalization the received signal of (4.1) becomes

$$R'_{l,k} = e^{j2\pi \frac{lN_s}{N}\phi_k} \frac{\sin(\pi\phi_k)}{\sin(\pi\frac{\phi_k}{N})} X_{l,k} + \sum_{i=0,i\neq k}^{N-1} e^{j\pi\phi_{k,i}} e^{j2\pi \frac{lN_s}{N}\phi_i} \frac{\sin(\pi\phi_{k,i})}{\sin(\pi\frac{\phi_{k,i}}{N})} X_{l,i} \frac{H_{l,i}}{H_{l,k}} + n'_{l,k} \quad (4.19)$$

Where $n'_{l,k}$ is the noise component changed due to channel equalization; this will be different depending upon the type of equalization scheme used. Zero Forcing algorithm causes noise enhancement at low SNR conditions. However, for the situation under analysis it is assumed that the data will be modulated using higher order QAM modulation, i.e. 256-QAM, 64-QAM, 16-QAM, etc. These require high values of SNR are greater than 15dB, and hence even with Zero Forcing channel equalization the noise enhancement will not be significantly large.

The proposed low complexity residual phase tracking algorithm in the *semi blind* system is presented next and compared against the performance of an exact algorithm. The 'exact algorithm' will be described later. It computes the exact phase angle using the inverse tangent function. Whereas, the proposed low complexity algorithm avoids the computation of the complex inverse tangent function.

The following symbols shall be used in the algorithm: $\beta_{l,k} = e^{j\theta_{l,k}} = e^{j2\pi l \frac{lN_s}{N}\phi_k}$ and $\alpha_{l,k} = e^{j\Delta\theta_k} = e^{j2\pi \frac{N_s}{N}\phi_k}$. It is further defined that $\beta_{0,k} = \alpha_{0,k} = 1, \quad \forall \quad k =$ pilot sub–carrier index. In this work pilot sub–carrier indices will be indicated by p instead of the usual k. It is also to be noted that p_i denotes the i^{th} pilot tone. The algorithm can now be written as

Step 1:

$$R'_{l,p}.\beta^*_{l-1,p} = \left(e^{j2\pi \frac{lN_s}{N}\phi_p} \frac{\sin(\pi\phi_p)}{\sin(\pi\frac{\phi_k}{N})} X_{l,p} + \sum_{i=0,i\neq p}^{N-1} e^{j\pi\phi_{p,i}} e^{j2\pi \frac{lN_s}{N}\phi_i} \frac{\sin(\pi\phi_{p,i})}{\sin(\pi\frac{\phi_{p,i}}{N})} X_{l,i} \frac{H_{l,i}}{H_{l,k}} + n'_{l,p} \right) e^{-j2\pi(l-1)\frac{lN_s}{N}\phi_p} \quad (4.20)$$

Under high SNR the second and the third term can be considered small and the multiplication of the complex exponential does not change their power, thus the equation can be approximated to

$$R'_{l,p}.\beta^*_{l-1,p} \approx e^{j2\pi \frac{N_s}{N}\phi_p} \frac{\sin(\pi\phi_p)}{\sin(\pi\frac{\phi_p}{N})} X_{l,p} \quad (4.21)$$

With a further assumption, that residual frequency offset is small, it can be approximated as

$$\begin{aligned} \mathrm{R}'_{\mathrm{l,p}}.\beta^{*}_{\mathrm{l-1,p}} &\approx \mathrm{e}^{\mathrm{j}2\pi\frac{\mathrm{N_s}}{\mathrm{N}}\phi_{\mathrm{p}}}\mathrm{X}_{\mathrm{l,p}} \\ &= \mathrm{e}^{\mathrm{j}\Delta\theta_{\mathrm{p}}}\mathrm{X}_{\mathrm{l,p}} = \mathrm{R}''_{\mathrm{l,p}} \end{aligned} \tag{4.22}$$

Where $R''_{l,p}$ denotes the estimate of the modulated pilot. This can be demodulated depending on the scheme used for modulating the pilot tones. Accordingly if a BPSK is used

$$\hat{\mathrm{X}}_{\mathrm{l,p}} = \begin{cases} +1 & \text{if Real}(\mathrm{R}''_{\mathrm{l,p}}) > 0 \\ -1 & \text{if Real}(\mathrm{R}''_{\mathrm{l,p}}) < 0 \end{cases} \tag{4.23}$$

The demodulation algorithm for QPSK can be derived similarly. Next it can be written that

$$\mathrm{R}''_{\mathrm{l,p}}.\hat{\mathrm{X}}^{*}_{\mathrm{l,p}} = \mathrm{e}^{\mathrm{j}\Delta\theta_{\mathrm{p}}}\mathrm{X}_{\mathrm{l,p}}\hat{\mathrm{X}}^{*}_{\mathrm{l,p}} = \alpha_{\mathrm{l,p}} \quad \text{since} \quad |\mathrm{X}_{\mathrm{l,p}}| = 1 \tag{4.24}$$

Continuing further with the algorithm, the following steps needs to executed next:

$$\hat{\alpha}_{\mathrm{l,p}} = \nu\hat{\alpha}_{\mathrm{l-1,p}} + (1-\nu)\mathrm{R}'_{\mathrm{l,p}}\hat{\mathrm{X}}_{\mathrm{l,p}}\mathrm{R}'^{*}_{\mathrm{l-1,p}}\hat{\mathrm{X}}^{*}_{\mathrm{l-1,p}} \tag{4.25}$$

$$\hat{\beta}_{\mathrm{l,p}} = \nu\hat{\beta}_{\mathrm{l-1,p}}\hat{\alpha}_{\mathrm{l,p}} + (1-\nu)\mathrm{R}'_{\mathrm{l,p}}\hat{\mathrm{X}}^{*}_{\mathrm{l,p}} \tag{4.26}$$

$$\text{where} \quad \hat{\alpha}_{\mathrm{l,p}} = \frac{\hat{\alpha}_{\mathrm{l,p}}}{|\hat{\alpha}_{\mathrm{l,p}}|}, \quad \hat{\beta}_{\mathrm{l,p}} = \frac{\hat{\beta}_{\mathrm{l,p}}}{|\hat{\beta}_{\mathrm{l,p}}|} \tag{4.27}$$

where ν is the memory of the algorithm, which is a design parameter. For the environment under discussion, a suitable value is $\frac{3}{4}$ which is found from simulation. The values of $\hat{\beta}$ are obtained at the pilot locations. With the help of the piecewise linear interpolation, the compensating complex factors can be computed. It has to be noted that instead of computing the phase angle, rather the complex exponential of the phase angle is computed in this algorithm. This will become more evident when compared with the steps of the exact algorithm which is explained in the next section. The straight solid line in Fig. 4.4 is the *actual phase* that needs to be estimated, while the curve is the sinusoid of the phase. In Fig. 4.4, $\xi = \delta$f, and C is a constant term. Estimation of the sinusoid at the pilot locations is being done here. There will be a sine and a cosine term, only one component is shown to retain the simplicity of the figure. They are approximated to be piece–wise–linear for small angles. Then the

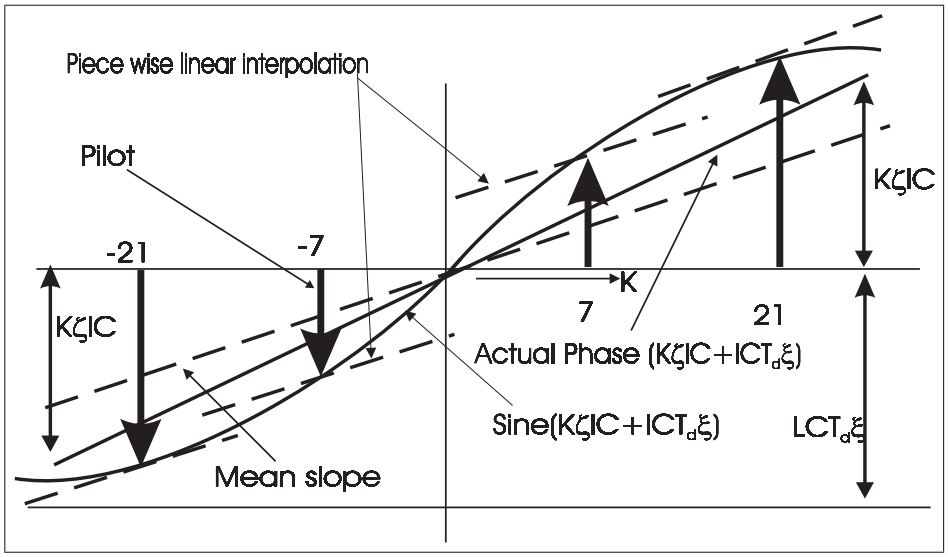

Figure 4.4: Piece-wise linear interpolation

mean slope of each of them is estimated as given below in (4.28).

$$m_l = \frac{1}{2}\left(\frac{\widehat{\beta}_{l,p_{21}} - \widehat{\beta}_{l,p_{-7}}}{21-(-7)} + \frac{\widehat{\beta}_{l,p_7} - \widehat{\beta}_{l,p_{-21}}}{7-(-21)}\right) \tag{4.28}$$

The subscripts of the pilot indexes denote the sub carrier index where pilots sub carrier are present. It needs to be noted that $\hat{X}_{l,p}$ is used in the algorithm. $\hat{X}_{l,p}$ is the estimated pilot symbol, reconstructed after detection, whereas in data aided algorithms, $P_{l,p}$ is used instead, which is the known pilot. The values in (4.28) are in reference to the IEEE 802.11a/g OFDM PHY standard.

Piece–wise–linear–interpolation is done to find the complex multiplication factor for each subcarrier for compensating the residual phase error as states below.

$$y_{l,k} = \widehat{\beta}_{l,p} - m_l(p-k) \tag{4.29}$$

Where p indicates the nearest pilot index to k^{th} subcarrier. Then for compensation we use $R'''_{l,k} = R'_{l,k} \cdot y^*_{l,k}$. The maximum errors that may occur will be at the farthest sub carriers (due to sampling frequency offset) where the difference is largest because of larger sub-carrier index (see (4.19) & Table 4.2).

The exact algorithm The exact algorithm which has been mentioned previously is described here. To follow the exact algorithm, (4.19)is taken as the starting point.

With the initial value of $\theta_{0,\mathrm{p}} = 0$, the algorithm can be started as

$$\mathrm{R}''_{\mathrm{l,p}} = \mathrm{R}'_{\mathrm{l,p}}.\mathrm{e}^{-\mathrm{j}\theta_{\mathrm{l}-1,\mathrm{p}}} \tag{4.30}$$

$\mathrm{R}''_{\mathrm{l,p}}$ denotes the estimate of the modulated pilot which is demodulated as explained in the previous section. Continuing further with the exact algorithm, the following can be stated.

$$\varphi_{\mathrm{l,p}} = \nu\varphi_{\mathrm{l}-1,\mathrm{p}} + (1-\nu)\mathrm{angle}(\mathrm{R}'_{\mathrm{l,p}}\hat{\mathrm{X}}_{\mathrm{l,p}}\mathrm{R}'^{*}_{\mathrm{l}-1,\mathrm{p}}\hat{\mathrm{X}}^{*}_{\mathrm{l}-1,\mathrm{p}}) \tag{4.31}$$

$$\vartheta_{\mathrm{l,p}} = \nu(\vartheta_{\mathrm{l}-1,\mathrm{p}} + \varphi_{\mathrm{l,p}}) + (1-\nu)\mathrm{angle}(\mathrm{R}'_{\mathrm{l,p}}\hat{\mathrm{X}}'^{*}_{\mathrm{l,p}}) \tag{4.32}$$

where $\mathrm{angle}(x) = \arctan(\frac{\mathrm{Imagimary}(x)}{\mathrm{Real}(x)})$ The phase angles estimated above are at the pilot locations. It is to be noted, that for this method, the inverse tangent function has to be executed two times, which becomes extremely computation intensive. Table look up is often used to avoid the complexity of its implementation, but this procedure is also limited when high resolution is required for small sized, low cost and low powered devices. Cordic implementation is also limited under such conditions of operation since they are slow. For compensation, the phase angles are interpolated using piece wise linear interpolation to all the data sub carrier indexes. The phase angles at the pilot locations can be explained as is depicted in Fig. 4.4. The mean slope of the phases at the pilot locations can be computed as

$$\psi_{\mathrm{l}} = \frac{1}{2}\left(\frac{\vartheta_{\mathrm{l,p}_{21}} - \vartheta_{\mathrm{l,p}_{-7}}}{21-(-7)} + \frac{\vartheta_{\mathrm{l,p}_{7}} - \vartheta_{\mathrm{l,p}_{-21}}}{7-(-21)}\right) \tag{4.33}$$

Piece–wise–linear–interpolation is done to find the compensating phase angle for each subcarrier as:

$$\hat{\vartheta}_{\mathrm{l,k}} = \vartheta_{\mathrm{l,p}} - \psi_{\mathrm{l}}(\mathrm{p}-\mathrm{k}) \tag{4.34}$$

Where p indicates the nearest pilot index to k^{th} subcarrier. For compensation the following needs to be used

$$\mathrm{R}'''_{\mathrm{l,k}} = \mathrm{R}'_{\mathrm{l,k}} \cdot \mathrm{e}^{-\mathrm{j}\hat{\vartheta}_{\mathrm{l,k}}} \tag{4.35}$$

In a data aided, non blind situation, the $\hat{\mathrm{X}}_{\mathrm{l,p}}$ is replaced by $\mathrm{P}_{\mathrm{l,p}}$ (known pilot sequence at receiver) in the steps of the above two algorithms described.

4.4 Simulation and Discussion

Simulation Parameters The parameters used for simulation are similar to that in IEEE 802.11g [11]. The carrier frequency is taken as 5.4 GHz. Sampling frequency offset is taken as 20 ppm, with 20 MHz of sampling frequency. Different values of *residual* carrier frequency offset are used and are mentioned in the simulation result curves. The number of sub carriers N is taken as 64. Number of zero sub carriers = 12, number of data sub carriers were 48 and number pilot sub carriers were 4. The GI $T_g = 0.8\mu$s, while the symbol duration $T_s = 4\mu$s and the useful symbol duration $T_u = 3.2\mu$s is used. Different combinations of data sub carrier modulation and pilot modulation is used. They are described on the simulation result curves.

The proposed low complexity algorithm is represented as alg1 (solid lines) in the figures. The exact algorithm is denoted by alg2 (dotted lines) which is run in the proposed semiblind environment. A completely data aided OFDM based system, following the IEEE 802.11a/g frame format, using the exact algorithm is marked as alg3 in the figures.

In WLAN environment, the channel is assumed to be quasi static during the entire period of a packet. Therefore Doppler frequency spread can be neglected. The proposed semi blind pilot scheme is to be used when data sub carriers will have high order modulation. This occurs only when the average SNR is quite high. The channel estimation using the long training sequence can be considered to suffer from little error under these conditions. Further the residual phase error is independent of the channel properties. Therefore for simplicity AWGN channel has been used in the analysis here. FEC is not used.

Results and Discussion The simulation related to Fig. 4.5 has data sub carriers modulated with 64–QAM, while the pilot sub carriers modulated with BPSK. The CFO mentioned in the figures indicates the *residual* carrier frequency offset in *ppm*. The result in Fig. 4.6 shows performance of the algorithms similar the previous case but with QPSK modulation on the piots. An important observation to be made in these two results is that, the performance of the exact algorithm, be it the proposed semi blind case or the commonly used completely data aided case(alg 2 and alg 3), is almost the same. Therefore, it is now seen that the known sequence of pilot as is transmitted in WLAN systems based on IEEE 802.11a/g frame format is not a necessity. It is also seen that the exact algorithms (alg 2 and alg 3), perform slightly better (on an average about 2dB) than the proposed low complexity algorithm (alg1).

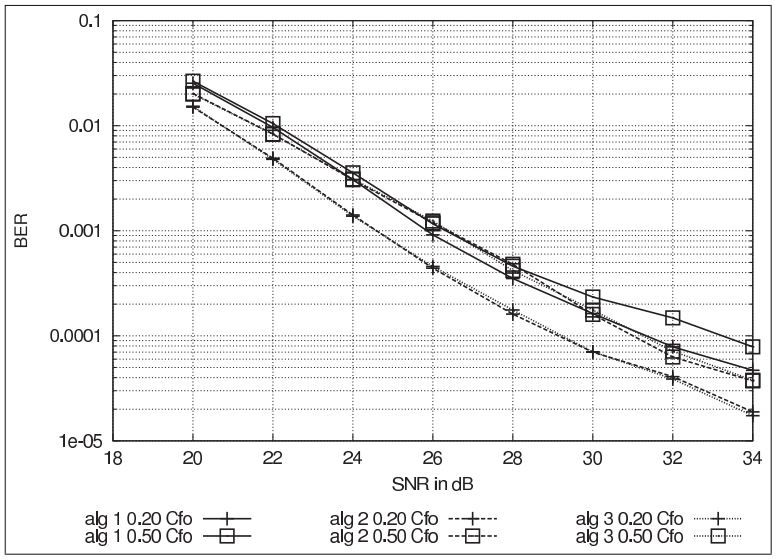

Figure 4.5: BER Vs SNR, Data→64-QAM, pilot→BPSK.
alg3 → completely data aided pilot based OFDM system, using the exact algorithm.
alg2 → the exact algorithm in the proposed semiblind environment.
alg1 → the proposed low complexity, approximated algorithm.

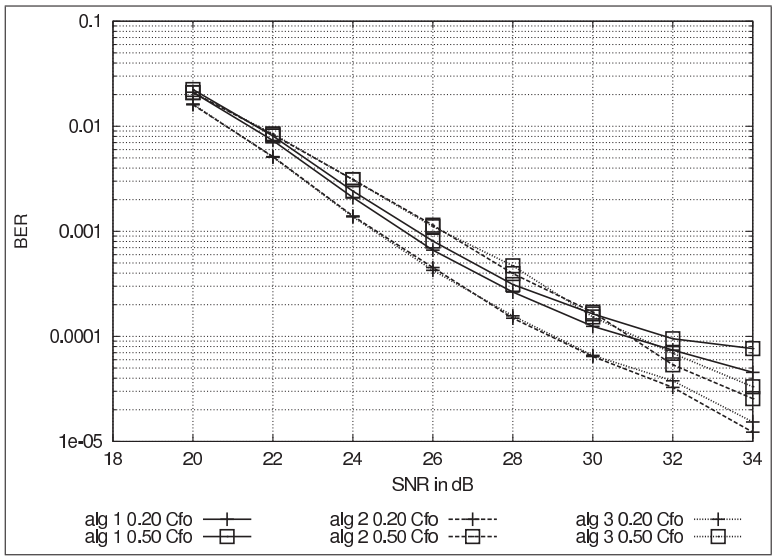

Figure 4.6: BER Vs SNR, Data→64-QAM, pilot→QPSK

Viewed in another way, the degradation of the low complexity algorithm is less than one order in terms of Bit Error Rate (BER), at a given Signal to Noise Ratio (SNR). Therefore it can also be said that the approximate algorithm, can be used in low complexity, low powered devices due to significant amount of reduction in complexity without much loss in performance.

The result in Fig. 4.7 has data sub carriers modulated with 16–QAM, while BPSK is used for the pilots. It has similar characteristics as previous results for lower residual phase error. An important observation to be made is that for high residual phase errors (near and above CFO = 0.5 ppm), the exact algorithms (2 and 3) fail, while the proposed approximate low complexity one continues to perform well. The reason for this behavior is that the residual phase error increases with OFDM symbol index, i.e. with time. If the accumulated residual phase reaches values near $\pi/2$, the exact algorithm using inverse tangent function becomes unstable. This is not the case for the proposed algorithm, which completely avoids the computation of the inverse tangent function. This is one of the added benefits of the proposed algorithm. Results in figures 4.8 and 4.9 are in accordance with the above.

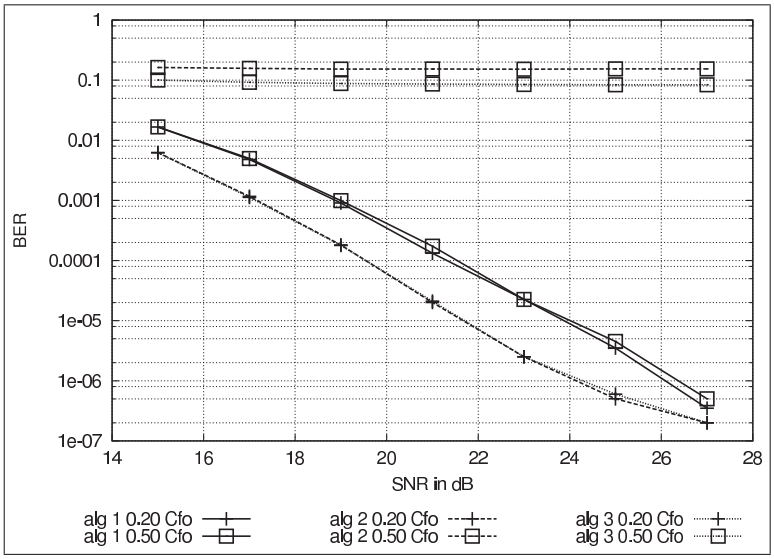

Figure 4.7: BER Vs SNR, Data→16-QAM, pilot→BPSK

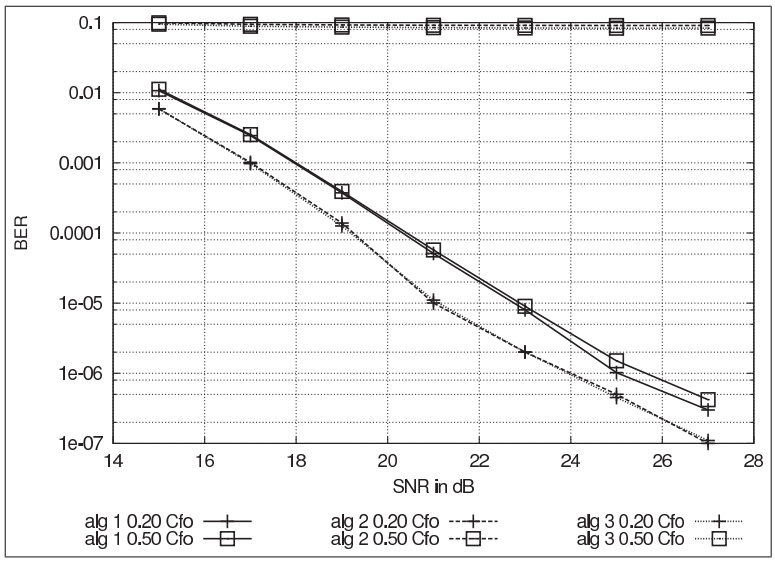

Figure 4.8: BER Vs SNR, Data→16-QAM, pilot→QPSK

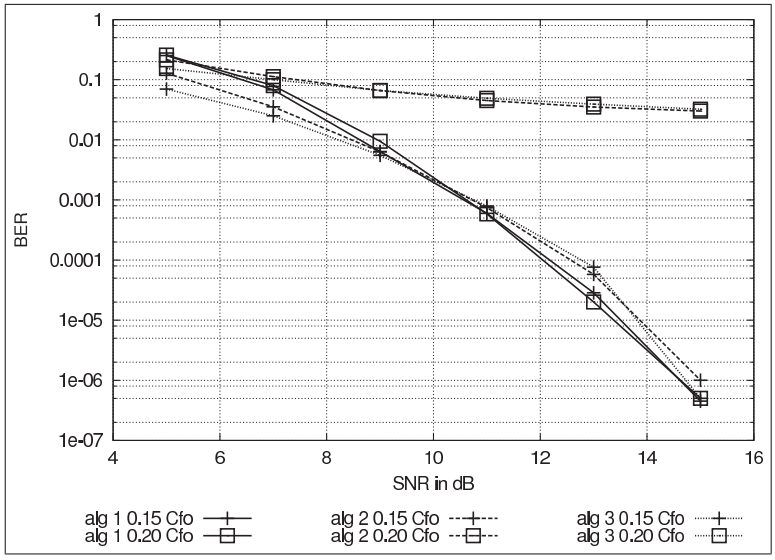

Figure 4.9: BER Vs SNR, Data→QPSK, pilot→BPSK

The additional data rate gained in this scheme can be computed as $\frac{N_p.N_{bp}}{T_s}$. N_p represents the number of pilots, N_{bp} indicates number of bits carried by each pilot. The percentage gain can be computed by the formula $100.\frac{N_p.N_{bp}}{N_{bd}.N_d}$, where N_{bd} implies, number of bits per data sub carrier and N_d implies, number of data sub carriers. The increase in data rate is summarized in Table 4.3. These values are based on IEEE 802.11a/g frame structure, which is a single user system. Much higher gain can be achieved in systems which need more pilots, especially for outdoor and multi–user OFDMA schemes.

Table 4.3: Semi Blind Configurations and gains

data-rate (mbps)	data-modulation	pilot-modulation	increase (Mbps)	% gain	Enhanced rate (Mbps)
12/18	QPSK	BPSK	1	∼5-8	19
12/18	QPSK	QPSK	2	∼11-16	20
24/36	16-QAM	BPSK	1	∼3-4	26
24/36	16-QAM	QPSK	2	∼5-8	38
48/54	64-QAM	BPSK	1	∼2-3	50(51)
48/54	64-QAM	QPSK	2	∼4-6	56(57)

4.5 Conclusion

In this chapter it has been shown that the proposed semiblind pilot scheme is viable, i.e. it is possible to transmit data information on the pilot tones, without loss in performance or requiring additional resource. This proposed technique provides up to two Mbps increase in data rate. An algorithm has been described to implement the proposed scheme. Depending on the data rate chosen, pilot sub carrier can be loaded with QPSK or BPSK adaptively based on the SNR margin available. In systems where more pilots are necessary, the proposed scheme can yield much more benefit.

Since with the proposed semi blind pilot scheme, the overhead due to pilot sub carriers can be reduced, therefore, instead of transmitting additional information bits, the proposed semiblind pilot technique can be exploited to add more pilots to the system for better estimation of the residual phase error which will lead to better BER performance. Adding more pilot sub carriers would require a higher overhead, however since the pilots can carry some data bits now, the pilot overhead can be compensated by overloading the pilots with the bits as described in this Chapter.

In addition to the above, a low complexity residual phase tracking algorithm in a semi blind system has been proposed to avoid the use of the highly complex inverse tangent function. The algorithm has also been compared against the exact algorithm, which uses the inverse tangent function to compute the residual phase, operating in a completely data aided system. The results show, that the performance degradation of the low complexity algorithm is within 1–2 dB, for very small residual phase. For comparatively larger residual phase errors the proposed low complexity algorithm is found to be more stable as compared to the exact algorithm. The reduction in complexity achieved by the proposed algorithm for residual phase tracking is quite significant when small, low powered, low complexity hand held and body worn next generation wireless communicating devices are considered. The algorithm reduces complexity by avoiding the computation of the highly complex inverse tangent function, which requires more than sixty arithmetic operations for series expansion implementation.

Finally it can be concluded that the proposed semi blind system performs as good as the currently used data aided phase tracking system. This gives a scope of increasing the efficiency of a standard OFDM based WLAN system by up to sixteen percent for IEEE 802.11a/g type systems. Much more gain is expected for schemes which need more pilots such as outdoor multi–user OFDMA systems. The good performance of the proposed low complexity algorithm in the semi blind environment makes it even more attractive.

5

Adaptive Sub Carrier Bandwidth

In the previous chapter, a technique to overload the pilot sub carriers in order to increase the spectral efficiency of the system has been discussed. The focus of this chapter is to present another novel transmission technique which has the potential to enhance the spectral efficiency of OFDM in Doppler frequency spread channel conditions. The proposed scheme does not demand a significant increase in the signal processing complexity of User Equipment (UE) to improve the spectral efficiency.

OFDM based wireless systems support very high spectral efficiency, but their performance is severely impaired by Inter Carrier Interference (ICI). ICI is introduced by frequency synchronization errors. Doppler frequency spread, due to terminal mobility, is one of the major contributors to ICI in OFDM systems. Many schemes to reduce ICI have been proposed, but they are very complex and some reduce system efficiency. ICI is proportional to the received signal strength and Doppler frequency spread. In a wide area since users will experience various signal strength due to path loss and shadowing, and since the amount of Doppler will be different for each user because of independent velocities, the ICI experienced by the users will vary over a wide range. For a certain amount of frequency shift, the ICI is inversely proportional to the sub carrier bandwidth. Therefore, it is proposed in this work to dynamically adapt the sub carrier bandwidth along with adaptive bit loading to overcome the

effect of ICI. This scheme avoids the need for complex interference algorithms at the receiver while making the system optimum for each situation. The focus of this chapter is to describe the architectures and analyze the performance of the proposed Adaptive Sub Carrier Bandwidth (ASB)-OFDM systems. Results show that ASB can provide higher throughput than its Fixed Sub Carrier Bandwidth (FSB) counterpart when both may use adaptive bit loading per sub carrier.

This chapter contains two sections. Each section analyzes a different implementation architecture for adaptive sub carrier bandwidth.

5.1 Adaptive Sub Carrier Bandwidth in TDM-OFDM

Frequency synchronization errors come from residual carrier frequency offset, sampling frequency offset, phase noise and Doppler frequency spread. Residual carrier offset is present due to non ideal performance of the carrier synchronization algorithm at the receiver. Sampling frequency offset is present due to clock frequency mismatch [45]. Phase noise arise because of imperfections in the local oscillators [68]. Doppler frequency spread is caused due to user mobility and movement of reflectors. Doppler frequency spread consists of multiple of frequency offsets as each multi path may have a different frequency shift [20]. Since carrier synchronization algorithms are designed to track only one frequency offset, it becomes difficult to eliminate the frequency spread due to Doppler. These impairments cause loss in orthogonality between the sub carriers and give rise to ICI and which severely limits the performance of OFDM systems [69],[70]. ICI is proportional to the received signal strength. It is also proportional to the square of the residual carrier offset plus Doppler frequency spread and is inversely proportional to the sub carrier bandwidth. Most approaches to combat ICI are towards using frequency synchronization or interference cancelation [19, 21]. They are usually very complex and sometimes there is loss in bandwidth efficiency. An important aspect which is not considered by these methods is that the amount of ICI is not same in all receivers under one coverage area. This is because the signal strength and mobility conditions of users, on which the amount of ICI is dependent, vary across a wide range. Another consideration is that different users will have different BER requirements depending on the service. These algorithms do not address this issue.

In all existing systems, the sub carrier bandwidth is kept constant. The bandwidth is chosen large enough to tolerate a certain amount of Doppler spread. In a different approach to mitigate ICI, Adaptive Sub Carrier Bandwidth (ASB) can

be used since ICI is inversely proportional to the sub carrier bandwidth for certain maximum frequency offset. Such methods are expected to relieve the receiver from implementing the complex ICI cancelation schemes. Authors in [71] shows the impact of varying the number of sub carriers[1] but do not discuss its dynamic realization. To address the target of satisfying a required bit error rate (BER) while maximizing the throughput, adaptive bit loading [26] can be used in conjunction with ASB.

This kind of a novel OFDM system, which can adaptively select the sub carrier bandwidth and bit loading based on Doppler condition, signal strength and BER requirement is being proposed and analyzed here.

5.1.1 System Description

One implementation of ASB can be based on Time Division Multiplexing (TDM) system. The number of sub carriers in different slots may be changed to generate different sub carrier bandwidths. Users with similar requirement of sub carrier bandwidth may share a time slot. The time frequency diagram can appear as in Figure 5.1. This model is used for analysis via simulation in this work. Among other possible

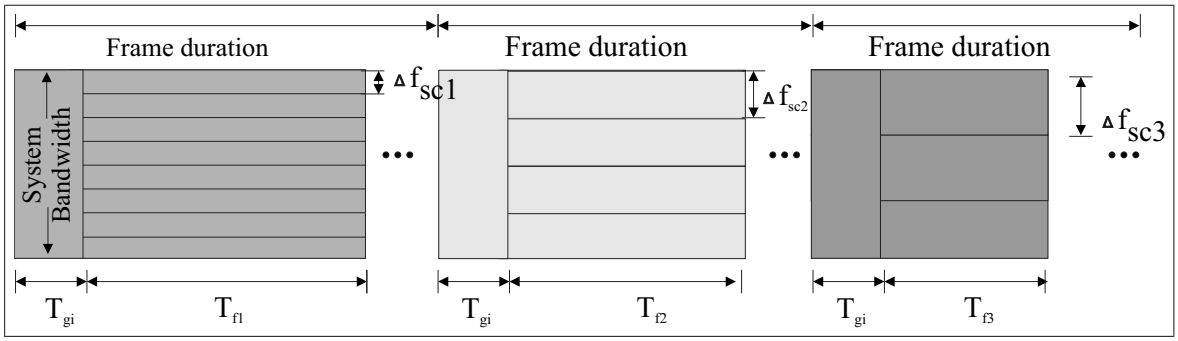

Figure 5.1: Time frequency diagram for the proposed TDM based ASB OFDM

implementations, another one can be Band Division Multiplexing (BDM) based as in Fig. 5.2. The entire available bandwidth may be divided into sub–bands with different sub carrier bandwidth in each sub band for example a 100 MHz may be divided into chunks of 20 MHz, 10 MHz or 5 MHz. Each sub band can be operated on by an IFFT with different number of sub carriers. The User Equipment (UE) is assumed to require only one type of sub carrier bandwidth and hence will operate on only one sub–band. Therefore only one Programable FFT [72] is needed for the user equipment. With a changing requirement of the sub carrier bandwidth the clock

[1]For a given system bandwidth varying the number of sub carriers implies a variation in the sub carrier bandwidth.

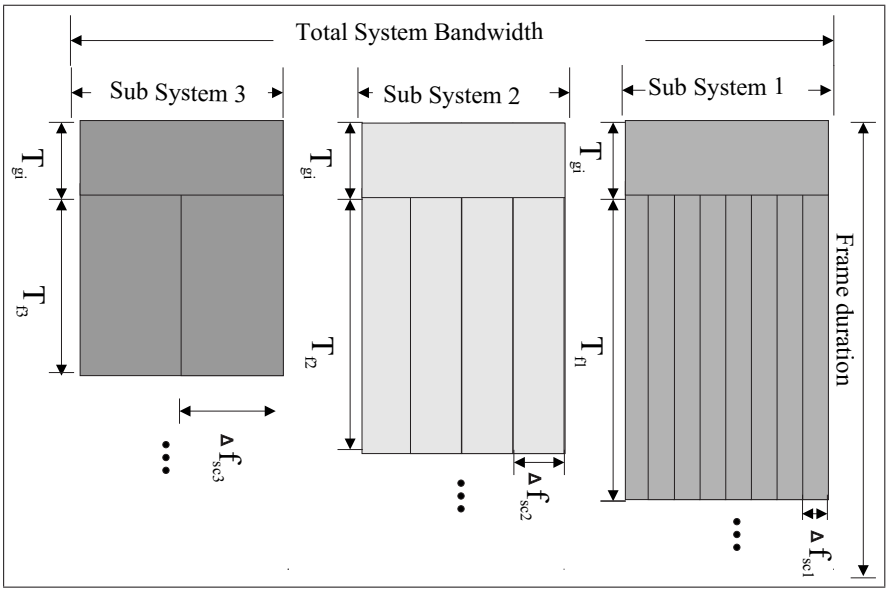

Figure 5.2: Time frequency diagram of the proposed ASB with BDM OFDM

and the FFT size of the programable FFT may be dynamically configured. At the base station, as many FFTs may be used as there are different types of sub carrier bandwidths.

As mentioned earlier, adaptive bit loading is done along with ASB. Though joint bit and power adaption is optimal, it has been observed that the gain obtained in keeping power constant while varying the rate is very close to being optimal [26]. Therefore the power per sub carrier is fixed and equally distributed on all data sub carrier. The rate is varied on each sub carrier by means of adaptive modulation. The study will be restricted to systems without forward error control (FEC) coding, as was done in [26] to analyze potential of the scheme.

5.1.2 Analytical Model

The time domain signal of the s^{th} transmitted OFDM symbol is defined in (2.19) – (2.22). The received signal is given in (3.11)– (3.14). In continuation to the above $\phi(k, k', \epsilon) = k - k' + \epsilon$, $\omega[s, k']$ is taken as the frequency domain noise component per sub carrier bandwidth. The symbol $H[s, k']$ is used as the channel coefficient for k'^{th} sub carrier of s^{th} OFDM symbol instead of $H_s[k']$ which was used earlier. For the simplicity of notation, the index s is dropped where ever it is not needed. $X[s, k']$ is zero mean, which implies that the interference term is also zero mean. The power of

the interference term due to ICI is then the same as its variance, which becomes,

$$\sigma^2_{\mathrm{ICI}_{\mathrm{X[k']}}} = \mathrm{E}[|\mathrm{X[k]}|^2] \sum_{\substack{\mathrm{k}=-\frac{\mathrm{N_f}}{2}, \\ \mathrm{k}\neq\mathrm{k}^{'}}}^{\frac{\mathrm{N_f}}{2}-1} |\mathrm{H[k]}|^2 \mathrm{sinc}^2\left(\pi(\frac{\delta \mathrm{f}}{\Delta \mathrm{f_{sc}}} + \mathrm{k} - \mathrm{k}^{'})\right), \tag{5.1}$$

where 'E' is the expectation operator. Replacing $\mathrm{E}[|\mathrm{X[k]}|^2]$ by $\mathrm{P_{X[k]}}$ which is the average power per sub carriers, and, $|\mathrm{H[k']}|^2$ by $\mathrm{P_{H[k']}}$, the ICI power at the receiver on sub carrier 'k$^{'}$' is:

$$\sigma^2_{\mathrm{ICI}_{\mathrm{X[k']}}} \approx \mathrm{P_{X[k]}P_{H[k']}} \sum_{\substack{\mathrm{k}=-\frac{\mathrm{N_f}}{2}, \\ \mathrm{k}\neq\mathrm{k}^{'}}}^{\frac{\mathrm{N_f}}{2}-1} \mathrm{sinc}^2\left(\pi(\frac{\delta \mathrm{f}}{\Delta \mathrm{f_{sc}}} + \mathrm{k} - \mathrm{k}^{'})\right). \tag{5.2}$$

It is assumed that the coherence bandwidth is large enough, so that the channel coefficients are the same for the most significant (neighboring) sub carriers [45]. Also, for small values of $\delta \mathrm{f} \Delta \mathrm{f_{sc}}$ [45],

$$\sigma^2_{\mathrm{ICI}_{\mathrm{X[k']}}} \approx \sigma^2_{\mathrm{ICI}_{\mathrm{X[k']}}} \approx \frac{1}{3}\mathrm{P_{X[k]}P_{H[k']}}(\pi\frac{\delta \mathrm{f}}{\Delta \mathrm{f_{sc}}})^2. \tag{5.3}$$

Therefore signal to interference plus noise ratio (SINR) is

$$\Upsilon_{\mathrm{rx}}[\mathrm{k}^{'}] \approx \frac{\mathrm{P_{X[k']}P_{H[k']}sinc}(\pi\frac{\delta \mathrm{f_c}}{\Delta \mathrm{f_{sc}}})^2}{\sigma^2_{\omega} + \frac{1}{3}\mathrm{P_{X[k]}P_{H[k']}}(\pi\frac{\delta \mathrm{f}}{\Delta \mathrm{f_{sc}}})^2}. \tag{5.4}$$

Figure 5.3 shows the plot of the average SINR vs sub carrier bandwidth for different velocity conditions. Each curve is for a particular velocity. It can be seen from this figure, that SINR improves with increasing sub carrier bandwidth for a given Doppler spread. But this does not ensure a monotonically increasing throughput with increasing sub carrier bandwidth. This can be seen from Figure 5.4. This figure shows that the throughput, for a given Doppler velocity, is maximum for a certain sub carrier bandwidth only. The throughput curves have been obtained by considering adaptive bit loading per sub carrier, which is discussed later. The decrease in throughput after a certain sub carrier bandwidth can be attributed to the increasing sub carrier bandwidth which causes the OFDM symbol duration to decrease thereby increasing the overhead due to guard interval. This can be understood by referring to (1.1). The

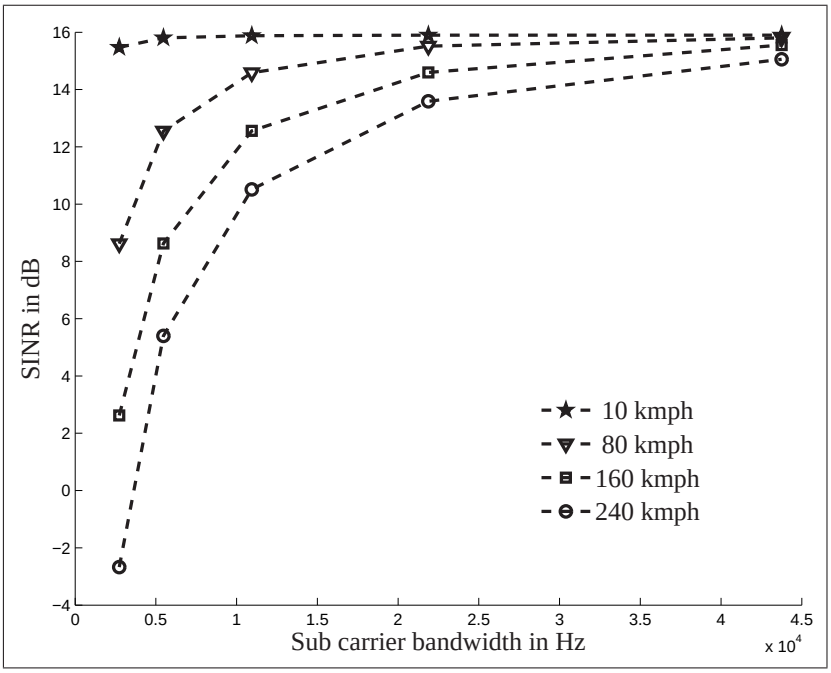

Figure 5.3: SINR vs sub carrier bandwidth at 15dB SNR

Guard Interval (GI) which is decided based on the channel delay spread is mostly fixed and should not change with the change in sub carrier spacing. As long as the length of GI is sufficiently large so that ISI is within tolerable limits the choice of sub carrier bandwidth and choice of GI can be treated independently. The next chapter of this thesis presents an analysis on the choice of GI. For the above it can be seen that by choosing the appropriate sub carrier bandwidth there is potential for significant improvement in throughput.

5.1.3 Algorithm for Adaptive Bandwidth for Sub Carriers

An algorithm is proposed here to dynamically select the appropriate sub carrier bandwidth and bit load per sub carrier to maximize the throughput while satisfying a required BER constraint. The sub carrier bandwidth can be chosen as

$$\Delta f_{chosen} = \arg\max_{\Delta f_m}[Thpt(\Delta f_m)], \quad (5.5)$$

such that

$$\Delta f_m < B_c, \text{ where } B_c \text{ is the coherence bandwidth, and} \quad (5.6)$$

$$T_s < T_c, \text{ where } T_c \text{ is the coherence time. [34]} \quad (5.7)$$

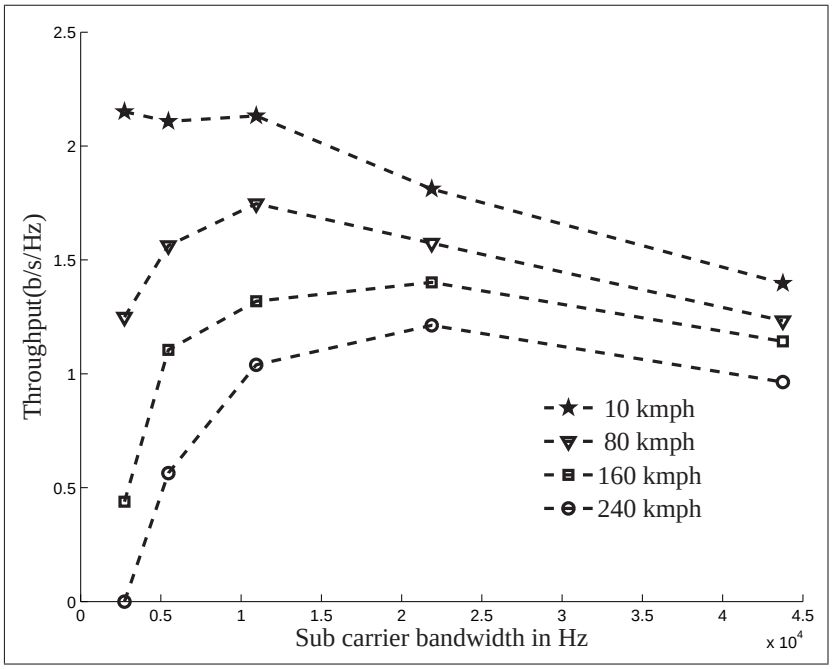

Figure 5.4: Throughput vs sub carrier bandwidth at 15dB SNR

The index 'm', runs through the allowable sub carrier bandwidths (out of a finite number of options) while meeting the constraints of coherence bandwidth and coherence time as mentioned above. The estimated throughput $\mathrm{Thpt}(\Delta \mathrm{f_m})$ in (5.5) can be written as

$$\frac{1}{\mathrm{B_w}(\frac{1}{\Delta \mathrm{f_m}} + \mathrm{T_{gi}})} \sum_{\mathrm{k}=-\frac{\mathrm{N_f}}{2}}^{\frac{\mathrm{N_f}}{2}-1} \mathrm{b_L}(\mathrm{k}, \Delta \mathrm{f_m})(1 - \mathrm{b_o}(\mathrm{k}, \Delta \mathrm{f_m})). \tag{5.8}$$

In the above expression $\mathrm{B_w}$ denotes the system bandwidth. The bit load estimate per sub carrier used in (5.8), assuming square constellation (QAM) can be expressed from [26] as,

$$\mathrm{b_L}(\mathrm{k}, \Delta \mathrm{f_m}) = 2\lfloor \frac{1}{2} \log_2 \left(1 \ - \frac{1.6}{\ln(\frac{\mathrm{b_{o\ req}}}{0.2})} \Upsilon_{\mathrm{rx}}(\mathrm{k}, \Delta \mathrm{f_m}) \right), \rfloor \tag{5.9}$$

where $\lfloor . \rfloor$ is the floor operation, which has been introduced as a square constellation such as QAM in considered to be used. In the above, $\mathrm{b_{o\ req}}$ is the target BER which is to be satisfied. The BER associated with the chosen bit load is [26]

$$\mathrm{b_o}(\mathrm{k}, \Delta \mathrm{f_m}) = 0.2e^{-\frac{1.6\Upsilon_{rx}(\mathrm{k}, \Delta \mathrm{f_m})}{2^{\mathrm{b_L}(\mathrm{k}, \Delta \mathrm{f_m})}-1}}, \tag{5.10}$$

which is tight for high SNR and has been claimed in [26] to be valid within 1.5dB for 4-QAM to 1024-QAM for bit error rate BER$\leq 10^{-3}$. The expression $\Upsilon_{rx}(\mathrm{k}, \Delta\mathrm{f_m})$ used above is taken as

$$\Upsilon_{\mathrm{rx}}(\mathrm{k}, \Delta\mathrm{f_m}) \approx \frac{\mathrm{P_{X[k]}P_{H[k]}sinc}(\pi\frac{\delta\mathrm{f}}{\Delta\mathrm{f_m}})^2}{\sigma_\omega^2 + \frac{1}{2}(\frac{\pi\delta\mathrm{f}}{\Delta\mathrm{f_m}})^2\mathrm{P_{X[k]}P_{H[k]}}}. \tag{5.11}$$

Executing of the Algorithm for ASB: The following steps may be executed in sequence to implement the above algorithm.

1. Select one sub carrier bandwidth from the available options.
2. Evaluate (5.11), i.e. SINR at each sub carrier for the selected sub carrier spacing. For the calculations, δf has to be estimated using advanced schemes such as [73].
3. Use the above in finding bit load for this chosen value of sub carrier spacing following (5.9).
4. Calculate the associated BER for each sub carrier for the chosen bit load using (5.10).
5. Use the above calculations of bit load and related BER for each sub carrier in calculating the throughput for the chosen sub carrier bandwidth following (5.8).
6. Store the value of the estimated throughput along with the value of sub carrier bandwidth and associated bit loads per sub carrier.
7. Repeat the above steps for all possible values of sub carrier bandwidth.
8. Finally execute (5.5) to select the sub carrier bandwidth and bit loads per sub carrier which has the highest estimated throughput.
9. The rate of change of Doppler condition and average channel quality is much slower compared to the rate of change of channel coefficients. Therefore it can be considered to adapt the sub carrier spacing, which is related to the Doppler and average SNR condition, at a slower rate than adapting the bit load which is related to the instantaneous channel gains. The bit loading should be done once per coherence time of the channel coefficients. i.e. once a sub carrier spacing is selected, it may be used until the Doppler condition or the average signal strength changes significantly and hence step 1 and step 7 may be skipped, and step 8 may be modified to read: Finally execute (5.5) to select bit loads per sub

carrier which has the highest estimated throughput for the chosen sub carrier bandwidth.

The overhead for signalling the bit load and chosen sub carrier bandwidth depends on the rate of signalling, number of bits used and also on the feedback mechanism. For simplicity of analysis but to keep the results realistic, it is assumed that BPSK is used for signalling the feedback information. It is also assumed that number of bits per feedback is taken as '$\log_2$[n(X)]', where 'n(X)' denotes the number of signalling levels for 'X' where 'X' is the feedback parameter. The rate of feedback of the bit loading parameter which depends on the channel gains is done once per coherence time per coherence bandwidth, while that for the maximum Doppler frequency offset which affects the selection of the sub carrier spacing is done once per second. This overhead which will vary as a function of the channel statistics is considered in the simulations. An example of a typical overhead calculations is shown in the later chapters on Link Adaptation.

5.1.4 Results and Discussion

Each coefficient of the time domain channel impulse response is taken as Rayleigh distributed with Jakes' [34] spectrum. Exponential power delay profile with rms delay spread of 2 micro seconds is used. Bandwidth of 5 MHz at carrier of 3.6 GHz is considered. The target BER is kept at 10^{-2}. To implement Adaptive Sub Carrier Bandwidth (ASB) in the simulations the TDM mode (Figure 5.1) is taken. Number of bits that can be loaded on a sub carrier are 0,2,4,6,8 and 10, where '0' means no transmission. The curves labeled 2048, 1024,...,128, are for systems with fixed sub carrier bandwidth using as many sub carriers for the 5 MHz channel bandwidth. These numbers correspond to 2.4 KHz to 39.063 KHz of sub carrier bandwidth. The options for number of sub carries (sub carrier bandwidth) for the proposed ASB system is selected from this range. The curve labeled with ASB, is for the proposed adaptive sub carrier bandwidth system.

Figure 5.5 shows the average sub carrier spacing selected by ASB scheme for different values of velocity at a received SNR of 15 dB. The increase in average value of sub carrier bandwidth selected with increasing velocity can be easily seen.

Now the throughput of ASB system is compared against FSB systems. The throughput of FSB system is computed considering adaptive bit loading per sub carrier as is considered for the ASB system. If Δf_{sc} is the sub carrier bandwidth, then the throughput is calculated using (5.8)–(5.11) where Δf_m is replaced by Δf_{sc}.

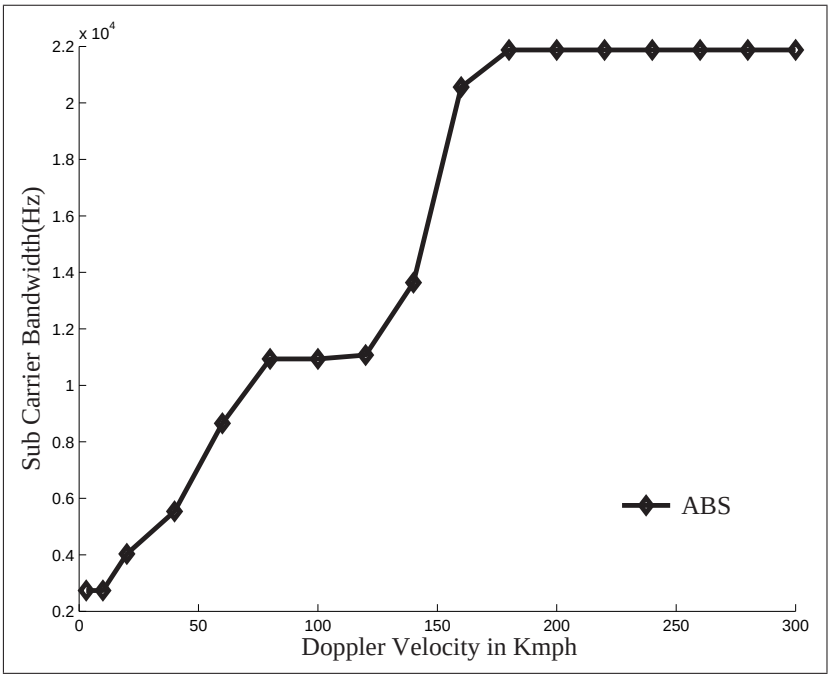

Figure 5.5: Sub carrier bandwidth selected by the proposed ASB system.

Figure 5.6 compares the throughput for ASB scheme against standard OFDM systems with fixed number of sub carrier bandwidth for different values of the number of number carriers at 15 dB SNR. It is clearly seen that a given sub carrier bandwidth has the highest throughput over a small range of velocity, while ASB has the highest throughput over the entire range. The system with 2048 sub carriers ($\Delta f_{sc} = 2.4$KHz) is best for mobility less than 10kmph. Between 10 and 40 kmph system with 1024 sub carriers ($\Delta f_{sc} = 4.88$KHz) has the highest performance. Between 40 kmph and 140 kmph, the one with 512 sub carriers ($\Delta f_{sc} = 9.77$KHz) is the most efficient, beyond which the system with 256 sub carriers ($\Delta f_{sc} = 19.531$KHz) is the best. It can be noted that the ASB system rides the envelope, i.e. it has the highest throughput over all velocities.

In the low mobility region ASB is better than one using 512 sub carrier by about 12% and about 25% better than one using 256 sub carriers. In the high mobility region (near 200 kmph) ASB is better than system with 512 sub carriers by about 25% and by more than 30% over system with 1024 sub carriers, when the one with 2048 sub carriers which is best for low mobility almost fails.

Figure 5.7 shows similar curves as above but for a higher SNR (25 dB). Comparing with the previous figure, one can clearly find that the difference in received signal strength has caused the optimal range for each OFDM system (with different but fixed sub carrier bandwidth) to change, but ASB is still the most efficient in the

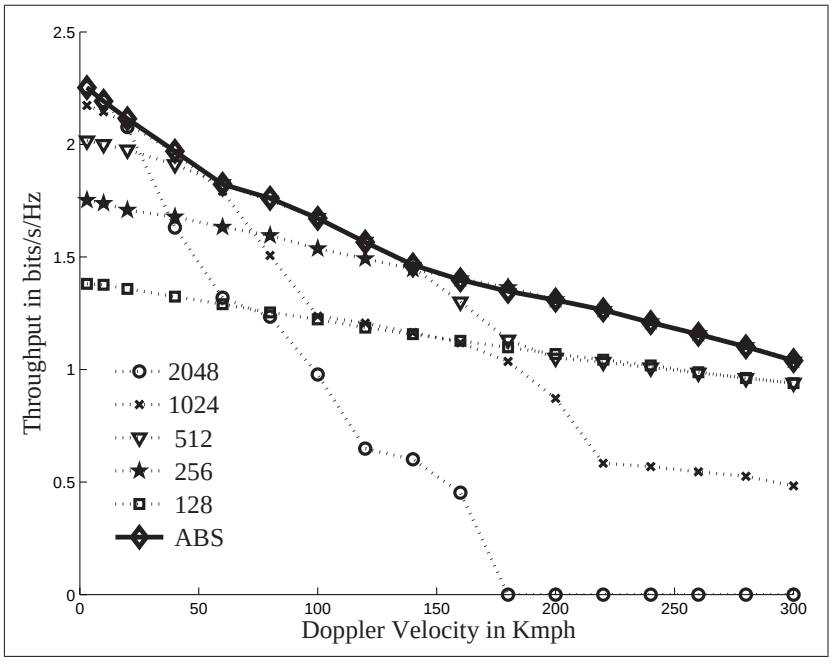

Figure 5.6: Throughput comparison of the proposed ASB vs standard FSB OFDM systems, at 15 dB SNR.

entire range. Between 0 and 10 kmph, it is seen that 2048 has the highest efficiency, between 10 and 50 kmph, the system with 1024 sub carriers is found to be optimal, between 50 kmph and 90 kmph, the system with 512 sub carriers is optimal, beyond which it is seen that the system with 256 is optimal. The ASB scheme is better than the fixed sub carrier bandwidth system by about 10% to 30% in different velocity regions. Finally Figure 5.8 shows the BER curves for all systems. It can be observed that by use of Adaptive Bit Loading (ABL), the BER is maintained below the target level (10^{-2}) for all system and for all velocities. Though the target BER is satisfied by both schemes (ASB and FSB) using ABL, it can be said that ABL alone is not sufficient for FSB OFDM system to be efficient in all Doppler conditions. ASB with ABL improves the throughput by a significant amount.

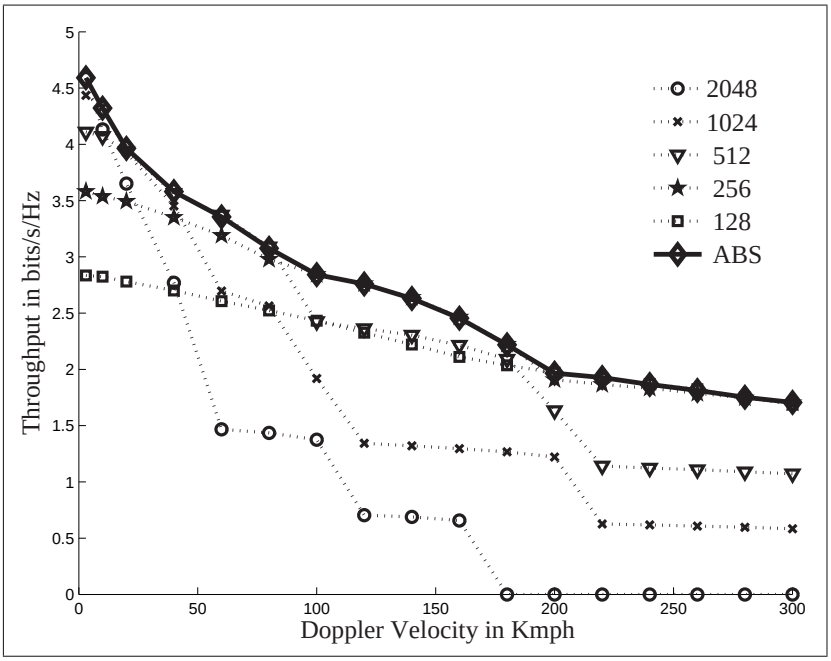

Figure 5.7: Throughput comparison of the proposed ASB vs FSB OFDM systems, at 25 dB SNR.

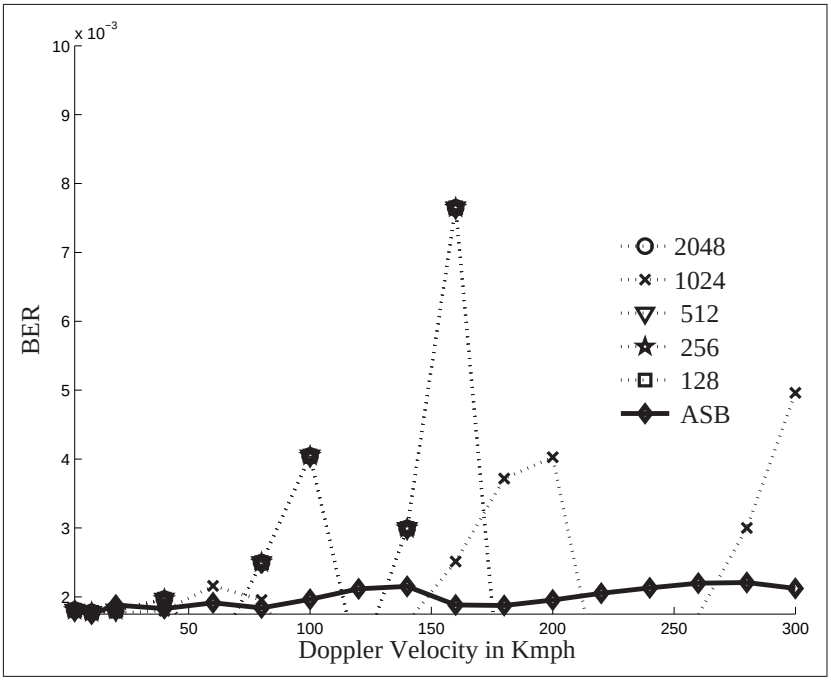

Figure 5.8: BER of the proposed ASB and FSB OFDM systems at 15 dB SNR, when target BER is 0.01

5.1.5 Conclusion

It can be concluded that the proposed Adaptive Sub Carrier Bandwidth (ASB) system in Doppler frequency spread scenario with varying received signal strength conditions has the potential to improve the performance of Fixed Sub Carrier Bandwidth (FSB)-OFDM system by 10% to 30% in different situations. While the latter system with a chosen but fixed sub carrier bandwidth is optimum only over a small range of velocities and received signal strength, the proposed ASB has optimum performance over all conditions. ASB avoids the complex compensation or interference cancelation mechanism at the receiver, thereby allowing lower complexity receivers. Thus the advantage of increased throughput with possibility of low complexity receivers makes the proposed ASB a potential candidate for consideration in future systems. The promising results pave the path for further investigation with realistic impairments such as channel information feedback delay, channel estimation error, along with the use of forward error control coding.

5.2 OFDMA Framework

In this section a different system architecture for implementing ASB will be described. This kind of architecture can be very well suited for OFDMA systems. The derivations presented in this chapter are unique as they provide the analysis of the interference generated OFDM systems when two OFDM system with different symbol durations are lie next to each other on orthogonal sub carriers. The analysis is very generic as it covers several different combination of the ratio of symbol durations. Interestingly when this condition occurs then the orthogonality of neighboring sub carriers is lost however since a set of sub carriers use similar symbol duration, the impact is not severe as detailed in the signal to interference plus noise ratio analysis detailed in this Section. For analysis we shall consider a system whose baseband transmitter architecture at the Base Station (BS) is given in Figure 5.10. The system of the proposed ASB OFDM is also referred to as Variable Sub Carrier Bandwidth (VSB) OFDM equivalently. The system is assumed to support multiple users simultaneously across different sub carriers. There are different groups of sub carriers, where the groups have different sub carrier bandwidths. Each IFFT spans the entire system bandwidth by using the same sampling period. In each IFFT, N1, N2, N3, etc. denotes the number of sub carriers, where larger numbers generate narrower sub carriers bandwidths. It can be noted that only a fraction of the sub carriers in each IFFT is activated (the number of active sub carriers in each IFFT can be made to vary), and that the active sub carriers of the different groups are selected such that the frequency band spanned by the different groups do not overlap. The frequency domain view of such a configuration is given in Fig. 5.9. A user must be allocated to

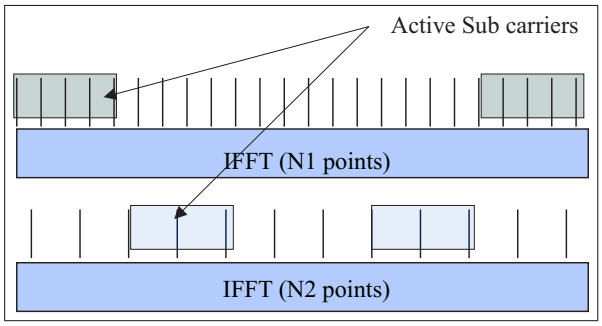

Figure 5.9: Frequency domain configuration of VSB OFDM

a particular sub carrier group, whose sub carrier bandwidth suits the requirement of the user conditions optimally. At the receiver a flexible FFT can be implemented [72] as a user will need only one type of sub carrier at a time, while at the base station as

many IFFTs are used as sub carrier types. The time frequency diagram of the signal can be represented as in Figure 5.2 except that there need not be any guard band between the sub-bands. It can be seen that since sub bands are next to each other, and since the symbol duration are not the same, the orthogonality will no longer be maintained. Therefore the system can also be called non-orthogonal frequency division multiplexing. However, not all sub carriers will be non orthogonal. Some sub carriers whose frequencies are integer multiple of another will still be orthogonal. The receiver at the BS can be as in Figure 5.11.

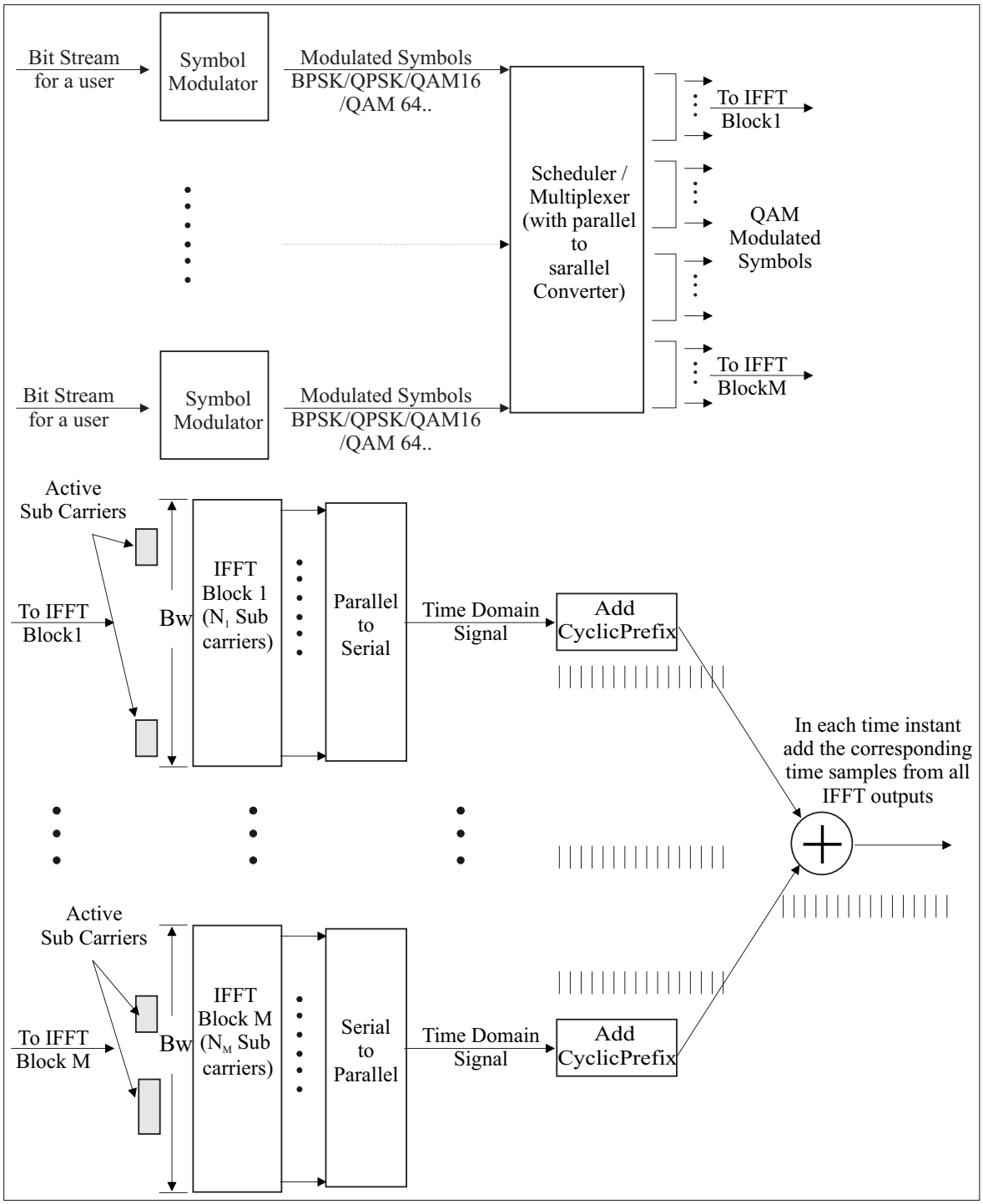

Figure 5.10: Downlink Transmitter for the proposed VSB OFDMA at the base station

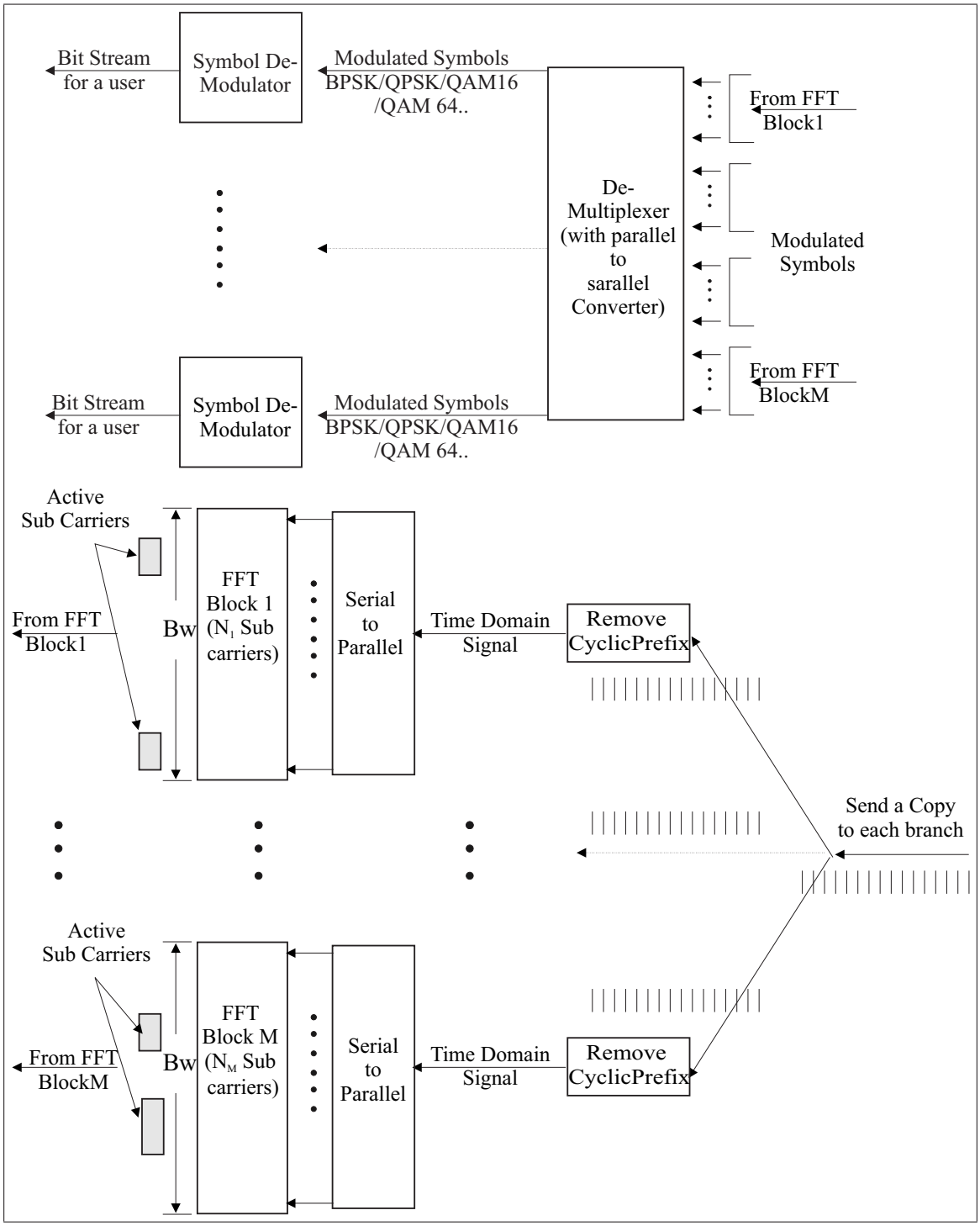

Figure 5.11: Up link Receiver for the proposed VSB OFDMA at the base station

5.2.1 Analytical Model

Table 5.1: List of Symbols

Symbol	Explanation
g	Index of the group, each group indicates a type of sub carrier
k_g	Sub carrier index for group
s_g	OFDM symbol index for group
X_{k_g,s_g}	sub carrier symbol
P_{k_g,s_g}	Power on sub carrier
T_{s_g}	OFDM symbol period
T_{f_g}	DFT period for a group
T_{gi_g}	Guard period for a group
f_c	Carrier Frequency
T	Sampling period
t	Time
$\Xi_{T_s}(t)$	Gate Function [46]
$H[t, k_g]$	Channel Transfer Function for sub carrier k_g
$\nu(t)$	Noise Term
$N_{gi_{\acute{g}}}$	Number of samples in the guard period
$N_{f_{\acute{g}}}$	Number of samples in the FFT
$N_{s_{\acute{g}}}$	Number of samples in an OFDM symbol

The band pass signal for OFDM transmitted through a system as shown in Figure 5.10 can be written as

$$x(t) = \mathrm{Re}\{\sum_{g}\sum_{s_g}\sum_{k_g} X_{k_g,s_g}\sqrt{P_{k_g,s_g}}e^{j2\pi\frac{k_g}{N_{f_g}T}(t-s_gT_{s_g}-T_{gi_g})} .\Xi_{T_s}(t-s_gT_{s_g})e^{j2\pi f_c t}\}, \quad (5.12)$$

where the symbols are defined in Table 5.1. After passing through the channel, the signal can be represented as [20],

$$r(t) = \mathrm{Re}\{\sum_{g}\sum_{s_g}\sum_{k_g}\sqrt{P_{k_g,s_g}}X_{k_g,s_g}\int_0^{\tau_{max}} h(t,\tau) e^{j2\pi(f_c+f_{d\tau})(t-\tau)}e^{j2\pi\frac{k_g}{N_{f_g}T}(t-s_gT_{s_g}-T_{gi_g}-\tau)} \Xi_{T_s}(t-s_gT_{s_g}-\tau)\,d\tau\} + \nu(t), \quad (5.13)$$

where τ_{max} is the maximum tail of the channel impulse response, $\nu(t)$ is the noise component and $f_{d\tau}$ is the Doppler frequency for delay τ. To simplify the above

expression, we use f_{max}, the maximum Doppler frequency instead of $f_{d\tau}$ in all delays in the above equation. This will also give us the worst case scenario. Then (5.13) becomes,

$$r(t) = Re\{\sum_{g}\sum_{s_g}\sum_{k_g}\sqrt{P_{k_g,s_g}}X_{k_g,s_g}\int_{0}^{\tau_{max}} h(t,\tau) \\ e^{j2\pi(f_c+f_{max})(t-\tau)}e^{j2\pi\frac{k_g}{N_{f_g}T}(t-s_gT_{s_g}-T_{gi_g}-\tau)} \\ \Xi_{T_s}(t-s_gT_{s_g}-\tau)\,d\tau\} + \nu(t). \quad (5.14)$$

If the guard interval is larger than maximum channel impulse response tail and considering that $h(t,\tau)e^{j2\pi(f_c+f_{max})(-\tau)}$ is inseparable from $h(t,\tau)$, then the above can be written as

$$r(t) = Re\{\sum_{g}\sum_{s_g}\sum_{k_g}\sqrt{P_{k_g,s_g}}X_{k_g,s_g}H[t,k_g] \\ e^{j2\pi(f_c+f_{max})(t)}e^{j2\pi\frac{k_g}{N_{f_g}T}(t-s_gT_{s_g}-T_{gi_g})} \\ \Xi_{T_s}(t-s_gT_{s_g})\,d\tau\} + \nu(t). \quad (5.15)$$

At the receiver the signal is down converted by multiplying the above by $e^{-j2\pi f_c^{'}}$, where $f_c^{'}$ is the frequency of the local oscillator at the receiver and $f_c^{'} = f_c + \delta f_c$, where δf_c is the carrier frequency offset error. After passing through a low pass filter the signal can be written as

$$r(t) = \sum_{g}\sum_{s_g}\sum_{k_g}\sqrt{P_{k_g,s_g}}X_{k_g,s_g}H[t,k_g]e^{j2\pi(\delta f_c+f_{max})(t)} \\ e^{j2\pi\frac{k_g}{N_{f_g}T}(t-s_gT_{s_g}-T_{gi_g})}\Xi_{T_s}(t-s_gT_{s_g})\,d\tau + \nu(t). \quad (5.16)$$

The received signal is then truncated, with a gate function as below

$$r_{s_{\acute{g}}}(t) = r(t)\Xi_{T_{f_{\acute{g}}}}(t-s_{\acute{g}}T_{s_{\acute{g}}}-T_{gi_{\acute{g}}}). \quad (5.17)$$

At the receiver the signal is then sampled. We assume transmit and receive clock synch error is negligible. The sampled signal can be written as [45]

$$r_{s_{\acute{g}}}(n) = r(n)\Xi_{N_{f_{\acute{g}}}}(n-s_{\acute{g}}N_{s_{\acute{g}}}-N_{gi_{\acute{g}}}). \quad (5.18)$$

The sub carrier at the receiver constructed by an FFT operation (considering ideal

timing synch) is

$$R_{s_{\acute{g}},k_{\acute{g}}^{'}} = \frac{1}{N_{f_{\acute{g}}}} \sum_{n=s_{\acute{g}}N_{s_{\acute{g}}}+N_{gi_{\acute{g}}}}^{(s_{\acute{g}}+1)N_{s_{\acute{g}}}} r_{s_{\acute{g}}}(n) e^{-j2\pi \frac{k_{\acute{g}}^{'}}{N_{f_{\acute{g}}}}(n-s_{\acute{g}}N_{s_{\acute{g}}}-N_{gi_{\acute{g}}})}. \quad (5.19)$$

Considering that the channel is almost static over one coherence time, which is larger than the largest OFDM symbol in the group, one can write the noiseless part of the received sub carrier as [45]

$$R_{s_{\acute{g}},k_{\acute{g}}^{'}} = \sum_{g}\sum_{s_g}\sum_{k_g} \sqrt{P_{k_g,s_g}} X_{k_g,s_g} H[k_g,s_g] e^{-j2\pi\phi(k_{\acute{g}}^{'},k_g)}$$
$$e^{j2\pi N_{f_{\acute{g}}}\psi(\delta f_c+f_{max},k_{\acute{g}}^{'},k_g)} \mathrm{sinc}(N_{f_{\acute{g}}}\pi\psi(\delta f_c+f_{max},k_{\acute{g}}^{'},k_g)), \quad (5.20)$$

where

$$\phi(k_{\acute{g}}^{'},k_g) = \frac{k_g}{N_{f_g}}(s_g N_{s_g}+N_{gi_g}) - \frac{k_{\acute{g}}^{'}}{N_{f_{\acute{g}}}}(s_{\acute{g}}N_{s_{\acute{g}}}+N_{gi_{\acute{g}}}) \quad (5.21)$$

$$\psi(\delta f_c+f_{max},k_{\acute{g}}^{'},k_g) = (\delta f_c+f_{max})T + \frac{k_g}{N_{f_g}} - \frac{k_{\acute{g}}^{'}}{N_{f_{\acute{g}}}}. \quad (5.22)$$

Therefore the desired signal is

$$A(k_{\acute{g}}^{'},s_{\acute{g}}) = \sqrt{P_{k_{\acute{g}}^{'},s_g}} X_{k_{\acute{g}}^{'},s_g} H[k_{\acute{g}}^{'},s_g] e^{j2\pi N_{f_{\acute{g}}}\psi(\delta f_c+f_{max})}$$
$$\mathrm{sinc}(N_{f_{\acute{g}}}\pi\psi(\delta f_c+f_{max})). \quad (5.23)$$

Thus the power of the desired signal is

$$E_{|A(k_{\acute{g}}^{'},s_{\acute{g}})|^2} = P_{k_{\acute{g}}^{'},s_g}|H[k_{\acute{g}}^{'},s_g]|^2 \mathrm{sinc}^2(N_{f_{\acute{g}}}\pi\psi(\delta f_c+f_{max})). \quad (5.24)$$

We assume $E_{|X_{k_g,s_g}|^2}=1$. The interference from the sub carriers of similar type ($g=\acute{g}$, but $k_g \neq k_{\acute{g}}^{'}$) is

$$B(k_{\acute{g}}^{'},s_{\acute{g}}) = \sum_{k_{\acute{g}}\neq k_{\acute{g}}^{'}} \sqrt{P_{k_{\acute{g}},s_{\acute{g}}}} X_{k_{\acute{g}},s_{\acute{g}}} H[k_{\acute{g}},s_{\acute{g}}] e^{-j2\pi\phi(k_{\acute{g}}^{'},k_{\acute{g}})}$$
$$.e^{j2\pi N_{f_{\acute{g}}}\psi(\delta f_c+f_{max},k_{\acute{g}}^{'},k_{\acute{g}})} \mathrm{sinc}(N_{f_{\acute{g}}}\pi\psi(\delta f_c+f_{max},k_{\acute{g}}^{'},k_{\acute{g}})). \quad (5.25)$$

The power of this interference is

$$\mathrm{E}_{|\mathrm{B}(\mathrm{k}_{\acute{g}}^{'},\mathrm{s}_{\acute{g}})|^2} = \sum_{\mathrm{k}_{\acute{g}} \neq \mathrm{k}_{\acute{g}}^{'}} \mathrm{P}_{\mathrm{k}_{\acute{g}},\mathrm{s}_{\acute{g}}} |\mathrm{H}[\mathrm{k}_{\acute{g}},\mathrm{s}_{\acute{g}}]|^2 \mathrm{sinc}^2(\mathrm{N}_{\mathrm{f}_{\acute{g}}} \pi \psi(\delta \mathrm{f_c} + \mathrm{f_{max}}, \mathrm{k}_{\acute{g}}^{'}, \mathrm{k}_{\acute{g}})) \tag{5.26}$$

The *orthogonality loss* due to the structure of the transmitter being analyzed can be understood by noting that even if $\delta \mathrm{f_c} + \mathrm{f_{max}}$ is made zero in the above expression, the term $\mathrm{sinc}^2(\mathrm{N}_{\mathrm{f}_{\acute{g}}} \pi \psi(\delta \mathrm{f_c} + \mathrm{f_{max}}, \mathrm{k}_{\acute{g}}^{'}, \mathrm{k}_{\acute{g}}))$ does not vanish as seen from (5.22) since the number of sub carriers in the IFFTs is different, i.e. the symbol periods are different.

The interference from sub carriers of other types ($\mathrm{g} \neq \acute{\mathrm{g}}$) is

$$\begin{aligned} \mathrm{C}(\mathrm{k}_{\acute{g}}^{'}, \mathrm{s}_{\acute{g}}) = \sum_{\mathrm{g} \neq \acute{g}} \sum_{\mathrm{k_g}} \sqrt{\mathrm{P}_{\mathrm{k_g},\mathrm{s_g}}} \mathrm{X}_{\mathrm{k_g},\mathrm{s_g}} \mathrm{H}[\mathrm{k_g}, \mathrm{s_g}] e^{-j2\pi\phi(\mathrm{k}_{\acute{g}}^{'}, \mathrm{k_g})} \\ e^{j2\pi \mathrm{N}_{\mathrm{f}_{\acute{g}}} \psi(\delta \mathrm{f_c} + \mathrm{f_{max}}, \mathrm{k}_{\acute{g}}^{'}, \mathrm{k_g})} \mathrm{sinc}(\mathrm{N}_{\mathrm{f}_{\acute{g}}} \pi \psi(\delta \mathrm{f_c} + \mathrm{f_{max}}, \mathrm{k}_{\acute{g}}^{'}, \mathrm{k_g})) \end{aligned} \tag{5.27}$$

The power of this interference is $\mathrm{E}_{|\mathrm{C}(\mathrm{k}_{\acute{g}}^{'},\mathrm{s}_{\acute{g}})|^2} =$

$$\sum_{\mathrm{g} \neq \acute{g}} \sum_{\mathrm{k_g}} \mathrm{P}_{\mathrm{k_g},\mathrm{s_g}} |\mathrm{H}[\mathrm{k_g}, \mathrm{s_g}]|^2 \mathrm{sinc}^2(\mathrm{N}_{\mathrm{f}_{\acute{g}}} \pi \psi(\delta \mathrm{f_c} + \mathrm{f_{max}}, \mathrm{k}_{\acute{g}}^{'}, \mathrm{k_g})). \tag{5.28}$$

The received SINR can thus be written as

$$\Upsilon_{rx}(\mathrm{k}_{\acute{g}}^{'}, \mathrm{s}_{\acute{g}}) = \frac{\mathrm{E}_{|\mathrm{A}(\mathrm{k}_{\acute{g}}^{'},\mathrm{s}_{\acute{g}})|^2}}{\mathrm{E}_{|\mathrm{B}(\mathrm{k}_{\acute{g}}^{'},\mathrm{s}_{\acute{g}})|^2} + \mathrm{E}_{|\mathrm{C}(\mathrm{k}_{\acute{g}}^{'},\mathrm{s}_{\acute{g}})|^2} + \mathrm{N_o} \Delta \mathrm{f}_{\mathrm{N}_{\mathrm{f}_{\acute{g}}}}}. \tag{5.29}$$

The capacity expression for the above SINR is,

$$\mathrm{Cap}(\mathrm{k}_{\acute{g}}^{'}, \mathrm{s}_{\acute{g}}) = \log_2(1 + \Upsilon_{\mathrm{rx}}(\mathrm{k}_{\acute{g}}^{'}, \mathrm{s}_{\acute{g}})) \frac{\mathrm{N}_{\mathrm{f}_{\acute{g}}}}{\mathrm{N}_{\mathrm{s}_{\acute{g}}}}. \tag{5.30}$$

5.2.2 Results and Discussion

For numerical analysis, bandwidth of 5 MHz with a carrier frequency of 3.6 GHz is used. Exponential power decay profile with an average rms delay spread of 1.5 μs is considered for the channel.

Figure 5.12 shows the SINR of a standard OFDM system at a received signal to noise ratio (SNR) of 20dB. The legend, for example 1024, denotes a standard FSB-OFDM system with as many sub carriers. It is seen that with decreasing number of sub carriers, i.e. increasing sub carrier bandwidth, the resilience to ICI is increased. It may follow that the system with smallest number of sub carriers is the best, but such

is not observed from the capacity curves in Figure 5.13. The anomaly is understood by considering the capacity expression (5.30) which includes the impact of guard interval (GI). GI depends only on the maximum channel impulse response length and should not be changed when the FFT size changes. It can be seen from Figure 5.13 that each OFDM system with a different sub carrier bandwidth is best in only a range of the velocity.

Figure 5.14 shows similar curves but when the received SNR is 10dB. It can be observed that the optimal region for a certain sub carrier bandwidth is changed compared to Figure 5.13. It is clear that a particular configuration of OFDM systems (a particular sub carrier bandwidth) is optimal only over a certain Doppler region and a certain received SNR situation.

Next, Figure 5.15 shows the average capacity of different sub carrier types at a received SNR of 20dB for the proposed VSB-OFDM system shown in Figure 5.10.

Though the new system introduces some amount of non-orthogonality, yet the impact is not significant as found by comparing Figure 5.13 and Figure 5.15. In a FSB OFDM system, the interference power is almost same across all sub carrier on an average. In case of the proposed Variable Sub Carrier Bandwidth (VSB), since different sub carrier bandwidths are implemented, the interference on the sub carriers is different.

At 10dB received SNR condition, the performance of the sub carriers of the new system is found similar to that of Figure 5.14 and hence not repeated. The structure as in Figure 5.10 provides the flexibility to implement the different sub carrier bandwidths in the same system simultaneously.

Different users having different SNR and Doppler conditions can be allocated to the sub carrier type which best suits the situation, i.e. the sub carrier bandwidth with highest capacity for the user situation can be used for the user. Such a situation is created with two types of users, i.e. one type with very low mobility and the other type with very high mobility. The capacity of the FSB systems is compared with that of the proposed VSB under these situation. The comparison is given in Figure 5.16. When the proposed VSB is used, the sub carrier bandwidth with highest capacity for a user is selected and allocated. The fraction of system bandwidth for high mobility users with respect to the total system bandwidth is changed from zero to unity, i.e between the situation when only low mobility users exist and when only high mobility users exits. The mark 0.5 denotes situation when both high and low mobility users exists in equal proportion. For simplicity of analysis all users are supposed to be at the same received SNR condition of 20dB. The capacity of the proposed VSB system

is compared with that of FSB in Figure 5.16. The x–axis denotes the fraction of system bandwidth used by high mobility users to the total available bandwdith. The curve labeled 1024 is for FSB OFDM with 1024 sub carriers (sub carrier bandwidth = 4.88 KHz). Similarly the curves labeled 512 and 256 represent FSB system with as many sub carriers and hence with 9.76 KHz and 19.5 KHz of sub carrier spacing. The curve labeled VSB is the one which can support the proposed variable sub carrier bandwidth by using multiple sub carrier bandwidths (options used in this work are 4.88 KHz, 9.76 KHz and 19.5 KHz) simultaneously at the transmitter. In this system, the users with smaller values of effective carrier offset use sub carriers with a smaller sub carrier bandwidth while those with higher Doppler frequency spread use wider subcarrier spacing. In this situation when there are users with different Doppler condition, it can be seen that any one type of FSB is efficient for only a small range of values of user distribution, while the proposed VSB has the highest capacity for all possible distribution of user mobility conditions. It is seen here that when more low mobility users are present, 1024 system is very good, but its effectiveness decreases steeply with increasing portion of high mobility users. In the same way FSB with 256 sub carries is good when more high mobility users are present. When more users are present who are almost static, the gain of the proposed VSB over FSB with 256 carriers is about 16%, and about 8% over FSB with 512 sub carriers. When most users are highly mobile, then VSB has gain of 20% over FSB with 1024 sub carriers, and about six percent over FSB with 512 carriers while it has similar capacity as 256 sub carrier system.

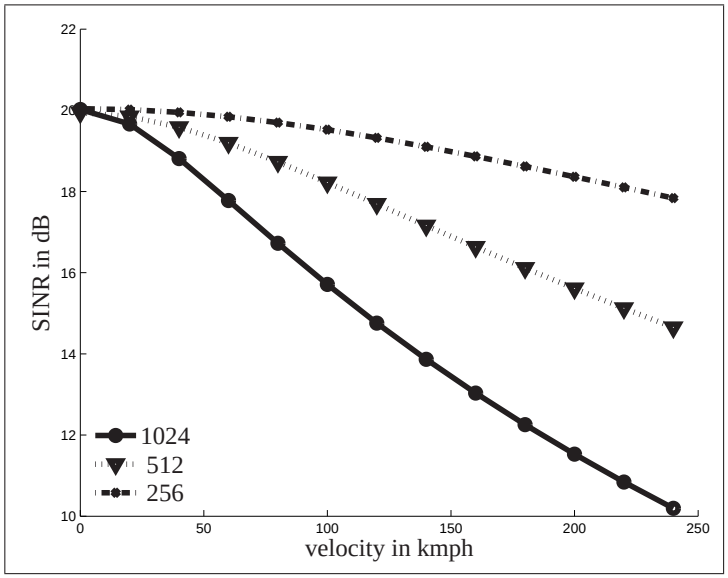

Figure 5.12: SINR of standard OFDM systems at 20dB SNR

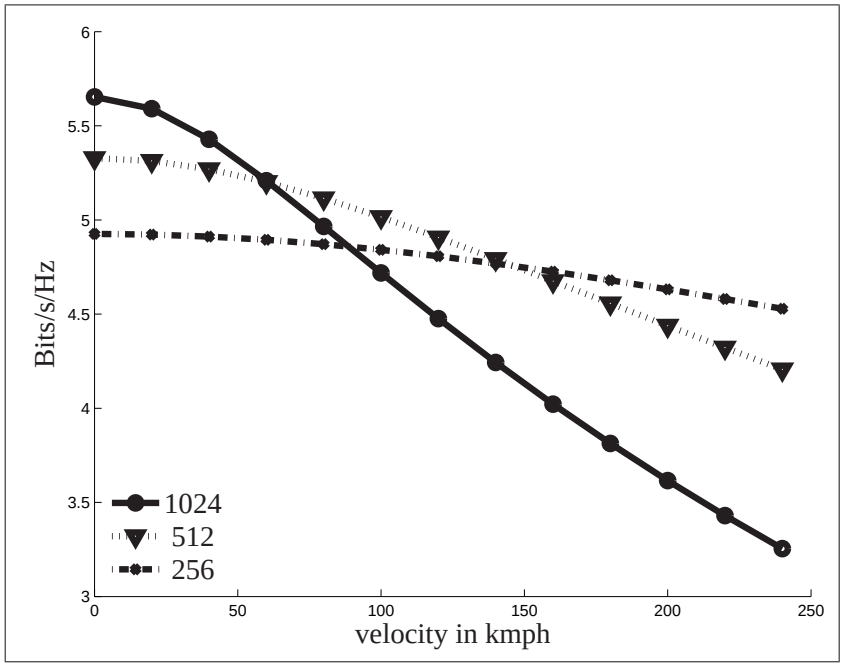

Figure 5.13: Capacity of standard OFDM systems at 20dB

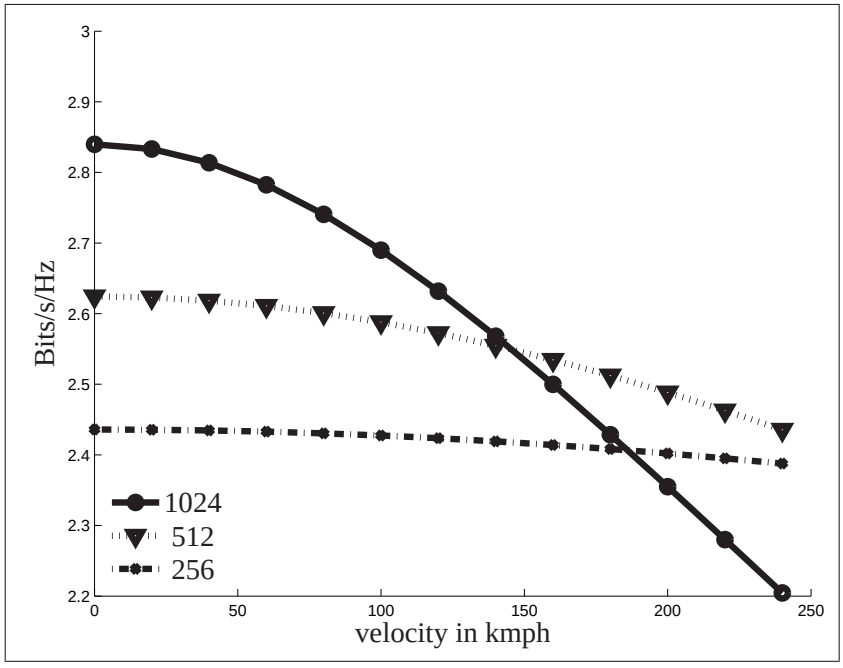

Figure 5.14: Capacity of standard OFDM systems at 10dB

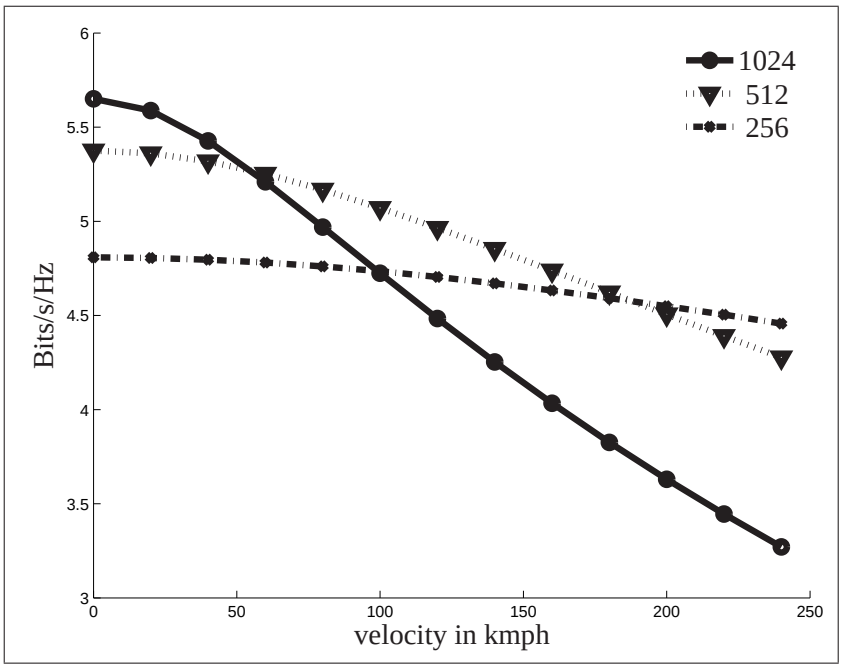

Figure 5.15: Capacity of VSB OFDM at 20dB

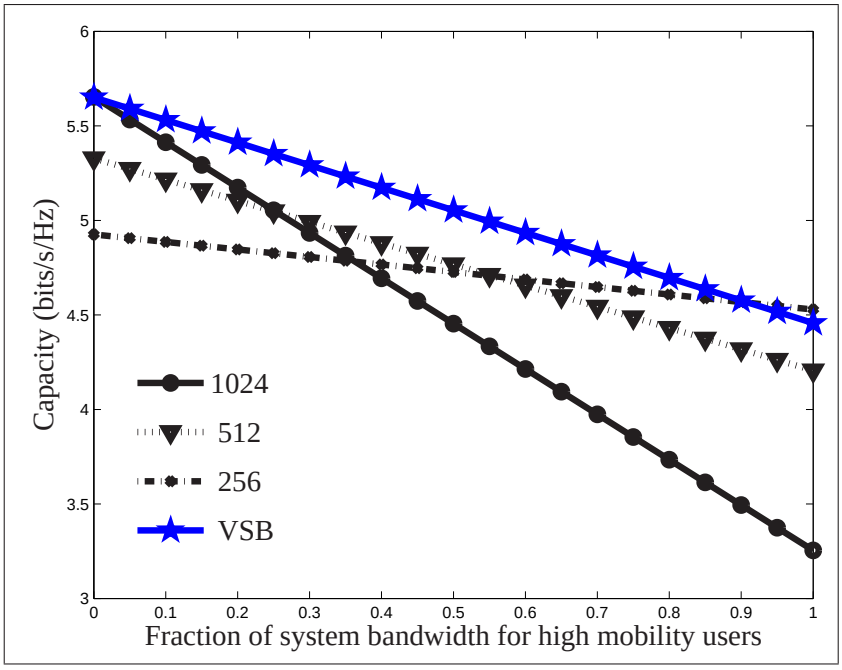

Figure 5.16: Capacity comparison when users with different mobility conditions coexist

5.2.3 Conclusion

It has been found that a chosen sub carrier bandwidth for a FSB OFDM system is optimum only over a small range of velocity and received signal strength conditions. When different users with various mobility conditions suffer from different amount of ICI, FSB OFDM system is found to be optimal only for a certain range of mobility distributions. A system which can support multiple sub carrier bandwidths simultaneously is proposed and analyzed in this work. Variable sub carrier bandwidths are used in the proposed system to overcome the impact of ICI since ICI is inversely proportional to the sub carrier bandwidth. This avoids complex ICI cancelation schemes at the receiver. Depending on the condition of ICI power, which is a function of the received signal strength and Doppler condition, users may use different sub carrier bandwidths. The new scheme analyzed can vary the sub carrier bandwidth and the number of sub carrier for each type of sub carrier bandwidth. In this way it can optimally cater to different types of user conditions simultaneously. The gains of the proposed VSB system over FSB OFDM system is in the range of eight to twenty percent in terms of capacity. The promising results of this analysis proves the potential of the proposed VSB scheme to enhance the performance of FSB OFDM systems though further investigations are needed to compare the gains when non ideal channel estimation and Doppler frequency spread estimations are encountered.

5.3 Summary

- In this Chapter, a new technique namely adaptive sub carrier bandwidth system has been introduced and evaluated for its effectiveness in tolerating a variety of Doppler conditions.

- It is found to be very robust and effective over OFDM systems using fixed sub carrier bandwidths.

- Two different architectures have been presented.

  - The first one uses standard OFDM system and principles of normal OFDM can be used in evaluating or designing the system.

  - The second architecture on the contrary does not maintain orthogonality among the sub carriers but provides more flexibility to the system deployment where different FFTs with different sizes but having the same

sampling clock and using orthogonal frequency bands for the active regions are used.

- The first system has the benefit that it supports different sampling frequencies, which in turn means it can simultaneously provide support to systems requiring different bandwidths. This is highly important if different equipments with different data rate capabilities are required to operate optimally in terms of power consumption in the same system. This is because a high sampling frequency drains the power, which is unnecessary for users requiring a low data rate. Therefore users with high and low data rate can be separated and each can optimize the power usage.

- The second architecture does not allow this as the sampling frequency of all FFTs with different sizes must be same. Of course it opens up the analysis for the case where a mixed architecture may be developed. Its advantage is that there is minimum loss in bandwidth since there is no need for guard band between two FFTs which is needed in the previous case.

- The concern for both the systems is the frame structure. It will require detailed design and might challenge existing framework.

- This kind of systems can be very useful for vehicle to vehicle communication as well, where devices will encounter large variety of Doppler conditions frequently.

- The proposed methods do not use complex receiver algorithms to cancel ICI, instead avoids it in the an efficient way, thereby reducing the complexity of the UE.

6

Variable Guard Interval

In the previous chapter the sub carrier bandwidth was adapted to overcome ICI and increase the spectral efficiency. However, the Guard Interval (GI) was assumed to be fixed. The focus of this chapter is to use dynamic adaptation of GI to improve the spectral efficiency further.

GI, in the form of Cyclic Prefix (CP), is used in OFDM systems between two consecutive OFDM symbols to avoid Inter Symbol Interference (ISI). The GI duration used normally is taken to be more than the maximum excess delay of the channel. Though the use of GI is important for a simple receiver implementation, it reduces the spectral efficiency of the system. On the other hand using a short GI introduces ISI thereby degrading the performance. The GI required, depends on the propagation environment. Instead of using the maximum excess channel delay as the design factor, dynamic selection of GI can be made to decrease the loss in spectral efficiency. An algorithm for implementing dynamically varying GI length is proposed in this chapter. The required GI is derived in this work as a function of several important system and channel parameters which is not available in existing literature to the best of the author's knowledge. The performance of the algorithm is analyzed for dynamic channel conditions. Results show that the algorithm can reduce GI significantly and thus can improve the throughput. The proposed method

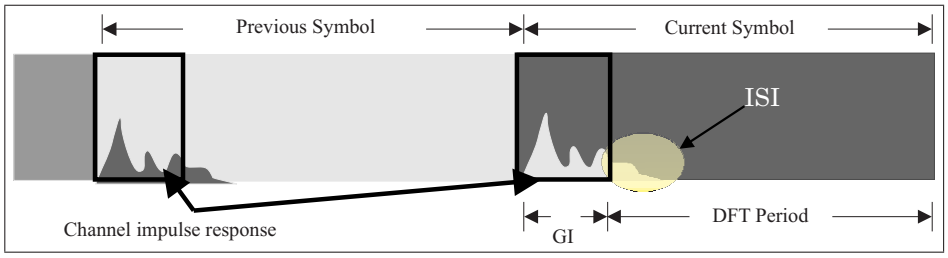

Figure 6.1: Effect of small GI.

performs well even in vehicular speed.

6.1 Introduction

To overcome ISI effects in the hostile multipath wireless environment, a GI is used between consecutive OFDM symbols. This helps in using one tap equalizer per sub carrier at the receiver. The GI is usually designed to be longer than the maximum channel delay; its length is selected after channel measurements in the desired implementation scenario. A GI shorter than the maximum excess channel delay causes ISI, as depicted in Figure 6.1. The short GI also introduces ICI due to loss in orthogonality among sub carriers. It is important here to note that carrier frequency offset and Doppler effect also cause ICI [70],[45],[74].

Cyclic prefix (CP) or zero padding (ZP) [75] are usual implementations of GI. CP causes an additional wastage of energy on top of spectral efficiency loss, whereas ZP only adds the overhead, but [76] shows that cyclic prefixed OFDM is more stable compared to other schemes. In IEEE standards 802.11a/g, 802.16a,e [11, 14, 15], as much as 25% of the OFDM symbol duration is CP.

It is seen from several measurements [77, 78, 31] that the local rms delay spread varies from few tens of nano seconds to few micro seconds. In such environments, using fixed GI (chosen more than the maximum delay in the environment) causes devices which experience smaller rms delay spread to use an unnecessarily large GI. There is a wastage of costly resource from a network point of view and power from the user device perspective, where battery life is a major concern.

This background motivates the use of Variable Guard Interval (VGI). This scheme is suitable when a preamble [14] is used for synchronization and channel estimation. There may be a concern for the timing synchronization algorithms which use GI for synchronization. However, using the VGI scheme is not expected to influence the performance of such algorithms much as it is seen that the mean square error in

the estimation of timing and frequency offset using the GI does not improve notably after a certain length of GI [79].

The loss due to a fixed GI, can be reduced by using VGI as discussed above. A preliminary form of this is in IEEE 802.16a,e. The Base Station (BS) can choose several GI lengths. But once a BS chooses a GI, all User Equipment (UE), in the cell covered by the BS, will use the same GI. Therefore, there is only one GI, which is the maximum of the required GIs considering all users in the coverage area of the BS. In this work, we consider the situation where, different GI lengths coexist simultaneously under one BS or Access Point (AP).

A few of the relevant works in this area are as follows. [80] presents the degradation when GI length is less than the channel impulse response, but its relation to rms delay spread of the channel is not discussed. Authors in [81] present the detailed analysis of the impact of insufficient GI in OFDM systems. But the expressions are too complex to use in a dynamic GI estimation procedure. The work in [82] presents ISI and ICI cancelation scheme and it requires highly complex interference cancelation scheme at the receiver. In [83], the authors propose not to use GI, but this is from synchronization perspective and does not consider the impact of ISI. The article [84] provides method for equalization where a filter is designed, which on convolution with the channel yields an effective channel with a compressed impulse response. This method is elegant but would increase the receiver complexity and signalling overhead.The authors in [85] also advocate the use of ISI cancelation algorithm at the receiver and the use of redundant carrier to combat ICI. Such mechanisms have high receiver complexity which prohibit the use of low end devices and also have loss in efficiency due to use of redundant carriers.The scheme in [86] uses different lengths of GI but by adjusting the sampling rate of the system. This scheme may be useful but may not be permissible in many simple receivers. In this scheme the receiver has to adjust the sampling rate which may create problems in synchronization of OFDM and internal receiver components. Moreover, in this scheme the number of sub carriers is dependent on the GI length needed. The number of sub carriers impact the sub carrier bandwidth which is usually decided based on the tolerance level to Doppler frequency spread and carrier offset. Therefore it has conflicting design parameters.

In this chapter an algorithm is proposed which selects the GI dynamically. A simplified closed form expression for maximum limit of interference and lower limit for desired signal power is used in this chapter to arrive at the the received SINR due to insufficient GI. This is used to derive the expression for the required GI which can be computed dynamically. The required GI is shown to be a function the rms delay

spread of the channel, the discrete fourier transform duration, the required SNR, which is not presented in any of the previous works by the others.

6.2 System Description

In this work, it is assumed that each transmission burst, which can be referred to as a frame (consisting of a sequence of OFDM symbols) may have a different GI as per the need of the user transmitting or receiving the frame. If multiple users share one transmission burst then the maximum length of required GI among the users sharing the burst is used. Higher level algorithms may be used to group users with similar requirement of GI in such a case.

In down link, the Access Point (AP), or the BS uses a GI based on the requirement of the users. The GI to be used in a frame has to be estimated and this information needs to be present at the transmitter. In Frequency Division Duplex (FDD) mode, the intended receivers can estimate the required GI, at a previous time, and feed back the information in the reverse link. For Time Division Duplex (TDD) mode, channel reciprocity may be used. In such a case, the required GI can be estimated from the reverse link channel estimate at the transmitter (AP/BS) and used in the subsequent forward link transmission. To feed back the required GI, a device may need up to 4 bits to indicate 16 levels of GI. This overhead is very small compared to the frame length. In the forward link , the GI used by the AP/BS in a frame can be signalled in the header for each frame. The required GI may be estimated every frame, and fed back only when there is a change required thereby further reducing the overhead. These are very much implementation specific.

6.3 Required GI

The time domain signal model for OFDM is defined in (2.19) – (2.22). The received sub carrier symbol in (3.11) can be expanded as

$$\begin{aligned}
\mathrm{X_s[k']} =& \frac{1}{\sqrt{\mathrm{T_f}}} \int_{\mathrm{sT_s+T_{gi}}}^{\mathrm{(s+1)T_s}} \mathrm{r_s(t)} e^{-\mathrm{j}2\pi \frac{\mathrm{k'}}{\mathrm{T_f}}(\mathrm{t-sT_s-T_{gi}})}\, d\mathrm{t} \\
=& \frac{1}{\mathrm{T_f}} \int_{\mathrm{sT_s+T_{gi}}}^{\mathrm{(s+1)T_s}} \left(\int_0^{\tau_{\max}} \mathrm{h}(\tau) \left(\sum_{\mathrm{k}=-\frac{\mathrm{N_f}}{2}}^{\frac{\mathrm{N_f}}{2}-1} \mathrm{X_s[k]} e^{\mathrm{j}2\pi \frac{\mathrm{k}}{\mathrm{T_f}}(\mathrm{t-sT_s-T_{gi}}-\tau)} \Xi_{\mathrm{T_s}}(\mathrm{t-sT_s}-\tau) \right) d\tau + \nu(\mathrm{t}) \right) \\
& . e^{j2\pi \mathrm{t} \frac{\epsilon}{\mathrm{T_f}}} \Xi_{\mathrm{T_f}}(\mathrm{t-sT_s-T_{gi}}) e^{-\mathrm{j}2\pi \frac{\mathrm{k'}}{\mathrm{T_f}}(\mathrm{t-sT_s-T_{gi}})}\, d\mathrm{t}. \qquad (6.1)
\end{aligned}$$

Results exist for situations where the GI is sufficiently large, but here we consider $\mathrm{T_{gi}} < \tau_{\max}$, i.e. the channel impulse response is not completely covered by the GI, and therefore interference from previous OFDM symbol creeps in. The OFDM symbol number 's' will have influence from the previous OFDM symbol. Figure 6.1 shows the effect of previous OFDM symbol on the current OFDM symbol. The highlighted portion inside the circle introduces ISI due to insufficient GI, and ICI due to the loss of orthogonality among sub carriers. Exponential power decay profile is considered for the channel model. Channel taps are taken as Rayleigh distributed. Following such a model, $\tau_0 = \tau_{\mathrm{m}} = \tau_{\mathrm{rms}}$ [87] ([88] also shows linear relationship between τ_{m} and τ_{rms}), where τ_0 is the decay constant of the channel model chosen, τ_{m} is the mean excess delay and τ_{rms} is the rms delay spread of the channel.

The transmit pulse for the $(\mathrm{s}-1)^{th}$ OFDM symbol is given by

$$\begin{aligned} \Xi_{\mathrm{T_s}}(\mathrm{t}-(\mathrm{s}-1)\mathrm{T_s}-\tau) = &\quad 1, \\ \text{for, } (\mathrm{s}-1)\mathrm{T_s}+\tau \leqslant &\quad \mathrm{t} < \mathrm{sT_s}+\tau \\ = &\quad 0, \text{otherwise.} \end{aligned} \tag{6.2}$$

At the receiver, the pulse used is

$$\begin{aligned} \Xi_{\mathrm{T_f}}(\mathrm{t}-\mathrm{sT_s}-\mathrm{T_{gi}}) = &\quad 1, \text{ for, } \mathrm{sT_s}+\mathrm{T_{gi}} \leqslant \mathrm{t} < (\mathrm{s}+1)\mathrm{T_s} \\ = &\quad 0, \text{otherwise.} \end{aligned} \tag{6.3}$$

The integral over 't' in (6.1) is non zero over the period

$$\begin{aligned} \max\left((\mathrm{s}-1)\mathrm{T_s}+\tau, \mathrm{sT_s}+\mathrm{T_{gi}}\right) \leqslant \mathrm{t} < \min\left((\mathrm{s})\mathrm{T_s}+\tau, (\mathrm{s}+1)\mathrm{T_s}\right) \\ \mathrm{sT_s}+\mathrm{T_{gi}} \leqslant \mathrm{t} < \mathrm{sT_s}+\tau. \end{aligned} \tag{6.4}$$

The coherence time is assumed to be greater than at least two OFDM symbols. Therefore (6.1) reduces to

$$\begin{aligned} \mathrm{X_s}[\mathrm{k}']_I = &\frac{1}{\sqrt{\mathrm{T_f}}} \sum_{\mathrm{k}=-\frac{\mathrm{N_f}}{2}}^{\frac{\mathrm{N_f}}{2}-1} \mathrm{X_{s-1}}[\mathrm{k}] \int_{\mathrm{T_{gi}}}^{\tau_{\max}} \mathrm{h}(\tau) e^{-j2\pi \mathrm{k}\frac{\tau}{\mathrm{T_f}}} e^{\phi(\mathrm{k},\mathrm{k}',\mathrm{s},\mathrm{T_f},\mathrm{T_s},\mathrm{T_{gi}})} e^{j\frac{2\pi}{\mathrm{T_f}}\phi(\mathrm{k},\mathrm{k}',\epsilon)(\mathrm{sT_s}+\mathrm{T_{gi}})} \\ &. e^{j\frac{\pi}{\mathrm{T_f}}(\tau-\mathrm{T_{gi}})} (\tau-\mathrm{T_{gi}}) \mathrm{sinc}(\pi\phi(\mathrm{k},\mathrm{k}',\epsilon)\frac{\tau-\mathrm{T_{gi}}}{\mathrm{T_f}})\, d\tau, \end{aligned} \tag{6.5}$$

where

$$\phi(\mathrm{k},\mathrm{k}^{'},\mathrm{s},\mathrm{T_f},\mathrm{T_s},\mathrm{T_{gi}}) = j2\pi\left(\frac{\mathrm{T_{gi}}}{\mathrm{T_f}}(\mathrm{k}^{'}-\mathrm{k}) - \frac{\mathrm{T_s}}{\mathrm{T_f}}\{\mathrm{sk}^{'}-(\mathrm{s}-1)\mathrm{k}\}\right)$$

and

$$\phi(\mathrm{k},\mathrm{k}^{'}\epsilon) = \mathrm{k}-\mathrm{k}^{'}+\epsilon. \tag{6.6}$$

The power for this term can be calculated as

$$\mathrm{E}_{\left[\mathrm{X_s[k']}_I \mathrm{X_s[k']}_I^*\right]} = \mathrm{E}_{\frac{|\mathrm{X_{s-1}[k']}|^2}{\mathrm{T_f}^2}} \sum_{\mathrm{k}=-\frac{\mathrm{N_f}}{2}}^{\frac{\mathrm{N_f}}{2}-1} \int_{\mathrm{T_{gi}}}^{\tau_{\max}} \mathrm{E}_{|\mathrm{h}(\tau)|^2}(\tau-\mathrm{T_{gi}})^2 \mathrm{sinc}^2(\pi\phi(\mathrm{k},\mathrm{k}^{'},\epsilon)\frac{\tau-\mathrm{T_{gi}}}{\mathrm{T_f}})\,d\tau$$

$$\text{where, } \mathrm{E}_{|\mathrm{h}(\tau)|^2} = \frac{1}{\tau_0}e^{-\frac{\tau}{\tau_0}} \text{ i.e. exponential power decay profile.} \tag{6.7}$$

Therefore

$$\mathrm{E}_{\left[\mathrm{X_s[k']}_I \mathrm{X_s[k']}_I^*\right]} = \mathrm{E}_{\frac{|\mathrm{X_{s-1}[k']}|^2}{\pi^2}} \frac{1}{\tau_0} \sum_{\mathrm{k}=-\frac{\mathrm{N_f}}{2}}^{\frac{\mathrm{N_f}}{2}-1} \frac{1}{(\mathrm{k}-\mathrm{k}^{'}+\epsilon)^2} \int_{\mathrm{T_{gi}}}^{\tau_{\max}} e^{-\frac{\tau}{\tau_0}} \sin^2\left(\pi(\mathrm{k}-\mathrm{k}^{'}+\epsilon)\frac{\tau-\mathrm{T_{gi}}}{\mathrm{T_f}}\right). \tag{6.8}$$

Using the identity [89]

$$\int \mathrm{e^{ax}sin^2(bx)d\,x} = \mathrm{e^{ax}}\left[\tfrac{1}{2\mathrm{a}} - \tfrac{1}{\mathrm{a^2+4b^2}}\left(\tfrac{\mathrm{a}}{2}\mathrm{Cos(2bx)} + \mathrm{bSin(2bx)}\right)\right] \tag{6.9}$$

and neglecting the terms with coefficients $e^{-\frac{\tau_{\max}}{\tau_0}}$ and considering that $\pi\epsilon\frac{\tau-\mathrm{T_{gi}}}{\mathrm{T_f}}$ to be quite small such that the 'sine' term can be assumed to be very small and the 'cosine' can be approximated to unity, the earlier expression can be reduced to

$$\mathrm{E}_{\left[\mathrm{X_s[k']}_I \mathrm{X_s[k']}_I^*\right]} \leqslant \mathrm{E}_{|\mathrm{X_{s-1}[k']}|^2} \sum_{\mathrm{k}=-\frac{\mathrm{N_f}}{2}}^{\frac{\mathrm{N_f}}{2}-1} \frac{2e^{-\frac{\tau}{\tau_0}}\frac{{\tau_0}^2}{\mathrm{T_f}^2}}{1+4\frac{\pi^2{\tau_0}^2}{T_f^2}(\mathrm{k}-\mathrm{k}^{'}+\epsilon)^2}. \tag{6.10}$$

Using the identity [89]

$$\coth(\pi\mathrm{x}) = \frac{1}{\pi\mathrm{x}} + \frac{2\mathrm{x}}{\pi}\sum_{\mathrm{a}=1}^{\infty}\frac{1}{\mathrm{a}^2+\mathrm{x}^2} \tag{6.11}$$

the interference from the previous OFDM symbol due to insufficient GI can be ap-

proximated as

$$\mathrm{E_{intfI}} \leqslant \mathrm{E}_{|\mathrm{X_{s-1}[k]}|^2} \frac{\tau_0}{\mathrm{T_f}} e^{-\mathrm{T_{gi}}/\tau_0}, \tag{6.12}$$

where $\mathrm{E}_{|\mathrm{X_{s-1}[k]}|^2}$ is the average power in the previous OFDM symbol. For very large $\mathrm{T_{gi}}$ ($\mathrm{T_{gi}} \gg \tau_0$) the term becomes negligible. It is seen that, for the interference from the previous OFDM symbol on the current one, the impact of insufficient GI dominates that due to carrier offset. Figure 6.2 compares the expression with the simulated interference value, marked in the figure as 'interference 1'. It is seen that the expression agrees very closely with the simulated value. Now we consider the

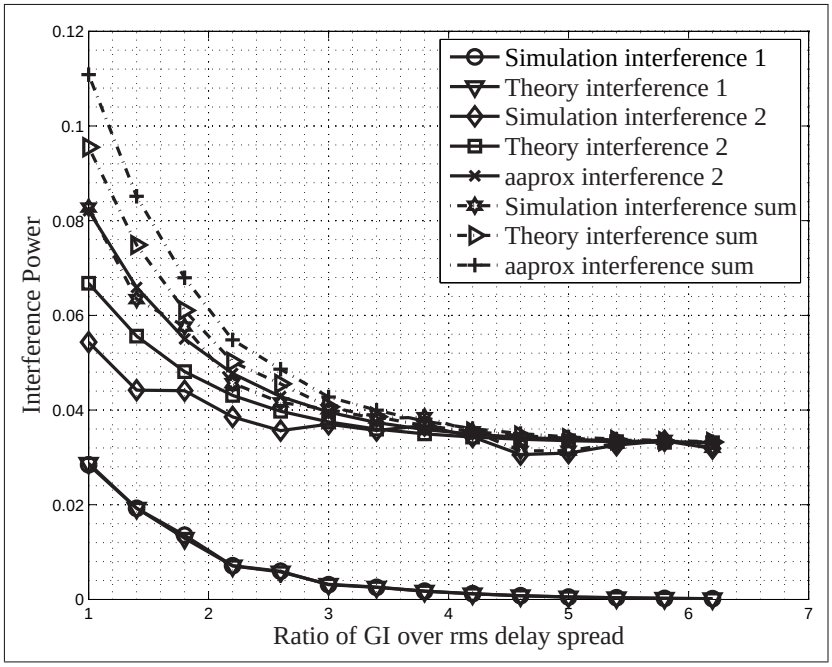

Figure 6.2: Interference Power due to previous OFDM symbol vs Ratio of GI over rms delay spread.

s^{th} OFDM symbol. For the region $0 < \tau \leqslant \mathrm{T_{gi}}$, there is the useful part and the interference due to ICI from carrier frequency offset. The contribution of this part of the received signal is given by

$$\mathrm{X_s[k']}_{II} = \frac{1}{\sqrt{\mathrm{T_f}}} \sum_{\mathrm{k}=-\frac{\mathrm{N_f}}{2}}^{\frac{\mathrm{N_f}}{2}-1} \mathrm{X_s[k]} \int_0^{\mathrm{T_{gi}}} \mathrm{h}(\tau) e^{-j2\pi \mathrm{k}\frac{\tau}{\mathrm{T_f}}} e^{\phi(\mathrm{k,k',s,T_f,T_s,T_{gi}})} e^{j\frac{2\pi}{\mathrm{T_f}}\phi(\mathrm{k,k',}\epsilon)(\mathrm{sT_s+T_{gi}})}$$
$$.e^{j\frac{\pi}{\mathrm{T_f}}(\tau-\mathrm{T_{gi}})}(\tau-\mathrm{T_{gi}})\mathrm{sinc}(\pi\phi(\mathrm{k,k'},\epsilon)\frac{\tau-\mathrm{T_{gi}}}{\mathrm{T_f}})\,d\tau. \tag{6.13}$$

The power of this term is given by $\mathrm{E}_{\left[\mathrm{X_s[k']}_{II}\mathrm{X_s[k']}^*_{II}\right]} =$

$$\mathrm{E}_{|\mathrm{X_s[k']}|^2}\sum_{\mathrm{k}=-\frac{\mathrm{N_f}}{2}}^{\frac{\mathrm{N_f}}{2}-1}\int_0^{\mathrm{T_{gi}}}\mathrm{E}_{|\mathrm{h}(\tau)|^2}\mathrm{sinc}^2(\pi\phi(\mathrm{k},\mathrm{k}^{'},\epsilon))\,d\tau, \tag{6.14}$$

neglecting terms with coefficients $e^{-\frac{\tau_{\max}}{\tau_0}}$, the component of the desired signal power ($\mathrm{k}=\mathrm{k}^{'}$) can be approximated using [45] as

$$\mathrm{E}_{\mathrm{usefulI}} \approx \mathrm{E}_{|\mathrm{X_s[k']}|^2}\mathrm{sinc}^2(\pi\epsilon)(1-e^{-\frac{\mathrm{T_{gi}}}{\tau_0}}), \tag{6.15}$$

while the inter carrier interference ($\mathrm{k}\neq\mathrm{k}^{'}$) can be approximated as

$$\mathrm{E}_{\mathrm{intfII}} \approx \mathrm{E}_{|\mathrm{X_s[k']}|^2}\frac{(\pi\epsilon)^2}{3}(1-e^{-\frac{\mathrm{T_{gi}}}{\tau_0}}). \tag{6.16}$$

Next the region between $\mathrm{T_{gi}}<\tau<\tau_{\max}$ is considered. As shown earlier, the transmit pulse for the s^{th} OFDM symbol is given by,

$$\begin{aligned}\Xi_{\mathrm{T_s}}(\mathrm{t}-\mathrm{sT_s}-\tau) =& 1,\ \text{for, } \mathrm{sT_s}+\tau\leqslant\mathrm{t}<(\mathrm{s}+1)\mathrm{T_s}\\ =& 0, \text{otherwise.}\end{aligned} \tag{6.17}$$

At the receiver, the portion after the GI is taken away, the pulse used is given in (6.3). The integral over 't' in (6.1) is non zero over the period

$$\begin{aligned}\max\left(\mathrm{sT_s}+\tau,\mathrm{sT_s}+\mathrm{T_{gi}}\right)\leqslant&\min\left((\mathrm{s}+1)\mathrm{T_s}+\tau,(\mathrm{s}+1)\mathrm{T_s}\right)\\ \mathrm{sT_s}+\mathrm{T_{gi}}\leqslant&\,\mathrm{t}<(\mathrm{s}+1)\mathrm{T_s}.\end{aligned} \tag{6.18}$$

Then the received sub carrier component is given by

$$\begin{aligned}\mathrm{X_s[k']}_{III} =& \frac{1}{\mathrm{T_f}}\sum_{\mathrm{k}=-\frac{\mathrm{N_f}}{2}}^{\frac{\mathrm{N_f}}{2}-1}\mathrm{X_s[k]}\int_{\mathrm{T_{gi}}}^{\tau_{\max}}\mathrm{h}(\tau)e^{-j2\pi\mathrm{k}\frac{\tau}{\mathrm{T_f}}}e^{\phi(\mathrm{k},\mathrm{k}^{'},\mathrm{s},\mathrm{T_f},\mathrm{T_s},\mathrm{T_{gi}})}e^{j\frac{2\pi}{\mathrm{T_f}}\phi(\mathrm{k},\mathrm{k}^{'},\epsilon)(\mathrm{sT_s}+\mathrm{T_{gi}})}\\ &.e^{j\frac{\pi}{\mathrm{T_f}}(\mathrm{T_s}-\tau)}(\mathrm{T_s}-\tau)\mathrm{sinc}(\pi\phi(\mathrm{k},\mathrm{k}^{'},\epsilon)\frac{\mathrm{T_s}-\tau}{\mathrm{T_f}})\,d\tau.\end{aligned} \tag{6.19}$$

The power of this component is computed as

$$\mathrm{E}_{\left[\mathrm{X_s[k']}_{III}\mathrm{X_s[k']}^{*}_{III}\right]} = \mathrm{E}_{\frac{|\mathrm{X_s[k']}|^2}{\mathrm{T_f}^2}} \sum_{\mathrm{k}=-\frac{\mathrm{N_f}}{2}}^{\frac{\mathrm{N_f}}{2}-1} \int_{\mathrm{T_{gi}}}^{\tau_{\max}} \mathrm{E}_{|\mathrm{h}(\tau)|^2} (\mathrm{T_s}-\tau)^2 \mathrm{sinc}^2(\pi\phi(\mathrm{k},\mathrm{k}',\epsilon)\frac{\mathrm{T_s}-\tau}{\mathrm{T_f}})\, d\tau. \tag{6.20}$$

For $\mathrm{k} = \mathrm{k}'$, it is the desired sub carrier and (6.20) becomes

$$\begin{aligned}
\mathrm{E}_{\mathrm{usefulII}} &= \frac{\mathrm{E}_{|\mathrm{X_s[k']}|^2}}{{\mathrm{T_f}}^2} \int_{\mathrm{T_{gi}}}^{\tau_{\max}} \frac{e^{-\frac{\tau}{\tau_0}}}{\tau_0} ({\mathrm{T_s}}^2 - \tau^2 - 2\tau\mathrm{T_s}) d\,\tau \\
&\qquad \text{neglecting terms with coefficients } e^{-\frac{\tau_{\max}}{\tau_0}} \\
&\approx \frac{\mathrm{E}_{|\mathrm{X_s[k']}|^2}}{{\mathrm{T_f}}^2} e^{-\frac{\mathrm{T_{gi}}}{\tau_0}} \left({\mathrm{T_s}}^2 - (({\mathrm{T_{gi}}}+\tau_0)^2 + {\tau_0}^2) - 2(\mathrm{T_{gi}}+\tau_0)\mathrm{T_s}\right),
\end{aligned} \tag{6.21}$$

for $\mathrm{k} \neq \mathrm{k}'$, it is the interference component

$$\begin{aligned}
\mathrm{E}_{\mathrm{intfIII}} &\approx \frac{\mathrm{E}_{|\mathrm{X_s[k']}|^2}}{\pi^2} \frac{1}{\tau_0} \sum_{\mathrm{k}=-\frac{\mathrm{N_f}}{2}}^{\frac{\mathrm{N_f}}{2}-1} \frac{1}{\mathrm{k}-\mathrm{k}'+\epsilon} \int_{\mathrm{T_{gi}}}^{\tau_{\max}} e^{-\frac{\tau}{\tau_0}} \sin^2\left(\pi(\mathrm{k}-\mathrm{k}'+\epsilon)\frac{\mathrm{T_s}-\tau}{\mathrm{T_f}}\right) \\
&\leqslant \frac{\mathrm{E}_{|\mathrm{X_s[k']}|^2}}{\pi^2} \frac{1}{\tau_0} \sum_{\mathrm{k}=-\frac{\mathrm{N_f}}{2}}^{\frac{\mathrm{N_f}}{2}-1} \frac{1}{\mathrm{k}-\mathrm{k}'+\epsilon} \int_{\mathrm{T_{gi}}}^{\tau_{\max}} e^{-\frac{\tau}{\tau_0}}.
\end{aligned} \tag{6.22}$$

Since the above leads to a loose upper bound of this component of the interference, we use the average power of the 'sine' function, and hence have it as

$$\mathrm{E}_{\mathrm{intfIII}} \leqslant \frac{\mathrm{E}_{|\mathrm{X_s[k']}|^2}}{2\pi^2} \frac{1}{\tau_0} \sum_{\mathrm{k}=-\frac{\mathrm{N_f}}{2}}^{\frac{\mathrm{N_f}}{2}-1} \frac{1}{\mathrm{k}-\mathrm{k}'+\epsilon} \int_{\mathrm{T_{gi}}}^{\tau_{\max}} e^{-\frac{\tau}{\tau_0}}, \tag{6.23}$$

which can be evaluated to

$$\mathrm{E}_{\mathrm{intfIII}} \leqslant \frac{1}{6} \mathrm{E}_{|\mathrm{X_s[k']}|^2} e^{-\frac{\mathrm{T_{gi}}}{\tau_0}} \tag{6.24}$$

but after simulation, it was found that a tighter bound is approximately given by

$$\mathrm{E}_{\mathrm{intfIII}} \leqslant \frac{1}{8} \mathrm{E}_{|\mathrm{X_s[k']}|^2} e^{-\frac{\mathrm{T_{gi}}}{\tau_0}}. \tag{6.25}$$

Figure 6.2 compares the simulation result for the interference power for this compo-

nent against the two approximations, marked in the Figure with 'interference 2'. The legend 'Theory' is for the latter expression in (6.25) while 'approx' is for the earlier one in (6.24). Both theoretical expressions upper bound the result obtained from simulations. The gap between the expression for small value of the ratio of GI over rms delay spread is due to the approximations made but this gap becomes very small for value of the ratio above 2. The total interference power is computed by adding up each interference contribution, i.e.

$$\begin{aligned}\mathrm{E_{intf}} =& \mathrm{E_{intfI}} + \mathrm{E_{intfII}} + \mathrm{E_{intfIII}} \\ =& \mathrm{E}_{|\mathrm{X_{s-1}[k]}|^2}\frac{\tau_0}{\mathrm{T_f}}e^{-\mathrm{T_{gi}}/\tau_0} + \mathrm{E}_{|\mathrm{X_s[k']}|^2}\frac{(\pi\epsilon)^2}{3}(1-e^{-\frac{\mathrm{T_{gi}}}{\tau_0}}) + \frac{1}{8}\mathrm{E}_{|\mathrm{X_s[k']}|^2}e^{-\frac{\mathrm{T_{gi}}}{\tau_0}}. \end{aligned} \quad (6.26)$$

Figure 6.2 shows the total interference power of simulation as compared against the theoretical formula derived. The curves labeled as 'sum' is the total interference power at a received sub carrier. The theoretical formulas are indeed upper bounds as can be seen from the figure. As indicated earlier, the legend 'simulation' is for the result obtained via simulation, 'theory' is obtained from the derived expressions, while 'approx' is obtained from the expression using approximations as described earlier. Similar observation is made in this case also regarding the expression and their relation to the simulation curves as in the case of 'interference 2'. The total useful signal power is given by

$$\begin{aligned}\mathrm{E_{useful}} &= \mathrm{E_{usefulI}} + \mathrm{E_{usefulII}} \\ &\approx \mathrm{E}_{|\mathrm{X_s[k']}|^2}\mathrm{sinc}^2(\pi\epsilon)(1-e^{-\frac{\mathrm{T_{gi}}}{\tau_0}}) + \frac{\mathrm{E}_{|\mathrm{X_s[k']}|^2}}{{\mathrm{T_f}}^2}e^{-\frac{\mathrm{T_{gi}}}{\tau_0}}({\mathrm{T_s}}^2 - (({\mathrm{T_{gi}}}+\tau_0)^2+{\tau_0}^2) - 2(\mathrm{T_{gi}}+\tau_0)\mathrm{T_s}). \end{aligned} \quad (6.27)$$

For large $\mathrm{T_{gi}}$ and $\epsilon = 0$, this term becomes $\mathrm{E}_{|\mathrm{X_s[k]}|^2}$, which is the ideal case. The expression is found to be a very close lower bound for the signal power. Since this is cumbersome to solve, we will use a simpler expression in evaluating the desired length of the GI. Instead of using (6.27) for $\mathrm{E_{useful}}$, only $\mathrm{E_{usefulI}}$ will used for the total useful signal power. This will of course reduce the estimate of SINR. SINR can thus be written as

$$\mathrm{SINR}\ (\tilde{\Upsilon}) \leqslant \frac{\mathrm{E_{useful}}}{\mathrm{E_{intfI}} + \mathrm{E_{intfII}} + \mathrm{E_{intfIII}} + \sigma^2_{\omega[\mathrm{k}]}}, \quad (6.28)$$

where $\sigma^2_{\omega[\mathrm{k}]}$ is the noise power per sub carrier. Figure 6.3 compares the SINR as

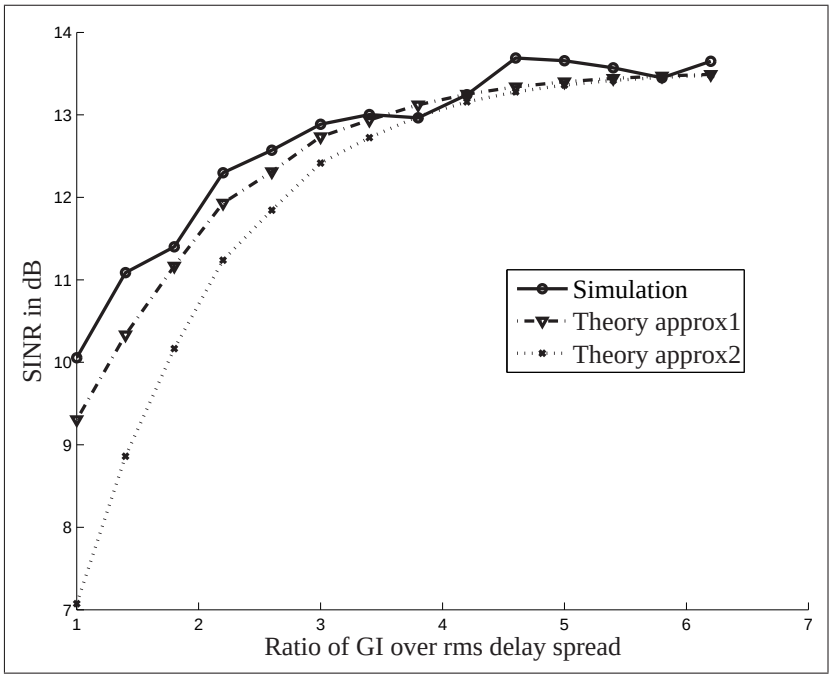

Figure 6.3: SINR vs Ratio of GI over rms delay spread

.

obtained from simulations, and that obtained from the derivations given above. The curve labeled 'Simulation' is the SINR obtained from simulation, while the one labeled 'Theory approx1', is obtained considering the tight bound, while 'approx2' is obtained using the relatively relaxed bound (for simpler computation complexity). It shows that the theoretical SINR predictions are lower bounds. Usually systems are required to satisfy a certain BER to meet a desired quality of service. The required BER, which has to be satisfied, can be mapped to a SINR value [26]. This value can be called the required SINR ($\tilde{\Upsilon}_{\text{req}}$). To compute the required GI, SINR ($\tilde{\Upsilon}$ as in (6.28)), due to the interference, is set to be greater than the required value, $\tilde{\Upsilon}_{\text{req}}$, i.e. $\tilde{\Upsilon} > \tilde{\Upsilon}_{\text{req}}$. Upon evaluating this expression, the required GI becomes

$$\mathrm{T_{gi}} \gtrapprox \tau_0 \log\left(\frac{\mathrm{A}}{\mathrm{B}}\right), \tag{6.29}$$

where A =

$$\tilde{\Upsilon}_{\text{req}}\{\frac{\tau_0}{\mathrm{T_f}} + \frac{1}{8} - \frac{\pi^2}{3}\epsilon^2\} + sinc^2(\pi\epsilon)$$

and

$$B = \mathrm{sinc}^2(\pi\epsilon) - \tilde{\Upsilon}_{\text{req}}\{\frac{\pi^2}{3}\epsilon^2 + \frac{1}{\Upsilon}\},$$

where $\Upsilon = \tilde{\Upsilon}_{\text{req}} + \Delta_{\tilde{\Upsilon}}$ in dB scale, where $\Delta_{\tilde{\Upsilon}}$ is extra SNR needed over the required

SNR, and $\Upsilon = \frac{\mathrm{E}_{|\mathrm{X_s[k]}|^2}}{\sigma^2_{\omega[\mathrm{k}]}}$. As can be observed from the above, *the required GI is thus found to be a function of the channel rms delay spread, required signal to interference plus noise power ratio, the signal to noise power ratio margin, and the DFT duration.*

The rms delay spread of the channel has to be estimated to compute the length of the required GI. The method in [90] may be used for such estimation. It can also be done following the definition of rms delay spread [34]. This will require channel coefficients which can be obtained by advanced channel estimation schemes. The GI used in the simulations is estimated following the definition, while the channel coefficients used in it are estimated following a Discrete Fourier Transform (DFT) based interpolation technique [91]. The estimated GI is used in the subsequent frame. Thus there will be a time lag between such estimation and use in a subsequent frame. In dynamic channel conditions, the required GI may change over the time lag period. The performance of systems using this VGI algorithm needs to be verified via simulation over such channel conditions, results for which will be presented in the following sections.

6.4 Performance and Discussion

To generate the time varying channel coefficients for each tap, the exponential power delay profile using Jake's Doppler spectrum with maximum velocity as 250 kmph is considered. The carrier frequency is taken as 3.6 GHz. Once the GI is estimated, it is used only in the next frame. Each frame is of 512 octets, with quadrature phase shift keying (QPSK) modulation scheme, while using rate 1/2 convolution coding with a constraint length of 7. The maximum tolerable relative carrier frequency offset has been kept at 2% of the sub carrier bandwidth.

To compare the performance of VGI in dynamic environment, first the mean BER is verified for different amount of time lag between estimation of GI and its use in subsequent OFDM symbols. Simulation conditions and results are given in Table 6.1. The symbol $T_{coh0.5}$ implies the coherence time for 50% correlation of the rms delay spread or mean excess delay. The term T_{coh0} implies the duration when the correlation function reaches zero for the first time. This point was calculated from the time correlation function of the channel. It can be seen from the table that the proposed VGI scheme does not compromise on BER. It maintains BER which is very close to the system using a large but fixed GI. This behavior can be explained from the condition which was used to derive the required GI. Since the GI is chosen such that the signal to interference plus noise ratio is maintained at the receiver there is no

Table 6.1: Bit Error Rate for SINR: 15 dB , rms delay spread: 1 μs, Carrier Frequency: 3.5 GHz, Bandwidth 20 Mhz bandwidth, Number of sub carriers: 1024, Guard length for fixed GI: 128.

Lag $\rightarrow$	NoDelay	$T_{coh0.5}$	T_{coh0}	$2xT_{coh0}$	$10xT_{coh0}$	Fixed GI
$\Delta_{\tilde{\Upsilon}} \downarrow$						
0.5	$5x10^{-5}$	$4x10^{-5}$	$3.5x10^{-5}$	$4x10^{-5}$	$5x10^{-5}$	$5x10^{-5}$
1	$3x10^{-5}$	$3x10^{-5}$	$2.7x10^{-5}$	$3x10^{-5}$	$4x10^{-5}$	$3x10^{-5}$
2	$1.25x10^{-5}$	$1.25x10^{-5}$	1.25^{-5}	1.25^{-5}	1.25^{-5}	$1.25x10^{-5}$

degradation in the BER. It also shows that the algorithm is robust to time variation of the rms delay spread and mean excess delay of the channel. Time variation of channel coefficients will give rise to time variations of the instantaneous rms delay spread [42]. Even though there is a large gap in the estimation of the required GI and the use in subsequent OFDM frames, there is not much degradation in the bit error rate. This means that as long as the average rms delay spread of the channel does not change significantly the estimated GI can be used quite satisfactorily. The over determination of interference and under estimation of the desired signal power leading to under estimation of SINR as discussed in the previous Section contributes to such phenomenon. Another issue to be considered is the discrete implementation of the GI. During implementation, the number of samples in the GI to be used is taken as $N_{gi_{used}} = \lceil \frac{T_{gi}}{T} \rceil$, where $\lceil \rceil$ means 'ceil' operation and T is the sampling period. Therefore only if the required GI changes by more than one sampling period, the required GI will change by one sampling period.

Now the impact of the several parameters that influence the selection of GI as given in (6.29) will be analyzed. Since the ratio of $\frac{\tau_0}{T_f}$ is small, the impact of variation of the ratio of $\frac{\tau_0}{T_f}$ on the required GI is very small. The impact of the parameters $\Delta_{\tilde{\Upsilon}}$, $\tilde{\Upsilon}_{req}$ and ϵ on the required GI is given in Figure 6.4. 'SNRgap' indicates the gap between $\tilde{\Upsilon}_{req}$ and Υ. It can be seen that for any given scenario, for non zero value of $\epsilon = 0.1$ ('ep2'), the required GI increases compared to when $\epsilon = 0.02$ ('ep1'). Without the knowledge of allowable ϵ, the required GI estimated would be less, and therefore there would be more interference and the required SINR will not be met. With increasing value of required SINR, the required GI also increases. This is because with increasing required SINR, the interference level must be kept at very low levels, hence a larger GI is required. It is also seen that with increasing gap between $\tilde{\Upsilon}_{req}$ and Υ, the required GI decreases. It will be shown, that increasing this gap indefinitely, does not give any benefit.

Figure 6.5 shows the bit error rate performance against increasing SNR when

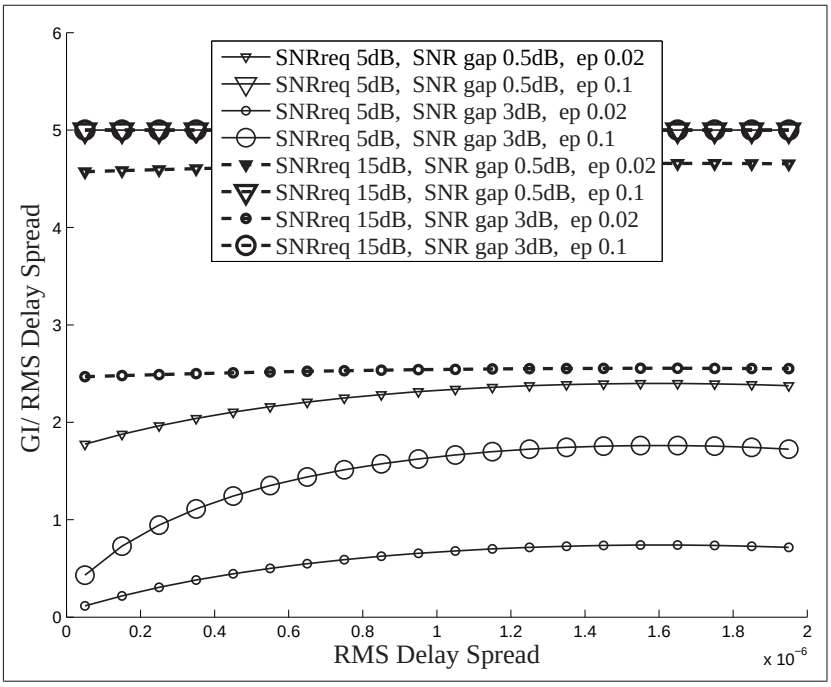

Figure 6.4: Ratio of GI Vs rms delay spread. Depicting variation of T_{gi} with respect to various $\Delta_{\tilde{\Upsilon}}$.

the required SNR is kept at 15 dB; i.e. 'SNRgap' is varied from 0.5 to 20 dB. It can be observed that even though the SNR is increased the bit error rate for VGI reaches an error floor. This is because the interference from the previous OFDM symbol will also increase with increasing signal power and thus perceived SINR will not increase and therefore BER curve will not improve beyond a certain value. It depends on implementation, how much extra power may be permissible. It has been seen that using 0.5 to 1 dB extra SNR may be a good tradeoff.

The distribution of the required GI, when the average rms delay spread is 1μs, (instantaneous rms delay spreads may vary, as was indicated with references in the introduction) is analyzed next. Figure 6.6 shows an empirical cumulative distribution plot of the required GI, obtained from the simulations, when the required SNR is 15 db and the SNR gap is 0.5,1 and 2 dB. The reduction in required GI with varying SNR gap can also be seen in these figures. In systems using fixed GI, the length of GI is usually taken about eight to ten times more than average rms delay spread(here the fixed GI was taken as 1/4 of the useful symbol duration, where the useful symbol period was kept as 51.2μs). Whereas in VGI it can be seen that in some cases as low as 3μs and maximum of about 6.2μs. This is because some of the extra GI is bought off by the additional SNR (SNR gap). Thus it can be seen that the required GI can be reduced by a huge margin of about 60% to 20%.

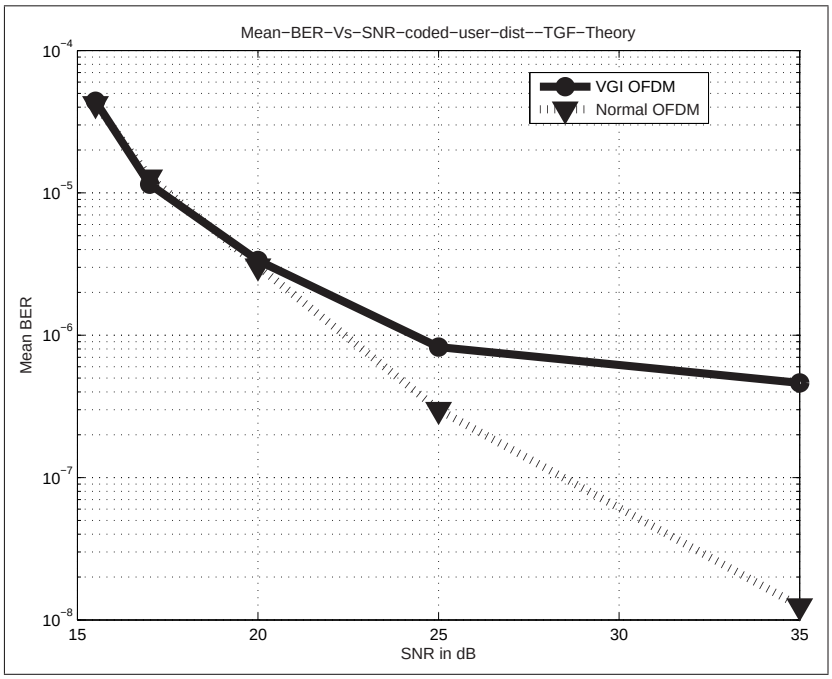

Figure 6.5: Performance with increasing SNR.

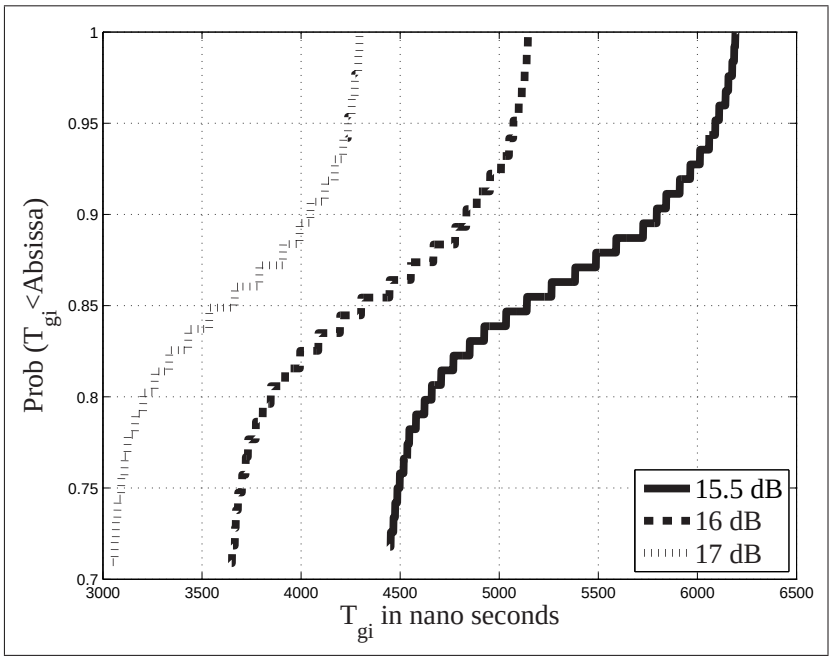

Figure 6.6: Cumulative Distribution Function of required GI.

In absolute terms the throughput increase is about 20% as can be seen in Figure 6.7, where 'VGI OFDM' is for the throughput distribution of the system using the proposed variable GI and 'Normal OFDM' is OFDM system using fixed GI. The legends 'Mean' marks the mean values of each throughput.

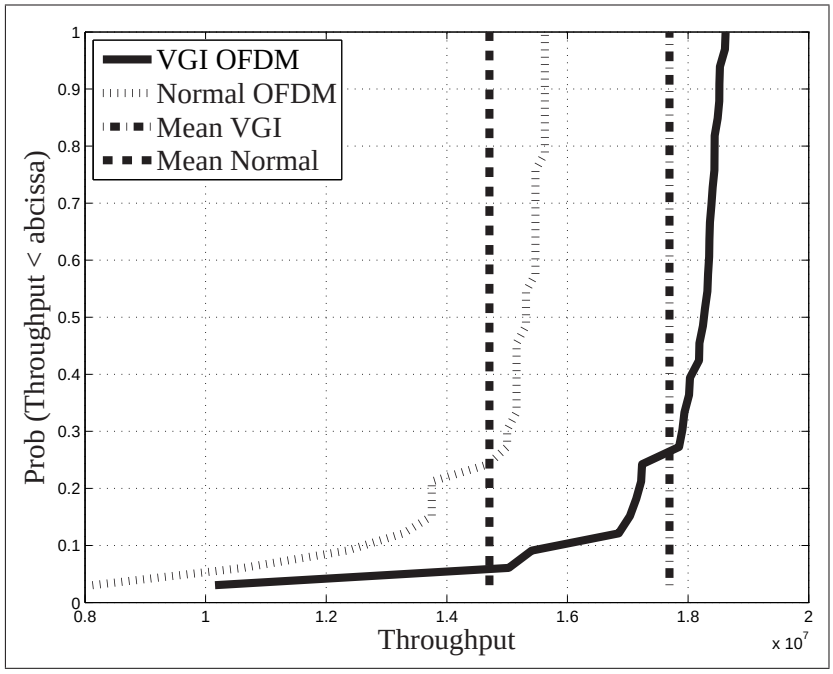

Figure 6.7: Gain in throughput of the proposed VGI over fixed GI system for 2dB extra SNR for 1μs rms delay spread.

6.5 Conclusion

In this work, an algorithm for implementing VGI for OFDM system in presence of carrier frequency offset in a dynamic wireless channel condition has been proposed. The algorithm is found to reduce required GI by about 60% and it also increases the mean throughput by about 20%, without compromising on BER but using 0.5–2 dB extra SNR. The performance is evaluated at 1 micro second average rms delay spread of the channel, at vehicular speeds of 250 kmph with 3.6 GHz of carrier frequency. The efficient performance of the algorithm makes it a good candidate for implementation in OFDM based wireless systems having such provisions.

7

Hybrid Link Adaptation

The goal of this thesis is to improve the spectral efficiency for OFDM systems, with minimum impact on User Equipment (UE) complexity. To this effect, hybrid Link Adaptation (LA) methods are proposed and analyzed in this Chapter.

In OFDM systems, there are several degrees of freedom in time and frequency domain, such as sub-band size, forward error control coding (FEC) rate, modulation, power level, modulation & coding rate adaptation interval and power adaptation interval. These can be exploited for Link Adaptation (LA) to achieve high spectral efficiency. The choice for adapting these parameters is dependent on dynamically changing channel parameters such as the instantaneous channel gains, the rms delay spread of the channel, Doppler frequency spread and average signal to noise ratio (SNR). Optimal adaptation implies highly complex systems and high signalling overhead. Hybrid strategies to tradeoff achievable efficiency and complexity are proposed and analyzed in this Chapter. *The term Hybrid is used because not only is the bit and power is being adapted but also the adaptation framework, i.e. the adaptation window for each of these parameters is also suggested to be adapted for achieving high spectral efficiency with optimum resolution of adaptation.*

7.1 Introduction

LA techniques are known to maximize spectral efficiency by exploiting the channel variability [92],[93]. LA schemes adapt transmission parameters, such as bit and power, according to the channel conditions so that the maximum bit rate is transmitted while keeping the error rate below a target [26]. Once the values of the adaptable parameters are selected they are kept constant over a region in time and frequency domain where the channel is relatively flat. There is advanced literature on adaptive modulation for single carrier systems [26]. OFDM has fine granularity of the minimum allocation unit which is the sub carrier. The flat fading experience by a sub carrier provides inherent support needed to exploit the advantage of LA [94],[95] in multiple dimensions. The optimal solution for achieving capacity is water filling method [96]. Due to its high implementation complexity, suboptimal solutions such as [94],[97], are used. There are several algorithms which address BER constraint along with spectral efficiency maximization [98] but these are mostly for uncoded systems. When a group of sub carriers are used instead of a single sub carrier and when forward error control coding is applied these results are no more applicable. The algorithm used in this work has been described in detail in Appendix B. The algorithm is however extended in this work in the sense that all references to a sub carrier are to be replaced by the sub band (group of neighboring sub carrier forming a data block).

The degrees of freedom that can be exploited by LA techniques increase when they are used in the OFDM framework with the benefit of improved spectral efficiency. However, this leads to increase in complexity of the system. LA involves adaptation of the modulation level (M), the FEC rate (C) and the power level (P) at the transmitter as per the channel state information fed back from the receiver. When applied in the OFDM framework, LA additionally includes selection of adaptation interval for M & C, adaptation interval for P, choice of sub-band size and bit–power loading algorithm. Other than the fast fading (instantaneous) of the channel gains, the dynamic variation of the channel parameters such as the root mean square (rms) delay spread, Doppler frequency spread, average SNR condition also heavily influence the values to be selected for some LA parameters. The authors in [27] discuss some of the channel effects but the work presented in this chapter provides a much more detailed analysis, covers many more situations and gives guidelines on Hybrid LA.

When a LA scheme tries to optimally adapt so many parameters which depend on another large set of varying channel conditions, then the system complexity is

bound to increase many folds. Therefore hybrid strategies, which limit some degrees of freedom by slowly varying some parameters, while using fast adaptation for the others are proposed and investigated in this work. The objective is to analyze the tradeoff between spectral efficiency loss and complexity and overhead reduction that can be obtained by the hybrid strategies.

7.2 System Model

The broad system model for LA is presented in Chapter 2. Fig. 7.1 elaborates the diagram for OFDM systems. As mentioned, in OFDM systems, the link adaptation is done in time and frequency domain. The Channel State Information (CSI) is fed back from the User Equipment (UE) to the Base Station (BS) in FDD systems or is measured at the BS in the reverse link in case of TDD systems. The CQI module feeds back the SNR of a sub band (a group of consecutive sub carriers). It may also feedback a change in the transmit power required to maintain the SNR. This information is used by the Link Adaptation Control unit at the transmitter. This unit selects the FEC coding rate, the modulation rate and the power level for each sub band according to the bit and power loading algorithm used in the system. It might also be used to select the sub band size, the adaptation interval, the power control interval, and a fixed coding rate when a single coding rate is to be used, details of which are discussed in this chapter. 3GPP-LTE [2] system parameters are used in this work and are given in Table 7.1 for reference.

Table 7.1: System Parameters

Parameter	**Value**
Carrier Frequency	2GHz
Bandwidth	5MHz
Sampling Frequency	7.68MHz
Sub Carrier Spacing	15 KHz
Rms delay spread	0.5μs–2μs
FFT size	512
Useful Symbol period	66.67μs
Cyclic Prefix	8.3μs
Code rates	$\frac{1}{3}, \frac{1}{2}, \frac{2}{3}$ convolution coding
Modulation	QPSK, 16-QAM, 64-QAM

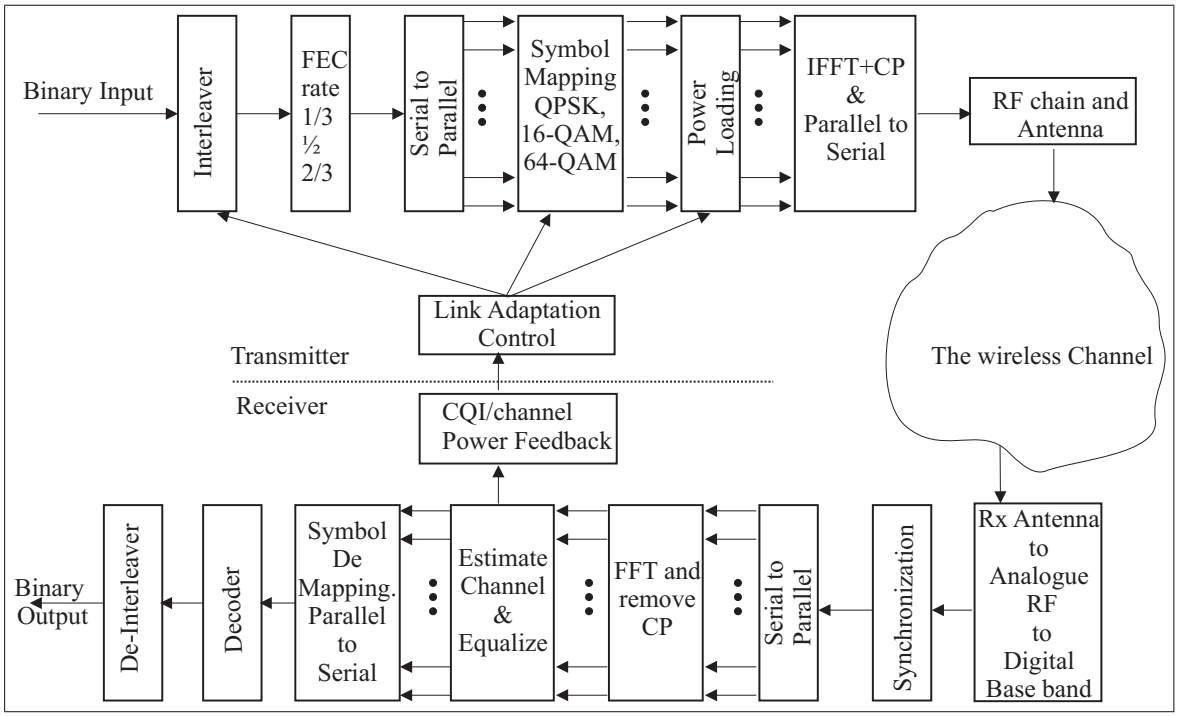

Figure 7.1: OFDM based link adaptation transceiver architecture

Frame Structure The frame structure fundamental to LA which is being considered in this work is given in Fig. 7.2. The sub-band size is defined by the number of consecutive sub carriers that make the block. The minimum unit over which FEC and interleaving are applied is called a block. The Block Error Rate (BLER) is calculated with respect to this block. It is a set of consecutive sub carriers which spans a successive sequence of OFDM symbols over a period of 0.5ms. The modulation level, code rate and power level are applied at the block level in this work. The block size can be made to vary in the frequency domain, by changing the sub band size. The modulation and coding level is adapted once every adaptation interval, which can be multiple of the block duration. Adaptation interval is the period in time over which the modulation and coding remains unchanged and power adaptation interval is the period between each power adaptation.

Link Adaptation Set up It is being considered that the UE receives the pilot signals at the Downlink (DL) transmission slot, and then it measures the received SNR. The received SNR is fed back to BS. The feed back information is sent to BS at Uplink (UL) time slot for TDD and uplink frequency band in FDD. CQI information conveys the channel information (SNR in this work). If no power control is needed then only the desired bit rate (a combination of modulation and coding

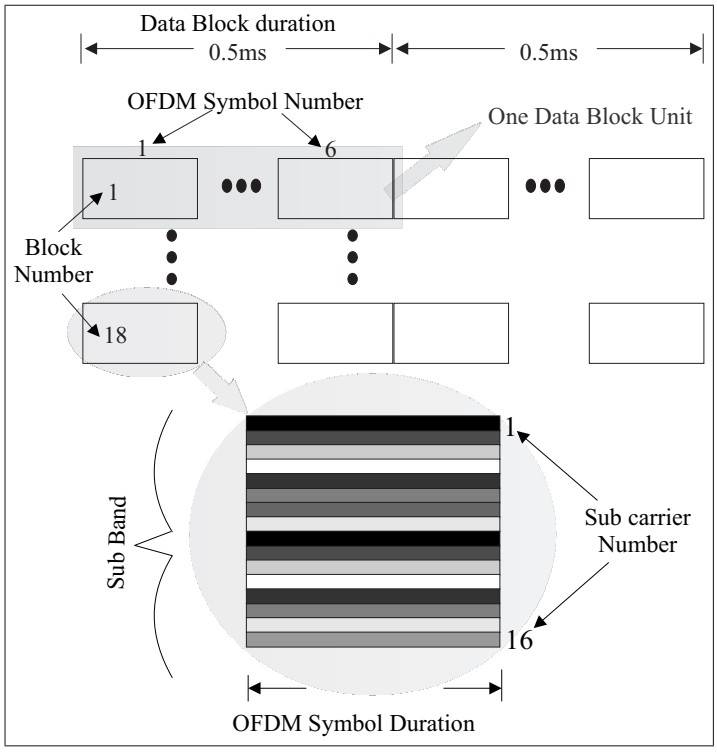

Figure 7.2: Link adaptation frame structure.

rate) may be used for CQI information, otherwise it may be quantized SNR in the dB scale or it might be a difference in power indicator. This depends very much on the LA algorithm in use. A typical time sequence of the channel estimation and feedback is in Fig. 2.22. At the beginning of each adaptation window, the resulting CQI for all blocks are sent back to BS, which is used to decide on LA method.

7.3 Hybrid LA strategies

Hybrid LA strategies being proposed here do not exploit all degrees of freedom simultaneously. As mentioned, several parameters can be adapted, namely, modulation level (M), the FEC code rate (C), power level (P), adaptation interval for M & C, adaptation interval for P, sub-band size and choice of bit–power loading algorithm. Different combination of slow and fast adaptation can be made between the available choices so that only few parameters are adapted instantaneously using immediate channel gains. Other parameters are adapted statistically, i.e. using average information such as, Doppler frequency spread, rms delay spread and average SNR. The interrelationships between the channel parameters and the link adaptation parameters are analyzed for simplified Hybrid LA in this chapter.

7.3.1 Different Link Adaptation Algorithms

Here two different link adaptation (bit and power loading) algorithms for various conditions of rms delay spread and Doppler conditions are considered.

- Adaptive Power, Modulation and Coding (APMC): In this algorithm power, modulation and coding rate are adapted simultaneously for each data block to achieve the best possible spectral efficiency. It uses iterative procedure to distribute power, and find bit loads, whose details are in [95]. The algorithm is also described in Appendix B.

- Adaptive Modulation and Coding with fixed Power (AMCfixP): In this algorithm, transmission power for each block is assumed to be equal at the beginning. Using the feedback CSI, the modulation and coding rate, which suits the SNR level, for each block are found. After this, the power is brought down so that the received SNR equals the threshold value. The purpose of bringing down the power is to save power and reduce interference when deployed in a cellular environment with aggressive frequency re-use. The difference with the earlier algorithm is that it avoids the iterations (of finding the best bit and power loading combination) and hence is significantly less complex.

The algorithms are evaluated in two different conditions. One has low diversity i.e. low rms delay spread and low Doppler while the other has high diversity i.e. high rms delay spread and high Doppler.

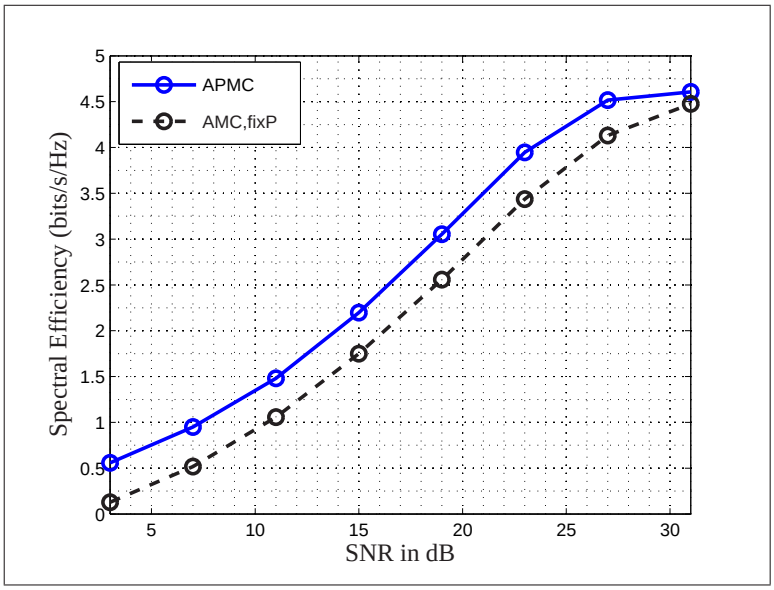

Figure 7.3: Spectral Efficiency for SISO with Fd=50Hz, $\tau_{rms} = 0.5\mu$s

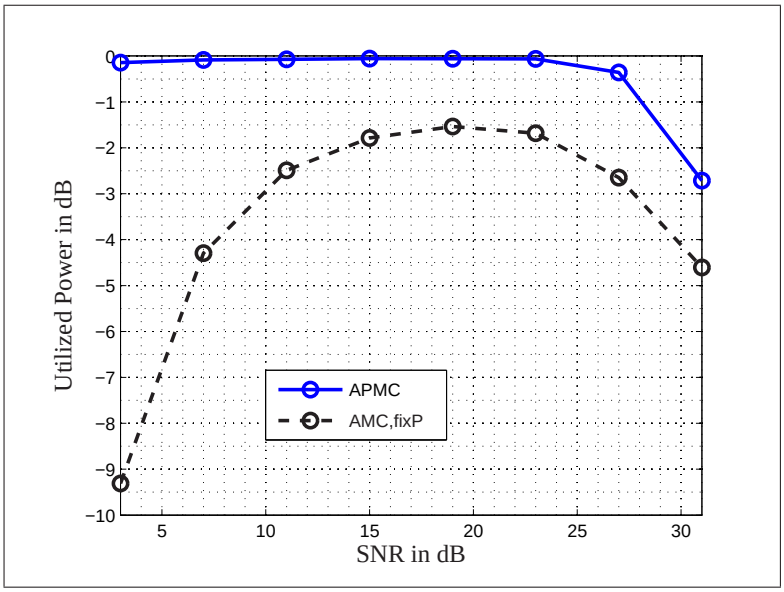

Figure 7.4: Power Utilization for SISO with Fd=50Hz, $\tau_{rms} = 0.5\mu$s

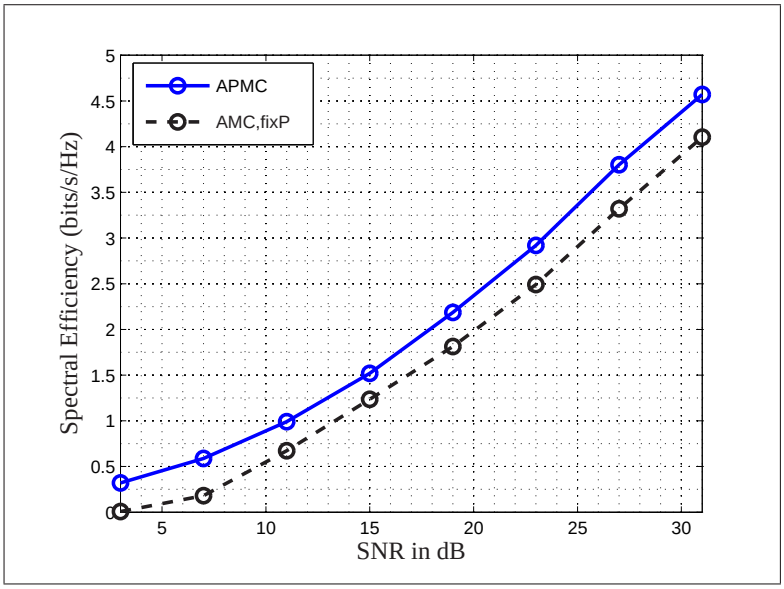

Figure 7.5: Spectral Efficiency for SISO with Fd=250Hz, $\tau_{rms} = 2\mu$s

Fig. 7.3 shows the spectral efficiency for the above mentioned LA algorithms in a Single Input Single Output (SISO) system for the low diversity conditions. From Fig. 7.3 it can be seen that APMC has quite improved performance compared to AMCfixP but at high SNR region the spectral efficiency of the two algorithms comes close to each other. This suggests that the low complexity AMCfixP can be used under the conditions of low diversity with high SNR. The behavior can be understood

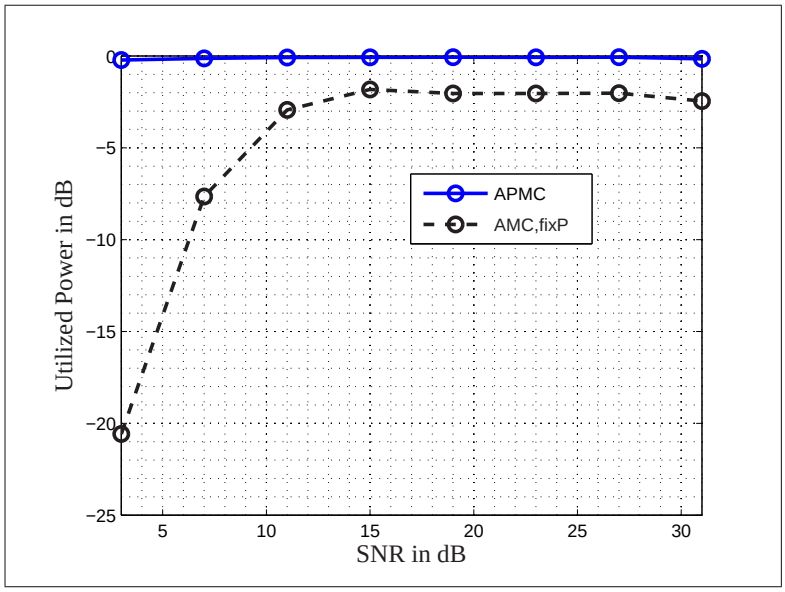

Figure 7.6: Power Utilization for SISO with Fd=250Hz, $\tau_{rms} = 2\mu$s

knowing that up to 64-QAM modulation have been used, therefore above a certain SNR condition, the spectral efficiency of the best bit and power loading algorithm cannot increase beyond certain limit. From the power utilization curves under these conditions as in Fig. 7.4 it can be concluded that AMCfixP algorithm consumes less power and therefore may cause less interference in a cellular scenario under strong interference.

Fig. 7.5 shows the spectral efficiency and Fig. 7.6 shows the power utilization performance for the same LA algorithms for high diversity conditions. In contrast to the earlier condition, it can now be seen from Fig. 7.6 that the gap in performance between the two algorithms has not decreased in the range of SNR under observation. Therefore the APMC algorithm proves to be better compared to the other LA algorithm. It can also be observed that the difference in power utilization for SNR above 10 dB is not more than 2 dB, while in the previous case there was much larger power saving by the AMCfixP algorithm. Under high interference scenario the reduction in interference due to use of less power might not be noticeable.

Finally, under low diversity and high SNR conditions, i.e. small cell and near the base station it is worth using the AMCfixP in order to have less complexity while for high diversity scenarios it is suggested to use APMC algorithm. It must also be noted that the algorithm to load bit and power can be adapted as per statistical channel conditions at a very slow rate since the channel statistics are not expected to change as per the coherence time. Fast bit and power loading in combination

with slow algorithm selection can be used to obtain the best performance in terms of spectral efficiency and power consumption. It is called fast adaptation here when the adaptation interval is comparable to the coherence time of the channel coefficients, whereas, when the adaptation interval is larger than the coherence time of the channel coefficients, then it is called slow adaptation.

7.3.2 LA with Different Sub-channel Sizes

In this section, the influence of rms delay spread and Doppler spread on the performance of LA with different sub-channel sizes is evaluated. The APMC algorithm is used in all analysis unless otherwise mentioned. This is because the APMC algorithm achieves the highest spectral efficiency. While the LA window in time domain is fixed at 0.5 ms, the LA in frequency domain can be performed across sub-band size of 8, 16, 32 & 64. Like the previous situation, analysis will be made in low and high diversity channel conditions.

From Fig. 7.7 it can be seen that with small Doppler frequency and delay spread values, a small sub-band size will lead to high spectral efficiency compared to a large sub-band size. This is because with small Doppler frequency and delay spread, diversity is low, i.e. the channel over one data block does not vary much. So, link adaptation gains over a flat channel will dominate interleaving gain. A small sub-channel size means less variation within the LA window, which will lead to better performance. On the other hand, it can be seen from Figure 7.8 that with high Doppler frequency and delay spread values, the performance for different sub-channel size is quite similar. The reason is, with high Doppler frequency and delay spread values, diversity is high even with a sub-channel size of 8. i.e. the channel is not very flat over a data block consisting of even 8 sub carrier over 6 OFDM symbols. Moreover, a wide sub-band means higher interleaving gain, because of more variation in the channel. Thus it can be seen that a variation in the sub-band size does not change the spectral efficiency. From Fig. 7.7 and Fig. 7.8, it can be concluded that for low Doppler frequency and delay spread, it is better to use a small sub-channel size to maximize system performance while for high Doppler frequency and delay spread, it is suggested to use a large sub band size since it will use significantly low overhead and computation resources, while achieving the same performance.

Now it is important to recall that in Chapter 2, it is stated that some SNR threshold was needed to select a modulation and coding which yields the best throughput while satisfying the target error rate constraint. In the cases presented above it

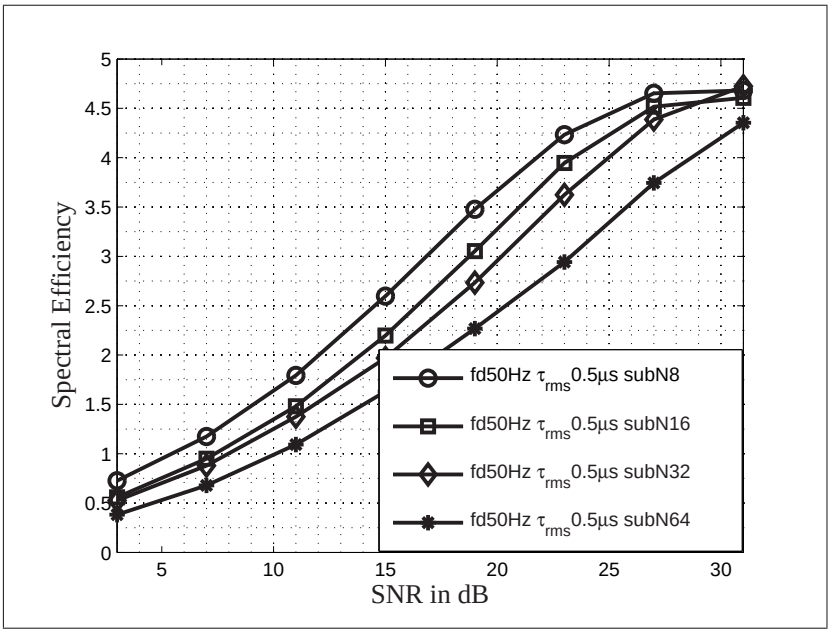

Figure 7.7: Spectral Efficiency with Doppler 50Hz, delay spread 0.5μs

can be noted that each situation, (which can be considered as a function of channel diversity condition, the LA duration, and the sub band size) demands a different switching threshold since the SNR required to meet a certain BLER is a function of the channel condition, the data block size in time, frequency and number of bits. The Look Up Table (LUT) used for one of the situations is presented in Table 7.2. The threshold values give an indication of the spectral efficiency performance. It can be seen in the LUT that the starting thresholds for each modulation and coding rate are increasing with increase in the sub band size for the 50 Hz Doppler scenario. This means that a certain modulation and coding level (a data rate) will be selected for a low SNR for the small sub band size as compared to a large sub band size to maintain the target BLER while maximizing the throughput. This in turn implies that at a lower SNR a higher data rate may be selected for the smaller sub band size, which has already been reflected in the spectral efficiency plot for this scenario. The BLER for this case on using these thresholds is in Fig. 7.9. It is shown in the figure that the BLER is almost satisfied in all conditions using the LUT given above, except for the very large sub band size, which means that the spectral efficiency curves are invalid and may shift even further to the right.

Finally it can be concluded that it is important to consider very slow rate sub band size adaptation to minimize feedback overhead along with fast bit and power loading to have a high spectral efficiency. The sub band size needs to be small for situations of flat channel over a data block while it can be large when the diversity

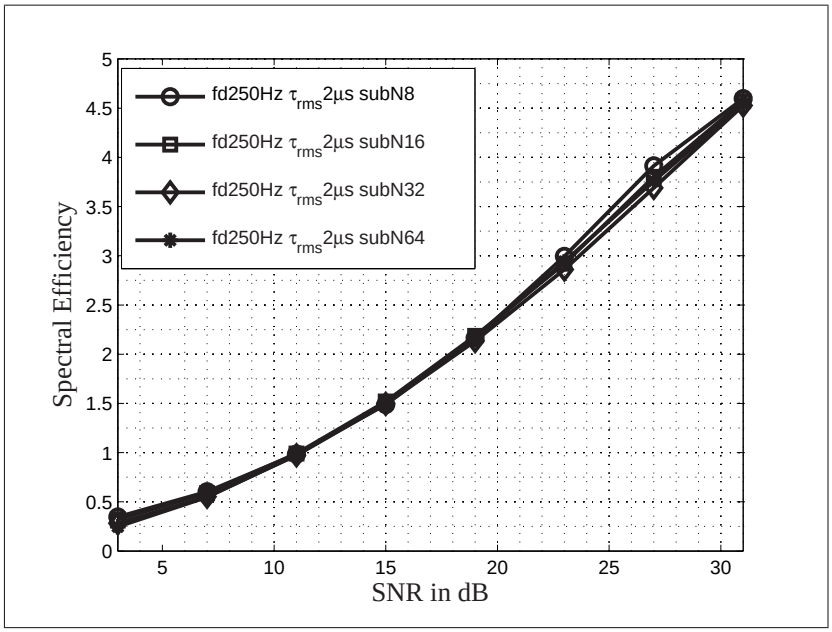

Figure 7.8: Spectral Efficiency with Doppler 250Hz, delay spread 2μs

Table 7.2: SISO,LA per 1 frame(s),BLER=0.05, tau_{rms}=0.5μs,fd=50Hz

SubN	Mod schemes	Rate2/3	Rate1/2	Rate1/3
8	4QAM	9.01dB	6.83dB	4.27dB
	16QAM	15.62dB	13.43dB	10.59dB
	64QAM	21.36dB	18.36dB	14.89dB
16	4QAM	10.43dB	7.83dB	4.96dB
	16QAM	17.14dB	14.29dB	10.81dB
	64QAM	22.98dB	20.19dB	16.09dB
32	4QAM	13.91dB	10.17dB	6.16dB
	16QAM	21.29dB	16.80dB	11.83dB
	64QAM	26.64dB	22.16dB	17.07dB
64	4QAM	17.38dB	11.54dB	6.60dB
	16QAM	23.35dB	17.84dB	12.61dB
	64QAM	29.83dB	22.83dB	17.48dB

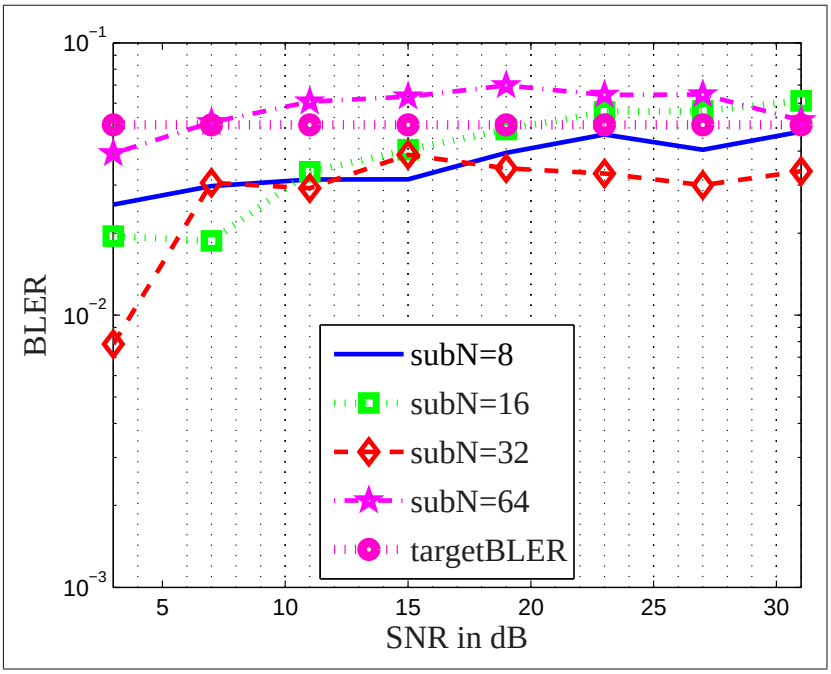

Figure 7.9: BLER for SISO,LA per 1 frame(s),BLER=0.05, τ_{rms}=0.5μs, fd=50Hz.

of the channel is quite high.

7.3.3 Fixed Coding Rate

In link adaptation studies [99],[27],[100],[101], it is found that adaptive bit loading is considered without any constraint on user devices. With optimal bit loading, there are situations where more than one coding rate is allocated to one user in consecutive data blocks, or more than one data block at a time. Though this leads to maximum spectrally efficiency, it may not be practically feasible to use more than once code rate for one UE. Using more than one code rate for a UE will put a heavy signal processing burden on the UE. Therefore using only one coding rate for a UE is advisable. In this situation it is important to identify the coding rate which might give the best performance. The focus of this section is to find the impact of different channel conditions on the fixed coding rate to be selected for a user. Therefore different fixed coding rates with adaptive modulation and power loading are considered. The benchmark performance is from adaptive modulation, coding and power control (APMC).

From Fig. 7.10 it can be seen that with small Doppler frequency and delay spread values, Adaptive Power and Modulation with Fixed Coding rate (APMfixC) with coding rate $\frac{2}{3}$ gives almost the same performance as APMC from 12 dB onwards;

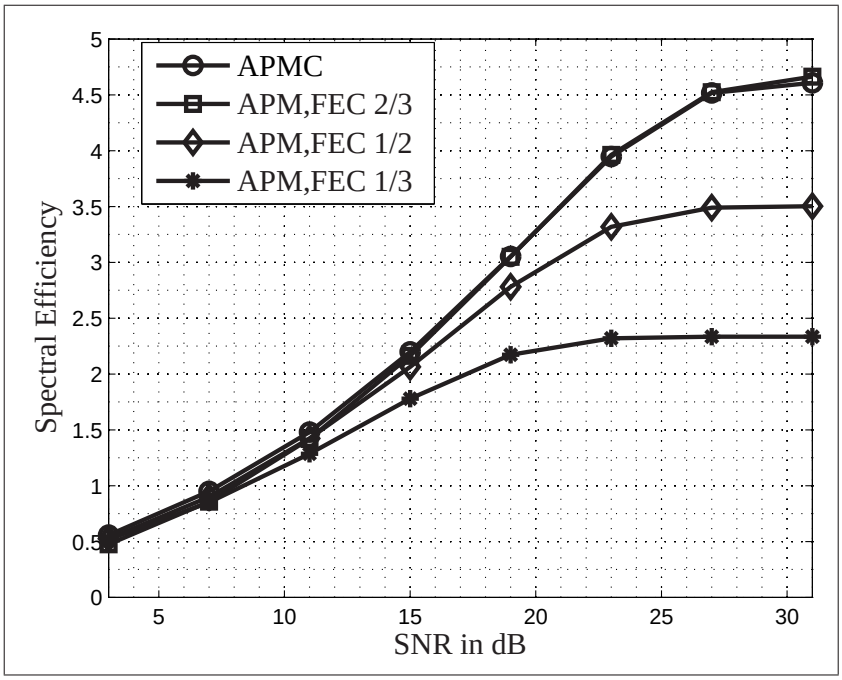

Figure 7.10: Spectral Efficiency with Doppler 50Hz, delay spread 0.5μs

while for SNR less than 12 dB coding rate $\frac{1}{2}$ has near optimal performance.

From Fig. 7.11 it can be said that rate $\frac{1}{3}$ can be used up to a SNR of 19dB, and rate $\frac{1}{2}$ up to SNR of 27 dB, while beyond this rate $\frac{2}{3}$ can be used for channel conditions with high diversity. These SNR values are average values measured over the whole bandwidth. By using the above thresholds, a UE can use only one coding rate yet have performance as close to adaptive coding as possible. This would require a much less complex system implementation while there would be negligible loss in performance.

In Table 7.3 the average SNR values for switching from one coding rate to another is given. The mark '-' indicates that the coding rate is the default rate to start with, while the SNR values indicate the starting average SNR from where the particular coding rate can be used and 'NA' indicates the corresponding coding rate not be used.

7.3.4 LA Rate

The effect of changing LA window in frequency domain have been studied in Section 7.3.2. In this part the performance of LA with different adaptation rate in time (every 1, 2, 5, 10 ms) is evaluated while using 16 sub carriers as the sub band size. The same extreme cases as in Section 7.3.2 are considered here, i.e. Doppler frequency

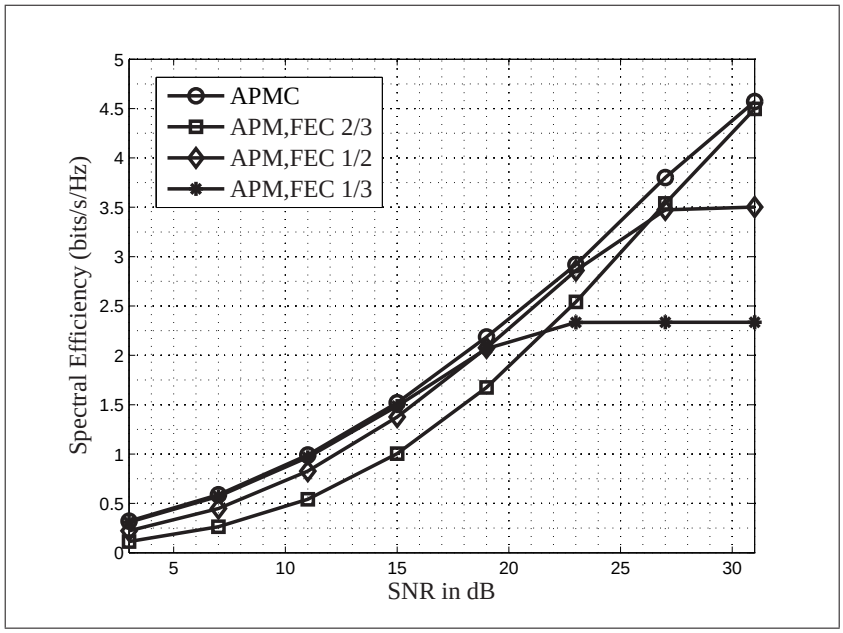

Figure 7.11: Spectral Efficiency with Doppler 250Hz, delay spread 2μs

50Hz, Delay spread 0.5μs and Doppler frequency 250Hz, Delay spread 2μs.

From Fig. 7.12 it can be seen that with small Doppler frequency and delay spread values, the performance for LA every 0.5ms is similar to the case of LA every 1ms and 2ms. This can be understood from the coherence time which is given by,

$$\mathrm{T_c} = \frac{9}{16\pi \mathrm{Fd}} = 3\mathrm{ms}. \tag{7.1}$$

The $\mathrm{T_c}$ is greater than 2ms. The channel is expected to be almost flat in this period. However, for LA every 5ms, there is a large performance drop, e.g. with 15dB SNR, spectral efficiency for LA every 2ms and 5ms is 2bps/Hz and 1.24bps/Hz, which is about 40% loss in performance. With LA every 10ms, the performance is even worse, i.e. only 1bps/Hz.

Fig. 7.13 shows the performance for the high diversity condition. It can be observed that the difference in performance between the highest rate of LA and lowest rate LA is less than the earlier case. The reason is, with Doppler frequency of 250Hz, the 50% coherent time is now:

$$\mathrm{T_c} = \frac{9}{16\pi \mathrm{Fd}} = 0.7\mathrm{ms}, \tag{7.2}$$

which means that the coherence time is comparable to the data block duration of 0.5ms. The gap between LA every 0.5 ms and 1 ms can thus be understood. The

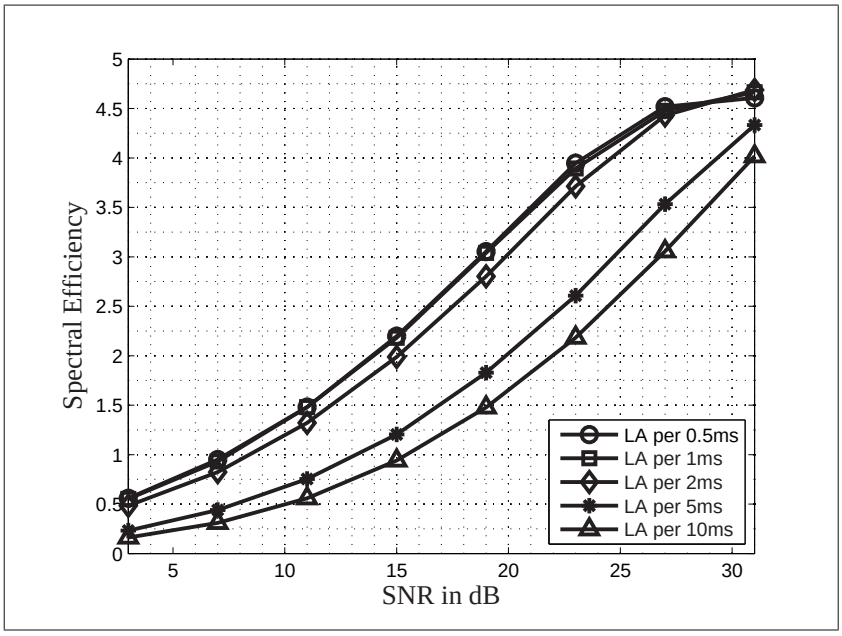

Figure 7.12: Spectral Efficiency with Doppler 50Hz, delay spread 0.5μs

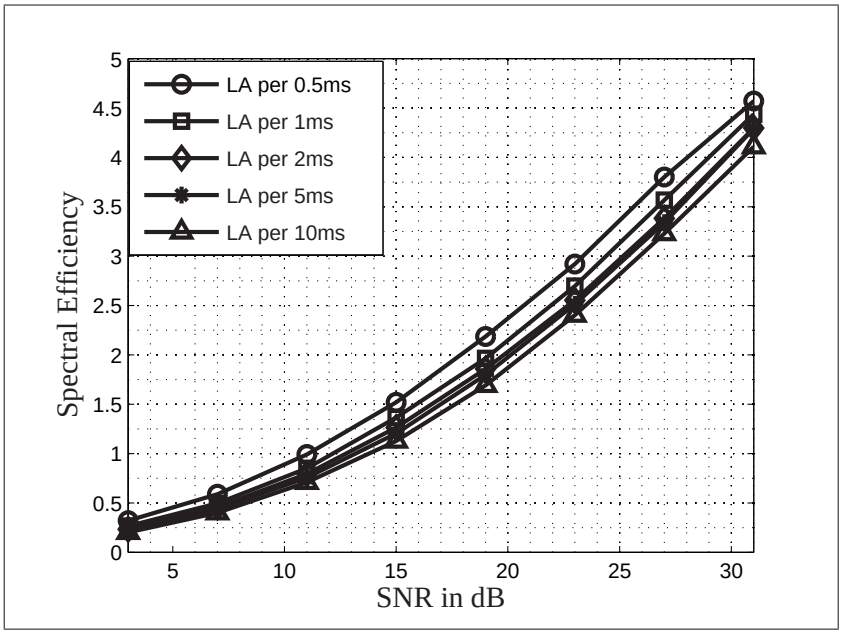

Figure 7.13: Spectral Efficiency with Doppler 250Hz, delay spread 2μs

Table 7.3: SNR Threshold for Coding Rate Switching

FEC		$\frac{1}{3}$	$\frac{1}{2}$	$\frac{2}{3}$	$\frac{1}{3}$	$\frac{1}{2}$	$\frac{2}{3}$	$\frac{1}{3}$	$\frac{1}{2}$	$\frac{2}{3}$	$\frac{1}{3}$	$\frac{1}{2}$	$\frac{2}{3}$
τ_{rms}	Fd	$subN = 8$			$subN = 16$			$subN = 32$			$subN = 64$		
0.5	50	NA	NA	-	NA	-	12	-	16	24	-	18	27
	150	NA	-	19	-	13	19	-	18	25	-	19	27
	250	NA	-	18	-	16	23	-	17	26	-	20	28
1	50	-	11	16	-	15	24	-	18	27	-	19	28
	150	NA	-	19	-	13	19	-	19	27	-	20	28
	250	NA	-	21	-	16	24	-	17	27	-	20	29
2	50	-	14	23	-	17	26	-	20	27	-	20	28
	150	-	16	24	-	19	26	-	18	27	-	20	28
	250	-	17	24	-	19	27	-	19	27	-	20	27

performance of the other LA rates also follow. It can be noted that the performance of the best case is already quite low compared to the earlier case which can be noted by comparing figures 7.12 & 7.13.

7.3.5 Different LA & PC Rates

In Section 7.3.4 the effect of different LA rates on the system performance was analyzed. The results show that if the LA time is much larger than the coherent time, the performance will be much worse as compared to LA at a fast rate. This implies that fast LA is needed in order to achieve a high spectral efficiency but a fast LA means high feedback overhead and more complex system as faster alteration of the system configuration is needed. In this section, the performance for slow LA but with fast Power Control (PC) is proposed and investigated. Fig. 7.14 shows the concept of slow LA with fast PC. The idea is to reduce the LA rate, i.e. using LA at periods larger than the coherence time of the channel to reduce complexity and overhead. There will be mismatch between the true SNR and the desired SNR to maintain a target error rate at the receiver, due to the time varying nature of the fading channel. To overcome this but in a cheaper way (in terms of overhead and complexity) fast power control is used between two bit loading intervals. Following the discussion in the earlier section on using fixed coding rate, the coding rate can be adapted at a much slower rate. However, if the modulation and coding rate are both adapted simultaneously in this analysis, then, the impact of using fast power control can be captured. Fast power control is done at least every 0.5 ms. Other adaptation intervals can be multiple of this. The power control uses feedback to increase, decrease the power levels. Based on the received information, the transmitter changes the transmit power by a certain

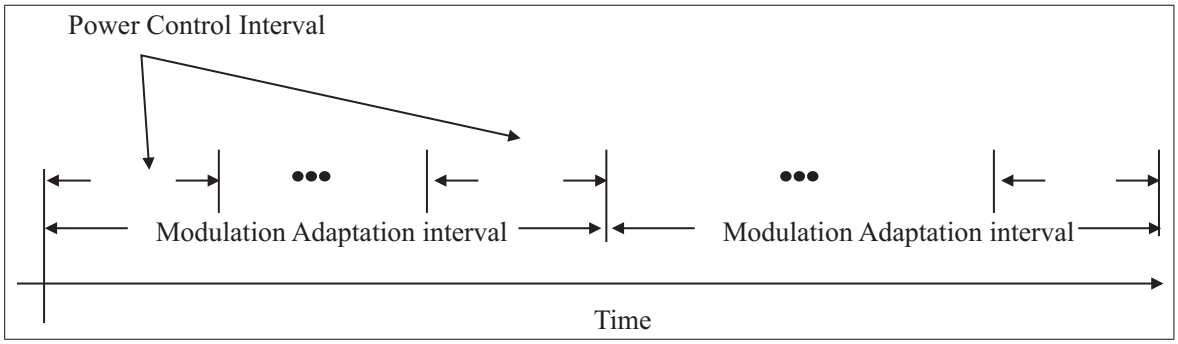

Figure 7.14: Combined slow LA with fast power control

percentage of the transmitted power in the previous data block in time. The details of the algorithm are given below. The feedback overhead of power control information is expected to be much lower than a complete SNR information feedback or rate control feedback. The feedback overhead is expected to be significantly reduced by engaging a combination of slow LA with fast power control. Further fast power control requires only stepping up or down of the transmit power and does not require re-orientation of the modulation/demodulation and the FEC/decoder blocks which is expected to reduce system complexity. The algorithm for the above is described below:

1. As depicted in Fig. 7.14, it can be considered that LA interval is of T_{la} s, and PC interval is of T_{pc} s, where $T_{la}/T_{pc} = K$ and K is an integer greater than or equal to one.

2. Within one data block, power, modulation and coding rate are calculated using the earlier mentioned LA algorithms. The modulation, coding rate and power are kept fixed during one data block.

3. In the beginning of the k^{th} PC window ($1 < k \leq K$), UE will compare the instantaneous channel gain with the previous PC window. If the difference between the two channel gains is within a certain limit L_{unchg}, then there is no need to change the power or modulation or coding levels.

4. Base Station (BS) collects the requirements for all data blocks. The BS first decreases the power for all the the data blocks which requires a decrease in power. However for those data blocks which need an increase in transmit power (since the channel conditions has become worse), the BS needs to consider the total power constraints. The granularity to bring down the power is always G_{down} dB, which is 20% and the maximum granularity for increasing power is G_{up} dB. The value of G_{up} dB can be decided dynamically. It can begin with

20% and then it can be decreased if the step size is not able to satisfy the requirements of the blocks requiring an increase in power level. Then the actual increase in power level $G_{up,actual}$ can be calculated as :

$$G_{up,actual} = G_{up} * \min\{1, (P_{av} + G_{down} * \sum_{n=1}^{N_{down}} P_{k-1,n})/(G_{up} * \sum_{n=1}^{N_{up}} P_{k-1,n})\} \quad (7.3)$$

where P_{av} is the available power, N_{down} is the number of blocks which need less power and N_{up} is the number of blocks which need more power. $P_{k-1,n}$ is the power assigned for the n^{th} block during the $k-1^{th}$ PC window. P_{av} is available power before redistributing the power and is calculated by:

$$P_{av} = P_T - \sum_{n=1}^{N} P_{k-1,n} \quad (7.4)$$

P_T is the total power constraint which indicates the up-limit for the total transmission power.

5. Step 3 is then repeated for each PC window within the same LA window. Step 2 and Step 3 are repeated for each LA window during the whole transmission time.

In this work, $G_{up} = G_{down} = 0.2$; $L_{lowlim} = 0.9$; $L_{uplim} = 1.1$. Like the earlier cases the two diversity conditions have been considered. The first one is the low diversity i.e. $\tau_{rms} = 0.5\mu$s, SISO, fd = 50Hz as in Fig. 7.15 which shows the performance for different LA & PC rates with subN = 16.

From this figure it can be seen that:

- When LA rate less than or equal to 1ms, there is no noticeable difference in performance compared to schemes using a fast power control.
- When LA is done every 2ms, a fast PC rate of every 0.5ms can increase the spectral efficiency by about 0.15 b/s/Hz, close to PC every 1ms.
- When LA is done every 5ms, both PC interval of 0.5ms and 1ms gives almost the same performance, which brings a maximum gain of about 67% in spectral efficiency over the case when only LA is done every 5ms.
- When LA is done every 10ms, both PC interval of 0.5ms and 1ms gives almost the same performance, which gives gain of about 50% improvement in spectral efficiency over the case when only LA is done every 10ms.

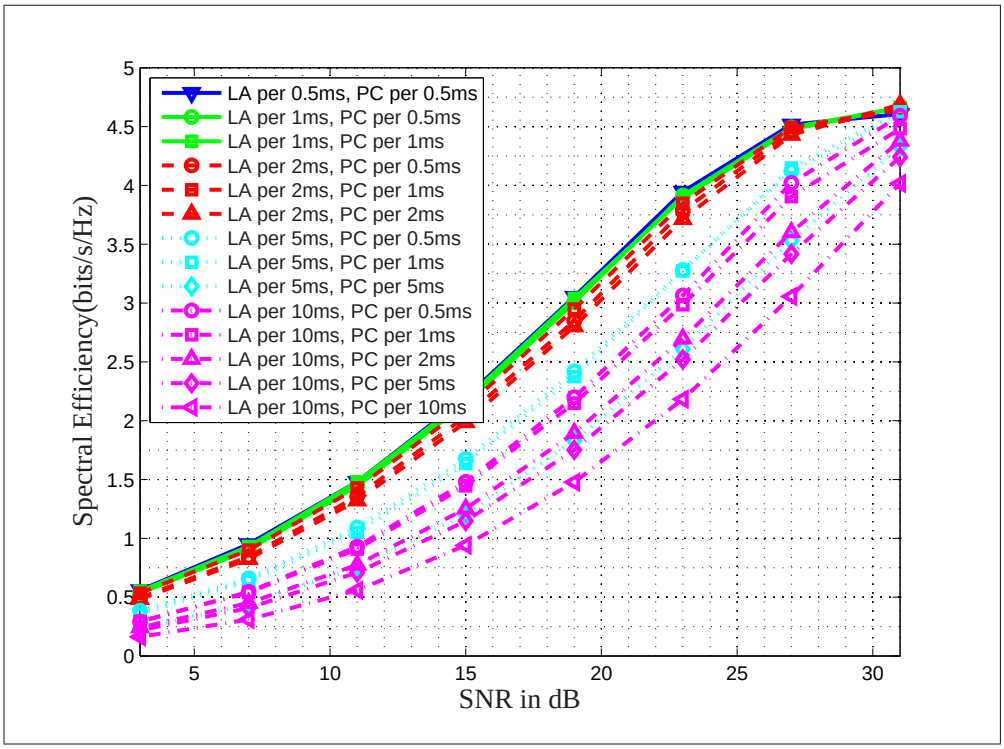

Figure 7.15: Spectral Efficiency for Different LA & PC Rates, Fd=50Hz,$\tau_{rms} = 0.5\mu$s

As has been seen before the decrease in the LA rate has a severe impact on the performance of the system. However, due to some constraints if the LA rate has to be kept slow, then the need for fast PC is clearly evident. It can be concluded that the combination of slow LA with fast PC appears to be very effective.

Figure 7.16 shows the performance for the high diversity case when Doppler frequency is 250Hz and rms delay spread is 2μs. It can be seen from this figure that PC gives very limited benefit as compared to the earlier case. This result is in accordance with Section 7.3.4.

Therefore it is seen that the slow LA with fast PC is very much effective in low diversity conditions, but when diversity of the channel increases, the gain from using fast PC does not yield a gain as significant as in the earlier case. The low diversity cases occur for small cells and near BS while the high diversity is expected for large cells and towards the cell boundary. Thus it can be said the slow LA with PC is better suited for micro cell scenarios.

Overhead calculation The signaling overhead to implement the different rates of power and modulation adaption is computed in this here. Parameters: N (total sub-carriers), $subN$ (No. of sub-carriers in one sub-channel) T_{LA} (LA interval), T_{PA}

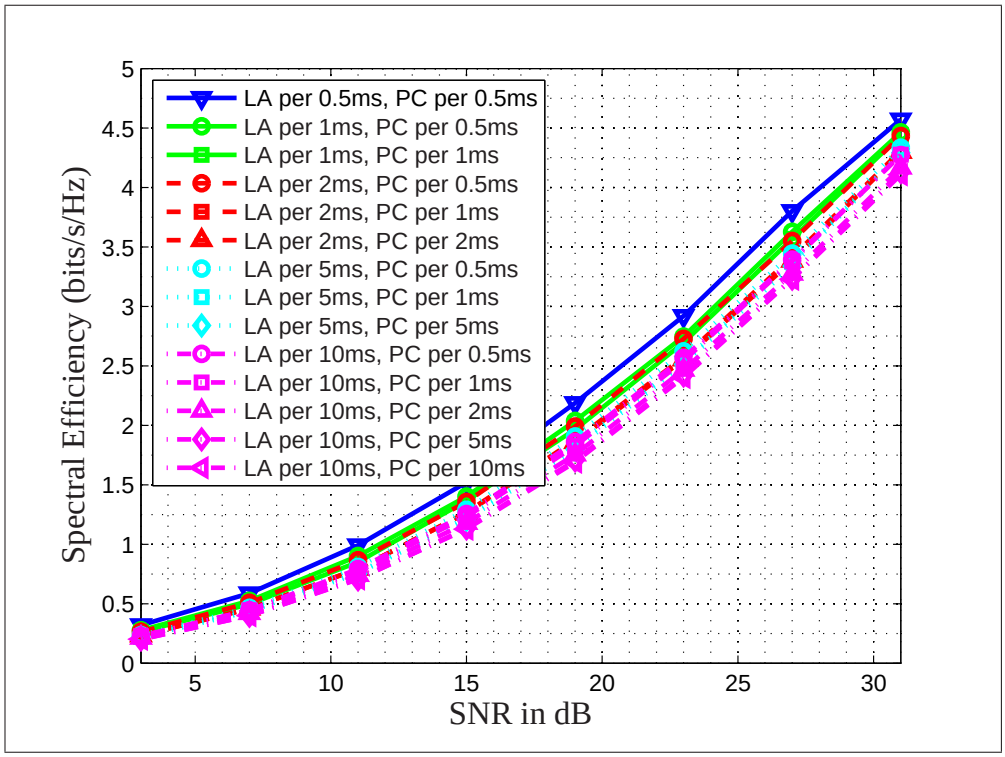

Figure 7.16: Spectral Efficiency for Different LA & PC Rates, fd=250Hz, $\tau_{rms} = 2\mu$s

(power adaptation interval), $n = T_{LA}/T_{PA}$ (integer number, LA over PA rate), PA_{ix} (the index of power adaptation times within one LA window).

For uplink (CQI feedback), 5 bits for one sub-band will be used. For power adaptation only 1 bit is needed to indicate whether the power should go up or down.

$$Overhead_{UL} = (5 + (\frac{T_{LA}}{T_{PA}} - 1))\frac{N}{subN}\frac{1}{T_{LA}} = \frac{(\frac{T_{LA}}{T_{PA}} + 4)N}{subN\ T_{LA}}$$

For downlink, i.e. to indicate the modulation and coding rate to be used, 4 bits for each sub band will be needed to indicate up to $2^4 = 16$ different rates. The overhead is presented in Table 7.4.

$$Overhead_{DL} = 4\frac{N}{subN}\frac{1}{T_{LA}} = \frac{4N}{subN\ T_{LA}}$$

$$Overhead_{total} = Overhead_{UL} + Overhead_{DL}$$

It has been seen that the best performance is achieved with LA interval of 1ms & PC interval of 1 ms i.e APMC every data block. However it is also seen in the previous section that LA interval can be increased up to 10 ms, which is several times more than the coherence time, without any notable performance deterioration. From

Table 7.4: Overhead in Mbps for Adapt Power LA

LAinterval	1ms	2ms		5ms		10ms
PC interval	1ms	0.5ms	1ms	0.5ms	1ms	1ms
subN=8	0.57	0.384	0.32	0.2302	0.1664	0.1152
subN=32	0.144	0.096	0.08	0.0575	0.0416	0.0288
subN=128	0.036	0.024	0.02	0.0144	0.0104	0.0072
subN=512	0.009	0.006	0.005	0.0036	0.0026	0.0018

Table 7.4, which gives an indication of the overhead needed for the different LA and PC intervals for different sub band sizes, it can be said that the overhead for case with 10 ms LA rate, has about five times less overhead, i.e a reduction of about 80% overhead is achievable.

7.3.6 Interaction between Spatial Diversity and Link Adaptation

The performance for APMC is evaluated for multiple antenna diversity situations. In this analysis a fixed sub-band size of 16 sub carriers is used. Doppler frequency is 50Hz and delay spread is 1μs. LA interval is varied from 0.5ms, to 10ms.

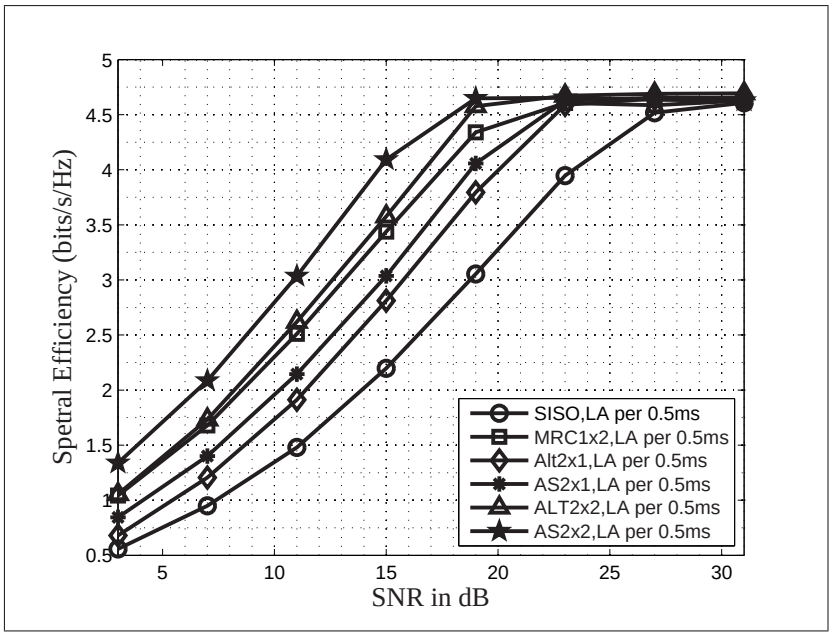

Figure 7.17: Spectral Efficiency for Multi-antenna Schemes, LA Per 0.5ms

From Figure 7.17 it can be seen that any form of multiple antenna technique bring in benefit over SISO system under the conditions investigated. Mul-

tiple Input Single Output (MISO)-Antenna Selection (ASc) has better performance than MISO-Alamouti among the 2x1 systems. Similarly Multiple Input Multiple Output (MIMO)-ASc outperforms MIMO-Alamouti significantly. This is because the Alamouti scheme has an averaging effect while ASc takes advantage of CSI knowledge at the transmitter in selecting the the link with the highest gain. Single Input Multiple Output (SIMO)-Maximal Ratio Combining (MRC), the simplest form of multiple antenna systems has performance close to MIMO-Alamouti. The MIMO-Alamouti has only little gain over SIMO-MRC since the extra antenna at the transmitter is used for diversity gain. When LA is made every 0.5 ms, as in Fig. 7.17, the following is the order of performance for SNR of up to 23 dB. ASc 2x2, Alamouti 2x2, MRC 1x2, ASc 2x1, Alamouti 2x1, SISO. This means that when channel state information is almost instantaneous, ASc makes the best use of this, and interestingly, using MRC 1x2, gives very close performance to Alamouti 2x2.

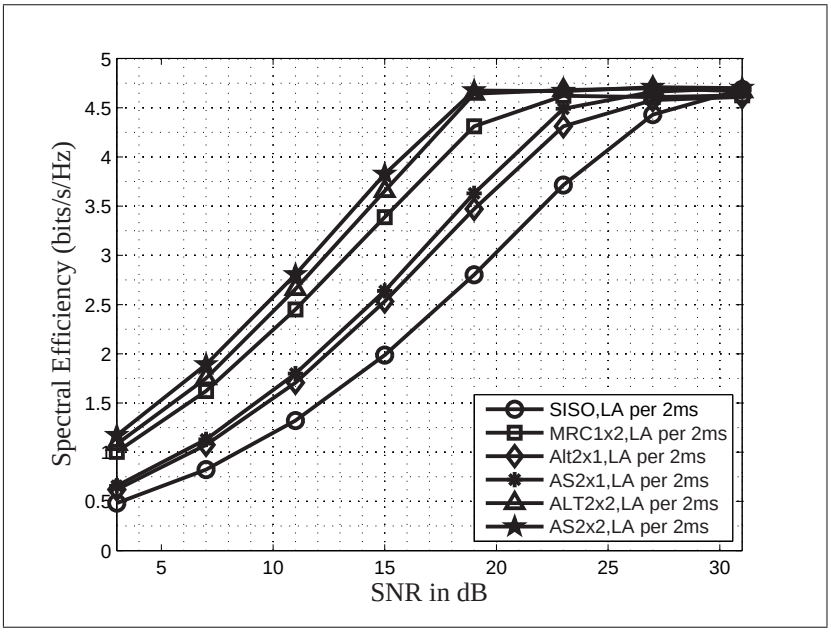

Figure 7.18: Spectral Efficiency for Multi-antenna Schemes, LA Per $2ms$

As the LA interval is increased, ASc fails to achieve its maximum potential due to outdated channel information (Fig. 7.18 through Fig. 7.20).

Therefore it can be concluded that when reliable CSI is available, it is better to use ASc.

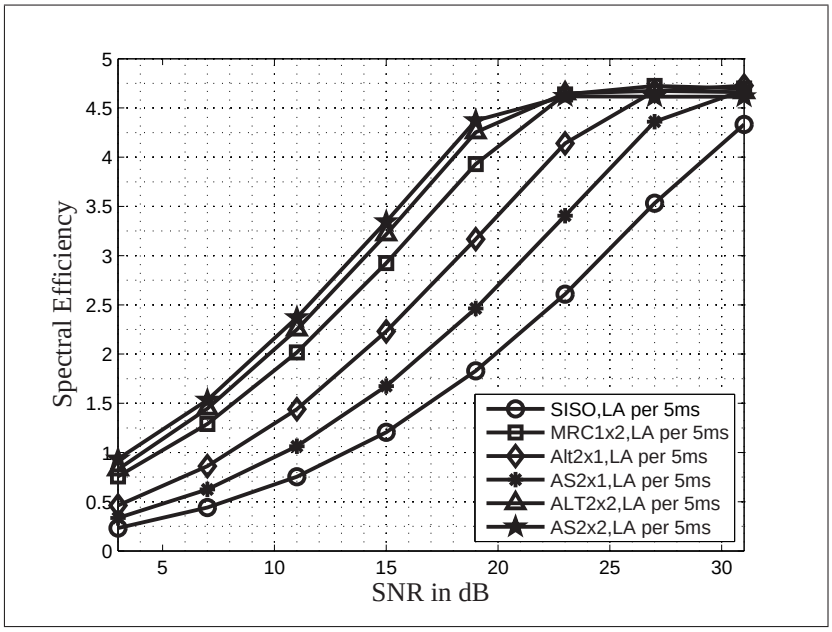

Figure 7.19: Spectral Efficiency for Multi-antenna Schemes, LA Per $5ms$

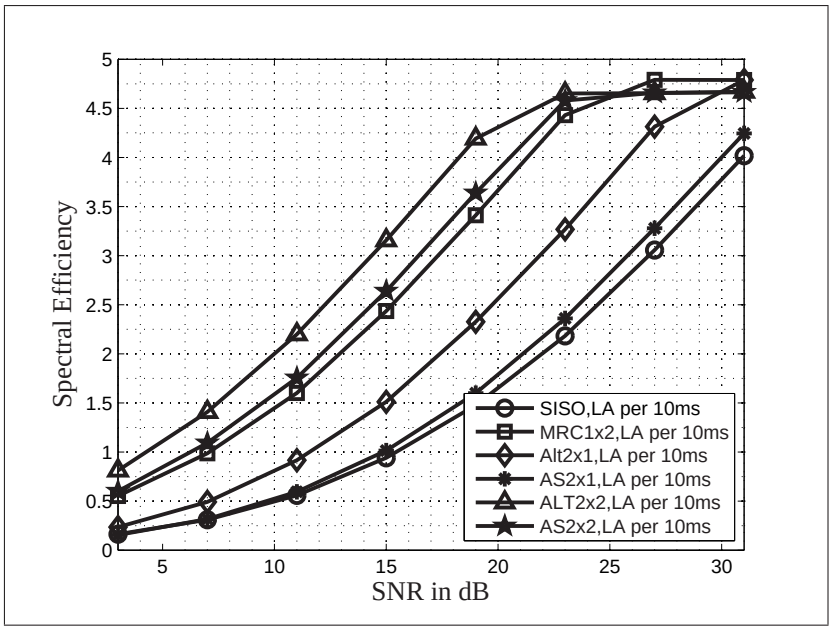

Figure 7.20: Spectral Efficiency for Multi-antenna Schemes, LA Per $10ms$

7.4 Discussion

Some channel parameters such as average SNR, rms delay spread and Doppler frequency spread can be classified as statistical measure, while channel gains for each sub band can be considered as instantaneous measure. Adaptation of the system parameters can be called slow (statistical) or fast (instantaneous) as per their dependence on the channel parameters. It is seen that bit and power loading algorithm selection, coding rate selection, sub band size can be made at a very slow rate using statistical channel parameters while modulation can be adapted at a medium rate using instantaneous channel gains if fast power control is applied in time domain. The combinations have been investigated in this chapter with the objective to arrive at systems with minimum complexity while having practically achievable maximum limits. The selection of the values for statistical adaptation depend heavily on the rms delay spread, Doppler frequency spread and average SNR values.

Some guidelines can be as follows.

- Adaptive Power, Modulation and Coding (APMC) should be used at low rms delay spread and Doppler condition, while Adaptive Modulation and Coding with fixed Power (AMCfixP) is suggested for high delay spread and high Doppler spread conditions.
- Coding rate 1/3 and 1/2 are expected to be used most often while 2/3 is used mainly for small sub band size. Coding rate selection can be based on the average SNR condition, the rms delay spread and Doppler frequency spread.
- Sub band size can be made small for low mobility and small delay spread while large sub band size is to be used for large variation of the channel.
- Power control is found to be very effective, since modulation and coding can be adapted at a medium rate, which simplifies LA implementation and reduces the overhead needed.
- Transmit diversity along with receive array gain , i.e. Alamouti-MRC combination is suggested for situation of large LA interval while ASc is highly recommended when LA interval is less than the coherence time.

Table 7.5[1] summarizes the investigations made in this Chapter.

[1]The "Yes" entry means that the particular adaptation parameter (row) is influenced by the channel parameter of the column.

Table 7.5: Summary of Hyrbid Link Adaptation

Option ↓	Doppler Spread	Rms Delay spread	Average SNR	Instantaneous SNR	Rate of adaptation
Bit and Power Loading Algorithm	Yes	Yes	Yes	No	Slow
Sub band size	Yes	Yes	Yes	No	Slow
Code rate	Yes	Yes	Yes	No	Slow
MIMO mode	-	-	Yes	No	Slow
Adaptation interval	No	Yes	No	No	Slow
Power control interval	No	Yes	No	No	Slow
Modulation selection	No	No	No	Yes	Medium
Power loading	No	No	No	No	Fast

7.5 Conclusion

The objective of this investigation is to arrive at the combinations of slow and fast adaptation of different link parameters which can provide maximum spectral efficiency yet will have minimum implementation complexity. Accordingly several aspects of link adaptation in OFDM systems has been analyzed. It is shown that for best performance the bit and power loading algorithm, sub band size, LA adaptation interval and PC interval, multiple antenna mode, FEC code rate, must be selected as per the channel statistics such as Doppler condition, RMS delay spread, average SNR while the selection of modulation level, and power loading, can be done as per the instantaneous channel gains. Therefore the proposed hybrid mechanisms maximizes the spectral efficiency while having minimum complexity and feedback overhead. It is found that using a single code rate for a user for all data blocks has very little loss in spectral efficiency compared to the algorithm which uses different coding rates in different data blocks. The selection of the single code rate is to be based on statistical channel parameters. Proposal to reduce the adaptation rate of the modulation level selection even further and to compensate the outdated channel information by using a fast power control to balance the SNR at the receiver has been made. This mechanism reduces overhead by more than 50% while realizing near maximum spectral efficiency performance. Such techniques reduce the degrees of freedom to be exploited at a given time but do not reduce the maximum spectral efficiency. These results are significant to provide valuable input to the upcoming wireless OFDM standards. The results are

also expected to trigger investigation in the joint resource allocation LA algorithms for multi user cellular environments.

An important consideration in the situations under investigation in this chapter is the use of outer loop link adaptation. In such systems the BER / BLER is tracked and if the target BER / BLER is not satisfied / over satisfied then the SNR thresholds for adaptive modulation and coding are re-adjusted so that spectral efficiency is maximized. The SNR threshold values are expected to change when the channel statistics change. The difficulty with these systems is that they are slow as there is a convergence period over which the BLER is stabilized. In contrast, the work described in this chapter presents the concept of using different LUT under different channel conditions. The assumption is that, an estimate of the channel statistics is available at the BS. With the use of the channel statistics the appropriate LUT can be used for bit and power loading. This procedure does not involve slow adaptation of the SNR thresholds but selection of a-priory SNR thresholds with the help of information on channel statistics. Further, the work in this chapter also considers the adaptation of modulation window, coding rate selection window and power control window in time and frequency domain based on channel conditions which is not inherent under the framework of outer loop link adaptation.

8

Link Adaptation under Transceiver Impairments

In the previous chapter various hybrid LA techniques have been discussed. However, the analysis considered ideal transmitter and receiver operation. On the other hand it is known that OFDM signal must go through the HPA, which has non linear transfer function. OFDM signal has high PAPR and this drives the HPA in to the non linear region. This chapter delves into the analysis of LA under such distortion. Modification to the LA methods to overcome the non linear distortion problem is also developed in this chapter. One of the pre-assumptions is that this kind of non linear distortion is not captured in the channel quality indicator which is fed back from the receiver. This kind of situations apply directly to WLAN type systems which use a low PAPR preamble as training sequence for channel estimation in front of the data symbols in a frame. Whether the channel quality indicator can carry the non linearity information in other systems is a matter of investigation. An important issue addressed here, which applies to all systems using link adaptation is the condition that different optimal Back of (BO) in the operating point of the HPA exists for different modulation and coding rates. Choosing a particular BO either causes a penalty in terms of coverage for some modulation and coding rates while it may increase the

BER / BLER degradation for others. This work presents the detailed analysis of such situations as well by considering different BO values. Further the influence of change in BER / BLER target on the optimal BO is also shown.

The analysis of LA in the presence of frequency synchronization problem is also analyzed in this chapter. It is assumed here that the residual frequency offset and maximum Doppler spread cannot be estimated at the UE due to low complexity implementation, but these impairments can be measured at the BS. This is in contrast to the analysis of Chapter 5 where it is considered that the maximum value of Doppler spread and residual carrier offset is measurable at the receiver. A method to overcome the effect of frequency synchronization error for LA schemes is proposed here.

The Hybrid Automatic Repeat-reQuest (HARQ) mechanism is generally combined with link adaptation to further improve the performance. Though the use HARQ mechanism may be expected to give some gain for Link Adaptation systems yet the performance of such schemes under self interference must be investigated. The HARQ mechanisms increase received SNR by combining repeated transmission of the same frame. It can be compared to increasing the SNR by increasing the number of receiver antenna branches. When there is self interference, then with increase in desired signal power there is a proportional increase in the interference power. Therefore the improvement in SINR is not a direct consequence. The SINR can be improved only if dedicated signal processing algorithms are used to cancel the interference / extract the desired signal out of the interference components which is beyond the scope of this work in its current state.

8.1 Influence of Non Linear HPA

OFDM is an elegant solution to tackle the frequency selective wireless channel and achieve high spectral efficiency using LA mechanism, but, it also has its problems. The output of the OFDM signal is the sum of a large number of sinusoids. If they combine constructively, then a large peak is created, thus giving rise to high PAPR [1]. When this signal goes through the HPA, before being transmitted to the air medium, the signal suffers from non linear distortion due to non ideal characteristics of the HPA. When the signal undergoes such non linear distortion, then spectral regrowth occurs which consists of in band intermodulation and out of band intermodulation [102]. These phenomenon affect the BLER performance and also introduce Adjacent Channel Interference (ACI) [103], [104].

Several algorithms to reduce PAPR in OFDM signals are available [105]. Some

of the schemes need side information [106], some use iterative techniques to reduce the PAPR [107], while others need additional processing at the receiver [108]. Which ever technique is used there is always a tradeoff between the PAPR reduction and performance degradation. Moreover some amount of PAPR always remains. To alleviate the problem of high peaks going into the non linear region of the HPA, usually a power Back of (BO) is used. The larger the BO, the more shifted is the operating point of the HPA to the linear region and thus better is the reduction of the distortion. However, BO also implies a reduction in the output power of the HPA. This reduces the coverage area of the system. So, a minimum BO which is a tradeoff between performance degradation and coverage is used. The other alternative is to use a very costly power amplifier which has a large operating range. This would increase the cost of the UE significantly. There will also be a huge power wastage due to large BO. Power wastage is a very important issue for UE where battery life is limited.

The amount of BO needed for optimum performance varies for different modulation and coding schemes [95]. It has been discussed in the earlier chapters, that LA dynamically adapts the modulation level, coding rate and power as per the time varying channel gain. In case of OFDM, the adaptation is also made across the frequency domain. The selection of the best data rate is made based on the SNR measured at the receiver. The SNR is usually measured using TS, which is also know as pilot symbol. The pilot symbols are designed in a way that the PAPR of the signal is very low [109],[110],[111] so that the pilot symbols suffer from very little non linear distortion. This is done to ensure proper channel estimation and synchronization at the receiver. Therefore, the SNR measured using the pilot symbols do not contain information about the non linear distortion in the DATA symbols which follow the pilot symbols. Existing works on LA do not analyze this situation.

Additionally, since LA uses varying modulation, power and coding rate for different sub-bands at the same time, using a fixed value of BO will not optimize the performance. It may be suggested to use the maximum BO. Though such a method will cause minimum distortion, it will be at the cost of coverage and power. Thus it is important to analyze the impact of nonlinearity in OFDM system using LA.

The focus here is to analyze the impact of non linear distortion on the performance of LA algorithms in OFDM systems and find suitable modification to the LA algorithm to overcome the problem. Hence PAPR reduction algorithm is not used. It is also to be noted that if a PAPR reduction algorithm is used then the results will be dependent on the PAPR reduction mechanism. Moreover neither the WLAN

nor the WMAN standards specify a transmit side signal processing procedure to reduce PAPR and this is open for implementation. For all these reasons, only BO has been used to reduce PAPR in the analysis in this work.

8.1.1 HPA Models

This section presents the HPA model used in the work. Its impact on the OFDM systems is also discussed. There are several models for HPA available in the literature which are mainly based on two types of amplifier. One is relatively older and is known as Traveling Wave Tube Amplifier (TWTA), which exhibits nonlinear distortion in both amplitude AM/AM and phase AM/PM conversion [112], [102],[113]. The other model is Solid State Power Amplifier (SSPA), which has nonlinear distortion in amplitude AM/AM only and is referred to as Rapp's Model [114].

Available literatures suggests that the AM/PM conversion for SSPA is small and hence is neglected in the model [1]. The Rapp's HPA model for AM/AM conversion is used in this work following [1]. The input output amplitude relation is given by [1]

$$g(x) = \frac{|x|}{(1 + |x|^{2p})^{\frac{1}{2p}}}, \tag{8.1}$$

where x is the signal amplitude and the variable p indicates the amount of nonlinearity. A good approximation of a practical HPA can be obtained by choosing p between 2 and 3. For large values of p, the model converges to a clipping amplifier, which is perfectly linear until it reaches the maximum output power level. It is very difficult to realize a linear HPA in practice.

Fig. 8.1 shows the input output signal amplitude relationship for the SSPA model. From the figure it can be seen that the higher the input power, the more is the chance that the signal will be in the nonlinear region. So, to operate in the linear region, the signal power needs to be reduced before feeding it to the amplifier input. This power reduction is referred to as Back of (BO). The figure also shows that when no BO is used, with p=2, for an input amplitude of 1, the output is 0.82. For 3 dB BO, i.e. reducing the input signal by a factor of half, the output is at 0.48 when the input is 0.5, BO by 6dB means reducing the input power by a factor of 0.25 and it can be seen that the output is very close, if not exactly same, as the input operating point. This shows the non linear effect. Thus BO is expected to improve BER performance but at the cost of capacity, coverage and power. To find

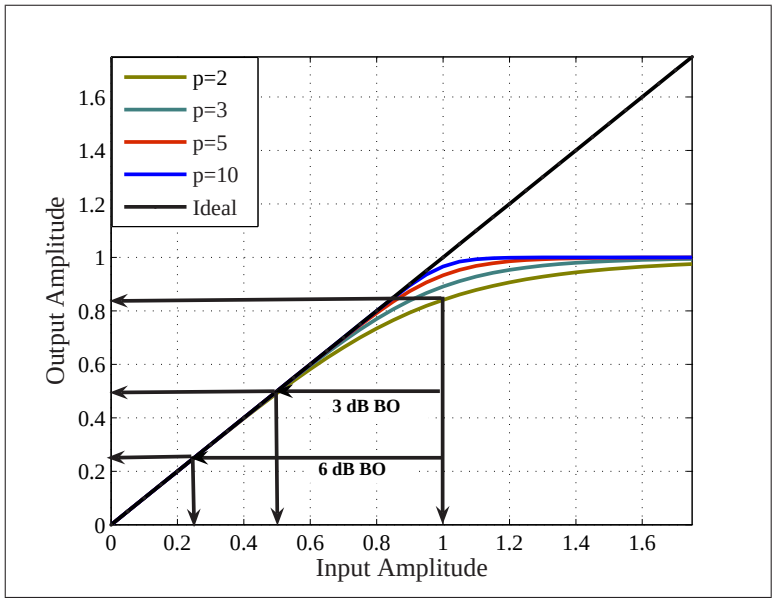

Figure 8.1: Power BO representation in Rapps Model

the amount of distortion caused by the amplifier only, the variation of power at the input and at the output of the amplifier is measured for different BO values and plotted in Fig. 8.2. It can be seen from the figure that with increasing BO power, the amount of distortion decreases, i.e. the signal operates more in the linear region.

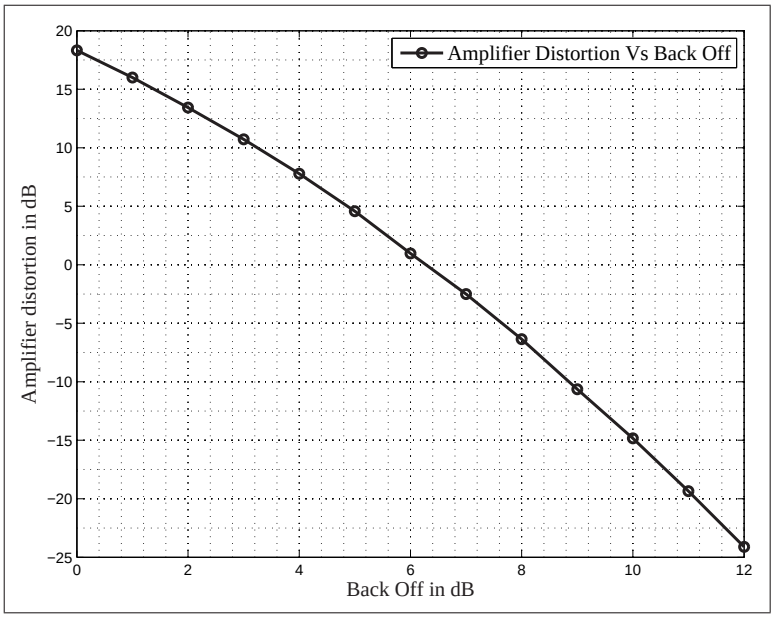

Figure 8.2: Relation between Amplifier Distortion and BO (in dB)

8.1.2 Effect of HPA on different Modulation and coding rates

Some fundamental results on PAPR issue in OFDM are briefly described in the Appendix D. The effect of modulation and coding schemes on PAPR for OFDM is also given in the Appendix D.

8.1.2.1 Effect on Power Spectrum

The frequency domain carrier arrangement for a typical OFDM system is given in Fig. 4.1. The high frequency components are set to zero to reduce ACI. The 0 frequency, is also set to zero to avoid unnecessary power wastage by DC transmission. The power spectrum of OFDM signal after the power amplifier is shown in Fig. 8.3 for different values of BO. It can be seen that the out of band emission decreases with increasing BO. With a change in signal power of 9 dB (BO of 10 dB to 1 dB) the out of band emission increases by about 34 dB. Along with the out of band emission it can be seen that the DC leakage increases as well and this is even slightly worse compared to the out of band emission. Thus it is seen that small BO results in large out of band emission which is a highly undesirable effect.

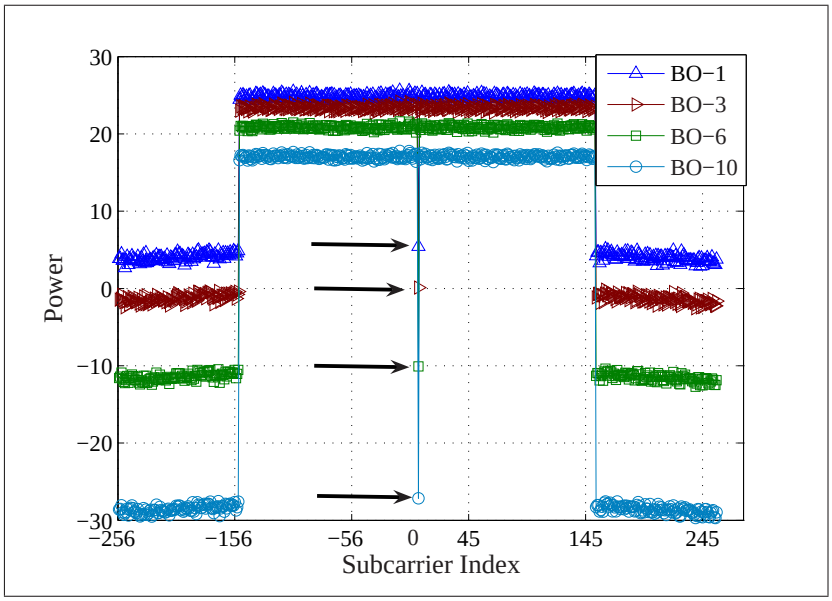

Figure 8.3: Spectrum plot of OFDM signal. 'BO' indicates BO value in dB.

8.1.2.2 Signal to Distortion plus Noise Ratio (SDNR) Plot

Signal to Distortion plus Noise Ratio (SDNR) helps to understand the true usable signal quality. SDNR can be measured both at the transmitter and at the receiver (post equalization). The output of the HPA depends on the nonlinearity parameter p given by the (8.1). Output of the HPA can be written as

$$y(t) = \alpha \cdot |x(t)|^2 \cdot e^{j\angle x} + n(t) = f(|x|^2, \alpha), \tag{8.2}$$

where α is an attenuation constant which depends on the BO value, x(t) is the input signal while n(t) is the uncorrelated noise generated due to the amplifier distortion. Variance of the distortion caused by the amplifier is given by,

$$\sigma_D^2 = E[x(t)|^2 - f(|x|^2, \alpha)] \tag{8.3}$$

The transmitter side SDNR is then given by,

$$SDNR_{Tx} = \frac{f(|x|^2, \alpha)}{\sigma_D^2 + \sigma_w^2} \tag{8.4}$$

where σ_w^2 is the variance of the white gaussian noise. When SDNR is measured at the receiver, it will include processed noise due to equalization as well. SDNR at the

receiver end can be expressed as,

$$\mathrm{SDNR} = \frac{1}{\mathrm{N}} \sum_{\mathrm{i}=0}^{\mathrm{N}-1} \frac{|\mathrm{X_i}|^2}{|\mathrm{X_i} - \hat{\mathrm{X}}_\mathrm{i}|^2}, \tag{8.5}$$

where, $\mathrm{X_i}$ is the transmitted constellation point at a sub carrier, $\hat{\mathrm{X}}_\mathrm{i}$ is the received constellation point and N is the number of sub carriers. Amount of SDNR does not depend on the modulation scheme used. However, for the same amount of SDNR, the effect on BLER performance of different modulation will be different. Since the decision boundaries for higher modulation in the constellation diagram are closer compared to the low order modulation, therefore, for the same amount of distortion the probability of correct decision for a symbol will be much lower for higher modulation order than that of a lower modulation order. Fig. 8.4 shows the SDNR at the receiver for AWGN channel, and Fig. 8.5 shows that for a fading channel for 4-QAM, i.e. QPSK. The curves for 16-QAM and 64-QAM are shown in D.7– D.10 for AWGN and fading channels. The impact of using a smaller BO on the BLER performance is clearly visible from these figures. The saturation of SDNR as seen in the figure, is where the distortion is significantly larger than the noise power. It can be realized that increasing the transmit power or reducing the noise level does not help in improving the received signal quality.

The figures also show that though the nature of SDNR curve is the same for both AWGN and fading channels. The amount of variation in SDNR (due to different values of BO) for fading channel is much lower than that of AWGN channel. This is because the fading channel has more influence on the SNR degradation than the non linear distortion. For example, in 4QAM system if the input power is 18 dB with BO of 8 dB, then the output power is 17 dB and 9dB for AWGN and fading channel respectively. Similarly, for modulation scheme of 16QAM with the same BO as above, but when the input power is 24 dB then the output power is 22 dB and 15 dB for AWGN and fading channel respectively.

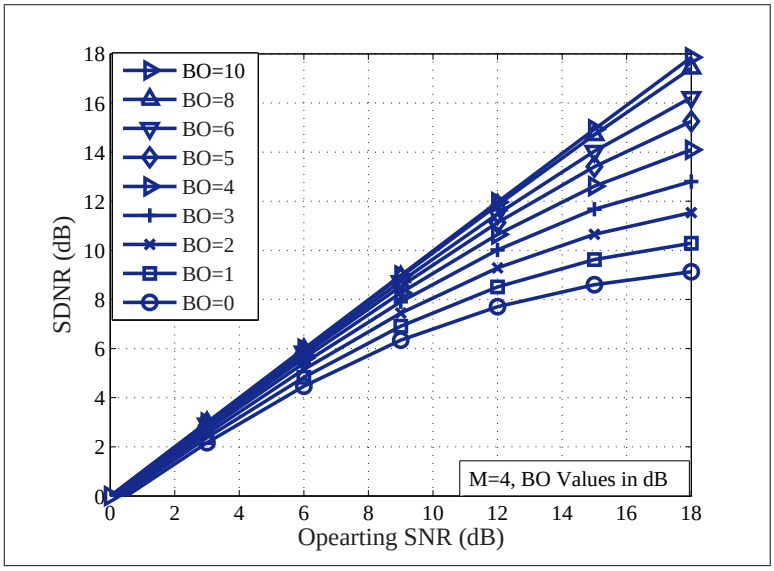

Figure 8.4: SDNR plot for 4QAM modulation in AWGN Channel.

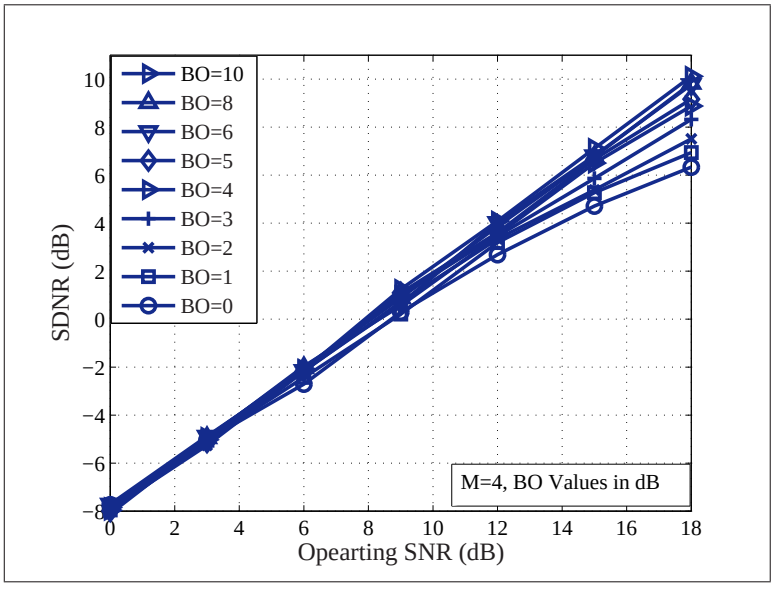

Figure 8.5: SDNR plot for 4QAM modulation in Fading Channel. The BO values are given in dB.

8.1.2.3 BLER Performance of Different Modulation and Coding

In this section the system performance is presented for individual modulation and coding schemes. Simulation parameters are as discussed in the last chapter (similar to 3GPP-LTE specification [2]) except that 16 sub carriers are used as the sub band size. Modulation schemes under investigation are 4QAM, 16QAM and 64QAM. BO is varied from 0 dB to 10 dB. It is seen from the CDF curves presented in Section D, that a power BO of 10 dB will accommodate almost all the high peaks and nonlinearity effect is mostly mitigated. Therefore, performance with 10 dB BO is considered as bench mark performance. The Doppler frequency for all the investigations was fixed at 50 Hz.

Effect of HPA and BO on all the modulation schemes are studied with FEC coding rate of $\frac{1}{3}$, $\frac{1}{2}$ and $\frac{2}{3}$. However, results for FEC = $\frac{1}{2}$ is presented here while the others are given in Appendix D. The main parameters, used to characterize the impact of nonlinearities to in this work is BLER. Since LA concerns spectral efficiency and BLER, the main concern here is the analysis of the effect of HPA distortion on these parameters for a given BO of the HPA[1].

It is worth mentioning that for convenience of using results obtained here in link adapted system, all the performance is plotted in terms of POST-SNR. POST-SNR is defined as the SNR measured at the receiver in each sub band while PRE-SNR is the SNR measured over the whole system bandwidth, i.e. across all sub bands. For AWGN channel, PRE-SNR and POST-SNR are the same since there is no channel variation. For each transmitted PRE-SNR, different sub carriers go through different amounts of channel fade, and thus the received SNR for different sub band vary. If the BLER is plotted against the PRE-SNR, then it will represent the average performance of different received SNR which will not exhibit the appropriate behavior of the system. In the simulations made, the SNR for each data block along with the information on the correctness of the data block is collected and then the BLER vs POST-SNR is plotted.

Fig. 8.6–Fig. 8.11 show the BER vs SNR for uncoded system and BLER vs SNR for FEC coded systems in fading channel. The results are shown for QPSK, 16-QAM and 64-QAM; For coded curves, the code rate of $\frac{1}{2}$ is used. It can be seen that the impact of HPA is quite different for coded and uncoded system. Since FEC coding and interleaving improve the performance, coding rate in conjunction with different modulation scheme has different impacts. The higher the modulation order,

[1]The selection of BO is achieved by striking a tradeoff between ACI and BLER degradation.

the greater is the impact of BO values. From the figures it can also be found that for uncoded case, 16-QAM and 64-QAM schemes show error floor quite early for a certain power BO as compared to the coded systems. It can also be seen that low order modulation like QPSK is minimally affected by even the smallest BO. This is because the HPA model being used in this work has only amplitude distortion with no phase distortion and QPSK is least affected by amplitude distortion compared to higher order QAM modulations. As stated earlier, BO shifts the operating point of the HPA to the linear region and thereby reduces the nonlinear distortion. It is clear that low modulation order does not require BO at all, as only little improvement is found between 3dB of BO applied in comparison to the case with no BO is used. However for 16QAM modulation, a 6dB BO gives us almost the same performance comparing to 10 BO case. This is inline with other available literatures [1], where it is reported that increasing the BO values more than the mean PAPR does not make much difference as the Cumulative Distribution Function (CDF) of PAPR is quite steep. For higher modulation, the impact of different BO values are more visible, since the distortions are more detrimental to dense constellation diagrams.

Further, it is observed in the CDF curve, the median and the 90 percentile value of the PAPR is very close. Beyond that, rest of the high peaks spans a wide area of SNR values. It can be said that high PAPR occurs very rarely. This is also evident from the BLER curves. For OFDM symbols with 512 subcarrier, median value of PAPR distribution is around 8 dB and it is seen from BLER curves for all modulation and coding rate that, there is not much performance improvement if 10 dB BO is used instead of 8dB. This means BO by median value might be good enough to mitigate the distortion effect. Increasing back off beyond that value will be of not much gain.

Since different modulation and coding rates show different behaviors for variation in BO power, the choices of suitable BO point for different modulations are different. Also, it is highly complex, if not impossible, to change the BO frequently with the change in modulation and coding rate in link adapted system. So finding an optimum BO point considering modulation and coding rate becomes necessary for optimum performance. In case of OFDM systems using LA, where more than one modulation order is expected to be used across the frequency domain in one OFDM symbol, it might not be possible to use a dynamic BO. For a proper analysis of the above scenario i.e. balancing the BO and BLER degradation can be made using Total Degradation (TDEG), which is defined for a certain BLER threshold as the amount of BO plus the SNR degradation in BLER performance as compared to the

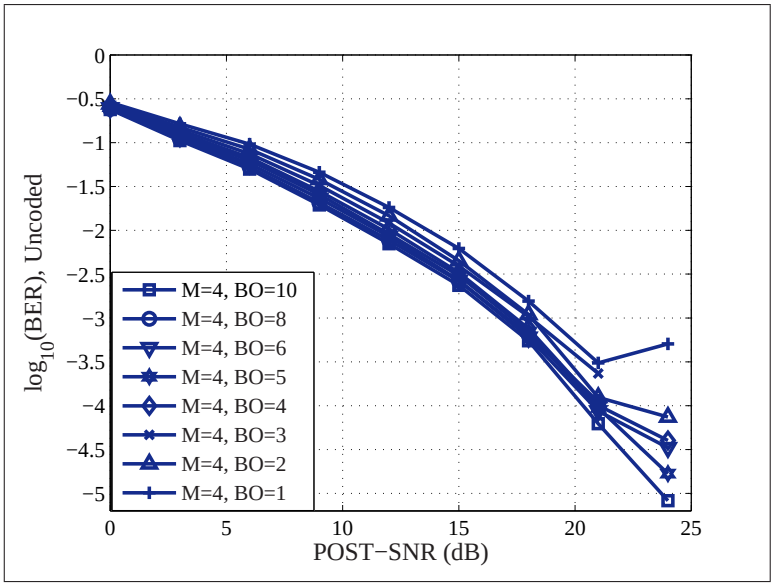

Figure 8.6: BER vs SNR curve for uncoded and M=4 in fading channel

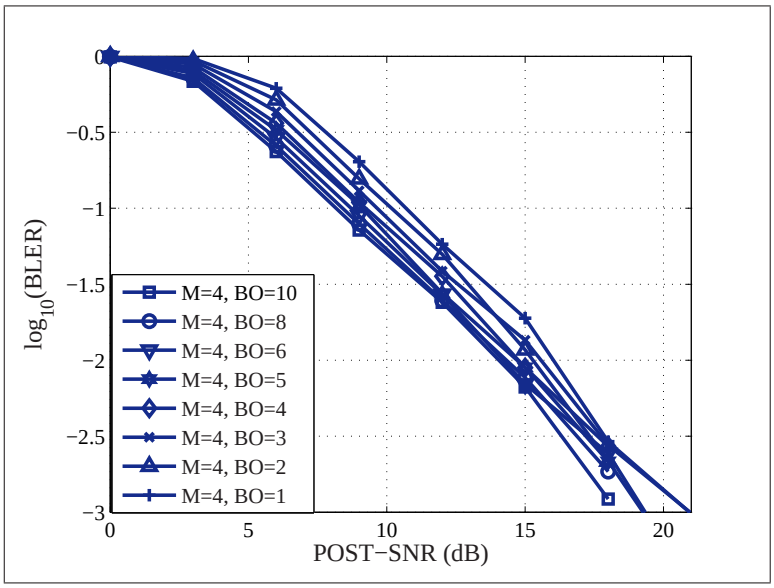

Figure 8.7: BLER vs SNR curve for $C = \frac{1}{2}$ and M=4 in fading channel

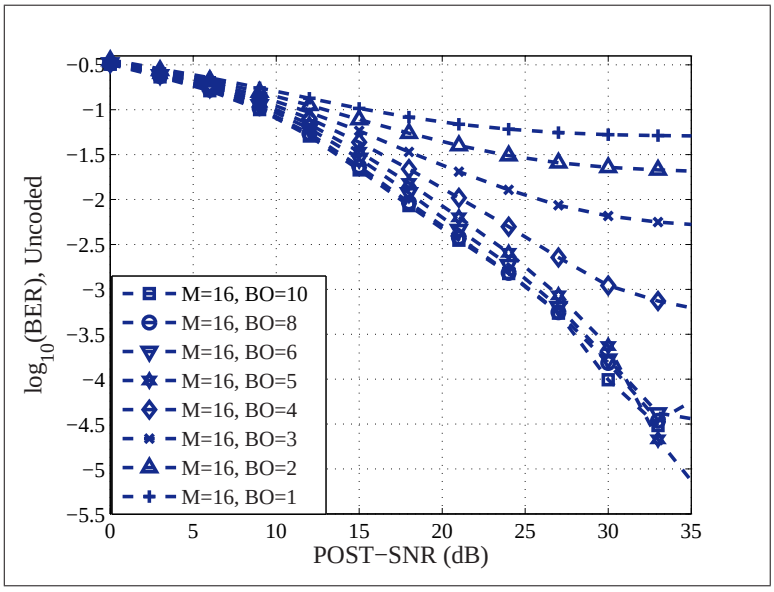

Figure 8.8: BER vs SNR curve for uncoded and M=16 in Fading channel

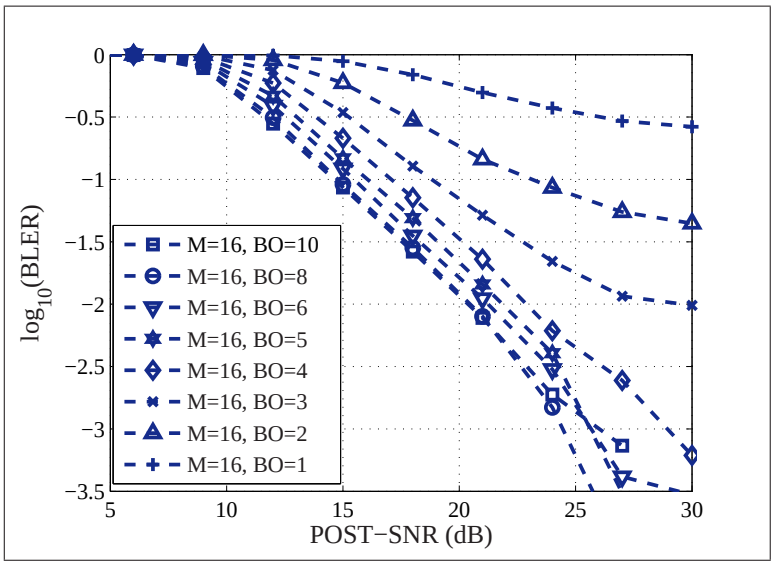

Figure 8.9: BLER vs SNR curve for $C = \frac{1}{2}$ and M=16 in fading channel

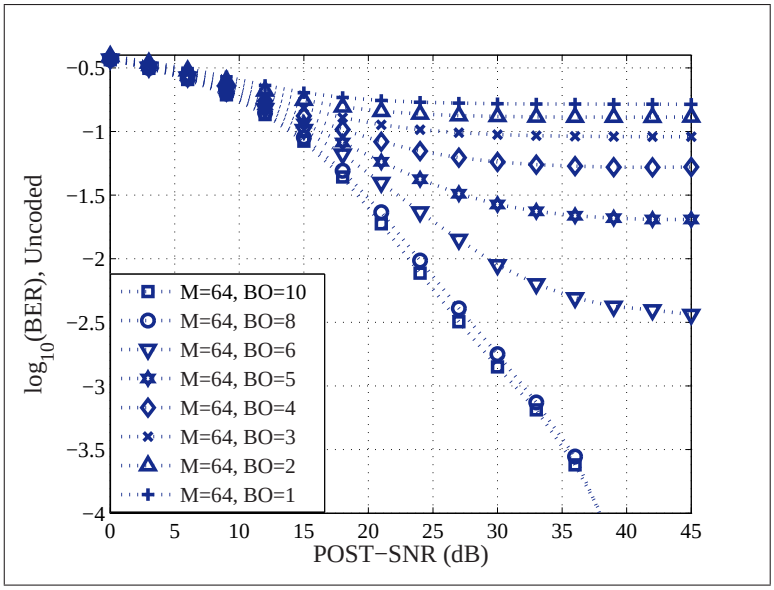

Figure 8.10: BER vs SNR curve for uncoded and M=64 in Fading channel

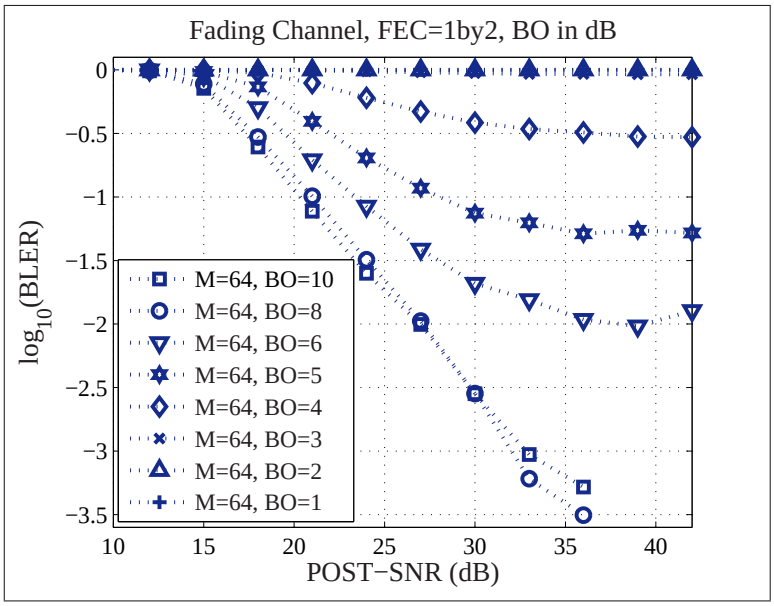

Figure 8.11: BLER vs SNR curve for $C = \frac{1}{2}$ and M=64 in fading channel

performance in the system without any distortion [102].

Table 8.1 explains how a TDEG can be found. This is for fading channel

Table 8.1: Table for Calculation of Total Degradation in dB

BO Values	Ideal($10dB$)	8	6	5	4	3	2
Measured SNR	14.6	14.7	15.6	16.3	17.2	18.9	23.1
Degradation	-	0.1	1.0	1.7	2.6	4.3	8.5
TDEG	-	8.1	7.0	6.7	6.6	7.3	10.5

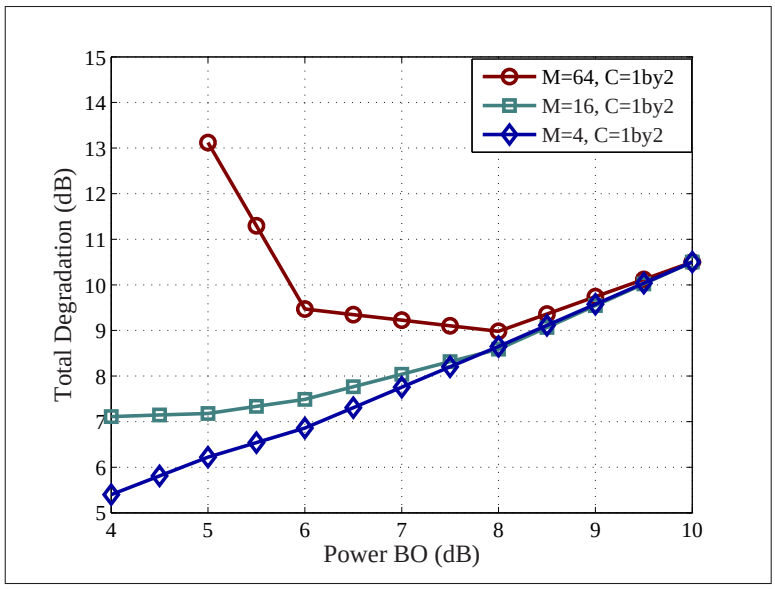

Figure 8.12: TD plot for $FEC = \frac{1}{2}$ with BLER Threshold= 0.1 in Fading Channel

with BLER threshold of 0.1, with 16-QAM and FEC coding rate of 0.5. In this table the reference performance is taken from that with 10 dB BO. For a certain value of BLER, the corresponding SNR without HPA system (or HPA with a BO of 10 dB or more) is used as the basic reference point. Then for that BLER threshold, the corresponding SNR values for different BO values for a particular modulation and coding rate is noted. The difference between this value and the reference value represents the degradation. The TDEG as defined earlier is the sum of the degradation and the corresponding power BO.

Fig. 8.12 and Fig. 8.13 show the TDEG curve for two different threshold of BLER 0.1 and 0.05 respectively. The optimum BO can be different for different BLER threshold. From the figures, it is seen that for 16-QAM coding rate 1/2, the minimum BO is 4dB and 5dB for BLER threshold of 0.1 and 0.05 respectively. So,

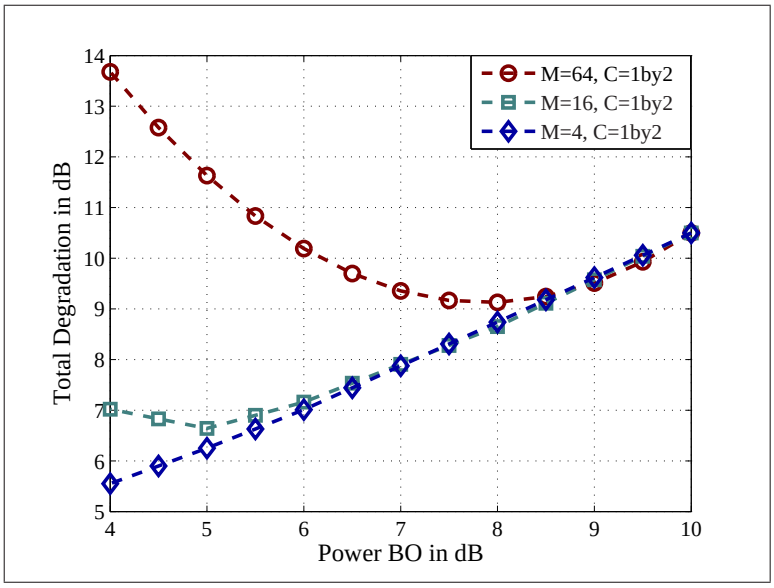

Figure 8.13: TD plot for $FEC = \frac{1}{2}$ with BLER Threshold= 0.05 in Fading Channel

it becomes important to look at the TDEG curves for different BLER threshold to satisfy different QoS criteria.

Several set of curves for different modulation and coding rates in AWGN and fading channel are given in Section D.

8.1.3 Link Adaptation under HPA Impairments

The LA algorithm considered in this chapter is simplified since the focus of investigation is the impact on non linear distortion on LA system and not the LA algorithm itself. Accordingly transmit power is brought down to maintain the SNR at the receiver for a chosen modulation level (identified by using a fixed transmit power in the PREAMBLE) while a coding rate of 1/2 is used, and hence it is mainly the modulation that is adapted as per the channel condition. The flow chart of the algorithm is given in Fig. 8.14. It is shown in [26] that the SNR threshold for switching the modulation level as per the channel gain is a function of the received SNR.

It is shown in (8.4) that the received SNR (actually SDNR) during the data symbol of an OFDM system includes distortion due to the non linear HPA and is a function of the BO. This implies that the thresholds are expected to be a function of the BO. This means that the Look Up Table (LUT), which contains the threshold values for different modulation and coding rates at a certain BLER, needs to be updated.

For uncoded system, it is possible to obtain analytical expression for revised

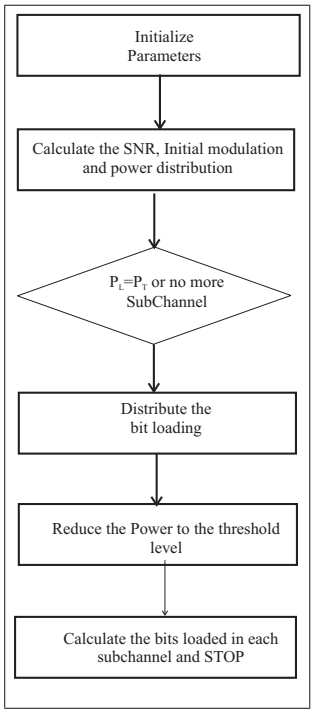

Figure 8.14: Flow chart of bit loading algorithm used for analyzing the influence of HPA in LA OFDM systems

threshold but, this will not be applicable to coded system and in those situations where a number of sub carriers form a sub band and when the system has to operate in varying channel conditions of rms delay spread and Doppler frequency spread. Since most practical systems such as 3GPP-LTE, WiMAX and IEEE 802.11g WLAN, use FEC coding, analytical expression obtained for uncoded system will not be usable. Therefore, computer based simulations are used in this work in order to find the additional margin needed to update LUT in order to maintain the QoS constraint.

8.1.3.1 Performance of LA based OFDM System

Performance of LA system is investigated for both AWGN and fading channel. From the basic BLER vs SNR curve for different BO values, the nature of performance degradation can be found. The reference LUT is prepared from the BLER vs SNR curves with 10 dB power BO since that does not introduce any non linear distortion. Results for LA based system presented here are for FEC= $\frac{1}{2}$. The required target BLER is set as 0.1.

Table 8.2: Variation in number of sub carriers Vs SNR.

SNR (dB)	-23	-21	-19	-17	-15	-10	-5	0	10	20
N	1.18	2.03	3.41	5.7	8.9	25.41	61.32	136.3	365.98	490.17
$\overline{\text{PAPR}}$	–	–	3.89	4.91	5.67	7.31	8.03	8.22	8.25	8.26

8.1.3.2 CDF of PAPR for LA System

From the expression of PAPR and also the Fig. D.1 it is clear that PAPR depends on the number for subcarrier used in a system. Though LA algorithm used in this work is a simplified version of the APMC, it is important to consider the class of algorithm such as APMC since they load different number of sub carriers as per the SNR condition. The link adaptation algorithm described in Appendix B uses power redistribution to the best sub carriers. This is because when the SNR is very low, the unused power from bad sub carriers is distributed to the better sub carriers to achieve a higher throughput. The relation between SNR and the number of loaded subcarrier is shown as in Table 8.2, where 'N' denotes the average number of sub carrier activated, and $\overline{\text{PAPR}}$ denotes the average PAPR in dB. The IFFT size has been 512. It can be seen that when the average SNR is very low, only few sub carriers are selected. This happens because the total power when distributed over these small number of carrier can cross the threshold for loading non zero number of bits. In these conditions, the mean PAPR is found to be quite low. The CDF of PAPR is shown in Fig. 8.15. There is hardly any change in PAPR for LA when the average SNR varies between -5 and 20 dB. The reason might be that high PAPR occurs rarely. When the number of sub carriers loaded exceed a certain threshold, there is not much influence on further increase in the number of sub carriers up to size of the IFFT. From this one may be led to conclude that since there is no change in the CDF of PAPR, there should not be any influence of the PAPR in the performance of LA based OFDM systems. However, the reverse has been partly observed in the earlier sections in this chapter and will also be observed in the upcoming sections as well.

8.1.3.3 Performance in AWGN Channel

Now, the performance of LA systems in OFDM will be analyzed with AWGN channel condition which will be followed by the more practical fading channel condition. The first row of the Table 8.3 shows the threshold for different modulation level when BLER constraint was set to 0.1. The Fig. 8.16 shows the performance with the ideal scenario, i.e. when HPA distortion is not taken into account and the first row the

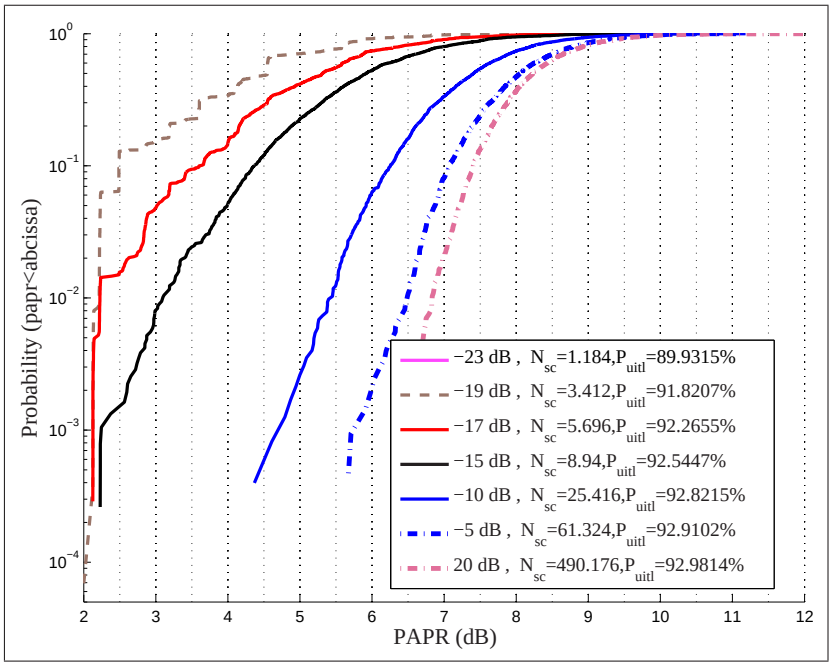

Figure 8.15: PAPR distribution for LA based OFDM system.

Table 8.3: LUT with basic and updated values for system with FEC= $\frac{1}{2}$ in AWGN Channel(Values in dB)

Power BO	None	QPSK	16QAM	64QAM
Ideal	0	5.1	11.6	17.3
6	0	5.1+0.5	11.6+0.9	17.3+2.9
5	0	5.1+0.8	11.6+1.5	17.3+7.1

table is used. It satisfies the BLER constraint. Fig. 8.19 gives the corresponding SE. However when the power amplifier distortion sets in, due to small BO, it clearly fails to satisfy the performance as is seen from Fig. 8.17. In this case the reference LUT is used while power BO less than 10 dB is considered. It can be seen that the performance of the system with 5 dB back off is worse than that of with 6dB back off power. This is expected as it is already found that the smaller the BO, larger the distortion and therefore, the greater the margin by which the system fails to meet the target BLER threshold. The Fig. 8.19 shows the severe impact on SE when not considering the impact of PAPR into LA systems. If however a power BO of 10 dB is used then the performance is same as reference system as shown in Fig. 8.16. But, this large amount of power back off drastically reduce the transmit power thereby reducing coverage which is not desired.

Therefore it is important to investigate methods which can compensate for the

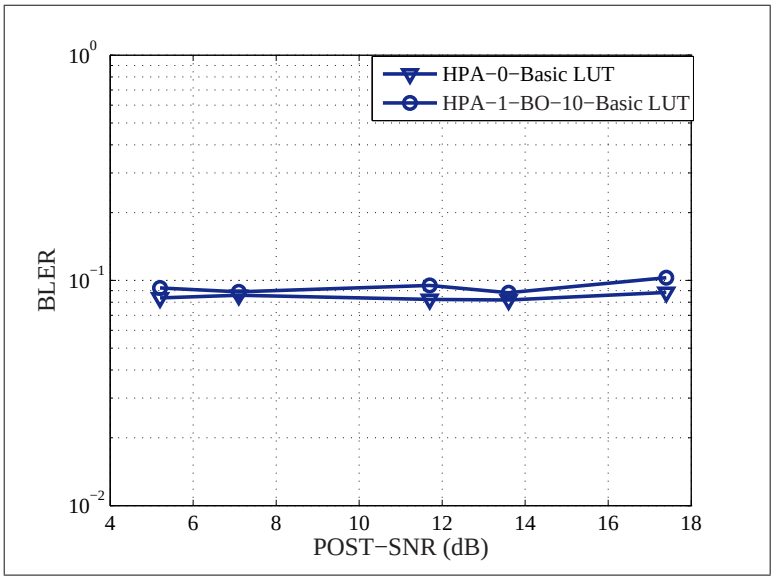

Figure 8.16: Performance of LA system with basic LUT when no power amplifier is applied. HPA-0 implies no HPA situation while HPA-1 implies that HPA is used in the simulation.

degradation. Modification of the LUT as discussed previously by adding extra margin may compensate for the BLER degradation. The margin will be different for different BO as it is already seen that the SDNR is a function of the power BO parameter. The less is the BO, the higher is the distortion which results in more BLER performance degradation and hence larger increment in threshold may be required. The Table 8.3 shows the ideal scenario as well as the added margin for non ideal cases with different BO and the above discussion is also reflected in the table. The Fig. 8.18 shows that the system satisfies the QoS constraint after adding the margin while Fig. 8.19 shows that spectral efficiency performance is restored to nearly the performance of the basic system.

The zigzag nature of the curves in Fig. 8.17 and in Fig. 8.18 when HPA is used is due to the power adaptation algorithm used in the system. For each sub channel, the measured SNR is used to switch the modulation level and the power for that sub channel is reduced to the threshold level which is just enough to maintain the SNR at the receiver. However, reducing power of the sub band is similar to BO by that amount which leads the sub band power to be closer to the linear region of the HPA and this improves the performance. Now for the same modulation level, there can be two different transmit power situation, one near the next lower threshold and the other near the next higher modulation threshold, depending on the channel condition. In the situation when the transmit power is near the next lower threshold, then the power BO is more compared to the other case, and hence the former is expected to

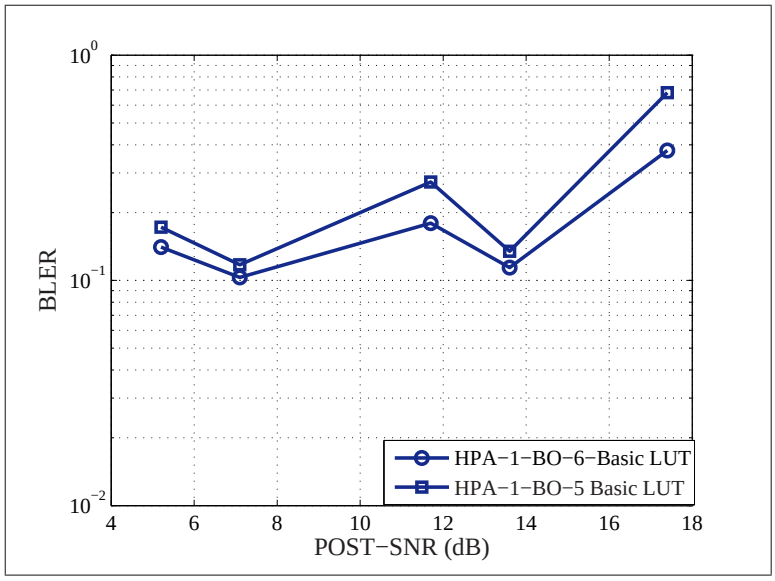

Figure 8.17: Performance of LA system with basic LUT when power amplifier is used

have a better BLER performance than the latter. This is observed in the nature of the curves shown in Fig. 8.17 and Fig. 8.18.

8.1.3.4 Performance in Fading Channel

The previous Section was dedicated to AWGN channel to show the influence of the nonlinear HPA. In this section, the fading channel is considered to get practical results. The LA issues for OFDM in fading channel are not similar to that of the AWGN channel. For AWGN channel, the PRE and POST-SNR values are identical. So the adaptation is based on the PRE-SNR, but for fading channel the PRE and POST-SNR are different quantities. While the PRE-SNR is the measure of the average SNR across the whole bandwidth the POST-SNR is the measured SNR across each sub band. At a certain PRE−SNR value, different sub channels can be loaded with different modulations and the satisfaction of the BLER criteria on the PRE-SNR level does not indicate the same for POST SNR values of the sub bands. In other words, for a given PRE-SNR, say 15 dB, there may be sub bands with POST-SNR varying between 5 to 20 dB (the range may be even wider). Therefore these sub bands will be loaded with different modulations. If the BLER is measured over the whole bandwidth and plotted against the PRE-SNR it will not give indication on the performance of each modulation level, i.e. it may happen that a particular modulation order does not meet the required BLER but the average BLER over the whole bandwidth does satisfy the target BLER, and this may not be desired. Therefore the analysis in this part

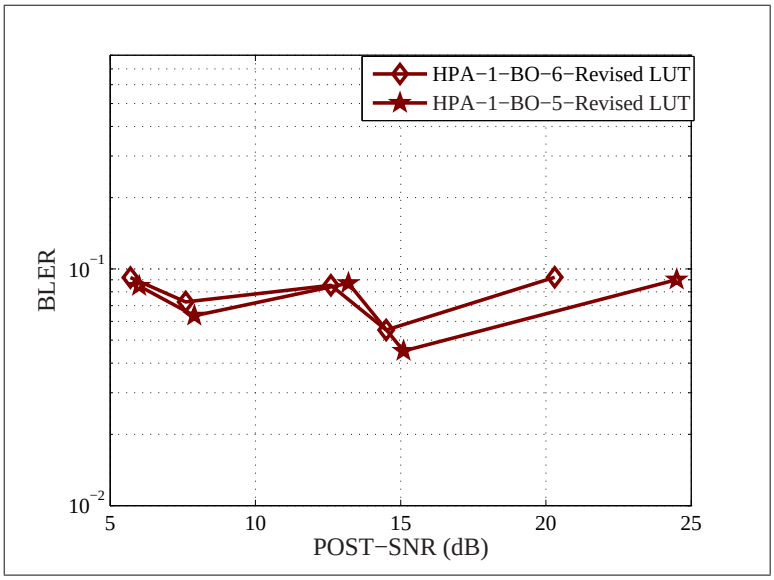

Figure 8.18: Performance of LA system with revised LUT when power amplifier is used

shows the BLER performance for different POST-SNR values. In the simulations, three different PRE−SNR values of 10 dB, 20 dB and 25 dB are chosen and the BLER performance vs the POST-SNR values is presented for each.

Table 8.4 shows the threshold of the reference system. System performance

Table 8.4: LUT with reference values for system with FEC = $\frac{1}{2}$ in Fading Channel(Values in dB)

Power BO	None	QPSK	16QAM	64QAM
Ideal	0	8.46	14.76	20.58

using the basic thresholds are shown in Figure 8.20 and 8.21 when 6 dB and 4 dB of BO is considered respectively. In both the cases system fails when 20 dB and 25 dB of transmit SNR is used, while the target BLER is satisfied when 10 dB PRE-SNR is used.

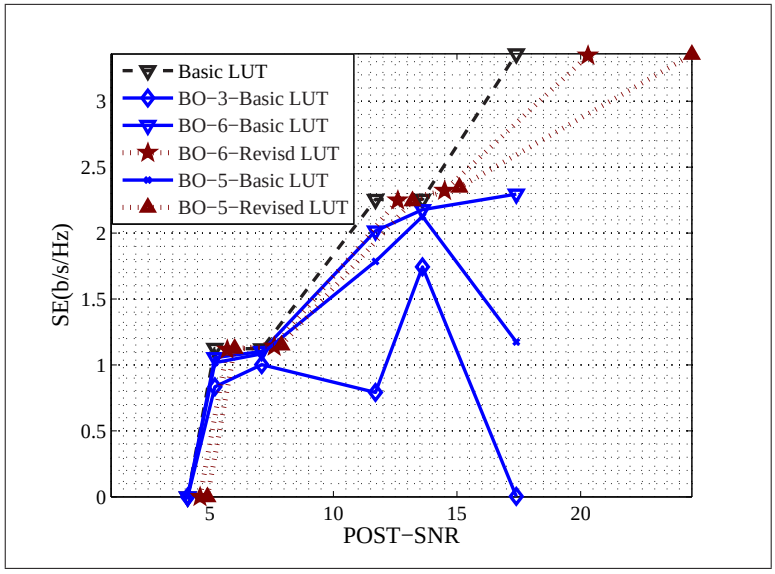

Figure 8.19: Spectral Efficiency comparison for LA system with and without PAPR consideration

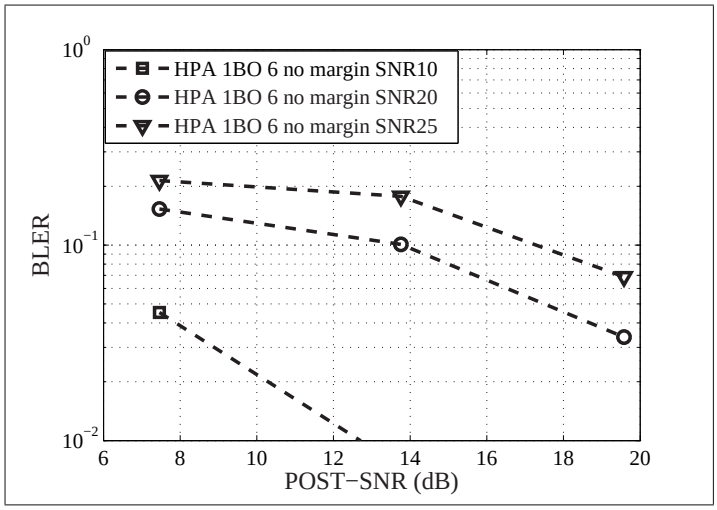

Figure 8.20: Performance of LA system with basic LUT for 6 dB of BO power

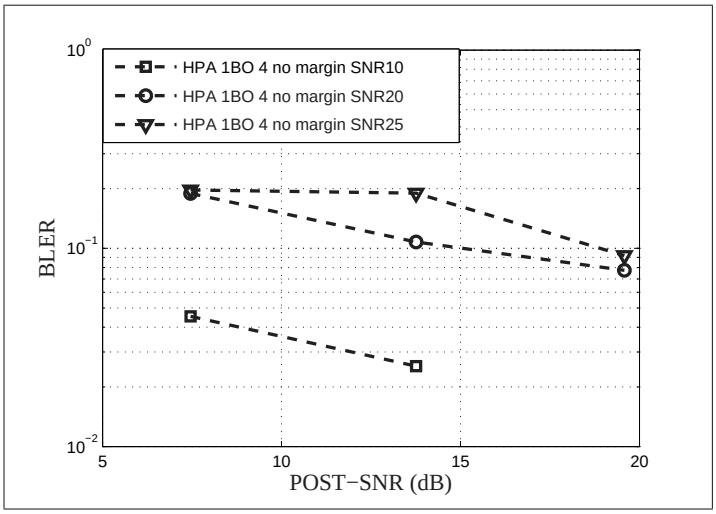

Figure 8.21: Performance of LA system with basic LUT for 4 dB of BO power

Then, extra margins are added to each threshold to satisfy the BLER constraint. The Table 8.5, 8.6 and 8.7 give the new LUT with additional margin required to satisfy the BLER constraint for 10, 20 and 25 dB of PRE−SNR.

Table 8.5: LUT with updated values for system with FEC = $\frac{1}{2}$ and PRE−SNR of 10 dB in Fading Channel(Values in dB)

Power BO	None	QPSK	16QAM	64QAM
10	-	8.46+0	14.76+0	20.58+0

Table 8.6: LUT with updated values for system with FEC = $\frac{1}{2}$ and PRE−SNR of 20 dB in Fading Channel(Values in dB)

Power BO	None	QPSK	16QAM	64QAM
6	-	8.46++1.75	14.76+0.3	20.58+0
4	-	8.46+2.5	14.76+0.5	20.58+0

Table 8.7: LUT with updated values for system with FEC = $\frac{1}{2}$ and PRE−SNR of 25 dB in Fading Channel(Values in dB)

Power BO	None	QPSK	16QAM	64QAM
6	-	8.46+2.5	14.76+1.65	20.58+0
4	-	8.46+4.0	14.76+1.75	20.58+0.5

The performances using the revised LUT are shown in Figure 8.22 and 8.23. When PRE−SNR is 10 dB, which is slightly higher than the switching threshold for QPSK, most of the sub carriers are expected to be loaded with QPSK and few of the subcarrier may experience very good channel and are loaded with 16QAM. As seen from the performance presented earlier in the chapter, QPSK is not much affected by HPA non linearities. This indicates that the target BLER level is satisfied for this modulation. The very few channels which are loaded with 16QAM might be experiencing a good average SNR over the sub channel. So they also satisfy the target BLER and hence no additional margin is required. This may be because of the nature of frequency domain fading of the channel. The fading characteristics may affect the performance of the FEC decoder. Since the interleaver distributes the bits within one data block, the gain from interleaving is also limited to the channel properties of a data block consisting of 16 consecutive sub carriers in the frequency domain and 6 OFDM symbols in the time domain. This can be substantiated by referring

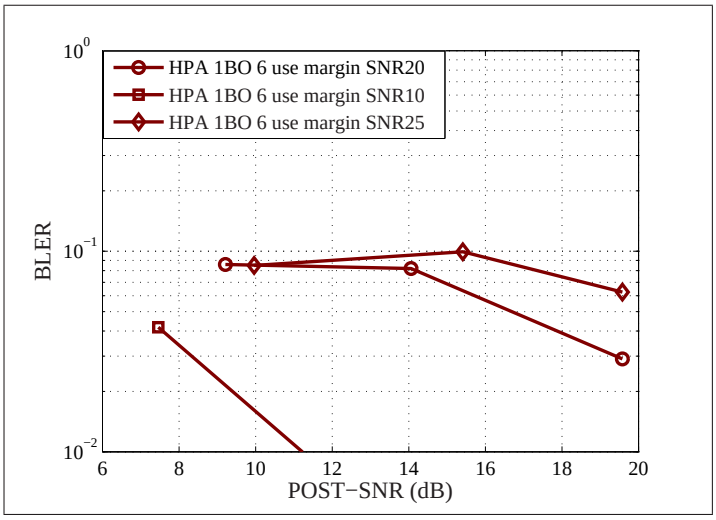

Figure 8.22: Performance of LA system with revised LUT for 6 dB of BO power

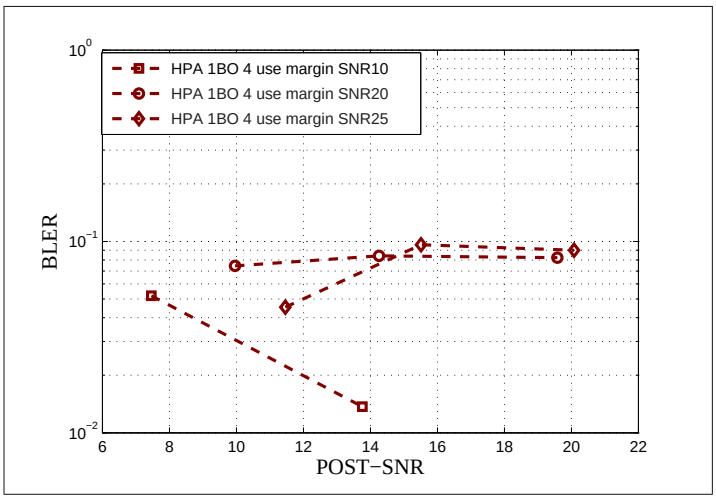

Figure 8.23: Performance of LA system with revised LUT for 4 dB of BO power

to the work [38], in Chapter 2 Section 3, which discusses the average bandwidth of fade vs, ratio of channel gain to the RMS channel gain. It is shown in the work that with increase in the channel gain relative to the RMS channel gain, the average bandwidth of fade increases. In other words, the work suggests that the good sub carriers will experience more flat channel in the frequency domain than the deeply faded sub carriers. This explains the result obtained in the LA. Interestingly it is worth comparing the additional margins being used for the AWGN situation and the fading channel situation. In the AWGN channel, the additional margin is solely because of the non linear distortions, whereas in fading channel the effect of frequency selectivity is more prominent as understood by the discussion above.

For PRE−SNR of 20 dB, most of the sub channels are likely to be loaded

with 16QAM and those experiencing high channel gains are loaded with 64 QAM. The sub channels which experience deep fades may get loaded with 4QAM. Even though they were loaded with 4QAM, it may be due to the extremely poor channel condition of some sub carriers that they fail to satisfy the BLER constraint. Hence, some additional margin is needed. This additional margin in turn implies that a particular modulation order is selected only if the average SNR over the sub channel exceeds an additional threshold thereby ensuring better channel condition suitable for the interleaver and FEC coder to satisfy the BLER target.

It can be seen from the Figure 8.22 and 8.23 that with additional margin the BLER requirement is successfully met. It can also be seen from the tables that higher the BO, lower is the additional margin required and this is accordance to the earlier discussion.

At a PRE-SNR of 25 dB more margin is needed for different modulation scheme as compared to that of 20 dB PRE−SNR. It can be noted here that threshold for switching of LA system changes depending on the PRE−SNR condition. This kind of revelation is not possible in the analysis made for single carrier systems [26]. Thus for implementing LA in OFDM based system, along with the primary distortion, it is also very important to consider the PRE-SNR condition for updating the SNR thresholds for switching the modulation and coding rate, otherwise though the average BLER might appear to be satisfied, the system may pay a penalty by not being able to transmit a particular modulation successfully and this especially affects the low order modulations.

8.1.4 Conclusion

It is seen that the distribution of PAPR in case of LA algorithms, which loads different number of sub carrier at different SNRs, is independent of SNR, when the average SNR is above 0 dB, i.e. PAPR of LA algorithms does not depend on how many sub carriers are loaded but the PAPR is similar to the case when all sub carriers of the IFFT are used. It has been found that high PAPR has severe impact on the LA based OFDM systems. It has been shown that LA-OFDM systems designed without considering the very important non linear distortion effects of the HPA will fail to meet a target BER. Additional margin must be used with the SNR switching thresholds for adaptive modulation and coding to meet the target BLER. It is also found that along with the effects of the distortion it is also vital to take into account the PRE-SNR condition while finding the SNR margins. In this section only FEC= $\frac{1}{2}$ is presented

which is representative of the kind of problem to be faced in these conditions. Results for other coding rates can be obtained following the discussion made in this work. With the modified algorithm for LA, that uses additional margin and updates the LUT (based on the BO information) to make the system maintain the BLER target, several LUT for different combination of back off power and coding rate may be needed which best fits the situation.

8.2 LA under ICI

In the previous section of this chapter the impairment at the transmitter end is presented. In this section the focus is on the impairment at the receiver end. The impact of ICI due to frequency synchronization is discussed in this section. A method to overcome the effect of ICI was presented in Chapter 5 of this thesis, where it was assumed that the maximum Doppler spread and residual frequency offset is estimated at the User Equipment (UE) and that the sub carrier bandwidth can be adapted to mitigate ICI. However in this section the influence on LA when the receivers do not have the capability to measure the frequency offsets and use fixed sub carrier bandwidth is analyzed. If the measured channel quality of the sub carriers does not include the ICI factor then there might be severe impact on the LA system which heavily depends on the feedback of measured signal strength. It is therefore necessary to analyze the performance of LA systems under these conditions. However, it is assumed that maximum Doppler spread and residual frequency offset are measurable at the BS. This information is used to make adjustments to LA.

8.2.1 Introduction

ICI in OFDM systems is caused by carrier offset due to frequency synchronization error [68],[45] and due to Doppler frequency spread [69],[70]. The analytical expressions for ICI are given in Chapter 5. It is seen that the amount of ICI is dependent on the ratio of effective carrier offset (residual carrier frequency offset and maximum doppler spread) to the sub carrier spacing and it also proportional to the received signal strength.

Figures 8.24–8.29 show the impact of the effective offset for different modulations for different SNR conditions for uncoded and rate half FEC coded system, in fading channel. In the analysis, 512 sub carriers in 5MHz bandwidth at 2 GHz carrrier frequency is considered. In all of the above cases the adaptation rate is considered to be 0.5ms. The channel rms delay spread of 2μs is used. It can be realized that for un coded system a target BER of 10^{-3} can hardly be maintained at high mobility conditions for high order modulations. For coded case the metric is BLER. In this case the error floor is not easily seen except for 64-QAM. But the impact of high Doppler frequency spread is evident. For QPSK, the performance degradation from 50Hz to 400Hz is about 5 dB at 10^{-1} BLER level. At the same BLER threshold, the performance degradation for 16-QAM is about 6dB and that for 64-QAM is about 17 dB. At lower BLER thresholds the performance degradation is even worse.

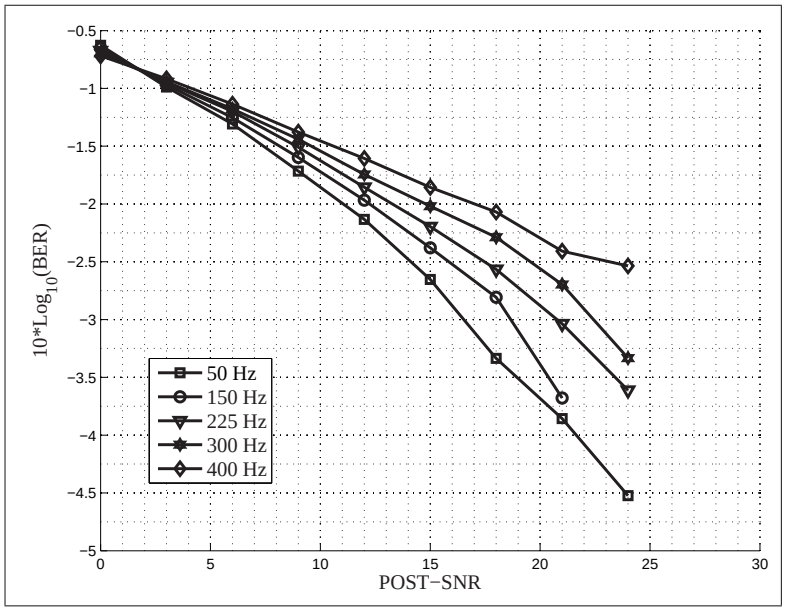

Figure 8.24: Impact of frequency offset on 4-QAM in fading channel.

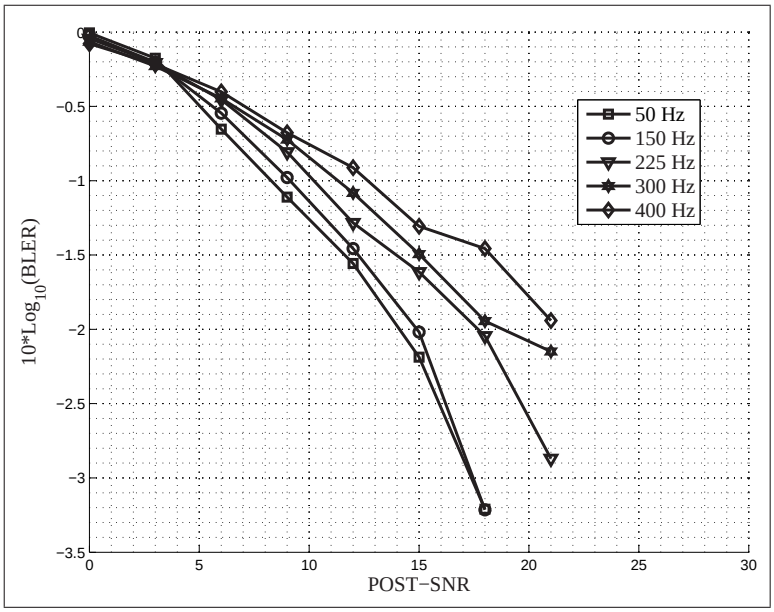

Figure 8.25: Impact of frequency offset on 4-QAM, FEC rate 1/2, in fading channel.

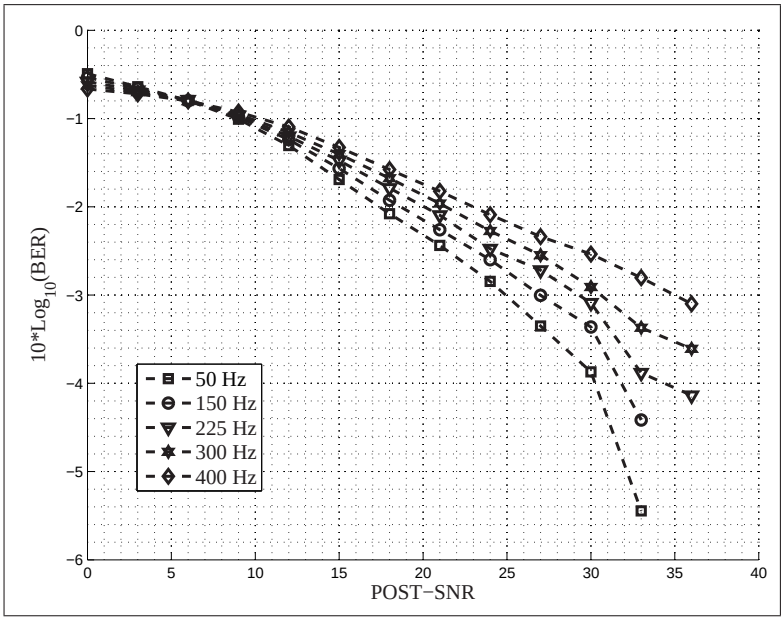

Figure 8.26: Impact of frequency offset on 16-QAM in fading channel.

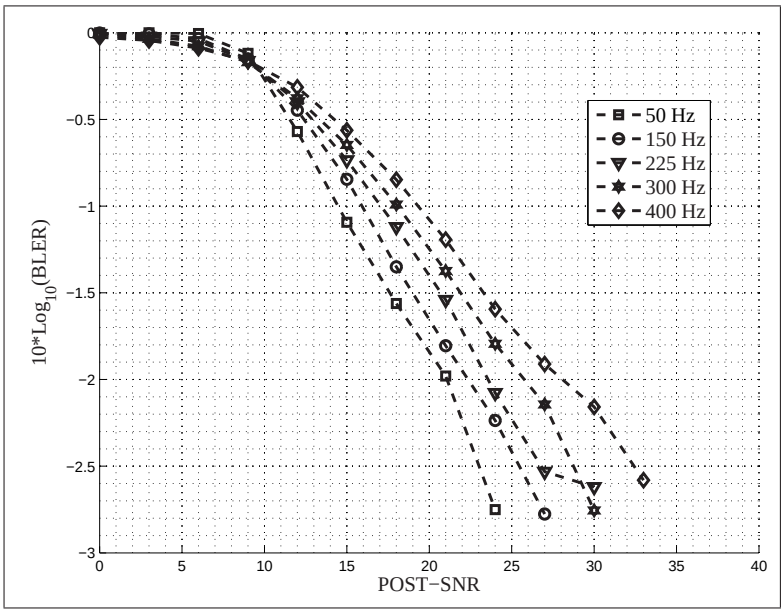

Figure 8.27: Impact of frequency offset on 16-QAM, FEC rate 1/2, in fading channel.

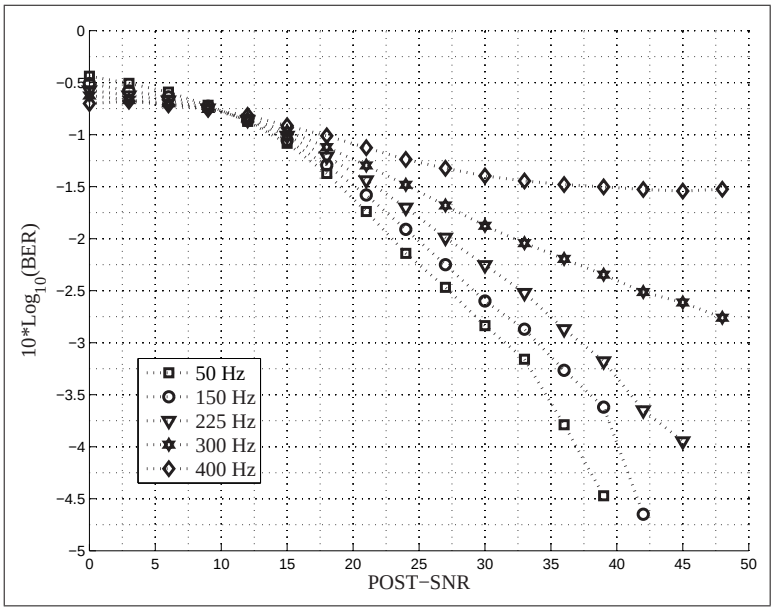

Figure 8.28: Impact of frequency offset on 64-QAM in fading channel.

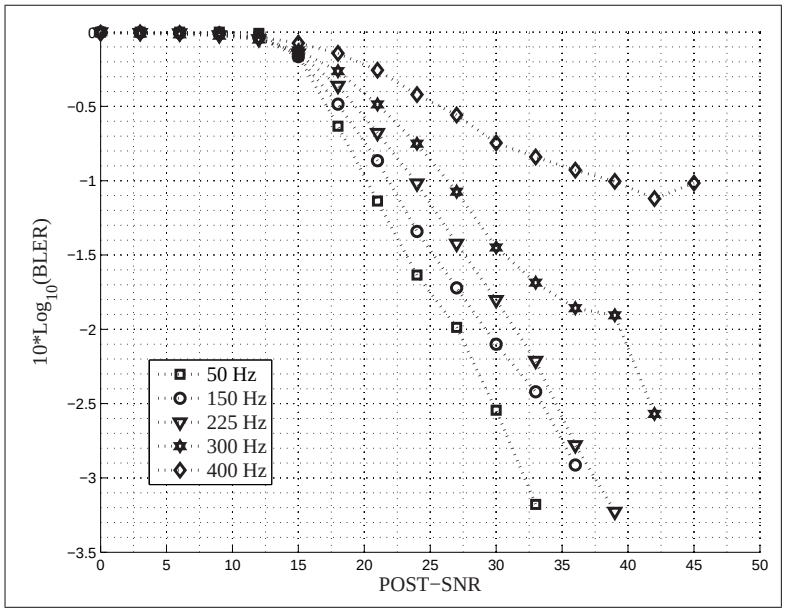

Figure 8.29: Impact of frequency offset on 64-QAM, FEC rate 1/2, in fading channel.

Table 8.8: LUT for different Doppler spread conditions for code rate of 1/2 at BLER threshold of 10^{-1}

Modulation	QPSK	16-QAM	64-QAM
SNR threshold in dB at 50 Hz	8.52	14.67	20.46
SNR threshold in dB at 150 Hz	10.52	16.67	22.46
SNR threshold in dB at 255 Hz	12.27	18.42	24.12
SNR threshold in dB at 300 Hz	13.52	19.67	25.46
SNR threshold in dB at 400 Hz	17.22	13.37	29.16

8.2.2 LA under undetected ICI

If the LUT for LA is generated based only one Doppler condition, say the 50Hz case, then the BLER performance for other Doppler conditions can be seen from Fig. 8.30. It can be seen that higher the Doppler frequency spread, the larger is the deviation of the BLER performance from the target BLER of 10^{-1}. This can be understood in the light of the increasing ICI with increase in Doppler frequency spread. It has been described before that the threshold to switch from one modulation to another or to select a modulation for a given coding rate depends on the SINR. In the above situation, it is assumed that the true Signal to Interference plus Noise Ratio (SINR) is not measured in the receiver. i.e. the ICI component has not been captured at the receiver in the SINR meaurement, i.e.

$$\mathrm{SINR} = \frac{\mathrm{E}[|\mathrm{X}|^2]|\mathrm{H}|^2\mathrm{sinc}^2(\pi\epsilon)}{\sigma^2} \tag{8.6}$$

where σ^2 is the noise power and ϵ is the relative frequency offset. Here the deterioration in SINR due to ICI is not considered and hence the wrong decision is made in selecting the modulation level. If receivers do not have the capability to estimate the residual carrier offset or the maximum Doppler spread then they are expected to be in this situation.

Following the above formula, the estimate of SINR is much more optimistic than the actual SINR. However as mentioned earlier it is assumed that the maximum Doppler offset is measurable at the Base Station (BS). Then to make the system meet the target BLER, the SNR thresholds must be modified. The updated LUT is given in Table 8.8. Though the UE may not have the capability to measure the residual offset, the BS my be able to do so and indicate to the UE to use a different SNR threshold corresponding to the Doppler condition.

The BLER of the system using the new threshold as defined in Table 8.8 is

given in Fig. 8.31. It can be seen that the system now satisfies the target BLER threshold at all Doppler conditions. The spectral efficiency curves for this system are in Fig. 8.32. At 20dB, there is about 17% decrease in spectral efficiency when the effective Doppler increases from 50 to 150 Hz, and the decrease is about 30% when the Doppler is about 225 Hz and when the Doppler is 400 Hz, the decrease in spectral efficiency is about 70%. The decrease in performance is due to the increased threshold which can be easily seen from the Table 8.8.

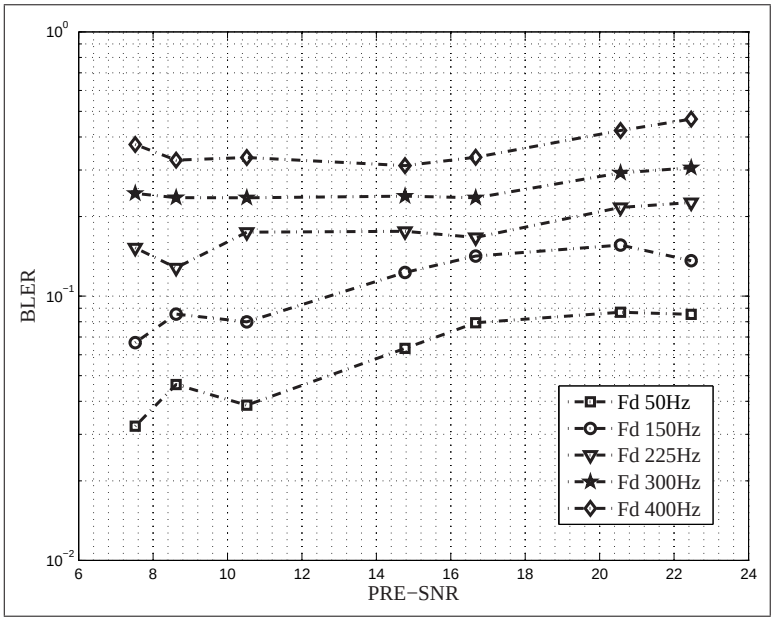

Figure 8.30: Bler performance without additional margin for coding rate 1/2

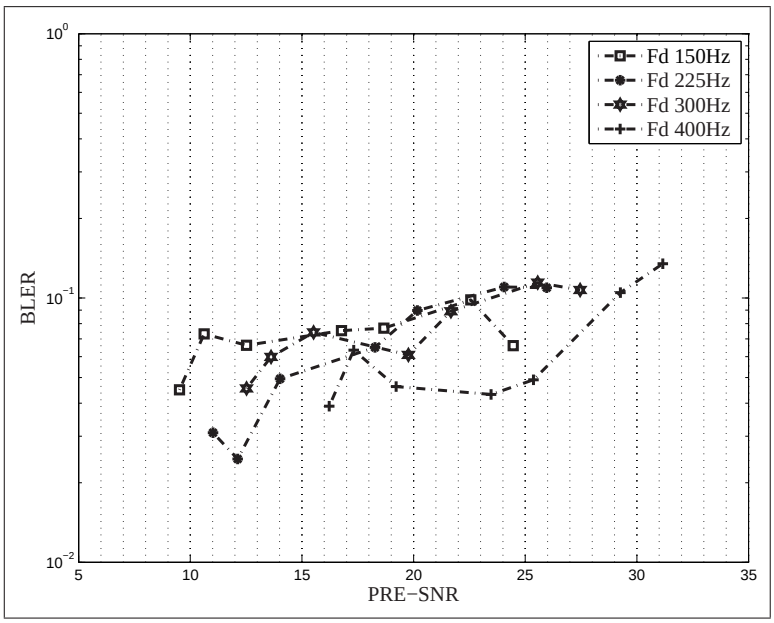

Figure 8.31: Bler performance with additional margin for coding rate 1/2

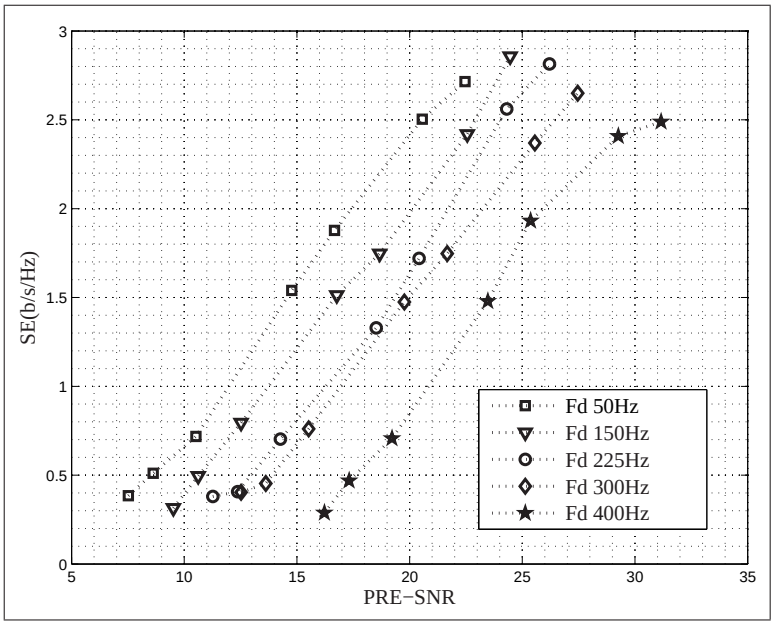

Figure 8.32: Spectral efficiency performance with additional margin for coding rate 1/2

8.2.3 Conclusion

In this section, it is shown that if the user equipment which feeds back the SNR to the BS in a LA system, cannot estimate the Doppler frequency spread, then the LA fails to meet the target error rate criteria. However, it is also shown that if the BS has the required capability to measure the Doppler frequency spread of a user, then a suitable adjustment to the SNR switching threshold for the adaptive modulation and coding can be made. This would allow the LA system to satisfy the error rate constraint while maximizing the spectral efficiency. Even though the LA system with the new thresholds can meet the required error rate there is a severe impact on the spectral efficiency of the systems. It is seen that when the Doppler frequency spread increases from 50Hz to 150Hz, the spectral efficiency drops by about 17%, while if the Doppler is about 400Hz, the performance drops by about 70%.

8.3 Summary

- In this chapter, the impairments at the transmitter and at the receiver ends have been considered for evaluating the performance of LA systems in OFDM framework

- At the transmitter side the influence of non linear power amplifier is analyzed.

- It is seen that non linear operation of the power amplifier has a detrimental effect on the LA systems. The target error rate criteria is not met by the LA when the HPA effects are not measured in the fed back SNR.

- The HPA introduces uncorrelated Gaussian noise, and the power of this noise increases with reducing power back off.

- The distortion introduced by the HPA is not measurable by a TS sequence since the TS design ensures that the time domain signal does not have a high PAPR. Therefore, the SNR fed back by the UE does not include the measure of the distortion although the effect is present in the data symbols which follow the TS.

- Since the BS has knowledge about the power BO and the size of FFT which gives an indication of the PAPR to be expected in a data symbol, it can leverage this information to adjust the SNR switching thresholds for the adaptive modulation and coding schemes.

- It is also shown that the optimum power BO obtained from the Total Degradation (TDEG) curves is different for each modulation and coding and that it varies with the required BLER.

- It is seen that higher order modulations require a higher SNR margin with respect to the reference SNR threshold for the same amount of power BO in the HPA. This is true because the higher order modulations have higher error probability for the same distortion noise power compared to a low order modulation.

- SNR margins required for fading channel condition when compared against the margins required for AWGN show quite distinct behavior. This is because the frequency selective fading nature of the channel has a very strong influence on the thresholds. In this case it is found that the SNR thresholds for the low order modulation need to be increased.

- Finally it is shown that by adjusting the SNR thresholds the LA schemes can maintain the required BLER and also maximize the throughput.

- In the second part of the chapter the influence of ICI due to Doppler frequency spread is analyzed.

- In contrary to an earlier chapter, it is assumed here that the maximum Doppler is not measurable at the UE. Therefore the SNR fed back does not include the effect of ICI.
- It is found that under such circumstances the LA systems fail to meet the BLER target.
- However if it is assumed that the BS has the signal processing capability to estimate the Doppler spread, then the SNR switching thresholds can be adjusted and the LA system can again be made to satisfy the BLER constraint.
- It is seen that even though the LA system can be made to satisfy the target BLER using the modified LUT, yet, there is a significant loss in spectral efficiency of the system. However, it is understood that with the modification in the LUT the system can sustain communication while meeting the target BLER even though the throughput is low, which is not possible without the mentioned modification.

9

Conclusions and Future Work

The main conclusions of this work and possible areas of further investigation are discussed in this chapter.

9.1 Conclusions

The focus of this work is to enhance the spectral efficiency of OFDM based wireless systems. Multi carrier spread spectrum based transmission schemes obtain frequency diversity due to spread spectrum properties and are robust against multi path fading due to the multi carrier architecture. However, for indoor conditions where the channel varies slowly with time and only a sub set of all sub carriers are allocated to one user, the outage performance of such systems is very low. It is proposed in Chapter 3, to use sub carrier hopping in such systems to overcome the low outage. The proposed sub carrier hopping with multi carrier spread spectrum is shown to improve the outage by 15%. It is also found that using interleaved sub carrier allocation is better than using consecutive sub carrier allocation for one user. Additionally it has been found that successive interference cancelation algorithms at the receiver are useful in only few scenarios. Several such guidelines are presented in this work.

Multi carrier spread spectrum techniques need additional signal processing

complexity over OFDM systems therefore the performance of such systems is compared against OFDM to find the better scheme. It is shown that, OFDM has better robustness to channel estimation errors than multi carrier spread spectrum systems when the systems are fully loaded. In partial load conditions, multi carrier spread spectrum schemes can provide a better BER performance than OFDM systems. Since, operating the system in full load gives higher data rate, and as it is found that OFDM is robust to receiver impairments under full load, therefore techniques to improve spectral efficiency of multi carrier based systems are investigated for OFDM systems.

Though OFDM is relatively more robust compared to multi carrier spread spectrum schemes, yet, it is not able to sustain the performance once the receiver impairments of channel estimation error and residual phase error exceed a certain amount. Therefore compensating for the receiver impairments is necessary to achieve a high performance. To track the residual phase error, pilot sub carriers are embedded among the data sub carriers. The pilot sub carriers are pre defined signals which are thus necessary overhead. It is found that the pilots enjoy a extra SNR. Therefore it is proposed in Chapter 4 to transmit additional information bits on pilot sub carriers to reduce the pilot overhead. Several combinations of modulation order to be loaded on pilot sub carriers and data sub carriers have been shown. The proposed scheme reduces the pilot overhead without performance degradation. It is seen that this scheme provides a gain between 5% and 15% depending on the scenario.

In outdoor condition a major contributor to the frequency synchronization errors is the Doppler frequency spread, which causes ICI. The ICI is dependent on the received signal strength and velocity of user and scatters in the environment. There is a large variation in the range of values of ICI. A novel technique of using adaptive sub carrier bandwidth to overcome inter carrier interference without using complex interference cancelation algorithms at the receiver is suggested in Chapter 5. Two different transmitter architectures are presented which provide a throughput gain in the range of 10% and 30% over OFDM system using fixed sub carrier bandwidth.

The performance of OFDM is also limited by the overhead due to GI, which is necessary to overcome the effect of ISI. An algorithm for selecting the GI duration dynamically, in OFDM systems, which is a function of the target SNR, the OFDM symbol duration, the maximum allowable carrier offset or Doppler frequency spread and the rms delay spread of the channel, is presented in Chapter 6. The scheme of using adaptive GI duration is seen to provide a throughput gain of up to 20% by reducing the GI overhead by as much as 60%.

To enhance the spectral efficiency of OFDM systems while maintaining a target

error rate link adaptation methods using adaptive modulation, coding, and power are under investigation. OFDM provides an ideal framework for implementation of LA schemes, but as the degrees of freedom increase when LA is combined with OFDM, the implementation complexity also increases. Therefore several schemes to adapt some parameters slowly while other parameters at a fast rate so as to limit the system complexity is proposed in Chapter 7. Among other useful results in this chapter, it is shown that by using fast power control along with slow adaptive modulation along with even slower coding rate adaptation the overhead can be reduced by more than 50% while maintaining the spectral efficiency nearly as much as the optimum performance. The need to adapt the sub band size and the suggestion for using only one FEC rate at a time for a user is also made in this chapter. Several valuable guidelines and important results have been obtained which can provide significant inputs to the upcoming OFDM based wireless communication standard.

Though the LA schemes in combination with OFDM are seen to provide very high spectral efficiency, the investigation of their performance under transmitter and receiver impairments is very important in order to understand the true potential of the schemes. Accordingly Chapter 8 presents the analysis of the LA - OFDM system under the influence of non linear HPA and the effect of ICI. The TS, which precedes the data symbols, is designed to have a much lower PAPR than that of the data symbols. Therefore the non linear distortion due to the HPA affects the TS much less than the data symbols. The received SNR measured using the TS will therefore not capture the non linear distortion due to the HPA. The erroneous SNR fed back by the UE causes the BS to select a modulation order and coding rate which cannot meet the target BLER. However, it is found that if the transmitter has a knowledge of the amount of non linear distortion, then suitable adjustments to the SNR switching thresholds can be made, which can ensure a high spectral efficiency while meeting the target BLER. In case of the ICI impairment, it is considered that the maximum Doppler spread or the residual carrier offset is not measurable by the user equipment due to limited complexity. However, it is considered that the base station has the capability to estimate these parameters. Under such situations a similar observation is made, i.e. the SNR switching thresholds need to be adjusted in order to meet the target BLER and maintain a high spectral efficiency.

Finally it can be concluded that using the transmission techniques proposed in this thesis, significant increase in spectral efficiency can be achieved for OFDM based wireless systems. Notably the gains of each of the proposed techniques are non overlapping. Therefore if these techniques are used simultaneously in future wireless

systems, then the benefit from each scheme will add up to provide a significant total improvement in spectral efficiency.

9.2 Future Works

Several methods to enhance the spectral efficiency of OFDM based wireless systems are proposed in this thesis. However there are many possible areas which can be explored further. It is found in this work that OFDM performs better than multi carrier spread spectrum under full load conditions where as the reverse is true for low load situations. Therefore hybrid adaptive multiplexing techniques which combine these two schemes suitably can be a possible issue for further investigation.

The use of semi blind pilot has been recommended in this work, which increases the spectral efficiency of OFDM systems. An extension of the analysis can be to devise systems which can dynamically adapt the pilot sub carrier density to further enhance the performance.

To overcome varying ICI conditions the use of variable sub carrier bandwidth is suggested here. The analysis presented assumes perfect estimation of maximum Doppler offset and SNR. Investigation on the effect of Doppler and SNR estimation error and algorithms for estimation of these parameters can be areas of further research.

To reduce the GI overhead of OFDM systems, an algorithm to dynamically choose the GI duration is given in this thesis, which considers ideal estimation of channel rms delay spread and SNR. Evaluation of the system under practical constraints of imperfect estimation of rms delay spread and SNR are possible issues of future investigation.

Algorithms for simplified link adaptation in OFDM framework have been presented in this work, but they are analyzed for single user scenario. As these algorithms are required to operate in multi user situations, joint link adaptation - resource allocation in a OFDMA framework for multicellular environments is foreseen as a natural extension of the work. It is found in this work that the non linear distortion and inter carrier interference have significant impact on the performance of LA - OFDM schemes. To tolerate the impairments, a large number of SNR look up tables are needed which increase the complexity of the system. Therefore reducing the complexity in this perspective can be investigated further.

A

Selected Publications Related to the thesis

A.1 Publications

A.1.1 IPR

1. "Enhancing spectral efficiency of OFDM systems by Data Transmission over Pilot Tones", September, 2004, Patent Application No 963/MUM/2004.

2. "A novel multirate orthogonal frequency division multiplexing system proposal to reduce intercarrier interference", September, 2004, Patent Application No 964/MUM/2004.

A.1.2 Journal

1. Suvra Sekhar Das, E. De Carvalho, and R. Prasad, "Variable sub-carrier bandwidth in OFDM framework" IEE Electronic Letters Vol 43 , Issue 1, Jan. 2006 pp. 46-48.

2. Suvra Sekhar Das, E. De. Carvalho, and R. Prasad, "Performance Analysis of OFDM systems with Adaptive Sub Carrier Bandwidth", accepted, IEEE Transactions in Wireless Communications.

3. Suvra Sekhar Das, E. De. Carvalho, and R. Prasad, "Dynamically Varying Guard Interval Length for OFDM Systems", to be submitted with revisions, IEEE Transactions in Wireless Communications.

4. Suvra Sekhar Das, E. De. Carvalho, and R. Prasad, "Hybrid Link Adaptation Strategies for OFDM systems", to be submitted.

5. Suvra Sekhar Das, E. De. Carvalho, and R. Prasad, "Adaptive Bit and Power Loading with PAPR and ICI Considerations for OFDM Based Systems", to be submitted.

A.1.3 Conference

1. Suvra S Das, Muhhamad Imadur Rahman, Nidcha Pongsuwanich, Fleming B. Fredericksen, Ramjee Prasad."Influence of PAPR on Link Adaptation Algorithms in OFDM Systems", IEEE VTC Spring 2007.

2. Suvra S Das, Muhhamad Imadur Rahman, Nidcha Pongsuwanich, Fleming B. Fredericksen, Elisabeth De Carvalho, Ramjee Prasad."Adaptive Modulation and Power Loading with PAPR Considerations for OFDM Based Systems", Accepted IEEE VTC Fall 2007.

3. Suvra Sekhar Das, Muhammad Imadur Rahman, Yuyane Wang, Fleming B. Fredericksen, Elisabeth De Carvalho, Ramjee Prasad. "Hybrid Link Adaptation Strategies for OFDM based systems". Accepted for publication in IEEE VTC Fall 2007.

4. Muhammad Imadur Rahman, Suvra Sekhar Das, Yuyane Wang, Fleming B. Fredericksen, Elisabeth De Carvalho, Ramjee Prasad. "Link Adaptation Strategies for Multi-Antenna Assisted WiMAX-like System", Accepted IST mobile summit 2007.

5. Suvra S Das, Muhammad Imadur Rahman, Yuyane Wang, Fleming B. Fredericksen, Ramjee Prasad, "Influence of Inter Carrier Interference on Link Adaptation Algorithms in OFDM Systems", Accepted IST mobile Summit 2007.

6. Suvra S Das, Elisabeth De Carvalho, Ramjee Prasad, "VGI OFDM in dynamic channel conditions", IEEE PIMRC 2006

7. Suvra Sekhar Das, Ramjee Prasad, et. al. "Variable Guard Interval OFDM in presence of carrier frequency offset", IEEE Globecom, November, 2005.

8. Suvra S Das, Elisabeth De Carvalho, Ramjee Prasad, "Time Correlation function for RMS delay spread of a channel model", IST Mobile Summit 2006, Myconos, Greece, June, 2006

9. Suvra Sekhar Das, Elisabeth De Carvalho, Ramjee Prasad, et. al." Variable SubCarrier Bandwidths in OFDM(A) Framework", IEEE VTC Spring 2007, Dublin, Ireland

10. Suvra S Das, Elisabeth De Carvalho, Ramjee Prasad, et. al . "Dynamically Adaptive Bandwidth for Sub Carriers in OFDM based Wireless Systems", IEEE WCNC 2007, Hongkong.

11. Das, S.S.; Rahman, M.I.; Fitzek, F.H.P.; "Multi rate orthogonal frequency division multiplexing",2005 IEEE International Conference on Communications , 2005. ICC 2005. Volume 4, 16-20 May 2005 Page(s):2588 - 2592

12. Suvra S Das, Rajeshwar Rao, Ramjee Prasad, "Performance of MultiCarrier Access Schemes with Receiver Impairments in Down LinkIndoor Environment", VTC Spring 2006, Melbourne, Australia.

13. Suvra S Das, Muhammad Imadur Rahman, Frank H.P. Fitzek, Ramjee Prasad "On Performance of SCH-OFDMA-CDM in Frequency Selective Indoor Environment", IEEE Vehicular Technology Conference Spring 2005 Wireless Access Stockholm, Sweden, May, 2005, conference proceedings.

14. Suvra S Das, et. al. "Using Pilots to Transmit Data Information in OFDM based WLANs", Wreless Personla Multimedia Communication WPMC 2004, September, 2004, Abano Terma Italy.

15. Suvra S Das, Ratnam V. Rajakumar, Muhammad I.Rahman, Arpan Pal,Frank H.P.Fitzek, Ole Olsen,Ramjee Prasad, "Low Complexity Residual Phase Tracking Algorithm for OFDM-based WLAN Systems", CSNDSP Symposium 2004, Fourth International Symposium 20-22 July 2004, Newcastle, UK, Juli, 2004, pp. 128-131

16. Suvra Sekhar Das, Muhammad Imadur Rahman, Frank H.P. Fitzek, Ramjee Prasad, et. al. "Low Complexity Semi Blind Residual Phase Tracking for OFDM based WLANs", WPMC 2005, Aalborg, Denmark, September, 2005,

A.2 Chapter wise Publications

Table A.1: Chapter wise Publications

Chapter Number	**Publication**
3	Conference: 12,13
4	Conference: 14,15,16. IPR: 1
5	Conference: 9,10,11. Journal: 1,2. IPR: 2
6	Conference: 6, 7, 8. Journal: 3
7	Conference: 3,4. Journal: 4
8	Conference: 1,2,5. Journal: 5

B

Link Adaptation

B.1 Bit and Power Loading Algorithm

An algorithm is presented here which has the highest possible throughput of the two algorithms referred [115, 94], while the complexity is between the two. The algorithm is referred to as simple adaptive modulation and power distribution algorithm(SAMPDA). It is designed based on the two algorithms, simple rate adaptation algorithm (SRA) [115] and adaptive power distribution (APDA) [94]. In the algorithm, greedy approach is used, but unlike the APDA, instead of starting from 0 power and 0 bits as the beginning, the algorithm is initiated with equal power for all sub-carriers. Then by comparing received signal to noise ratio (SNR) with the SNR-lookup table, loaded bits for each subcarrier can be found, and power required for each subcarrier is recalculated. The flow chart for the algorithm is in Figure B.1. The parameters used in describing the algorithm are given in Table B.1

The SAMPDA algorithm works as follows:

- **Step 1: Initialization** Equal power per sub carriers for SNR measurement at the receiver

$$P_n = P_T/N$$

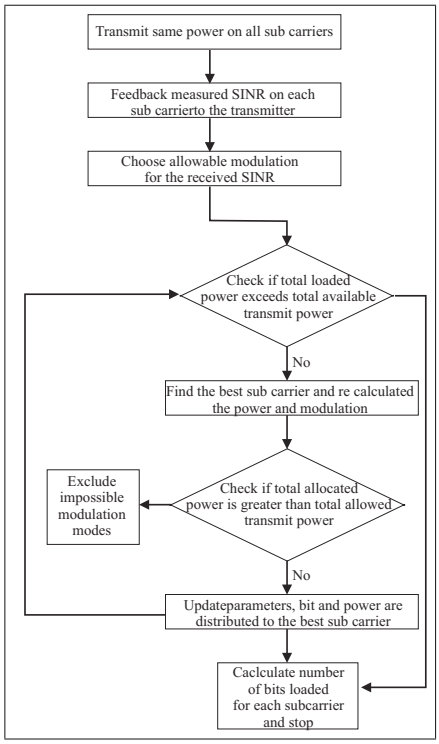

Figure B.1: Flow diagram of the SAMPDA algorithm

Table B.1: Parameter description

P_T	Transmit power threshold
P_L	Loaded power
N	Number of sub-carriers
F	The highest modulation level
$\psi_{mod} = [0, 1, ..., F]$	Usable modulation set
$P_{1\times N}$	Vector of power for each subcarrier
$k_{1\times N}$	Vector of loaded bits for each subcarrier
$M_{1\times N}$	Vector of Modulation scheme for each subcarrier
n	Sequence number of the subcarrier
g_n	Channel gain at the n^{th} subcarrier
$\frac{\Delta P}{\Delta k}{}_{1\times N}$	Incremental power per incremental bit
γ_n	Signal to noise ratio in each subcarrier
σ_n^2	Noise power in each sub-carrier
SNR^f	Required SNR to maintain the target BER for the f^{th} modulation level
NaN	Not a number
n^*	Sequence number of the BEST subcarrier which has the minimum value of $\frac{\Delta P}{\Delta k}$.

- **Step 2: Initial modulation scheme and power calculation** Find initial modulation scheme based on the feedback of SNR from the receiver.

$$\gamma_n = \frac{P_n g_n^2}{\sigma_n^2}$$

$$M_n = f_n \quad \text{where} \quad SNR^{f_n} \leq \gamma_n < SNR^{f_n+1}$$

$$P_n = \frac{SNR^{M_n}\sigma_n^2}{g_n^2}; \qquad P_L = \sum_{n=1}^{N} P_n$$

$$\frac{\Delta P}{\Delta k}_n = \frac{(SNR^{M_n+1} - SNR^{M_n})\sigma_n^2}{2g_n^2} \quad \text{if} \quad M_n \neq F$$

$$\frac{\Delta P}{\Delta k}_n = NaN \quad \text{if} \quad M_n == F$$

- **Step 3: Check the Termination Condition:** If $P_L = P_T$ or $min(M) = F$, go to step 6, else continue;

- **Step 4: Iteration starts:** Find the BEST subcarrier:

$$n^* = argmin_n \frac{\Delta P}{\Delta k}$$

Recalculate power and modulation scheme for the n^*th subcarrier:

$$M_{n^*} = M_{n^*} + 1; \quad P_{n^*} = \frac{SNR^{M_{n^*}}\sigma_n^2}{g_{n^*}^2}$$

- **Step 5: Check Whether the Distributed Power Overflows:** if $\sum_{n=1}^{N} P_n \geq P_T$, exclude the infeasible Modulations:

$$\frac{\Delta P}{\Delta k}_{n^*} = NaN; \quad M_{n^*} = M_{n^*} - 1$$

$$P_{n^*} = \frac{SNR^{M_{n^*}}\sigma_n^2}{g_{n^*}^2}$$

go to step 3, else update the parameters:

$$P_L = \sum_{n=1}^{N} P_n$$

$$\frac{\Delta P}{\Delta k}_{n^*} = \frac{(SNR^{M_{n^*}+1} - SNR^{M_{n^*}})\sigma_n^2}{2g_{n^*}^2} \quad if \quad M_{n^*} \neq F$$

$$\frac{\Delta P}{\Delta k}_{n^*} = NaN \text{ if } M_{n^*} == F$$

go to step 3;

- **Step 6: End:** Calculate bits loaded for each subcarrier:

$$k_n = log2(2^{2\times M_n}) = 2 \times M_n$$

and stop.

After these six steps, bit and power for each subcarrier are stored in the two N length vectors $k_{1\times N}$ and $P_{1\times N}$, which will be used for the transmission.

Analysis and Simulation Number of sub-carriers is taken as $N = 512$, system bandwidth, $B = 5$MHz, target bit error rate (BER) is taken as 10^{-2}. Baseband modulation schemes such as QPSK, 16-QAM, 64-QAM are considered switchable options. Number of symbols per frame is 10.

Analysis in terms of Spectral Efficiency From the spectral efficiency curves for the three algorithms in Figure B.2 it is seen that the SAMPDA algorithm achieves the same spectral efficiency as the APDA algorithm, which is better than the SRA by more than 30% between 10db and 20dB and by more than 15% between 20 and 30dB.

Complexity Analysis in terms of number of Iterations For the SNR region less than 10 dB, the algorithm uses the least number of iterations as shown by Figure B.3. Between 10dB and 30 dB SNR, the algorithm uses significantly less number of iterations than the APDA algorithm but slightly higher number compared to the SRA. Beyond 40dB the SAMPDA algorithm the number of iterations for the algorithms is very close to that of SRA. It is interesting to observe that where as the SAMPDA needs increasing number of iterations with increasing SNR, that for the algorithm is almost independent of the SNR until 40 dB.

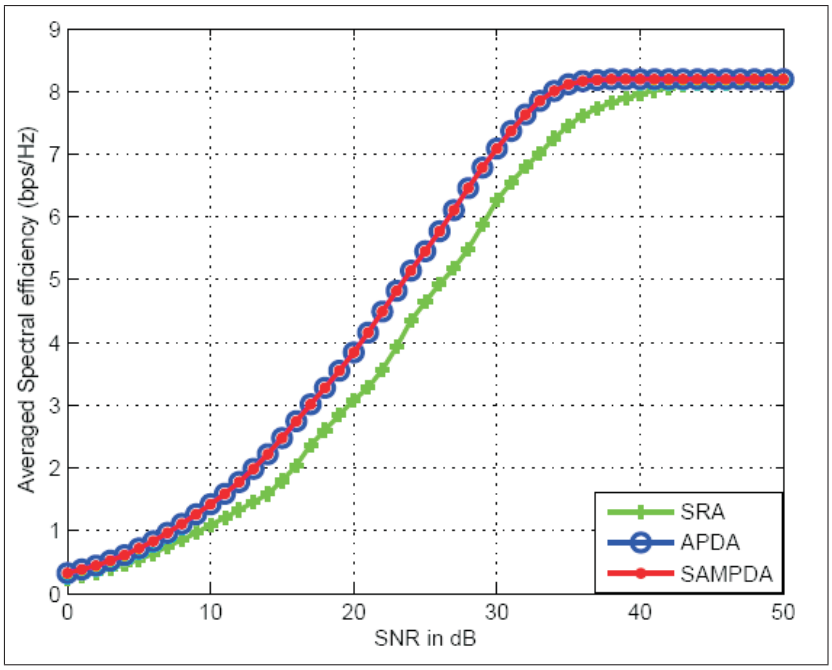

Figure B.2: Spectral efficiency achievement of the adaptation algorithms

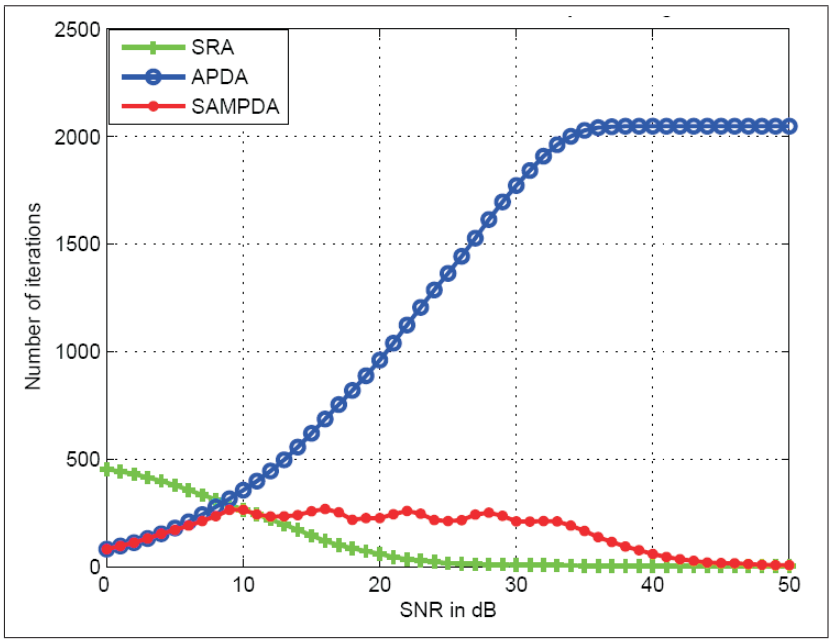

Figure B.3: Number of iterations required by different adaptation algorithms

C

Hybrid Link Adaptation

In this part the results for Hybrid Link Adaptation using WiMAX parameters are presented.

Bit and Power Loading Algorithms There can be some variation on the bit and power loading algorithm used for LA as discussed below. **Adaptive Power, Modulation and Coding (APMC):** APMC will adapt power, modulation and coding rate all together [115, 94]. It uses iterative procedure to distribute power, and find bit loads, whose details are in [95]. **AMCFP:** This case considers fixed power, i.e the iterations for bit and power loading are not used, which makes it very simple and fast.

AMC adapt P: In the AMCFP algorithm above, since power is fixed, one can expect some power to be wasted since signal to noise ratio (SNR) threshold required for the M& C rate selected for a block must be less than the available SNR. Therefore to save this power, the transmit power level can be adjusted so that the received SNR at the block is maintained just at the threshold required to maintain the target error rate.

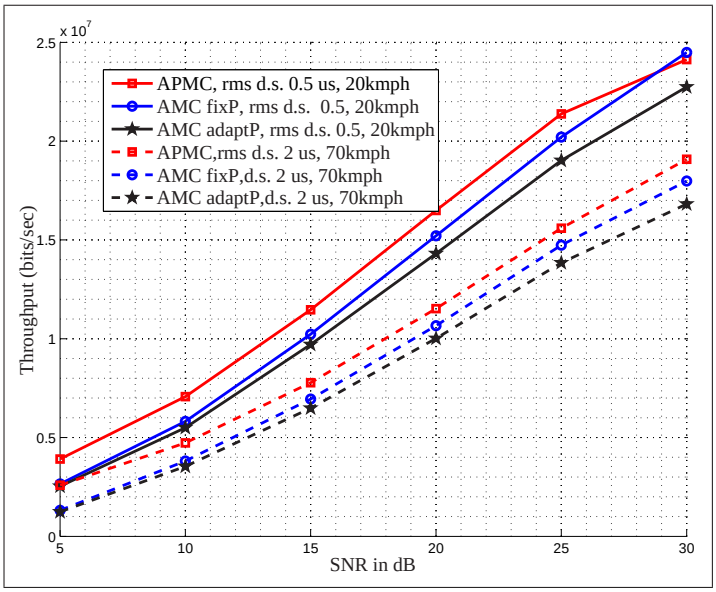

Figure C.1: Throughput comparison of different Link adaptation algorithms at 0.5 μs and 2.0 μs rms delay spread and Doppler condition for sub-band size of 8 sub carriers

Performance Comparison The throughput comparison of the three algorithms mentioned above is shown in Fig. C.1. The legend 'u' is used to represent 'micro seconds' which refers to the rms delay spread of the channel. In all cases the APMC has the best throughput. It is followed by AMCFP, while AMC adapt P has the worst performance. AMCFP has almost similar performance to APMC, when there is high diversity in the channel condition, i.e. large Doppler and rms delay spread, but it has notable performance loss in case of low Doppler and low rms delay spread condition. Therefore it can be suggested that for low Doppler and low rms delay spread condition, APMC be used, whereas when the diversity in the channel increases, it is better to use AMCFP. Finally it can be suggested to combine selection of bit and power loading algorithm at a very slow rate (based on statistical measure) along with fast (instantaneous) adaptation of modulation and coding rate.

Power Utilization Fig. C.2 shows the power utilization of the different algorithms. A low power utilization means low power transmission. This in turn means low interference condition in multi cellular scenario, where aggressive frequency re-use is followed. In such a scenario, the algorithm which has the lowest power utilization, may be the best one use. In this viewpoint the algorithm which brings down the transmit power to meet the threshold of the received SNR, but avoids iterative power distribution seems to have the best performance under all channel conditions. Considering the above results we will used fixed power in most of the analysis unless mentioned.

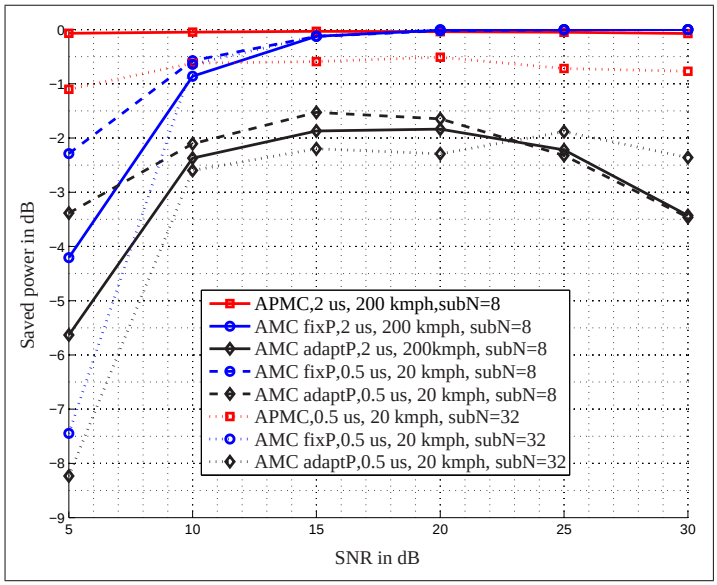

Figure C.2: Power utilization comparison of different Link adaptation algorithms at different rms delay spread and Doppler condition for sub-band size of 8 and 32 sub carriers

Sub band Size In this part the influence of rms delay spread and the Doppler velocity on different sub-band sizes (8,32,128 and 512 carriers) are investigated. Fig. C.3 shows the throughput for LA system when modulation (M) & coding rate (C) are adapted every 2ms while keeping P fixed. It can be seen from the figure that, when rms delay spread is small i.e. coherence bandwidth is large, and the velocity is also low, i.e. coherence time is large, then the sub-band size of 8 sub carriers has the highest throughput. It is followed by sub-band size of 32 which is followed by 512. Interestingly at high velocity and high rms delay spread i.e. small coherence bandwidth and small coherence time, the sub-band size of 8 sub carriers has very similar performance as that of sub-band with 128 sub carriers. Therefore it can be concluded that for very high velocity and high rms delay spread condition, it is better to use a large sub-band size since it will use significantly low overhead, whereas when velocity and rms delay spread are low, it is suggested to use small sub-band size. It must be noted that sub band size selection can be a statistical adaptation in combination with instantaneous adaption of modulation and coding rate.

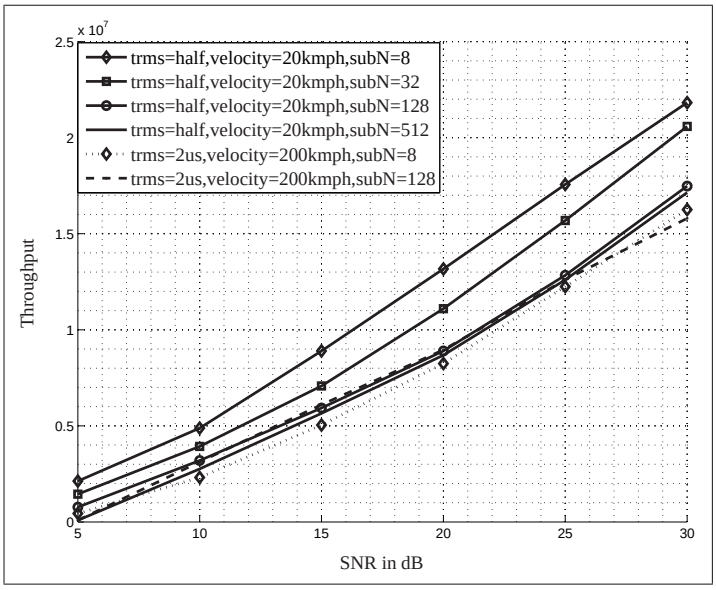

Figure C.3: Throughput performance of different sub-band sizes for different rms delay spread, Doppler velocity.

Fixed Coding rate In this part comparison of the scheme which adapts both modulation and coding every each frame, is made against the scheme which uses a single coding rate with adaptive modulation. Using multiple coding rates simultaneously for user means that the user equipment needs multiple FECs and decoders, which has prohibitive increase in implementation complexity of the transmitter and receiver. Therefore using only a single FEC coder (i.e only one FEC rate) for one user is highly desired. Then, selection of the FEC code rate becomes very important which is discussed in this section. Fig. C.4 shows the throughput comparison for sub-band with 8 sub carriers. In the figure 'RateAdapt' means adaptive modulation and coding simultaneously however as mentioned earlier, the power is kept constant. It can be seen that the performance of fixed coding rate is not far from the optimal adaptive modulation coding scheme. The channel statistics such as rms delay spread, Doppler velocity and average SNR are needed to choose the threshold for switching from one coding to another so that performance is close to being optimal. Similar behaviour has been found for different sub band size. In Table C.1 the average SNR values for switching from one coding rate to another is given. The mark '-' indicates that that coding rate is the default coding rate to start with, while the SNR values indicate the starting average SNR from where the particular coding rate can be used and 'NA' indicates the corresponding coding rate not be used. It can be concluded that if small sub-band size is used then all coding rates are important, but when large sub-band size is selected then coding rates '1/3' and '1/2' are enough.

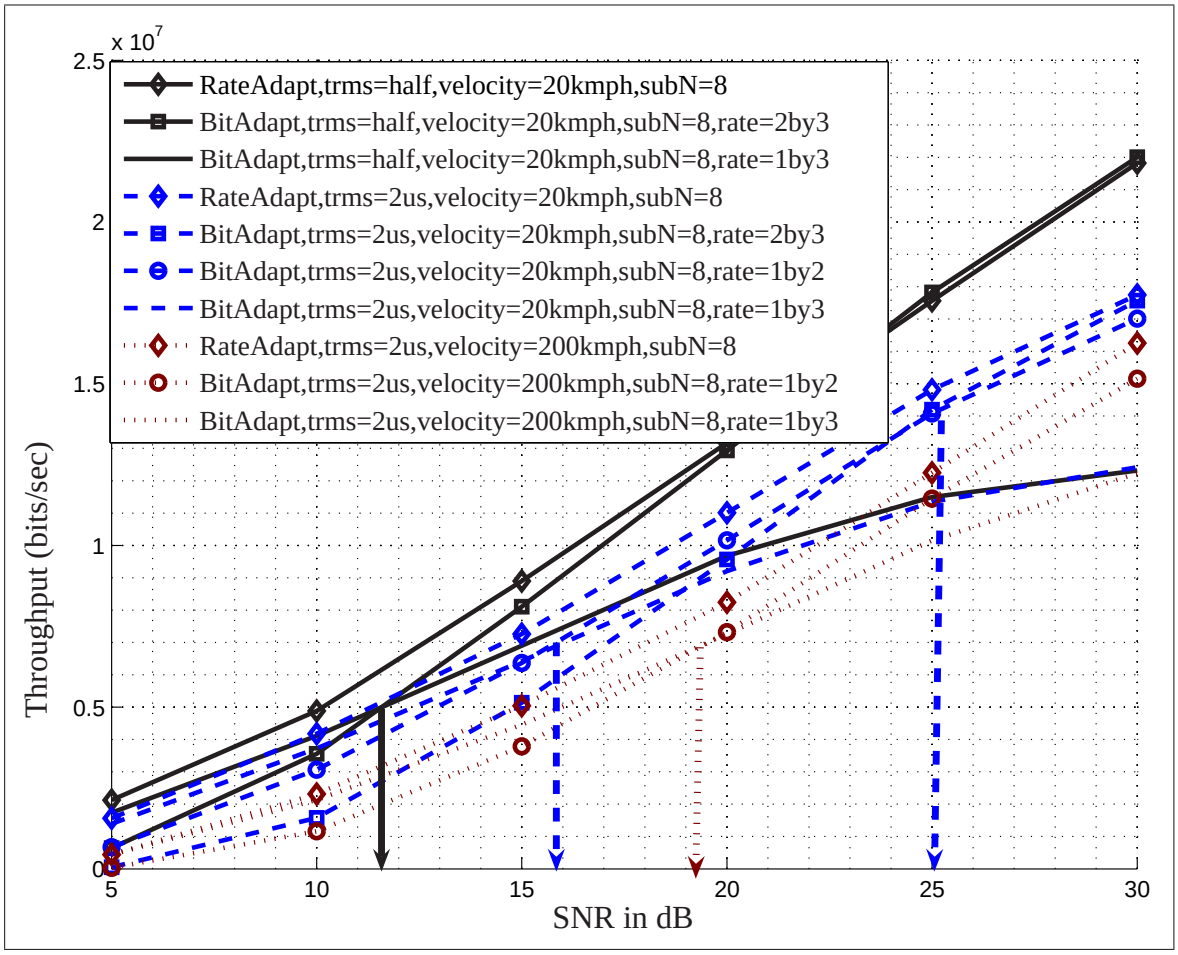

Figure C.4: Throughput performance comparison for fixed coding with adaptive modulation Vs adaptive modulation and coding for sub-band size of 8 sub carriers.

Table C.1: Average SNR thresholds (in dB) for switching coding rate for different rms delay spread and Doppler condition

	0.5μs, 20kmph			2μs, 20 kmph			2μs, 200 kmph		
subN$\downarrow$	Code rate								
	$\frac{1}{3}$	$\frac{1}{2}$	$\frac{2}{3}$	$\frac{1}{3}$	$\frac{1}{2}$	$\frac{2}{3}$	$\frac{1}{3}$	$\frac{1}{2}$	$\frac{2}{3}$
8	–	11.5	15.5	–	14.5	24	–	19.5	30
32	–	13.5	21.5	–	20.5	N.A.	–	20	N.A.
128	–	21.5	N.A.	–	21.5	N.A.	–	20	N.A.
512	–	23.5	N.A.	–	22	N.A.	–	22.5	N.A.

M & C Adaptation Rate Fig. C.5 shows the impact of different adaptation interval for rms delay spread of 0.5 μs and velocity 20 kmph. It can be seen that decrease in the adaptation rate has severe impact on the achievable spectral efficiency using adaptive modulation and coding when the size of sub band is up to 32 sub carriers. When the sub band size is larger, i.e. for subN=512 there is very little impact of decrease rate of adaptation. This happens because when a large sub band size is used, there is a large diversity gain and hence there will be little variation in the average channel gain and therefore even a large adaptation interval can be used easily.When sub band size is made large there is little impact on the adaptation time interval; i.e. short term adaptation in time domain is not necessary when the adaptation window is large in frequency domain even in low mobility conditions.

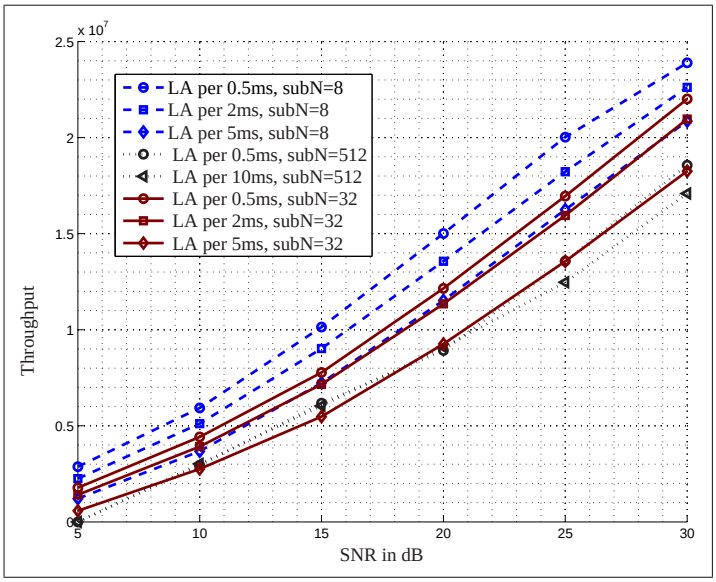

Figure C.5: Throughput comparison for different adaptation rates, for rms delay spread of 0.5μs at 20 kmph

D

LA in OFDM systems under HPA

PAPR in OFDM

OFDM symbol is generated by superimposing several carriers. These carriers may add up constructively which results in high amplitude and when it comes to power consideration, the problem is even worse. This problem is widely knows as Peak to Average Power Ratio (PAPR) problem. Large PAPR of a system makes the implementation of Digital to Analogue Converter (DAC) and Analogue to Digital Converter (ADC) to be extremely difficult. The design of RF amplifier also becomes increasingly difficult as the PAPR increases. Since the source of the problem is constructive addition of subcarrier, with the increase of subcarrier number in an OFDM symbol, PAPR will also increase. PAPR can be defined mathematically as:

$$\text{PAPR} = \frac{\max |\text{x(n)}|^2}{\overline{|\text{x(n)}|^2}} \tag{D.1}$$

Several methods have been proposed to reduce the nonlinear effect. Some technique directly deals with nonlinearity of the amplifier, such as pre-distortion, negative feedback, linear amplification with nonlinear component (LINC), feed forward etc. Other techniques reduce the PAPR of the OFDM signal so that operating point does

not fluctuate over a large range. There are several techniques to reduce PAPR. They are divided mainly in three category, namely *Signal Distortion Techniques*, *Coding Techniques* and finally the *Scrambling Technique*. A very good comparison of these methods can be found in [116].

CDF of PAPR

OFDM signal is generated using (2.19). There $X_s[k]$ when multiplied by the complex exponential forms a complex number, the real and imaginary parts are zero mean random numbers with uniform distribution. Due to the operation of the $\sum$ operator which adds a large number of such terms the output of the IFFT can be approximated to be Gaussian distributed, following the central limit theorum. As the output of the IFFT is a complex sequence, the amplitude of the OFDM signal can be considered Rayleigh distributed, while the power distribution is central chi squared distributed with two degrees of freedom. The cumulative distribution function of the power of the OFDM signal is therefore given by:

$$F(z) = \int_0^z \frac{1}{2 \cdot \sigma^2} \cdot e^{-\frac{u}{2 \cdot \sigma^2}} du = 1 - e^{-z} \tag{D.2}$$

where σ is the variance of the real or imaginary part. Assuming that the samples z to be mutually uncorrelated and the cumulative distribution function for the peak power per OFDM symbol is given by [117]:

$$P(PAPR \leq z) = F(z)^N = (1 - e^{-z})^N \tag{D.3}$$

where N is the number of subcarrier.

PAPR and Number of Subcarrier

The Figure D.1 shows the theoretical and simulated CDF of PAPR for different number of subcarrier. Theoretical curve is generated using the (D.3). It is seen that there is no difference between theoretical and simulation values except for the very low CDF. This because the probability of such situations are very low and it requires a very large number of simulations to get the exact curves. Here CDF for 128, 512 and 1024 subcarrier are shown and it shows that PAPR is proportional to the number of subcarrier.

The CDF of PAPR reaches 90 percentile value very quickly and rest of the values span over wide range of SNR.

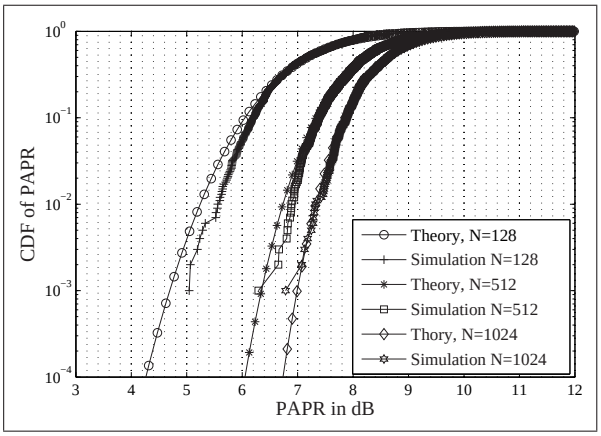

Figure D.1: Comparison of theoretical and simulated CDF of PAPR

Effect on Constellation points

Fig. D shows the performance for two different BO values, 3 dB and 6 dB. This can be compared with Fig. D.4 which shows the received constellation points for 16QAM modulation scheme when no power amplifier was used. It can be seen that the received constellation points become affected and scattered due to the effect of the nonlinear distortion of the HPA.

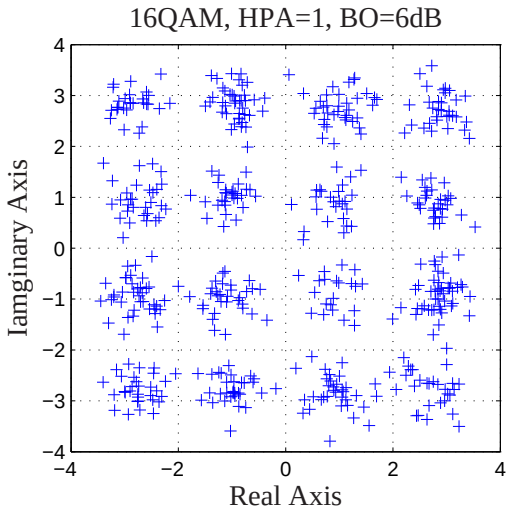

Figure D.2: Effect of BO of 6 dB on 16QAM constellation points

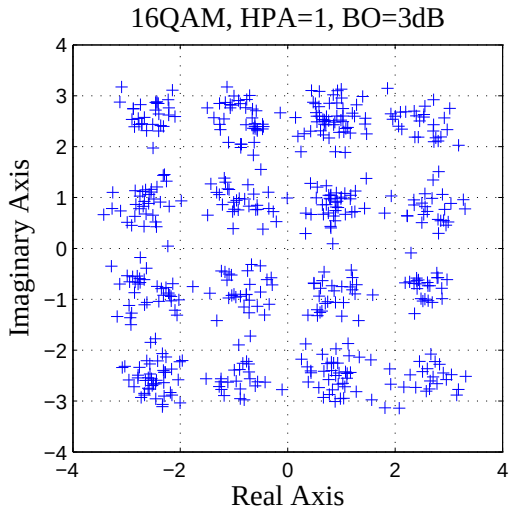

Figure D.3: Effect of BO on 16QAM constellation points

Effect Modulation and Coding Schemes on PAPR

The Fig. D.5 shows the effect of different modulation schemes for a rate $\frac{1}{2}$ coding rate when the IFFT size if 512. All curves overlap, which implies that PAPR for OFDM

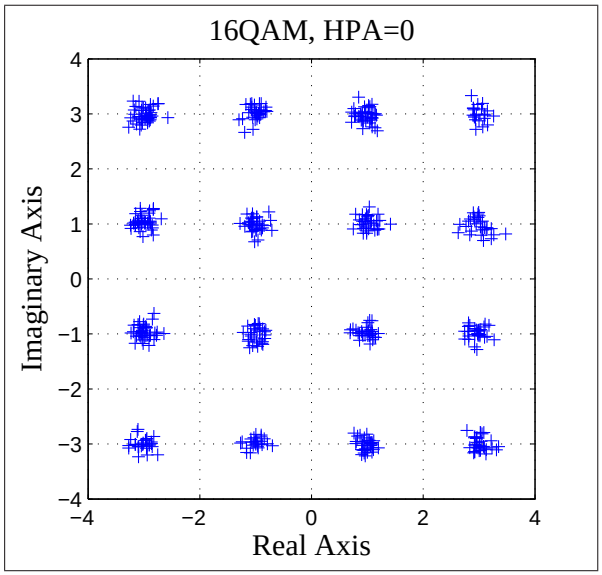

Figure D.4: 16QAM basic constellation points

is independent of modulation scheme.

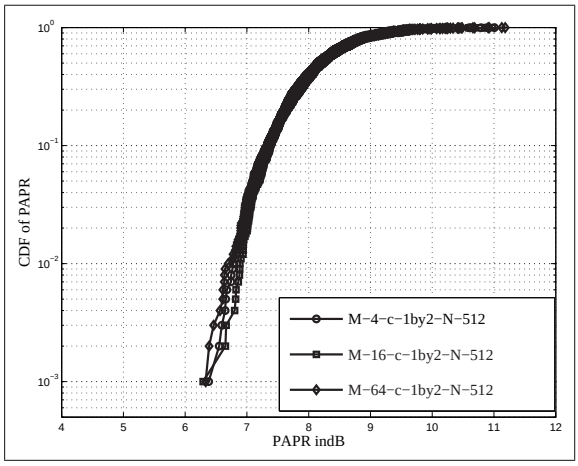

Figure D.5: Effect of different modulation scheme on CDF of PAPR when FFT size is 512. M indicates the modulation level, and C the coding rate.

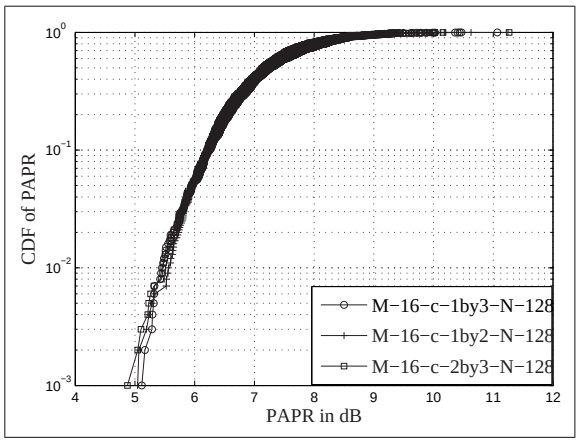

Figure D.6: Effect of different coding rate on the CDF of PAPR when FFT size is 128. M indicates the modulation level, and C the coding rate.

Fig. D.6 shows that PAPR is not affected by the coding rate. Here modulation and number of subcarrier were fixed to 16QAM and 128 respectively while coding rate was varied. And the result is same as mentioned above. i.e. there is no impact of coding rate on PAPR distribution. So, PAPR is an inherent property of the subcarrier of the symbol itself which is not influenced by the parameters like modulation, FEC coding etc.

SDNR Plots

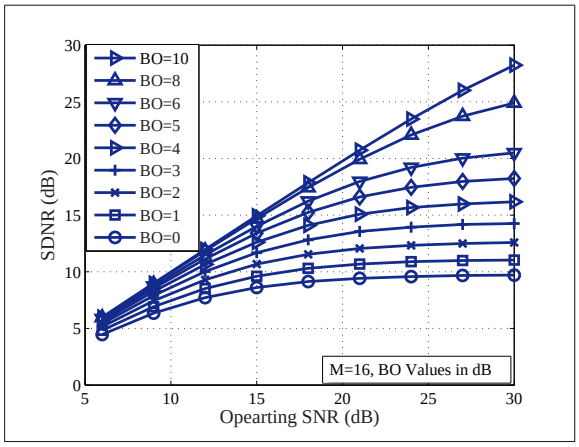

Figure D.7: SDNR plot for 16QAM modulation in AWGN Channel

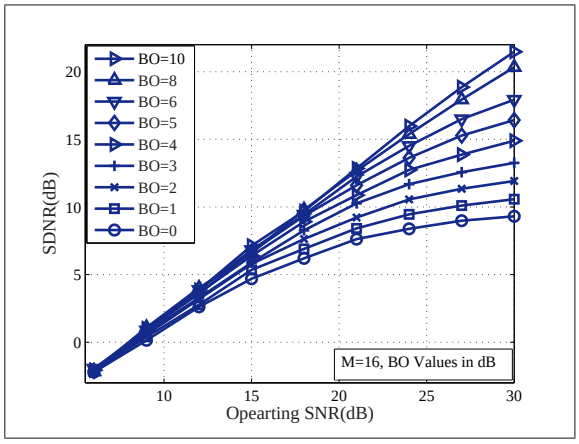

Figure D.8: SDNR plot for 16QAM modulation in Fading Channel

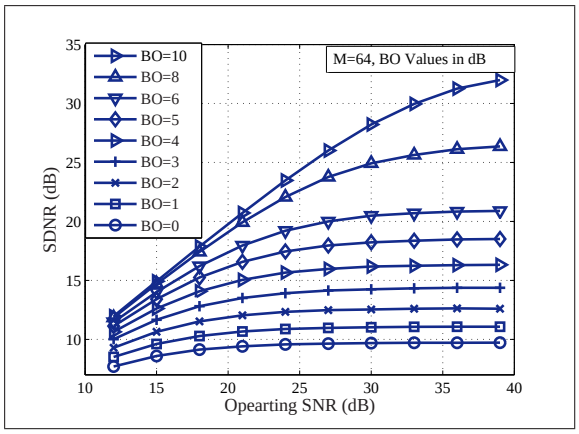

Figure D.9: SDNR plot for 64QAM modulation in AWGN Channel

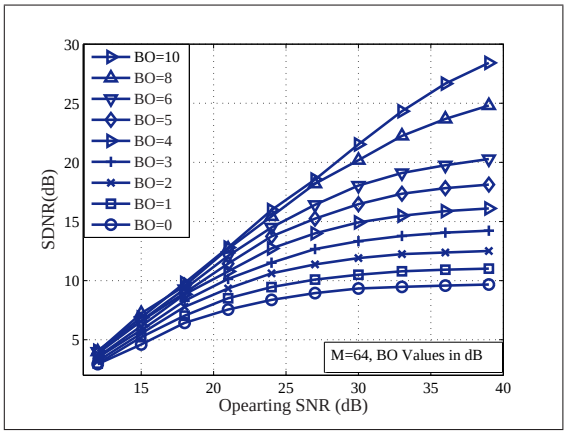

Figure D.10: SDNR plot for 64QAM modulation in Fading Channel

Performance of Different Modulation and Coding

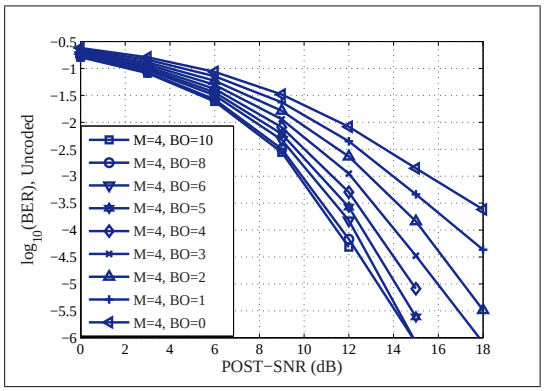

Figure D.11: BER vs SNR curve for uncoded and M=4 in AWGN channel

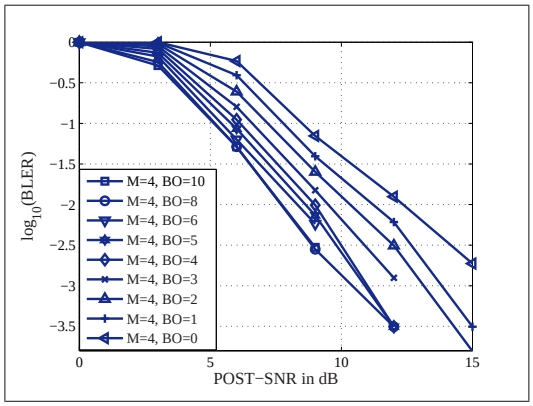

Figure D.12: BLER vs SNR curve for $C = \frac{1}{2}$ and M=4 in AWGN channel

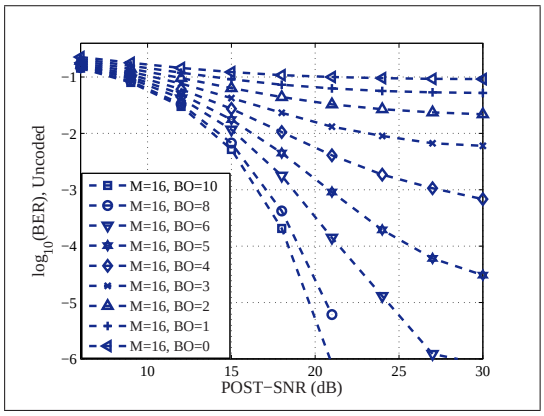

Figure D.13: BER vs SNR curve for uncoded and M=16 in AWGN channel

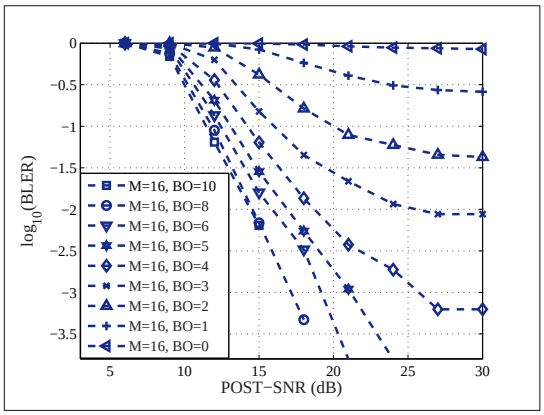

Figure D.14: BLER vs SNR curve for $C = \frac{1}{2}$ and M=16 in AWGN channel

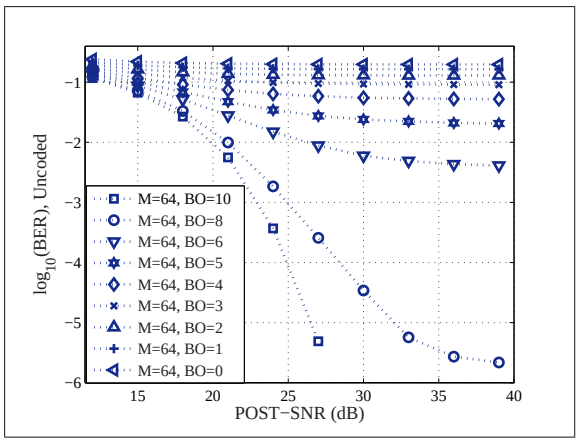

Figure D.15: BER vs SNR curve for uncoded and M=64 in AWGN channel

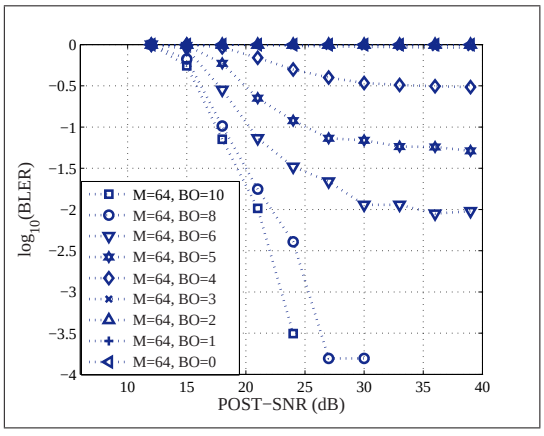

Figure D.16: BLER vs SNR curve for $C = \frac{1}{2}$ and M=64 in AWGN channel

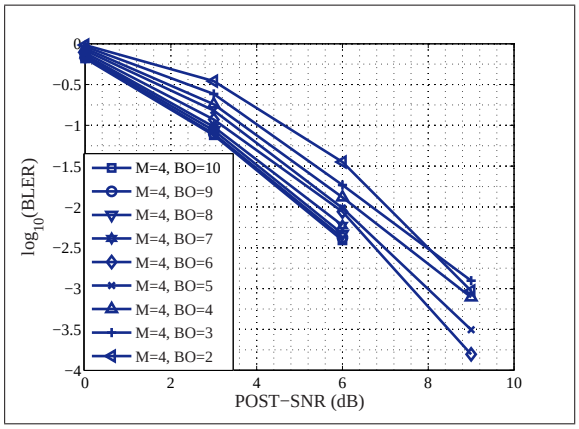

Figure D.17: BLER vs SNR curve for $C = \frac{1}{3}$ and M=4 in AWGN channel

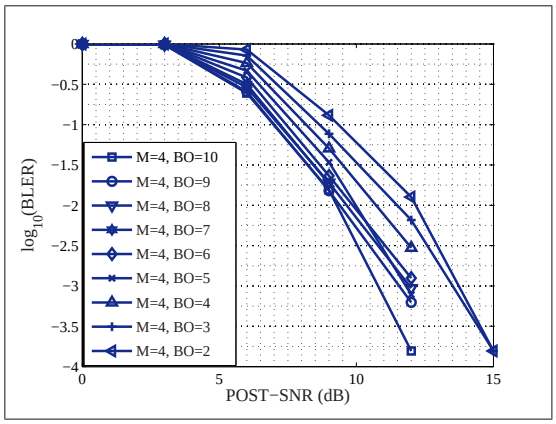

Figure D.18: BLER vs SNR curve for $C = \frac{2}{3}$ and M=4 in AWGN channel

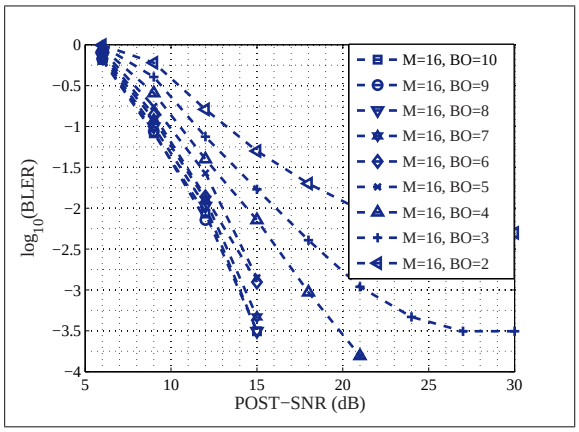

Figure D.19: BLER vs SNR curve for $C = \frac{1}{3}$ and M=16 in AWGN channel

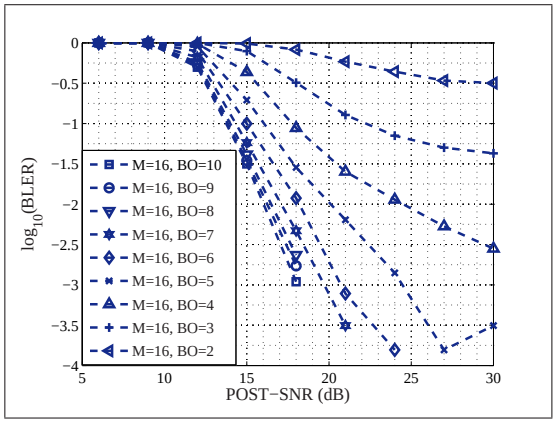

Figure D.20: BLER vs SNR curve for $C = \frac{2}{3}$ and M=16 in AWGN channel

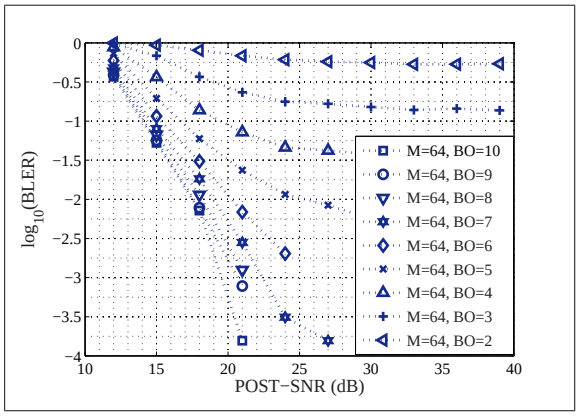

Figure D.21: BLER vs SNR curve for $C = \frac{1}{3}$ and M=64 in AWGN channel

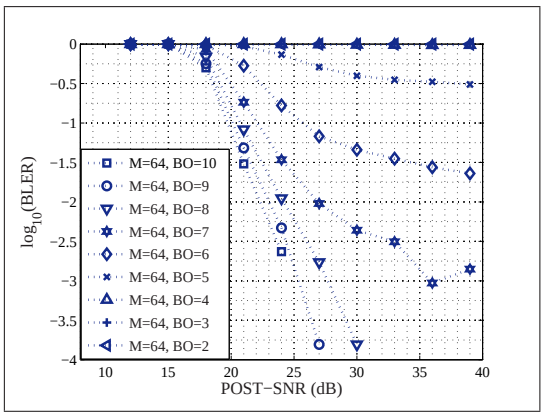

Figure D.22: BLER vs SNR curve for $C = \frac{2}{3}$ and M=64 in AWGN channel

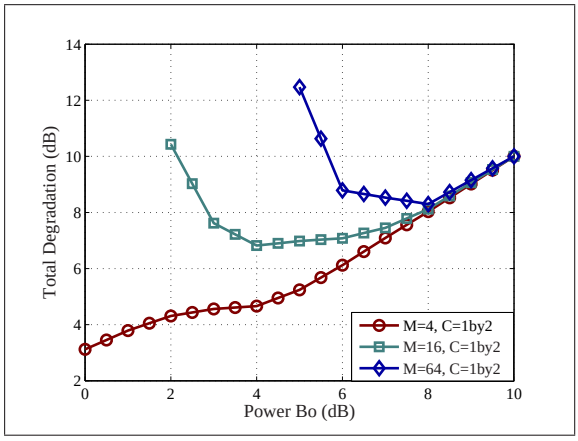

Figure D.23: TD plot for $FEC = \frac{1}{2}$ with BLER Threshold= 0.1 in AWGN

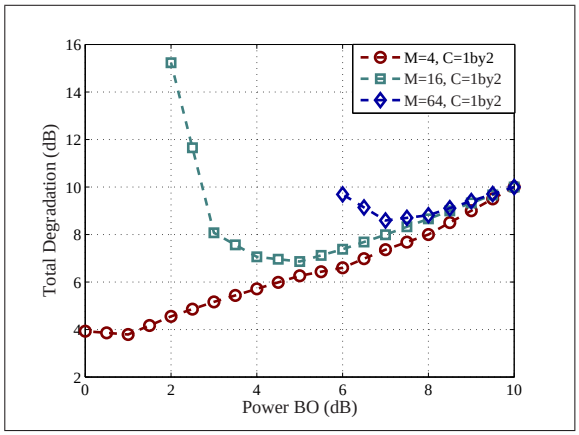

Figure D.24: TD plot for $FEC = \frac{1}{2}$ with BLER Threshold= 0.05 in AWGN

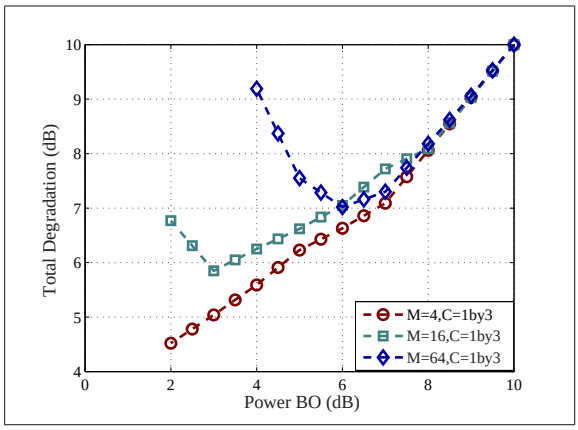

Figure D.25: TD plot for $FEC = \frac{1}{3}$ with BLER Threshold= 0.1 in AWGN

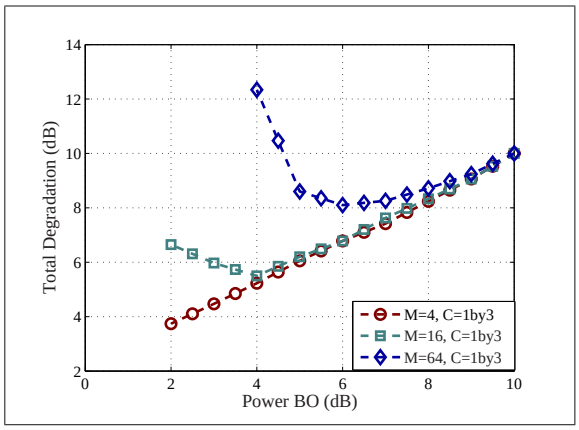

Figure D.26: TD plot for $FEC = \frac{1}{3}$ with BLER Threshold= 0.05 in AWGN

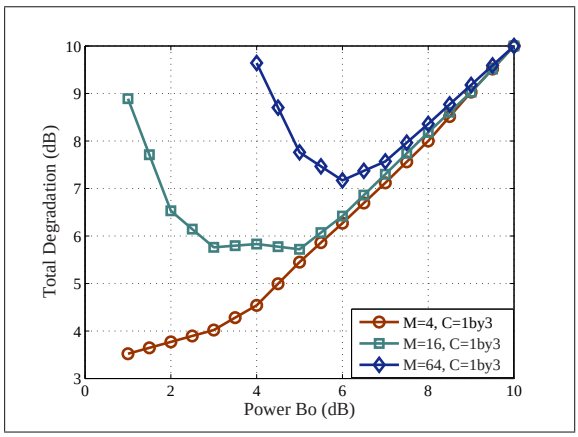

Figure D.27: TD plot for $FEC = \frac{1}{3}$ with BLER Threshold= 0.1 in Fading Channel

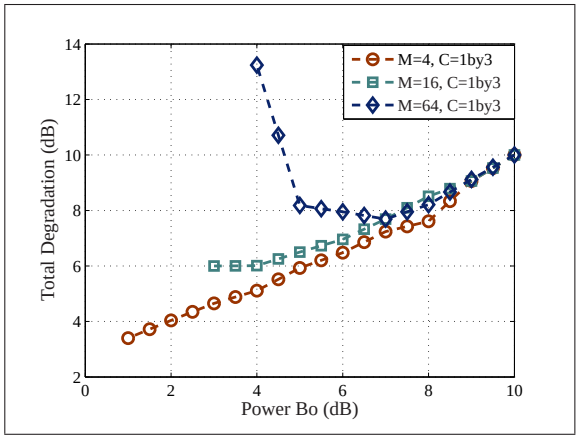

Figure D.28: TD plot for $FEC = \frac{1}{3}$ with BLER Threshold= 0.05 in Fading Channel

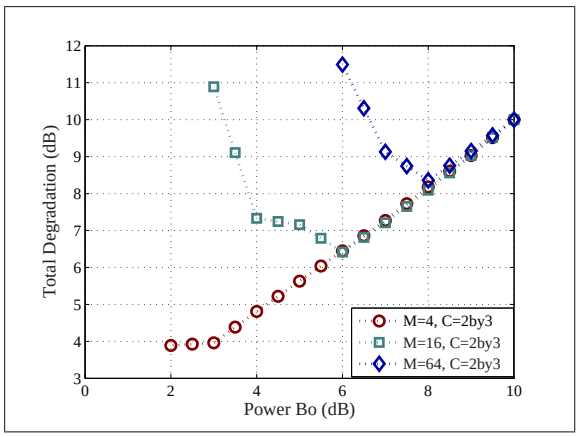

Figure D.29: TD plot for $FEC = \frac{2}{3}$ with BLER Threshold= 0.1 in AWGN

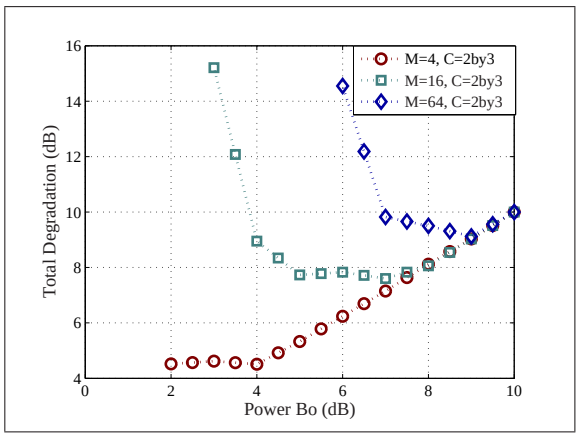

Figure D.30: TD plot for $FEC = \frac{2}{3}$ with BLER Threshold= 0.05 in AWGN

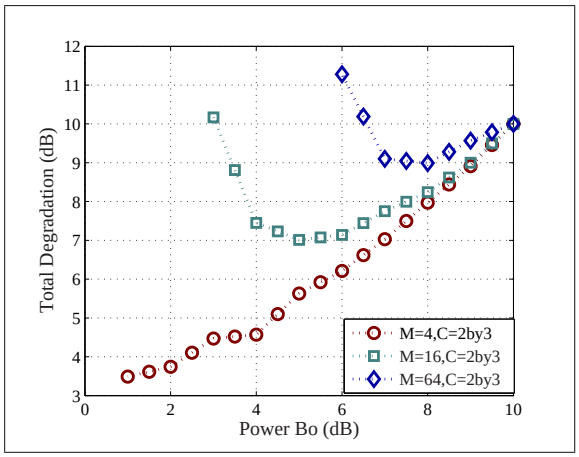

Figure D.31: TD plot for $FEC = \frac{2}{3}$ with BLER Threshold= 0.1 in Fading Channel

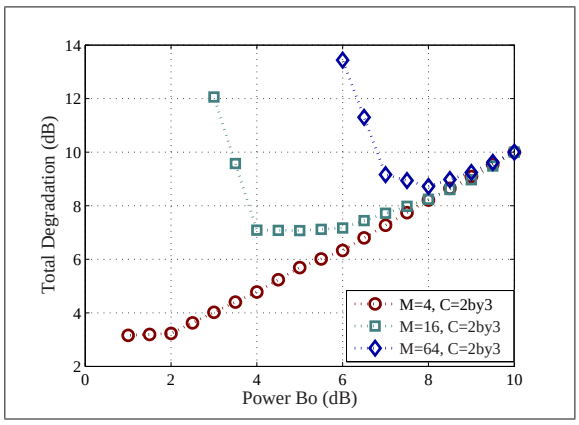

Figure D.32: TD plot for $FEC = \frac{2}{3}$ with BLER Threshold= 0.05 in Fading Channel

List of Abbreviations

ABL	Adaptive Bit Loading
ACI	Adjacent Channel Interference
ADC	Analogue to Digital Converter
ADSL	Asynchronous Digital Subscriber Line
APMC	Adaptive Power, Modulation and Coding
APMfixC	Adaptive Power and Modulation with Fixed Coding rate
AMCfixP	Adaptive Modulation and Coding with fixed Power
AP	Access Point
ASB	Adaptive Sub Carrier Bandwidth
ASc	Antenna Selection
AWGN	Additive White Gaussian Noise
BDM	Band Division Multiplexing
BER	Bit Error Rate
BLER	Block Error Rate
BO	Back of
BS	Base Station
CDF	Cumulative Distribution Function
CDMA	Code Division Multiple Access

CP	Cyclic Prefix
CSI	Channel State Information
CQI	Channel Quality Index
DAB	Digital Audio Broadcasting
DAC	Digital to Analogue Converter
DFT	Discrete Fourier Transform
DL	Downlink
DVB	Digital Video Broadcasting
EGC	Equal Gain Combining
FDM	Frequency Division Multiplexing
FDD	Frequency Division Duplex
FEC	Forward Error Correction
FER	Frame Error Rate
FFT	Fast Fourier Transform
FSB	Fixed Sub Carrier Bandwidth
HARQ	Hybrid Automatic Repeat-reQuest
HDSL	High bit-rate Digital Subcarrier Lines
HPA	High Power Amplifier
GI	Guard Interval
ICI	Inter Carrier Interference
IFFT	Inverse Fast Fourier Transform
IO	Interfering Objects
ISI	Inter Symbol Interference
LA	Link Adaptation

LUT Look Up Table

MC-SS Multi Carrier Spread Spectrum

MC-SS-MA Multi Carrier Spread Spectrum Multiple Access

MIMO Multiple Input Multiple Output

MISO Multiple Input Single Output

MMSE Minimum Mean Square Error

MRC Maximal Ratio Combining

OFDM Orthogonal Frequency Division Multiplexing

OFDM-BDM Orthogonal Frequency Division Multiplexing - Band Division Multiplexing

OFDMA-CDM Orthogonal Frequency Division Multiple Acess with Code Division Multiplexing

OFDM-TDM Orthogonal Frequency Division Multiplexing - Time Division Multiplexing

OFDM-TDMA Orthogonal Frequency Division Multiplexing - Time Division Multiple Access

OFDMA Orthogonal Frequency Division Multiple Access

OFDMA-TDMA Orthogonal Frequency Division Multiple Access - Time Division Multiple Access

PAM Pulse Amplitude Modulation

PAPR Peak to Average Power Ratio

PC Power Control

PCs Personal Computers

PER Packet Error Rate

PSK Phase Shift Keying

QAM Quadrature Amplitude Modulation

QoS Quality of Service

QPSK Quadrature Phase Shift Keying

RF Radio Frequency

RMS Root Mean Square

SCH Subcarrier hopping

SCH-OFDMA-CDM Sub-Carrier Hopped Orthogonal Frequency Division Multiple Access with Code Division Multiplexing

SCH-MC-SS Sub-Carrier Hopped Multi Carrier Spread Spectrum

SDNR Signal to Distortion plus Noise Ratio

SE Spectral Efficiency

SIC Successive Interference Cancelation

SIMO Single Input Multiple Output

SINR Signal to Interference plus Noise Ratio

SISO Single Input Single Output

SNR Signal to Noise Ratio

SSPA Solid State Power Amplifier

TDD Time Division Duplex

TDEG Total Degradation

TDM Time Division Multiplexing

TS Training Sequence

TWTA Traveling Wave Tube Amplifier

UE User Equipment

UL Uplink

VDSL	Very High speed Digital Subscriber Line
VGI	Variable Guard Interval
VSB	Variable Sub Carrier Bandwidth
WiMAX	Worldwide Interoperability for Microwave Access
WLAN	Wireless Local Area Network
WMAN	Wireless Metropolitan Area Network
WPAN	Wireless Personal Area Network

Bibliography

[1] Prasad R., *OFDM for Wireless Communications.* Artech House Publishers, 2004.

[2] "Technical specification group radio access network; physical layer aspects for evolved universal terrestrial radio access (utra): Release 7," 3rd Generation Partnership Project, Draft Standard 3GPP TR 25.814 V7.1.0, 2006-09.

[3] Nee R. V. & Prasad R., *OFDM for Wireless Multimedia Communications.* Artech House Publishers, 2000.

[4] Hanzo L., Mūnster M., Choi B.J., Keller T., *OFDM and MC-CDMA for Boradband Multi-User Communications, WLANs, and Broadcasting.* Wiley, 2003.

[5] Kuipers B. W. M., "MULTICARRIER - ORTHOGONAL FREQUENCY DIVISION MULTIPLE ACCESS," Ph.D. dissertation, Aalborg University, 2006.

[6] Weinstein S.B., Ebert P.M., "Data Transmission by Frequency Division Multiplexing Using the Discrete Fourier Transform," *IEEE Transactions on Communications*, vol. 19, no. 5, Oct. 1971.

[7] Chow P.S. , Tu J.C., Cioffi J. M., "A Discrete Multitone Transceiver System for HDSL Applications," *IEEE Journal on Selected Areas in Communications*, vol. 9, no. 6, Sep. 1991.

[8] Chow P.S., Tu J.C. and Cioffi J.M., "Performance Evaluation of a Multichannel Transceiver System for ADSL and VHDSL services," *IEEE Journal on Selected Areas in Communications*, vol. 9, no. 6, Aug. 1991.

[9] ETSI, "Radio broadcasting systems; Digital Audio Broadcasting (DAB) to mobile, portable and fixed receivers," European Telecommunication Standard, Standard EN-300-401, May 1997.

[10] Hiperlan2, "Broadband Radio Access Networks (BRAN),HIPERLAN Type 2;Physical (PHY) layer," ETSI, Tech. Rep., 1999.

[11] "Part 11: Wireless lan medium access control (mac) and physical layer (phy) specifications amendment 4: Further higher data rate extension in the 2.4 ghz band," IEEE, Standard IEEE Std 802.11g.-2003, June 2003.

[12] ETSI, "Digital Video Broadcasting (DVB);Framing structure, channel coding and modulation for digital terrestrial television," European Telecommunication Standard, Standard EN-300-744, 2004-2006.

[13] ——, "Digital Video Broadcasting (DVB); Transmission System for Handheld Terminals (DVB-H)," European Telecommunication Standard, Standard EN-302-304, 2004.

[14] "Part 16: Air Interface for Fixed Broadband Wireless Access SystemsAmendment 2: Medium Access Control Modifications and Additional Physical Layer Specifications for 2-11 GHz," IEEE, Standard IEEE Std 802.16a-2003, 2003.

[15] "Part 16: Air interface for fixed broadband wireless access systems. amendment for physical and medium access control layers for combined fixed and mobile operation in licensed bands," IEEE, Standard IEEE Std 802.16e/D12,October 2005, 2005.

[16] Cherry, S, "Edholm's law of bandwidth," *IEEE Spectrum*, vol. 41, no. 7, pp. 58–60, July 2004.

[17] Kaiser S., Fazel K., "A flexible spread-spectrum multi-carrier multiple-access system for multi-media applications," in *The 8th IEEE International Symposium on Personal, Indoor and Mobile Radio Communications*, vol. 1, Sep. 1997, pp. 100–104.

[18] Narasimhan, R., "Performance of diversity schemes for OFDM systems with frequency offset, phase noise, and channel estimation errors," *IEEE Transactions on Communications*, vol. 50, no. 10, pp. 1561–1565, Oct. 2002.

[19] Zhao Y., Haggman, S. G., "Intercarrier interference self-cancellation scheme for OFDM mobile communication systems," *IEEE Transactions on Communications*, vol. 49, no. 7, pp. 1185 – 1191, July 2001.

[20] Stuber G.L., *Principles of mobile communication.* Kluwer Academic, 2001.

[21] Hou W, Chen B., "ICI cancellation for OFDM communication systems in time-varying multipath fading channels," *IEEE Transactions on Communications*, vol. 4, no. 5, Sep. 2005.

[22] Tomasin S, et al., "Iterative interference cancellation and channel estimation for mobile OFDM," *IEEE Transactions on Wireless Communications*, vol. 4, no. 1, pp. 238 – 245, 2005.

[23] Moose P.H., "A Technique for Orthogonal Frequency Division Multiplexing Frequency Offset Correction," *IEEE Transactions on Communications*, vol. 42, no. 10, pp. 2908–2914, Oct. 1994.

[24] Fletcher, P.N., "Iterative decoding for reducing cyclic prefix requirement in OFDM modulation," *IEE Electronic Letters*, vol. 39, no. 6, pp. 539–541, Mar 2003.

[25] Chen S.; Zhu C., "ICI and ISI analysis and mitigation for OFDM systems with insufficient cyclic prefix in time-varying channels," vol. 50, no. 1, pp. 78–83, Feb. 2004.

[26] Chung S. T., Goldsmith A. J., "Degrees of freedom in adaptive modulation: a unified view," *IEEE Transactions on Communications*, vol. 49, no. 1, pp. 1561–1571, Sep. 2001.

[27] Ahn, C.-J.; Sasase, I, "The effects of modulation combination, target BER, Doppler frequency, and adaptation interval on the performance of adaptive OFDM in broadband mobile channel," *IEEE Transactions on Consumer Electronics*, vol. 48, no. 1, pp. 167 – 174, 2002.

[28] Goldsmith A. J. and Greenstein L., "Effect of average power estimation error on adaptiveMQAM modulation," in *IEEE ICC, June 1997, pp. 11051109.*

[29] Medbo J., Andersson H., Schramm P., Asplund H., Berg J.-E. , "Channel models for HIPERLAN/2 in different indoor scenarios. COST–259," EURO-COST," Report, 1998.

[30] Erceg V., et al., "An Empirically Based Path Loss Model for Wireless Channels in Suburban Environments," *IEEE Journal on Selected Areas in Communications*, vol. 17, no. 7, pp. 1205 – 1211, July 1999.

[31] ——, "A Model for the Multipath Delay Profile of Fixed Wireless Channels," *IEEE Journal on Selected Areas in Communications*, vol. 17, no. 3, pp. 399–410, March 1999.

[32] ——, "Channel model for fixed wireless application," IEEE 802.16 working group, Tech. Rep., 2001.

[33] Emerson D.T., "THE WORK OF JAGADIS CHANDRA BOSE: 100 YEARS OF MM-WAVE RESEARCH," in *International Microwave Symposium Digest, 1997., IEEE MTT-S*, vol. 2. IEEE,, June 1997, pp. 553–556.

[34] Rappaport T. S., *Wireless Communications Principles and Practice*. Prentice Hall Inc., 1996.

[35] Proakis J.G., *Digital Communications*, 3rd ed. Mc Graw Hill, 1995.

[36] A. F. Molisch, *Wireless Communications*, 1st ed. John Wiley & Sons, 2005.

[37] Lawton, M.C.; Davies, R.L.; McGeehan, J.P., "An analytical model for indoor multipath propagation in the picocellular environment," in *Sixth International Conference on Mobile Radio and Personal Communications*, Dec. 1991, pp. 1–8.

[38] Witrisal K., "OFDM Air Interface Design for Multimedia Communications," Ph.D. dissertation, Delft University of Technology, The Netherlands, April 2002.

[39] Paetzold M., *Mobile Fading Channels: Modelling, Analysis, & Simulation, 1st Edition*. John Wiley & Sons, 2002.

[40] Greenstein L.J., et. al., "A New Path-Gain/Delay-Spread Propagation Model for Digital Cellular Channels," *IEEE Transactions on Vehicular Technology*, vol. 46, no. 2, pp. 477–485, May 1997.

[41] Cox D., Leck R., "Correlation Bandwidth and Delay Spread Multipath Propagation Statistics for 910-MHz Urban Mobile Radio Channels," *IEEE Transactions on Communications*, vol. 23, no. 11, pp. 1271–1280, 1975.

[42] Das S.S., Prasad R.,, "Time Correlation function for RMS delay spread of a channel model," in *IST Mobile Summit*, June 2006.

[43] X. Fuqin, *Digital Modulation Techniques*. Artech House Publishers, 2000.

[44] Standard

[45] Speth M., Fechtel S.A., Fock G., Meyr H., "Optimum Receiver Design for Wireless Broad-Band Systems Using OFDMPart I," *IEEE Transactions on Communications*, vol. 47, no. 11, pp. 1668 – 1677, Nov. 1999.

[46] Das S. S., et al., "Multi Rate Orthogonal Frequency Division Multiplexing," in *IEEE ICC 2005* , vol. 4, May 2005, pp. 2588 – 2592.

[47] N. Yee, J.P. Linnarz, G. Fettweis, "Multi-Carrier CDMA in indoor wireless radio networks," in *IEEE PIMRC '93*, Sep. 1993.

[48] A. Chouly, et al., "Orthogonal multicarrier technique applied to direct sequence spread spectrum CDMA systems," in *IEEE Telecommunication conference (GLOBECOM'93)*, Nov.-Dec. 1993.

[49] Fazel K., "Performance of CDMA/OFDM for mobile communication system," in *IEEE international conference on Universal Personal Communications (ICUPC'93)*, Oct. 1993, pp. 975–979.

[50] QingXin C., Elvano S. S., Pasupathy S., "Multicarrier CDMA with Adaptive Frequency Hopping for Mobile Radio Systems," *IEEE Journal on Selected Areas in Communications*, vol. 14, no. 9, Dec. 1996.

[51] Yang L-L, Hanzo L.,, "Performance of Generalized Multicarrier DS-CDMA Over Nakagami-m Fading Channels," *IEEE Transactions on Communications*, vol. 50, no. 6, pp. 956–966, June 2002.

[52] Pongsuwanich N., "PAPR issues in Link Adaptation for WiMAX like OFDM Systems," Masters Thesis, Aalborg University, Sep. 2006.

[53] Heiskala J.& Terry J., *OFDM Wireless LANs: A Theoritical and Practical Guide*, 2nd ed. Sams Publishing, July 2001.

[54] Prasad R., Hara S., "An Overview of Multi-Carrier CDMA," in *4th IEEE International Symposium on Spread Spectrum Tehcniques and Applications, ISSSTA96*, Sep. 1996,, p. 107114.

[55] Paulraj A., et al., *Introduction to Space Time Wireless Communiactions*. CAMBRIDGE, 2003.

[56] Steendam H., Moeneclaey M., "The Effect of Carrier Phase Jitter on MC-CDMA Performance," *IEEE Transactions on Communications*, vol. 47, no. 2, pp. 195–198, Feb. 1999.

[57] Legouable R, et al., "Performance Comparison between OFDM/TDMA vs MC-CDMA and DS-CDMA vs Techniques in HIPERLAN/2," in *IST Mobile and Wireless Telecommunications Summit, Aveiro, Portugal, 15-18th June 2003*, Aveiro, Portu, June 2003.

[58] Hanzo, L.; Lie-Liang Yang; Manster, M.; Byoung-Jo Choi;, "Recital on multicarrier communications: space-time coded versus adaptive OFDM/MC-CDMA," in *IST Workshop on Mobile Future, 2004 and the Symposium on Trends in Communications.*, 24-26 Oct. 2004, pp. x – xxviii.

[59] Tsumura S., Mino R., Hara S., Hara Y., "Performance comparison of OFDM-FH and MC-CDM in single- and multi-cell environments," in *61st IEEE Vehicular Technology Conference, VTC Spring*, vol. 3, June 2005, pp. 1730–1734.

[60] M. Tanda, "Blind symbol-timing and frequency-offset estimation in OFDM systems with real data symbols," *IEEE Transactions on Communications*, vol. 52, no. 10, pp. 1609–1612, Oct. 2004.

[61] Ma X. , Giannakis G.B: , Barbarossa S., "Non-data-aided frequency-offset and channel estimation in OFDM and related block transmissions," in *IEEE ICC* , 2001, pp. 1866–1870.

[62] M. Speth, et al., "Optimum Receiver Design for Wireless Broad-Band Systems Using OFDM - Part II: A case study," *IEEE Transactions on Communications*, vol. 49, no. 4, April 2001.

[63] Yang B., Letaief K.B., Cheng R.S. & Cao Z. ,, "Timing Recovery for OFDM Transmission," *IEEE Journal on Selected Areas in Communications*, vol. 18, no. 11, Nov. 2000.

[64] Yang B., Ma Z., Cao Z., "ML-oriented DA sampling clock synchronization for OFDM systems," *WCC - ICCT 2000*, vol. 1, pp. 781 – 784, Aug. 2000.

[65] Abhayawardhana,V.S., Wassell, I.J.,, "Residual frequency offset correction for coherently modulated OFDM systems in wireless communication," in *IEEE Vehicular Technology Conference Spring*, vol. 2, 2002, pp. 777–781.

[66] Miaoudakis,et al., "An all-digital feed-forward CFO cancellation scheme for HIPERLAN/2 in multipath environment," in *The 13th IEEE International Symposium on Personal, Indoor and Mobile Radio Communications, 2002*, 4, Ed., Sep. 2002, pp. 15–18.

[67] Das S. S., et al., "Low Complexity Residual Phase Tracking Algorithm for OFDM-based WLAN Systems," in *Proceedings of CSNDSP 2004*, July 2004.

[68] Pollet T., Bladel V. M., Moeneclaey M., "BER sensitivity of OFDM systems to carrier frequency offset and Wiener phase noise," *IEEE Transactions on Communications*, vol. 43, no. 234, pp. 191 – 193, Feb.-March-April 1995.

[69] Robertson P., Kaiser S.,, "The effects of Doppler spreads in OFDM(A) mobile radio systems," in *IEEE VTC 50th Vehicular Technology Conference*, vol. 1, Sep. 1999, pp. 19–22.

[70] Wang T., et al., "Performance Degradation of OFDM Systems Due to Doppler Spreading," *IEEE Transactions on Wireless Communications*, vol. 5, no. 6, pp. 1422–1432, June 2006.

[71] Steendam H., Moeneclaey M., "Analysis and Optimization of the Performance of OFDM on Frequency-Selective Time-Selective Fading Channels," *IEEE Transactions on Communications*, vol. 47, no. 12, pp. 1811–1819, Dec. 1999.

[72] Hung C. P., Chen S. G., Chen K. L.,, "Design of an efficient variable-length FFT processor," in *ISCAS*, vol. 2, May 2004, pp. 833–836.

[73] Cai J., Song W., Li Z., "Doppler spread estimation for mobile OFDM systems in Rayleigh fading channels," *IEEE Transactions on Consumer Electronics*, vol. 49, no. 4, pp. 973–977, Nov. 2003.

[74] Zhao Y., Haggman S. -G., "Sensitivity to Doppler shift and carrier frequency errors in OFDM systems-the consequences and solutions," in *IEEE VTC 1996*, vol. 3, pp. 1564 – 1568.

[75] Muquet B., et al., "Cyclic prefixing or zero padding for wireless multicarrier transmissions?" *IEEE Transactions on Communications*, vol. 50, no. 12, Dec. 2002.

[76] Manton J. H., "Dissecting OFDM: The Independent Roles of the Cyclic Prefix and the IDFT Operation," *IEEE Communications Letters*, vol. 5, no. 12, pp. 474–476, Dec. 2001.

[77] Rappaport, T.S., Seidel, S.Y., Takamizawa K.,, "Statistical channel impulse response models for factory and open plan building radio communicate system

design," *IEEE Transactions on Communications*, vol. 39, no. 5, pp. 794 – 807, May 1991.

[78] Mohr, W., "Radio propagation for local loop applications at 2 GHz," in *Third Annual International Universal Personal Communications*, Oct. 1994, pp. 119–123.

[79] Beek V. D., et al., "ML estimation of time and frequency offset in OFDM systems," *IEEE Transactions on Signal Processing*, vol. 45, no. 7, pp. 1800–1805, July 1997.

[80] Seoane J.L. et al., "Analysis of intertone and interblock interference in OFDM when the length of the cyclic prefix is shorter than the length of the impulse response of the channel," vol. 1. IEEE Globecom'97.

[81] Pollet T., et al., "Performance Degradation of Multi–Carrier Systems Caused by an Insufficient Guard Interval," in *International Workshop on Coppler Wire Access Systems "Bridging the last copper drop"*, Oct. 1997.

[82] Toeltsch M., Molisch, A.F., "Efficient OFDM transmission without cyclic prefix over frequency-selective channels," in *IEEE PIMRC 2000*, vol. 2, Sep.

[83] Bakker J.D., "Eliminating the OFDM cyclic prefix," in *IEEE PIMRC*, vol. 2, Sep. 2002, pp. 834–837.

[84] Schur R., "Impulse compression for OFDM transmission over time-varying multipath channels," in *IEEE 56th VTC 2002-Fall*, vol. 2, Sep.

[85] Park C.J., Im G-H. , "Efficient DMT/OFDM transmission with insufficient cyclic prefix," *IEEE Communications Letters*, vol. 8, no. 9, pp. 576–578, Sep. 2004.

[86] Lim C., et al., "Novel OFDM Transmission Scheme to Overcome ISI Caused by Multipath Delay Longer than Cyclic Prefix," in *IEEE VTC 2005-Spring*, vol. 3, June.

[87] Halford K., Webster M., "Multipath Measurements in Wireless LANs," intersil, Application Note AN9895.1, 2001.

[88] Rappaport T. S., "Characterization of UHF Multipath Radio Channels in Factory Buildings," *IEEE Transactions on Antennas and Propagation*, vol. 37, no. 8, Aug. 1989.

[89] Gradshteyn I.S., Ryzhik I.M., *Table of Integral, Series and Products.* Academic Press Inc., 1980.

[90] Tang X., Bar-Ness Y., "Maximum Likelihood Channel Delay Estimation with Limited Number of Samples Using Diagonal Matrix Approximation," *Wireless Personal Communication*, vol. 27, no. 3, pp. 183–194, 2003.

[91] Garcia F. -G., et al., "DFT-based channel estimation in 2D-pilot-symbol-aided OFDM wireless systems," in *IEEE VTC 2001 Spring*, vol. 2.

[92] Hayes J., "Adaptive Feedback Communications," *IEEE Transactions on Communications*, vol. 16, no. 1, pp. 29–34, Feb. 1968.

[93] Cavers, J, "Variable-Rate Transmission for Rayleigh Fading Channels," *IEEE Transactions on Communications*, vol. 20, no. 1, pp. 15–22, Feb. 1972.

[94] Toyserkani A. T. et al., "Sub-carrier based Adaptive Modulation in HIPERLAN/2 System," in *IEEE International Conference on Communications, 2004* , June.

[95] Das S.S., M.I. Rahman et al., "Influence of PAPR on Link Adaptation Algorithms in OFDM Systems," in *IEEE VTC Spring'07*, Dublin, Ireland, 22-25 April 2007.

[96] Viswanath P., "Asymptotically optimal water-filling in vector multipleaccess channels," *IEEE Transactions on Information Theory*, vol. 47, pp. 241–267, Jan. 2001.

[97] Chow P.S., Cioffi J.M., Bingham J.A.C., "A practical discrete multitone transceiver loading algorithm for data transmission over spectrally shaped channels," *IEEE Transactions on Communications*, vol. 43, pp. 773–775, Feb.-March 1995.

[98] Wyglinski A.M. et. al, "Bit Loading With BER-Constraint for Multicarrier Systems," *IEEE Transactions on Wireless Communications*, vol. 4, no. 4, pp. 1383–1387, July 2005.

[99] Wong C. Y., Cheng R.S., Lataief K.B., Murch R.D.,, "Multiuser OFDM with adaptive subcarrier, bit, and power allocation," *IEEE Journal on Selected Areas in Communications*, vol. 17, no. 10, pp. 1747–1758, Oct. 1999.

[100] Zhang Y. J.; Letaief, K.B., "Multiuser adaptive subcarrier-and-bit allocation with adaptive cell selection for OFDM systems," *IEEE Transactions on Wireless Communications*, vol. 3, no. 5, pp. 1566 – 1575, Sep. 2004.

[101] Kulkarni, G.; Adlakha, S.; Srivastava, M., "Subcarrier Allocation and Bit Loading Algorithms for OFDMA-Based Wireless Networks," *IEEE Transactions on Mobile Computing*, vol. 4, no. 6, pp. 652 – 662, Nov.-Dec. 2005.

[102] Paolo Banelli and Giuseppe Baruffa and Saverio Cacopardi, "Effect of HPA Non Linearity on Frequency Multiplexed OFDM Signals," in *IEEE Transaction on Broadcasting*, vol. 47, no. 2, June 2001, pp. 123–136.

[103] Ramjee Prasad , *OFDM for Wireless Communication.* Artech House Publishers, 2004.

[104] A. Molisch, *Wireless Communication.* IEEE Press, 2005.

[105] Han S. H., and Lee J.H. , "An Overview of Peak-to-Average Power Ratio Reduction Techniques for Multicarrier Transmission," *IEEE Transactions on Wireless Communications*, April 2005.

[106] Alsusa, E.; Yang, L., "Low-complexity post-IFFT PAPR reduction technique for OFDM systems," *IEE Electronic Letters*, vol. 42, no. 19, pp. 1123–1124, Sep. 2006.

[107] Nikookar, H.; Lidsheim, K.S., "Random phase updating algorithm for OFDM transmission with low PAPR," *IEEE Transactions on Broadcasting*, vol. 48, no. 2, pp. 123–128, June 2002.

[108] Park M.; et al., "PAPR reduction in OFDM transmission using Hadamard transform," in *IEEE International Conference on Communications ICC*, vol. 1, June 2000, pp. 430–433.

[109] You Y.-H.; et al., "Training sequence design and channel estimation of OFDM-CDMA broadband wireless access networks with diversity techniques," *IEEE Transactions on Broadcasting*, vol. 49, no. 4, pp. 354–361, Dec. 2003.

[110] Chong E. T., Wassell, I.J., "Near-optimum training sequences for OFDM systems," in *The 9th Asia-Pacific Conference on Communications, APCC*, vol. 1, Sep. 2003, pp. 119–123.

[111] Drieberg, M.; Yew Kuan Min; Jeoti, V.;, "Low PAPR preamble for IEEE802.16a OFDM system," in *13th IEEE International Conference on Networks, Jointly held with the IEEE 7th Malaysia International Conference on Communication.*, vol. 2, Nov. 2005.

[112] Adel A. M. Saleh, "Frequency-Independent and Frequency-Dependent Nonlinear Models of TWT Amplifiers," in *IEEE Transaction on Communication*, vol. COM-29, no. 11, November 1981, pp. 1715–1720.

[113] G Santella and F Mazzenga, " A hybrid analytical-simulation procedure for performance evaluationin M-QAM-OFDM schemes in presence of nonlinear distortions," in *IEEE Transactions on Vehicular Technology*, vol. 47, no. 1, February 1998, pp. 142–151.

[114] C. Rapp, "Effects of HPA-nonlinearity on a 4-DPSK/OFDM-signal for a digital sound broadcasting signal," in *ESA, Second European Conference on Satellite Communications (ECSC-2) p 179-184 (SEE N92-15210 06-32)*, Oct. 1991, pp. 179–184.

[115] Lei M., et al., "An Adaptive Power Distribution Algorithm for Improving Spectral Efficiency in OFDM," *IEEE Transactions on Broadcasting*, vol. 50, no. 3, pp. 347 – 351, Sep. 2004.

[116] S. H. Han and J. H. Lee, "An overview of peak-to-average power ratio reduction techniques for multicarrier transmission," in *IEEE Wireless Communications*, vol. 12, no. 2, April 2005, pp. 56– 65.

[117] Richard Van Nee and Ramjee Prasad , *OFDM Wireless Multimedia Communication.* Artech House Publishers, 2000.

Vita

Suvra Sekhar Das was born in 1977 in a small town Naihati, in the state of West Bengal in India. He did his schooling from St. Patrick's H.S. school in Asansol, West Bengal. He obtained his B.Eng. degree in Electronics and Communication Engineering from Birla Institute of Technology (Deemed University), Mesra, Ranchi, India in the year 2000 with a 'First Class with Distinction'. He joined Tata Consultancy Services (TCS), India an Assistant Systems Engineer (Trainee) in June 2000. He was involved with the multi media group where he was involved with building simulators for interactive video televisions. He joined the Embedded systems group in TCS Kolkata in the year 2001. For the next two years he was engaged in developing several digital signal processing applications and wireless LAN IEEE 802.11a receiver front end algorithms. Since September 2003, he has been posted at the Wireless Networking (WING) Group at Aalborg University (AAU) as a Researcher from TCS where he later started pursuing his PhD studies.

His current research interest is in optimization for wireless systems at the physical and medium access control layer for multi user cellular networks. He has been an active IEEE volunteer and has taken part in numerous IEEE activities, most notably as the TPC chair of the 1^{st} AAU IEEE Student Paper Conference, AISPC'07, held in Aalborg in January 2007.

Permanent Address: Center for TeleInFrastruktur (CTiF)
Aalborg University
Niels Jernes Vej 12
9220 Aalborg Ost
Denmark
e-mail: *ssd@es.aau.dk*